CRANFIELD UNIVERSITY

Karla Simone Gemkow

Modelling of Damage in Orthotropic Materials: Including Strain-Softening Effects in Dynamic Problems

School of Engineering
Department of Applied Mechanics and Astronautics

PhD Thesis
Academic Year: 2012 - 2013

Supervisor: Prof. Rade Vignjevic
October 2013

CRANFIELD UNIVERSITY

School of Engineering
Department of Applied Mechanics and Astronautics

PhD Thesis

Academic Year 2012 - 2013

Karla Simone Gemkow

Modelling of Damage in Orthotropic Materials: Including Strain-Softening Effects in Dynamic Problems

Supervisor: Prof. Rade Vignjevic
October 2013

This thesis is submitted in partial fulfilment of the requirements for the degree of PhD.

ABSTRACT

This work presents an examination of critical issues in damage modelling of materials with inelastic deformation within the continuum damage mechanics framework. In this the focus lies on stability issues in continuum damage mechanics models with strain-softening behaviour. It is well-known that strain-softening behaviour leads to an ill-posed boundary value problem and with this to a non-unique solution. Additionally, an application of these models in finite element codes is accompanied by a strong sensitivity of results on the chosen finite element spatial discretisation.

This work investigates the mathematical and numerical issues arising from continuum damage mechanics models with strain-softening. A longitudinal wave propagation problem, which is commonly used in literature in the context of strain-softening, will be examined in particular. This example is the strain-softening bar. It is simple in its nature but nevertheless it offers a closed-form analytical solution to a nonlinear problem, is able to capture the characteristic properties of the strain-softening solution and allows a comparison between different methods.

The groups of nonlocal and viscous regularisation schemes are investigated in more detail as they aim to remedy the problem of the ill-posed boundary value problem due to strain-softening. These methods introduce a characteristic length scale parameter, explicitly or implicitly, which confines the strain localisation area to a finite size and keeps the boundary value problem stable.

The scope of the presented works lies in showing that major improvements of damage modelling can be made by addressing the stability issues of the boundary value problem due to strain-softening. Firstly, it is shown that the meshless SPH method has nonlocal properties which can be exploited in the modelling of strain-softening, a use of SPH (total Lagrange form) which has not been considered previously. Then the concept of an “Equivalent damage force”, a unique approach at the time, is introduced which describes the influence of damage as a body force. It is shown analytically that this approach keeps the boundary value problem stable and leads numerically to mesh insensitivity of results to the used finite element spatial discretisation. The approach of an “Equivalent damage force” is extended analytically to fit the needs of materials with orthotropic material behaviour. This involves the definition of a symmetric and positive-definite 8^{th} order damage tensor which is not generic and has not been delivered in literature so far.

ACKNOWLEDGEMENTS

First of all, I would like to express my deepest gratitude to my supervisor Prof. Rade Vignjevic who has been my first choice as advisor and whom I have always admired for his seemingly endless knowledge. I am very grateful that he offered me the chance of realising my educational ambitions by offering me the PhD and securing funding which enabled me to focus my attention on my studies. His clear guidance, huge knowledge and expert advice were essential to the success of this PhD. Thank you very much for your support!

I would also like to thank all lecturers and researchers of the Crashworthiness, Impact & Structural Mechanics Group in Cranfield University for providing me with work materials and advice. Many thanks go as well to our group administrator Marion who always has had an open ear for the students and has helped them to find their way through Cranfield University.

I would also like to express my appreciation for my fellow PhD colleagues who also became my friends during the PhD process. Thanks for keeping up the motivation and making the office a pleasant place to go to.

I would also like to thank Simon for being a great friend and helping me through the last months of my PhD by proof reading my thesis. Also I would like to thank my friend Jekaterina who has accompanied me through my academic years and always offered moral support.

Last but not least I would like to thank my parents and my sister. It is almost impossible to put in words their love and support. However, it was most important that they have always believed in me.

TABLE OF CONTENTS

LIST OF FIGURES

LIST OF TABLES

LIST OF ACRONYMS

CDM	Continuum damage mechanics
CM	Continuum mechanics
FE	Finite element
PDE	Partial differential equation
RVE	Representative volume element
SPH	Smoothed particle hydrodynamics
1D	One-dimensional
2D	Two-dimensional
3D	Three-dimensional

1 Introduction

1.1 Problem Statement

Continuum mechanics is a sound approach to represent macroscopic material behaviour with constitutive equations using the well-known concepts of stress and strain. It has been used commonly for engineering applications and is widely used in finite element applications. However, continuum mechanics does not account for damaging processes on the microscale due to plastic deformation.

The continuum damage mechanics approach includes micromechanical damage processes into constitutive equations using averaging techniques. This is done by using a scalar or tensorial damage variable defined as loss of effective load-carrying area due to micromechanical damage. These models are not fit to represent objectively localised material behaviour due to damage and violate material stability in the sense of Hadamard [41] when the strength of the material is exceeded. This leads to a behaviour known as strain-softening. Strain-softening results analytically in an ill-posed boundary value problem and numerically into spurious mesh-sensitivity of results on the chosen spatial discretisation of the problem.

A number of methods have been introduced which address the issue of objectively representing the physical deformation localisation due to damage by limiting the fracture energy dissipated, such as cohesive method and smeared crack method. However, they have not been successful in solving the mathematical and numerical instability issues leading to mesh-dependency of results. The group of continuum-based regularisation methods, such as viscous and nonlocal methods, approaches the problems due to strain-softening by introducing higher-order terms of time or space which confines the strain-softening area to a finite size and keeps the boundary value problem stable. For this however, an additional parameter, namely a characteristic length parameter, needs to be known.

Regularisation methods are considered in literature to be the only group of methods able to maintain a stable boundary value problem in the presence of strain-softening. However, other possibilities of tackling the mathematical and numerical issues connected to strain-softening might exist. This is worth exploring to add further options to constitutive modelling in continuum damage mechanics.

1.2 Literature Overview

Composite materials are of increasing interest to aviation and automotive industry due to their high performance in strength compared to their overall weight. They are built from two main components, (1) the fibres and (2) a matrix material in which the fibres are embedded. The overall material achieves superior material properties through interdependency of fibres and matrix material in comparison to their single components [35; 55]. The fibres add strength and stiffness to the material. The matrix keeps the position of the fibres, protects them from external mechanical and deteriorating influences and distributes stresses evenly over the fibres. Typical fibre materials are carbon [124; 126], glass [13; 63; 101] and metals [94]. Matrix materials can be resins [14; 114], concrete [1; 31], ceramics [16; 94] or polymers [13; 122]. This variety of possible combinations makes composites a versatile material which allows combining suited material properties for the intended purpose.

However, the fibres have high strength and stiffness only in their longitudinal direction. Therefore, the overall material behaviour is directional and they are classified as orthotropic materials. This increases the complexity for the description of mechanical properties because more constants are needed to describe the material response [35; 55]. The use of finite element methods is wide spread in the development of structures because it offers the possibility to accelerate the development of concepts and designs and makes them more cost-efficient. [78]

A common approach to model the material behaviour of composites in finite element analyses is the use of strength-based failure criteria. These describe the macroscopic material behaviour as linear elastic up to a defined failure strength at which the stresses are set to zero instantaneously and the material is considered to have failed. These criteria are straightforward in their mathematical description and stable in their finite element representation, even in the case of orthotropy. Therefore, they have been popular for finite element purposes and a number of criteria have been developed over the last five decades [46; 55; 57]. Examples of widely used composite failure criteria are the Maximum Stress criteria [55], the Tsai-Wu critierion [113], the Hashin criteria [44] and the Chang-Chang criteria [23; 24].

Although the use of failure criteria has been stable for finite element purposes it has been found that they overly simplify real material behaviour. The behaviour of composites is not purely linear elastic up to a certain failure strength because during

the deformation process the material's microstructure experiences damage which leads to a degeneration of material properties on the macroscale and therefore leads to nonlinearities in the macroscopic material behaviour of materials. [78; 125]

Continuum damage mechanics accounts for changes of macroscopic material behaviour due to damage processes on the microscale. The micromechanical damage processes are introduced into the well-known constitutive equations of continuum mechanics by the definition of a damage variable which represents the reduction in effective load-carrying cross-sectional area. This approach was first introduced by Kachanov [56] who defined an isotropic damage variable, called 'continuity', defining the remaining effective load-carrying area. This approach was further developed by Rabotnov [98] who defined the isotropic damage variable as the effective surface of discontinuities. The definition used by Rabotnov is commonly used nowadays in continuum damage mechanics. Other researchers who have contributed greatly to this field are Lemaitre [64], Krajcinovic [61; 62], Chaboche [19-21], Murakami [82], Cordebois and Sidoroff [26] and Voyiadjis [121] among others. Subsequently, the continuum damage mechanics approach was extended for orthotropic and anisotropic material behaviour by defining tensorial damage variables of 2^{nd} [17; 26] and 4^{th} order [75; 106] able to capture directional damaging processes.

Continuum damage mechanics represents a more comprehensive description of macroscopic material behaviour than mere failure criteria due to the consideration of defects on the microstructure [77; 111]; however, continuum damage mechanics itself is a simplification of micromechanical influences on material behaviour as it uses average measures of material degeneration, namely the damage variable. Constitutive equations of continuum damage mechanics can only be used on a scale sufficiently large enough to be assumed homogeneous, this is the macroscale. This assumes that the microscale is homogeneous as well; however, the microstructure itself and damage processes are heterogeneous [77; 88].

Plastic deformation is dominated by the nucleation, growth and coalescence of voids and microcracks on the microstructure, eventually leading to material fracture. Figure 1 represents the microscopic damage process in 5 stages. The first stage is the formation of micro-voids. This stage of plastic deformation is considered as stable because voids are evenly distributed through the material. Therefore, the material is considered homogeneous from scales above the microscale. The actual microscopic localisation process, and with this the onset of instable macroscopic behaviour, starts

when voids grow and consequently accumulate in the critical area. This clustering leads to merging of voids and formation of cracks, called void coalescence. Once coalescence has started, the damaging process accelerates in the critical area leading to localisation of defects on the microscale. Simultaneously, areas outside the localisation zone, with homogeneously distributed voids, start to unload in an elastic fashion. Finally, the formed microcracks start to grow and merge themselves leading to crack propagation. [5; 85; 88; 97]

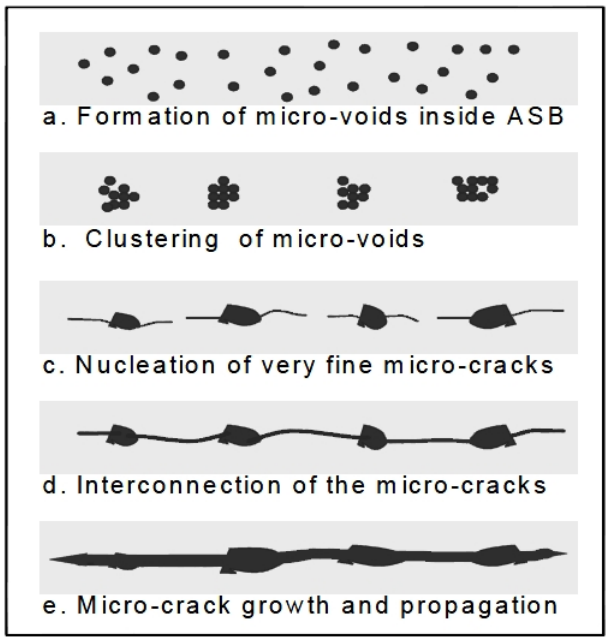

Figure 1: Microstructural localisation process [5]

The idea of damaging processes on the microscale is common for different types of materials, such as metals, concrete and composites. However, the influence which damage has on the macroscopic material behaviour depends on the type of material. An example for manifestation of microscopic damage on macroscopic localisation in metals is necking under tensile loads [15; 51] and cracking in concrete [112] and brittle failure in composites [36].

The damaging processes on the microscale have a significant impact on the observed macroscopic inelastic material behaviour resulting in observance of localisation on the macroscale too. However, on the macroscopic level deformation localisation is understood as instability in a solid's inelastic behaviour [15; 67] showing itself as bands of intense straining which precedes failure. Physical experiments have shown that the localised straining has a finite size in real materials which depends on the material's microstructure [60; 71].

Although continuum damage mechanics is a simplification of processes on the microstructure, continuum damage mechanics is capable of modelling linear elasticity, the influence of initiation and progression of damage on the macrostructure and finally failure. It represents a favourable approach for the description of macroscopic material behaviour because constitutive equations are based on the well-known concepts of stress and strain and continua obey fundamental physical laws. This makes it a common engineering tool and is widely used due to their computational effectiveness. Other finite element models considering the micromechanical composition of a material exist; however, their use is restricted by their practicality. These models tend to have a large number of elements which require a high amount of computational resources and require long termination times [51]. That restricts the use of micromechanical models in finite element methods strongly.

It has been shown that continuum damage mechanics has the issue of mathematical instabilities when the critical load of the material is exceeded. Continuum damage mechanics utilises engineering stress-engineering strain relationships which imply a homogeneously distributed deformation of the specimen. Engineering stress is defined as load over virgin cross-sectional area and engineering strain expresses the ratio of change in length and original length. But in the consideration of continuum damage mechanics damage reduces the effective load-carrying cross-sectional area. This leads to a negative slope in the engineering stress-engineering strain curve when the material's strength is exceeded. This behaviour is called strain-softening which is characterised by a decline of stress with simultaneous increase of strain. A qualitative example of an engineering stress-engineering strain curve is given in Figure 2. The negative slope in the stress-strain relationship indicates a loss of positive-definiteness of the tangent modulus which leads to severe mathematical issues as the material stability criterion is violated [41; 99]. As a consequence the type of partial differential equations changes, from elliptic to hyperbolic in static problems and from hyperbolic to elliptic in dynamic problems, and the boundary value problem is no longer well-posed and a unique solution cannot be achieved. The implementation of such a model in finite element methods also leads to severe numerical problems which manifest themselves as spurious deformation localisation leading to mesh-sensitivity of results on the used spatial discretisation [103]. This is accompanied by a non-physical deformation localisation in the softening zone and vanishing energy dissipation upon mesh refinement. [11; 96; 102; 110]

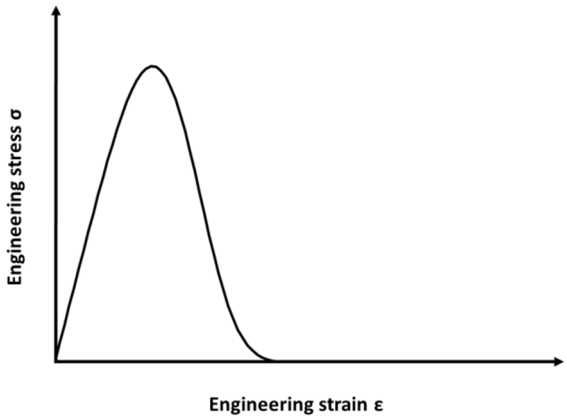

Figure 2: Example of stress-strain relationship with strain-softening

Strain localisation behaviour in continuum damage mechanics has been a concern for many researchers, e.g. Pijaudier-Cabot and Bažant [96], Sluys and de Borst [110], Rice [99] and Neilsen and Schreyer [86]. Unfortunately, the problem of strain-softening and localisation is highly nonlinear and analytical solutions to compare numerical results with are difficult to obtain. Bažant and Belytschko [6] derived as first an analytical solution for strain-softening for longitudinal wave propagation within a bar. This approach was adopted by a number of researches for investigations of dynamic strain-softening in continuum damage mechanics [11; 96; 102; 110]. This example has been very popular in analytical and numerical investigations of strain-softening because it has an exact solution of the nonlinear softening problem, uses well-established wave theory and can be used to compare different methods with each other.

The issue that continuum damage mechanics cannot represent localisation in a finite size, leads to non-physical results and severe numerical instabilities has been subject to extended research.

One of the first models dealing with material failure was the discrete cohesive method which is closely related to fracture theory [4; 32; 45]. In this method it is assumed that the localisation with finite size is small enough to be assumed as a line crack. This zone is modelled with cohesive elements between continuum elements which release energy during the fracturing process. This method leads to convergence with physical results due to the limitation of fracture energy; however, the position of the localisation area needs to be known, the method simplifies the localisation zone to a line crack and it does not address the issue of an ill-posed boundary value problem due to strain-softening.

Another method is the smeared crack method, introduced by Bažant and Oh [8], which brings the cohesive method to the continuum level by smearing the fracture energy over a band which has the width of an element which represents the localisation zone. The method estimates the correct amount of dissipated fracture energy if the size of the crack zone is estimated correctly. Unfortunately, that makes the results subjective to the used mesh refinement and it still does not address the issue of the ill-posed boundary value problem.

The Gurson model [40; 84; 115-117] links continuum mechanics with micromechanical void nucleation, growth and coalescence using a yield function including the void fraction as a damage parameter. Strain-softening is modelled as a consequence of increasing void fraction in the material. Although this model is a micromechanically justified model it lacks the stability of the boundary value problem and leads to spurious mesh-sensitivity in numerical simulations when strain-softening occurs.

The problems of the continuum damage mechanics approach in modelling the finite size of the localisation zone and spurious mesh-sensitivity due to the negative tangent modulus can be avoided when an intrinsic length scale is introduced into constitutive equations. This can be achieved with regularised continua which are enriched with higher-order derivatives of space or time and introduce a characteristic internal length scale. These methods are the viscous method, e.g. [83; 109], nonlocal method, e.g. [95; 96] and gradient-enhanced method, e.g. [2; 3]. These models have been used with success in keeping the boundary value problem stable [96]. But these methods depend on an appropriate choice of viscous parameter or internal length scale, depending on the method, and might require additional boundary conditions due to the introduction of higher-order terms.

1.3 Aims and Objectives

This work investigates the representation of damage and strain-softening behaviour within the continuum damage mechanics framework. The aim is to explore new methods, other than regularisation methods, which are capable of maintaining a stable boundary value problem in the presence of strain-softening, thus leading to a unique solution and an insensitivity of numerical results on the chosen finite element spatial discretisation. Additionally, this solution should include orthotropy to make it applicable to a wider range of different material behaviours, such as composites.

To reach this aim a number of objectives were identified:

- Understand the continuum damage mechanics approach and strain-softening behaviour in an analytical, numerical and physical way.
- Validate available material models of composites finite element modelling, including failure models and continuum damage mechanics models.
- Evaluate the strain-softening problem in the local continuum damage mechanics approach regarding their analytical and numerical instabilities.
- Review methods dealing with strain-softening and evaluate existing regularisation methods which remedy the ill-posed boundary value problem due to strain-softening.
- Explore and quantify capabilities of the meshless SPH method, in its total Lagrange form, as nonlocal method, representing a new application of the SPH method.
- Develop the concept of an “Equivalent damage force”, a unique approach at the time, in continuum damage mechanics to solve the analytical and numerical issues of strain-softening material behaviour.
- Test the concept of an “Equivalent damage force” numerically by using an isotropic material model with a scalar damage variable.
- Extend the concept of an “Equivalent damage force” to orthotropic material behaviour.

1.4 Outline

Chapter 2 provides the conceptual and mathematical background of continuum mechanics. The concept of stress and strain, which will be used throughout this work, will be clarified. The chapter also introduces the mathematics and notation of tensors which will be used commonly in this work.

Chapter 3 provides the general framework of continuum damage mechanics. Firstly, it will be explained how heterogeneous damage on the microscale is averaged and included in the constitutive equations of continuum mechanics through the damage variable. Then important principles and hypotheses, such as effective stress and strain equivalence, used for constitutive modelling are introduced. Then the mathematical background of material instabilities caused by strain-softening behaviour in continuum damage mechanics will be investigated as basis for further progress in this work. The chapter will close with the analytical investigation of a one-dimensional strain-softening problem, namely the strain-softening bar, a common test problem in literature regarding

strain-softening. This problem will be of paramount importance throughout this work as it allows for a closed-form solution due to its simplicity and illustrates clearly the characteristics and issues of the strain-softening solution.

Chapter 4 will provide a survey of composite failure and damage models commonly used in finite element codes. The most commonly used assumptions and theories will be introduced. Then a numerical analysis in LS-DYNA, using single element tests, will be conducted to investigate the capabilities of several readily available composite models. In another step the previously introduced strain-softening bar will be used to show the numerical instabilities connected to strain-softening in a readily available LS-DYNA continuum damage mechanics model. These results will be compared to the analytical solution for strain-softening which was investigated in Chapter 3. Finally, this chapter will close with a test of available stabilisation methods for numerical instabilities due to strain-softening which are readily available in the finite element codes LS-DYNA and ABAQUS. The example of the strain-softening bar will be used to investigate the characteristic behaviour of these stabilisation methods.

Chapter 5 will give a review on existing methods dealing with strain-softening. First a review on the cohesive method, smeared crack method and Gurson model will be given. However, the focus will be the investigation of regularisation methods, namely nonlocal integral, nonlocal gradient-enhanced and viscous methods, as they are addressing the issue of an ill-posed boundary value problem. It will be shown analytically that these methods keep the boundary value problem well-posed by preventing the change in type of partial differential equations.

Chapter 6 will apply the meshless smoothed particle hydrodynamics (also known as SPH) approach to strain-softening. SPH uses a smoothing function to define the interaction of particles. The author of this work presumes that the smoothing function makes SPH a nonlocal method by nature and that instabilities associated with strain-softening can be avoided by adjusting the smoothing function. The use of SPH in improving the nature of the boundary value problem in the presence of strain-softening has not been addressed in literature previously. Therefore, the characteristic properties of SPH for CDM models with strain-softening will be observed and quantified in this chapter. First the main aspects making SPH a nonlocal method will be pointed out. Then a numerical investigation with the in-house SPH code MCM using the strain-softening bar example will be carried out which will show clearly how the adjustment of the SPH smoothing function influences the strain-softening solution. It will be shown

that SPH is indeed acting like a nonlocal method and leads to a unique solution for strain-softening when the smoothing function is defined appropriately.

Chapter 7 will present the “Equivalent damage force” approach which was developed by the author of this work and is unique at the time. This approach describes the influence of damage on the material behaviour as body force. This approach isolates the influence of damage on the homogeneous part of the equation of motion which keeps the governing partial differential equations hyperbolic. Therefore the initial boundary value maintains its well-posedness. This concept will be first demonstrated analytically for a one-dimensional problem. Then a numerical evaluation of the approach will be done with an isotropic representation which was implemented in the DYNA3D code. The numerical evaluation is carried out first using the strain-softening bar as it shows clearly the characteristic properties of this approach. A second validation problem is the investigation of a concrete tension test which allows a comparison of the “Equivalent damage force” approach to experimental work and conventional regularisation methods. Finally, the approach of an “Equivalent damage force” will be extended to orthotropic material behaviour. This requires the definition of a symmetric and positive-definite 8^{th} order damage tensor. The definition of an 8^{th} order tensor and the proof of its symmetry and positive-definiteness is not generic and could not be deducted from present literature.

Chapter 8 provides conclusions and suggestions for future work.

2 Concepts of Solid Mechanics

Continuum mechanics (CM) focuses on the motion and deformation behaviour of continua. The microstructure of a material is neglected in CM. Instead a material is regarded on a scale sufficiently large enough to allow a homogenisation of the material properties. This scale is at least the mesoscale at which variables are homogenised over a representative volume element (RVE). However, in general the macroscale is considered.

CM distinguishes two main fields: solid mechanics and fluid mechanics. Fluid mechanics studies the physical behaviour of fluids; however, this branch is not part of the present work. This work focusses on solid mechanics.

Solid mechanics describes the behaviour of solids under the application of external forces. Solids are understood as continua which have a given resistance against changes in shape and volume. Solid mechanics distinguishes between a reversible deformation, regarded as elastic, and an irreversible deformation, regarded as plastic.

This chapter will provide most important background of CM and will introduce a considerable amount of notation used throughout this work.

2.1 Tensors

Physical quantities used in CM are independent of the used coordinate system. These quantities are expressed with tensors in mathematics. A tensor is described in a coordinate system by its components and can be expressed in any other coordinate system by a transformation of its components without changing its physical quantities.

Laws of CM are expressed with tensor equations. These equations are valid in any other coordinate system because transformations are linear and homogeneous. This is called invariance.

This work restricts its attention to Cartesian tensors. These tensors are defined in the Cartesian coordinate system which is an orthogonal system.

Tensors have a rank, also called order, which depends on the valid transformation law. The number of components possessed by a tensor is determined by n^N, where N is the order of the tensor in n-dimensional space. Many physical quantities are expressed with tensors of 0^{th}, 1^{st} or 2^{nd} order. Tensors of higher order are rather constructs used in mathematics of CM. Table 2-1 shows commonly used tensors of different quantities.

Table 2-1: Examples of common tensor quantities

Sign	Order	Quantity	Example
m	0th	scalar	mass
f_i	1st	vector	force
σ_{ij}	2nd	dyadic	stress
C_{ijkl}	4th	tetradic	stiffness tensor

Table 2-1 sets an example for a notation which is commonly used to represent components of a tensor: index notation. Indices are said to be free indices when they are not repeated in a term. The number of free indices states the order of a tensor. Repeated indices in a term are called dummy indices when the summation convention is used. This convention states that a term is summed up over the full range $1, 2, \dots n$ of the dummy index.

A 2nd order tensor is symmetric if an exchange of indices does not change the tensor.

$$D_{ij} = D_{ji} \tag{2-1}$$

Any tensor can be expressed in matrix form. An exchange of indices would correspond to the exchange of rows and columns in matrix representation. Therefore, a tensor written in matrix form is symmetric when its matrix is equal to its transpose.

$$\boldsymbol{D} = \boldsymbol{D^T} = \begin{bmatrix} D_{11} & D_{12} & D_{13} \\ D_{12} & D_{22} & D_{23} \\ D_{13} & D_{23} & D_{33} \end{bmatrix} \tag{2-2}$$

A 2nd order tensor is said to be skew-symmetric if it equals the conjugate's negative.

$$D_{ij} = -D_{ji} \tag{2-3}$$

The representation of skew-symmetry in matrix form is as shown below. A matrix is skew-symmetric if it equals the negative of the transpose.

$$\boldsymbol{D} = -\boldsymbol{D^T} = \begin{bmatrix} 0 & D_{12} & D_{13} \\ -D_{12} & 0 & D_{23} \\ -D_{13} & -D_{23} & 0 \end{bmatrix} \tag{2-4}$$

Any tensor can be decomposed in a symmetric and a skew-symmetric part.

$$D_{ij} = \frac{1}{2}\left(D_{ij} + D_{ji}\right) + \frac{1}{2}\left(D_{ij} - D_{ji}\right) \tag{2-5}$$

Tensors with higher order are said to have minor symmetries when indices in successive pairs are interchangeable, to have major symmetries when pairs of indices are interchangeable and super-symmetric when the tensor is symmetric in all indices.

$$A_{ijkl} = A_{jilk} \quad \text{Minor symmetry in } i \text{ and } j, \text{ and } k \text{ and } l \tag{2-6}$$

$$A_{ijkl} = A_{klij} \quad \text{Major symmetry in } ij \text{ and } kl \tag{2-7}$$

$$A_{ijkl} = A_{jilk} = A_{klij} \quad \text{Super-symmetry in all indices} \tag{2-8}$$

2.2 Stress Tensor

The stress tensor is a tensor of order two which describes the state of stress in a point of a continuum. It includes the stress information of three mutually perpendicular planes in the considered point. Figure 3 represents the stress tensor according to the given coordinate planes. The stress tensor is written in index notation σ_{ij} $(i, j = 1, 2, 3)$. The first index indicates the plane's normal and the second index indicates the direction of the stress.

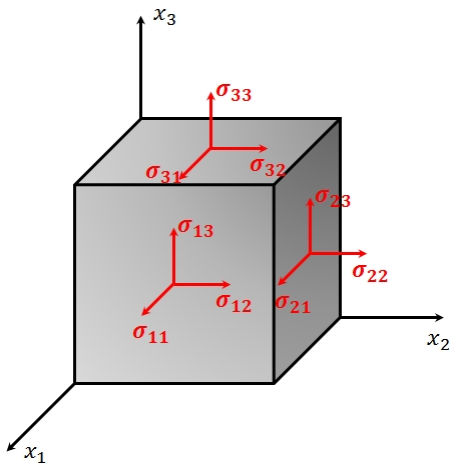

Figure 3: Components of the stress tensor with reference to the coordinate planes

The stress tensor is represented by a 3 × 3 matrix:

$$[\sigma_{ij}] = \begin{bmatrix} \sigma_{11} & \sigma_{12} & \sigma_{13} \\ \sigma_{21} & \sigma_{22} & \sigma_{23} \\ \sigma_{31} & \sigma_{32} & \sigma_{33} \end{bmatrix} \tag{2-9}$$

The diagonal components $(\sigma_{11}, \sigma_{22}, \sigma_{33})$ are called normal stresses and are normal to the plane. The off-diagonal components $(\sigma_{12}, \sigma_{13}, \sigma_{21}, \sigma_{23}, \sigma_{31}, \sigma_{32})$ are called shear stresses and are tangential to the planes.

The stress tensor is symmetric which can be proven by determining the moment equilibrium for the body in Figure 3.

$$\sigma_{ij} = \sigma_{ji} \tag{2-10}$$

2.3 Deformation and Strain

This section aims to study deformation of a continuum when it moves from an initial configuration to a new (current) configuration. Deformation is understood as a change in size and shape of the continuum.

It is assumed in CM that stress at a point within a material depends on the deformation of this specific point. The deformation of a continuum is described as the gradient of the displacement field u_k. u_k expresses the current position, x_k, of a point with reference to its original position, X_k.

Figure 4 shows a continuum displaced from its original configuration at $t = 0$ to a later configuration at $t = t$. The position of the point P_0 is described with the position vector $X_K\hat{\boldsymbol{I}}_K$ with respect to $OX_1X_2X_3$ and the later position of it is described with the position vector $x_k\hat{\boldsymbol{e}}_k$ with respect to $ox_1x_2x_3$. The coordinates $X_1X_2X_3$ are called material coordinates and the coordinates $x_1x_2x_3$ are called spatial coordinates. The vector $b_K\hat{\boldsymbol{I}}_K$ locates the origin of the spatial coordinate system with respect to the origin of the material coordinates. The vector $u_k\hat{\boldsymbol{e}}_k$ which connects P_0 and P is called the displacement vector.

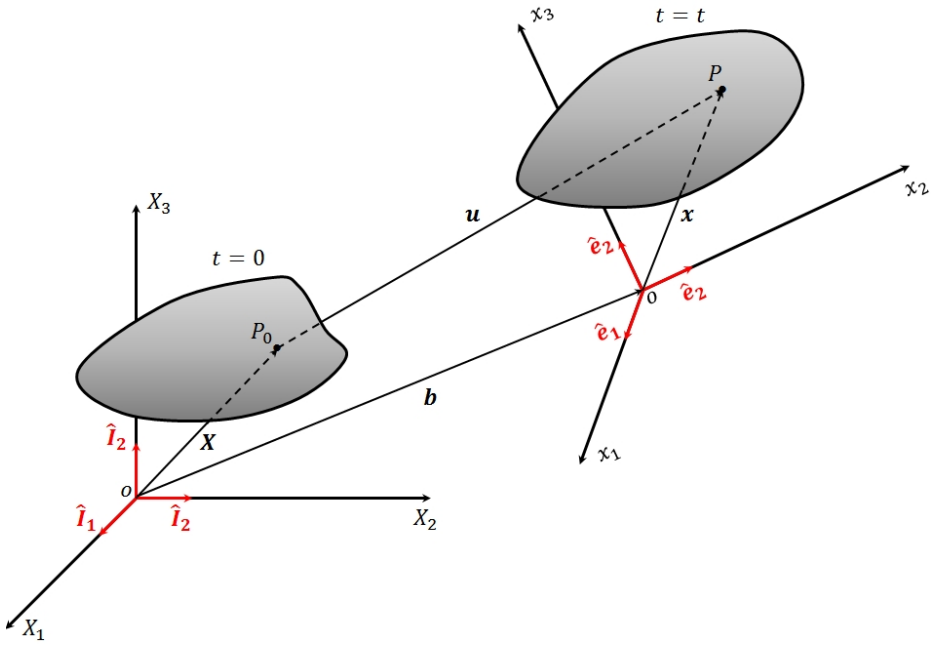

Figure 4: Displaced continuum description (adapted from [80])

The displacement vector can be constructed according to the relationships made in Figure 4. However, it is sufficient to assume that $OX_1X_2X_3$ and $ox_1x_2x_3$ coincide. Then the displacement vector reduces to:

$$u_k = x_k - X_k \tag{2-11}$$

During the deformation process the reference point P_0 changes its position as time progresses. The route it takes is called the path line. The movement of a continuum's particle is described by a mapping between the initial and current configuration. The mapping from initial to current configuration is known as Lagrangian formulation.

$$x_i = x_i(X_1, X_2, X_3, t) \tag{2-12}$$

The mapping from current to initial configurations is called Eulerian formulation.

$$X_i = X_i(x_1, x_2, x_3, t) \tag{2-13}$$

The Langrangian and Eulerian mappings, (2-12) and (2-13), are inverse to each other under the conditions that the mapping and its partial derivatives are continuous. This is true when the Jacobian determinant exists.

$$\mathcal{J} = \left|\frac{\partial x_i}{\partial X_j}\right| \neq 0 \tag{2-14}$$

The motion of a continuum is described by the gradient of the mapping. This operation produces a 2nd order tensor which is called deformation tensor. If the partial differentiation is conducted with respect to the initial configuration it is called material deformation gradient $\mathcal{F}$.

$$\mathcal{F} = \frac{\partial x_i}{\partial X_j} \tag{2-15}$$

The spatial deformation gradient $\mathcal{F}^{-1}$ describes the motion with respect to the current configuration.

$$\mathcal{F}^{-1} = \frac{\partial X_i}{\partial x_j} \tag{2-16}$$

Material and spatial deformation gradient are inverse to each other.

$$\frac{\partial x_i}{\partial X_j}\frac{\partial X_j}{\partial x_k} = \frac{\partial X_i}{\partial x_j}\frac{\partial x_j}{\partial X_k} = \delta_{ik} \tag{2-17}$$

δ_{ik} is the Kronecker delta which is defined as:

$$\delta_{ik} = \begin{cases} 1 & if \quad i = k \\ 0 & if \quad i \neq k \end{cases} \tag{2-18}$$

The description of the relative displacement between the points P_0 and P is given by the displacement gradient. The displacement gradient is found through a partial differentiation of the displacement vector in (2-11) which describes the difference between coordinates. The differentiation with respect to the initial configuration results in the material displacement gradient $\partial u_i / \partial X_j$. The spatial displacement gradient $\partial u_i / \partial x_j$ is achieved by a differentiation with respect to the current configuration. The displacement gradient is contained within the deformation gradient as it can be seen from (2-19) and (2-20).

$$\frac{\partial u_i}{\partial X_j} = \underbrace{\frac{\partial x_i}{\partial X_j}}_{\mathcal{F}} - \delta_{ij} \tag{2-19}$$

$$\frac{\partial u_i}{\partial x_j} = \delta_{ij} - \underbrace{\frac{\partial X_i}{\partial x_j}}_{\mathcal{F}^{-1}} \tag{2-20}$$

Figure 5 show the change in length between two initial points P_0 and Q_0 during motion. The distance is described by dX_i in the initial configuration and by dx_i in the current configuration.

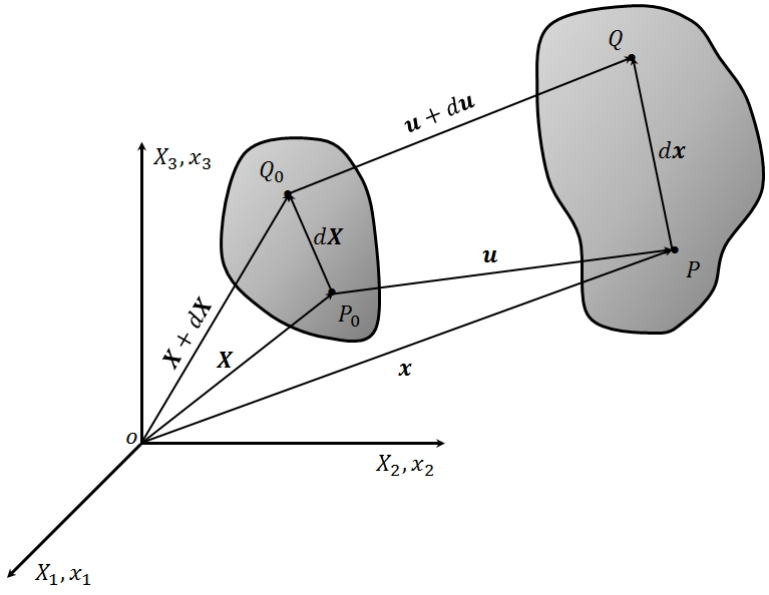

Figure 5: Description of relative displacement of two points (adapted from [80])

The differential distance dX_i between the neighbouring points P_0 and Q_0 can be expressed with reference to the current configuration.

$$dX_i = \frac{\partial X_i}{\partial x_j} dx_j \tag{2-21}$$

The differential distance dx_i between the neighbouring points P and Q can be expressed with reference to the initial configuration.

$$dx_i = \frac{\partial x_i}{\partial X_j} dX_j \tag{2-22}$$

The measure of deformation is defined by the change in the squared length of the differential element dX_i: $(dx)^2 - (dX)^2$. If this difference is equal to zero the continuum is rigid. The squared lengths of the differential elements are defined as follows:

$$(dX)^2 = dX_i dX_i = \delta_{ij} dX_i dX_j \tag{2-23}$$

$$(dx)^2 = dx_i dx_i = \delta_{ij} dx_i dx_j \tag{2-24}$$

The square of the initial distance in (2-23) can be expressed in the current configuration by using (2-21). The square of the current distance in (2-24) can be expressed in the initial configuration by using (2-22).

$$(dX)^2 = \frac{\partial X_k}{\partial x_i} \frac{\partial X_k}{\partial x_j} dx_i dx_j \tag{2-25}$$

$$(dx)^2 = \frac{\partial x_k}{\partial X_i} \frac{\partial x_k}{\partial X_j} dX_i dX_j \tag{2-26}$$

The measure of deformation will be expressed in the Lagrangian framework by a substitution of (2-23) and (2-26).

$$(dx)^2 - (dX)^2 = \left(\frac{\partial x_k}{\partial X_i} \frac{\partial x_k}{\partial X_j} - \delta_{ij} \right) dX_i dX_j \tag{2-27}$$

The 2nd order tensor contained in (2-27) is the Lagrangian finite strain tensor.

$$L_{ij} = \frac{1}{2} \left(\frac{\partial x_k}{\partial X_i} \frac{\partial x_k}{\partial X_j} - \delta_{ij} \right) \tag{2-28}$$

The measure of deformation will be expressed in the Eulerian framework by a substitution of (2-24) and (2-25).

$$(dx)^2 - (dX)^2 = \left(\delta_{ij} - \frac{\partial X_k}{\partial x_i}\frac{\partial X_k}{\partial x_j}\right) dx_i dx_j \tag{2-29}$$

The 2nd order tensor contained in (2-29) is the Eulerian finite strain tensor.

$$E_{ij} = \frac{1}{2}\left(\delta_{ij} - \frac{\partial X_k}{\partial x_i}\frac{\partial X_k}{\partial x_j}\right) \tag{2-30}$$

The Lagrangian and Eulerian finite strain tensors can be expressed in terms of the displacement gradient. This requires a substitution of (2-19) in (2-28) and a substitution of (2-20) in (2-30).

$$L_{ij} = \frac{1}{2}\left(\frac{\partial u_i}{\partial X_j} + \frac{\partial u_j}{\partial X_i} + \frac{\partial u_k}{\partial X_i}\frac{\partial u_k}{\partial X_j}\right) \tag{2-31}$$

$$E_{ij} = \frac{1}{2}\left(\frac{\partial u_i}{\partial x_j} + \frac{\partial u_j}{\partial x_i} - \frac{\partial u_k}{\partial x_i}\frac{\partial u_k}{\partial x_j}\right) \tag{2-32}$$

The small deformation theory is an important concept in CM. In this theory it is assumed that the displacement gradients are small in comparison to unity. Therefore products of the displacement gradient, as they appear in the Lagrangian and Eulerian finite strain tensors, are insignificant which leads to a linearisation of the strain tensors. This results in the definition of the Lagrangian and Eulerian infinitesimal strain tensors.

$$l_{ij} \approx \frac{1}{2}\left(\frac{\partial u_i}{\partial X_j} + \frac{\partial u_j}{\partial X_i}\right) \tag{2-33}$$

$$\epsilon_{ij} \approx \frac{1}{2}\left(\frac{\partial u_i}{\partial x_j} + \frac{\partial u_j}{\partial x_i}\right) \tag{2-34}$$

The assumption of small displacements and small displacement gradients makes the difference between material and spatial displacement gradients negligible. The Lagrangian and Eulerian infinitesimal strain tensors can be approximated to be equivalent as a consequence.

$$l_{ij} = \epsilon_{ij} \tag{2-35}$$

The result of this linearisation is the linear strain tensor.

$$\varepsilon_{ij} = \frac{1}{2}\left(u_{i,j} + u_{j,i}\right) \tag{2-36}$$

$$[\varepsilon_{ij}] = \begin{bmatrix} \varepsilon_{11} & \varepsilon_{12} & \varepsilon_{13} \\ \varepsilon_{21} & \varepsilon_{22} & \varepsilon_{23} \\ \varepsilon_{31} & \varepsilon_{32} & \varepsilon_{33} \end{bmatrix}$$

$$= \begin{bmatrix} \frac{\partial u_1}{\partial x_1} & \frac{1}{2}\left(\frac{\partial u_1}{\partial x_2} + \frac{\partial u_2}{\partial x_1}\right) & \frac{1}{2}\left(\frac{\partial u_1}{\partial x_3} + \frac{\partial u_3}{\partial x_1}\right) \\ \frac{1}{2}\left(\frac{\partial u_2}{\partial x_1} + \frac{\partial u_1}{\partial x_2}\right) & \frac{\partial u_2}{\partial x_2} & \frac{1}{2}\left(\frac{\partial u_2}{\partial x_3} + \frac{\partial u_3}{\partial x_2}\right) \\ \frac{1}{2}\left(\frac{\partial u_3}{\partial x_1} + \frac{\partial u_1}{\partial x_3}\right) & \frac{1}{2}\left(\frac{\partial u_3}{\partial x_2} + \frac{\partial u_2}{\partial x_3}\right) & \frac{\partial u_3}{\partial x_3} \end{bmatrix} \quad (2\text{-}37)$$

It can be easily seen that the linear strain tensor in (2-37) is symmetric.

2.4 Equation of Motion

A continuum with volume V is at any time subjected to two kinds of forces: body forces b_i and surface forces f_i. Body forces act on a volume element dV and are expressed as force per unit mass. They can be expressed as force per unit volume ρb_i as well. An example for a body force is gravity. Surface forces act through a surface element dS defined by the surface normal n_j, e.g. contact forces. A system of surface forces is expressed by the stress vector which is defined by Cauchy's stress principle.

$$t_i = \sigma_{ji} n_j \quad (2\text{-}38)$$

Static equilibrium of dV is achieved when the resultant force of body and surface forces vanishes.

$$\int_S \sigma_{ji} n_j \, dS + \int_V \rho b_i \, dV = 0 \quad (2\text{-}39)$$

The application of Gauss' divergence theorem allows a conversion of a surface integral to a volume integral. Therefore the equilibrium equation in (2-39) becomes:

$$\int_V \left(\sigma_{ij,j} + \rho b_i\right) dV = 0 \quad (2\text{-}40)$$

The volume of the continuum body is arbitrary and the volume integral can be neglected. The static equilibrium finally reads:

$$\sigma_{ij,j} + \rho b_i = 0 \quad (2\text{-}41)$$

A continuum in motion is subjected to a velocity field v_i.

$$v_i = \frac{du_i}{dt} \tag{2-42}$$

The rate of change of the linear momentum equals the resultant force of body and surface forces according to the principle of linear momentum.

$$\int_V \left(\sigma_{ij,j} + \rho b_i\right) dV = \frac{d}{dt}\int_V \rho v_i \, dV \tag{2-43}$$

The volume of the continuum body is arbitrary and the volume integral can be neglected. The equation of motion reads finally:

$$\sigma_{ij,j} + \rho b_i = \rho \dot{v}_i \tag{2-44}$$

2.5 Constitutive Equation

The constitutive equation for a linear elastic solid is given by the generalised Hooke's law. This law connects the stress tensor in (2-9) linearly with the strain tensor in (2-37). The connection of those 2nd order tensors can only be achieved through a 4th order tensor. This tensor is the stiffness tensor C_{ijkl}.

$$\sigma_{ij} = C_{ijkl}\varepsilon_{kl} \tag{2-45}$$

C_{ijkl} contains 81 independent components which describe the full elastic behaviour of a solid with their elastic constants. However, the number of independent constants is reduced to 36 by considering the symmetry of stress and strain tensor.

It is therefore possible to express C_{ijkl} with 36 components in matrix form.

$$\begin{bmatrix} C_{1111} & C_{1122} & C_{1133} & C_{1123} & C_{1131} & C_{1112} \\ C_{2211} & C_{2222} & C_{2233} & C_{2223} & C_{2231} & C_{2212} \\ C_{3311} & C_{3322} & C_{3333} & C_{3323} & C_{3331} & C_{3312} \\ C_{2311} & C_{2322} & C_{2333} & C_{2323} & C_{2331} & C_{2312} \\ C_{3111} & C_{3122} & C_{3133} & C_{3123} & C_{3131} & C_{3112} \\ C_{1211} & C_{1222} & C_{1233} & C_{1223} & C_{1231} & C_{1212} \end{bmatrix} \tag{2-46}$$

$$\cong \begin{bmatrix} C_{11} & C_{12} & C_{13} & C_{14} & C_{15} & C_{16} \\ C_{12} & C_{22} & C_{23} & C_{24} & C_{25} & C_{26} \\ C_{13} & C_{23} & C_{33} & C_{34} & C_{35} & C_{36} \\ C_{14} & C_{24} & C_{34} & C_{44} & C_{45} & C_{46} \\ C_{15} & C_{25} & C_{35} & C_{45} & C_{55} & C_{56} \\ C_{16} & C_{26} & C_{36} & C_{46} & C_{56} & C_{66} \end{bmatrix}$$

The constitutive equation in (2-45) will be written in Voigt notation for this purpose. Voigt notation changes the double index of the stress and strain tensors to a single valued index.

$$\begin{aligned} \sigma_{11} &= \sigma_1 & \sigma_{23} &= \sigma_{32} = \sigma_4 & \varepsilon_{11} &= \varepsilon_1 & 2\varepsilon_{23} &= 2\varepsilon_{32} = \varepsilon_4 \\ \sigma_{22} &= \sigma_2 & \sigma_{13} &= \sigma_{31} = \sigma_5 & \varepsilon_{22} &= \varepsilon_2 & 2\varepsilon_{13} &= 2\varepsilon_{31} = \varepsilon_5 \\ \sigma_{33} &= \sigma_3 & \sigma_{12} &= \sigma_{21} = \sigma_6 & \varepsilon_{33} &= \varepsilon_3 & 2\varepsilon_{12} &= 2\varepsilon_{21} = \varepsilon_6 \end{aligned} \tag{2-47}$$

The number of the stiffness tensor's indices in (2-45) is therefore reduced from four to two.

$$\sigma_K = C_{KM}\varepsilon_M \quad with \quad K, M = 1,2,3,4,5,6 \tag{2-48}$$

The stress and strain tensors are written as column matrices due to the reduction of indices.

$$\begin{bmatrix} \sigma_1 \\ \sigma_2 \\ \sigma_3 \\ \sigma_4 \\ \sigma_5 \\ \sigma_6 \end{bmatrix} = \begin{bmatrix} C_{11} & C_{12} & C_{13} & C_{14} & C_{15} & C_{16} \\ C_{12} & C_{22} & C_{23} & C_{24} & C_{25} & C_{26} \\ C_{13} & C_{23} & C_{33} & C_{34} & C_{35} & C_{36} \\ C_{14} & C_{24} & C_{34} & C_{44} & C_{45} & C_{46} \\ C_{15} & C_{25} & C_{35} & C_{45} & C_{55} & C_{56} \\ C_{16} & C_{26} & C_{36} & C_{46} & C_{56} & C_{66} \end{bmatrix} \begin{bmatrix} \varepsilon_1 \\ \varepsilon_2 \\ \varepsilon_3 \\ \varepsilon_4 \\ \varepsilon_5 \\ \varepsilon_6 \end{bmatrix} \tag{2-49}$$

It is known that the stiffness tensor is symmetric in successive indices, $ij = ji$ and $kl = lk$, due to the symmetry of the stress and strain tensor. It can be proven that C_{ijkl} is symmetric with respect to the index pairs ij and kl under certain conditions.

Internal energy is purely mechanical when thermal effects are insignificant. Then the internal energy is called strain energy du. The strain energy per unit volume is defined by:

$$du = \sigma_{ij} d\varepsilon_{ij} \tag{2-50}$$

A substitution of (2-45) in (2-50) leads to:

$$du = C_{ijkl}\varepsilon_{ij}d\varepsilon_{ij} \tag{2-51}$$

Integration leads to the strain energy function u^*. The existence of this function is fundamental for the further symmetry of the stiffness tensor.

$$u^* = \frac{1}{2}C_{ijkl}\varepsilon_{ij}\varepsilon_{kl} \tag{2-52}$$

The differentiation of the strain energy function with respect to the strain tensor ε_{ij} leads to the generalised Hooke's law.

$$\frac{\partial u^*}{\partial \varepsilon_{ij}} = C_{ijkl}\varepsilon_{kl} \tag{2-53}$$

Subsequent differentiation with respect to ε_{kl} results in the stiffness tensor.

$$\frac{\partial^2 u^*}{\partial \varepsilon_{ij}\partial \varepsilon_{kl}} = C_{ijkl} \tag{2-54}$$

However, the same holds true when the sequence of indices is changed.

$$\frac{\partial^2 u^*}{\partial \varepsilon_{kl}\partial \varepsilon_{ij}} = C_{klij} \tag{2-55}$$

It can be seen from (2-54) and (2-55) that the sequence of differentiation is arbitrary. The stiffness tensor with its 36 components is symmetric in itself as a consequence.

$$C_{ijkl} = C_{klij} \tag{2-56}$$

It can be concluded that the most general stiffness tensor has only 21 independent components. The matrix form is expressed by C_{KM}.

$$[C_{KM}]=\begin{bmatrix} C_{11} & C_{12} & C_{13} & C_{14} & C_{15} & C_{16} \\ C_{12} & C_{22} & C_{23} & C_{24} & C_{25} & C_{26} \\ C_{13} & C_{23} & C_{33} & C_{34} & C_{35} & C_{36} \\ C_{14} & C_{24} & C_{34} & C_{44} & C_{45} & C_{46} \\ C_{15} & C_{25} & C_{35} & C_{45} & C_{55} & C_{56} \\ C_{16} & C_{26} & C_{36} & C_{46} & C_{56} & C_{66} \end{bmatrix} \tag{2-57}$$

The stiffness tensor in (2-57) reflects the most general case of linear elasticity and is commonly known as anisotropy. Anisotropy indicates that the elastic properties are

directional. Further simplifications of the stiffness tensor can be conducted by exploiting symmetries of elastic behaviour.

The first simplification can be made by assuming a monoclinic material. A monoclinic material has one plane of elastic symmetry. The components of the stiffness matrix reduce to 20. 13 constants are independent if a strain energy function exists.

$$[C_{KM}] = \begin{bmatrix} C_{11} & C_{12} & C_{13} & 0 & 0 & C_{16} \\ C_{12} & C_{22} & C_{23} & 0 & 0 & C_{26} \\ C_{13} & C_{23} & C_{33} & 0 & 0 & C_{36} \\ 0 & 0 & 0 & C_{44} & C_{45} & 0 \\ 0 & 0 & 0 & C_{45} & C_{55} & 0 \\ C_{16} & C_{26} & C_{36} & 0 & 0 & C_{66} \end{bmatrix} \tag{2-58}$$

A material with a minimum of two planes of elastic symmetry is called an orthotropic material. The stiffness matrix has only 12 components of which 9 are independent in presence of a strain energy function.

$$[C_{KM}] = \begin{bmatrix} C_{11} & C_{12} & C_{13} & 0 & 0 & 0 \\ C_{12} & C_{22} & C_{23} & 0 & 0 & 0 \\ C_{13} & C_{23} & C_{33} & 0 & 0 & 0 \\ 0 & 0 & 0 & C_{44} & 0 & 0 \\ 0 & 0 & 0 & 0 & C_{55} & 0 \\ 0 & 0 & 0 & 0 & 0 & C_{66} \end{bmatrix} \tag{2-59}$$

Transversely isotropic materials have one plane in which the elastic properties are not directional. This specific plane is isotropic and the direction subscripts are interchangeable. The stiffness matrix depends on only 5 independent elastic constants.

$$[C_{KM}] = \begin{bmatrix} C_{11} & C_{12} & C_{12} & 0 & 0 & 0 \\ C_{12} & C_{22} & C_{23} & 0 & 0 & 0 \\ C_{12} & C_{23} & C_{22} & 0 & 0 & 0 \\ 0 & 0 & 0 & \frac{(C_{22} - C_{23})}{2} & 0 & 0 \\ 0 & 0 & 0 & 0 & C_{66} & 0 \\ 0 & 0 & 0 & 0 & 0 & C_{66} \end{bmatrix} \tag{2-60}$$

If a material's elastic properties possess full symmetry the material is called isotropic. An isotropic material has only 2 independent elastic constants.

$$[C_{KM}] = \begin{bmatrix} \lambda + 2\mu & \lambda & \lambda & 0 & 0 & 0 \\ \lambda & \lambda + 2\mu & \lambda & 0 & 0 & 0 \\ \lambda & \lambda & \lambda + 2\mu & 0 & 0 & 0 \\ 0 & 0 & 0 & \mu & 0 & 0 \\ 0 & 0 & 0 & 0 & \mu & 0 \\ 0 & 0 & 0 & 0 & 0 & \mu \end{bmatrix} \tag{2-61}$$

The two constants λ and μ in (2-61) are called Lamé constants and are defined by the Young's modulus E and Poisson's ratio ν. μ is also known as shear modulus G.

$$\lambda = \frac{\nu E}{(1 + \nu)(1 - 2\nu)} \tag{2-62}$$

$$\mu = G = \frac{E}{2(1 + \nu)} \tag{2-63}$$

The generalised Hooke's law in (2-45) for an isotropic material can be written in index notation:

$$\sigma_{ij} = \lambda \delta_{ij} \varepsilon_{kk} + 2\mu \varepsilon_{ij} \tag{2-64}$$

The generalised Hooke's law in (2-45) can be rearranged in a way that the strain tensor is expressed in terms of the stress tensor. The elastic behaviour of the solid is then described by the elastic constants of the compliance tensor S_{ijkl}.

$$\varepsilon_{ij} = S_{ijkl} \sigma_{kl} \tag{2-65}$$

The compliance is inverse to the stiffness tensor: $S_{ijkl} = C_{ijkl}^{-1}$. Therefore the compliance matrix of an isotropic material can be derived from (2-61), (2-62) and (2-63).

$$[S_{KM}] = \frac{1}{E} \begin{bmatrix} 1 & -\nu & -\nu & 0 & 0 & 0 \\ -\nu & 1 & -\nu & 0 & 0 & 0 \\ -\nu & -\nu & 1 & 0 & 0 & 0 \\ 0 & 0 & 0 & 2(1 + \nu) & 0 & 0 \\ 0 & 0 & 0 & 0 & 2(1 + \nu) & 0 \\ 0 & 0 & 0 & 0 & 0 & 2(1 + \nu) \end{bmatrix} \tag{2-66}$$

2.6 Summary

This chapter presented the basis of linear elasticity and introduced the index notation which will be used throughout this thesis. The concepts of solid mechanics are of high importance as they are used to describe material behaviour in FE software.

However, the presented concepts will be proven to be limited in the progress of this work. In the next chapter the continuum damage approach will be introduced. This approach enables the inclusion of degenerative processes of the microscale in constitutive equations which were presented in this chapter.

3 Continuum Damage Mechanics and Instabilities Associated with Strain-Softening

The influence of micromechanical damage processes on the macroscopic material behaviour cannot be described with the general approach of continuum mechanics. Continuum damage mechanics (CDM) includes the micromechanical damage process in constitutive equations by assuming a homogeneous distribution in a representative volume element (RVE). The degeneration of material properties is introduced into constitutive equations by applying an averaging technique in which material degeneration is described as loss of effective load-carrying area. This is designated with a damage variable which can be scalar or tensorial. Therefore, CDM is able to represent linear elastic material behaviour as well as the influence of initiation and progression of damage on the macroscopic material behaviour.

However, CDM is said to be a local approach to damage because the development of stress depends only on the deformation history of a single point x_i. The CDM approach is limited in its mathematical value when materials undergo a behaviour known as strain-softening. Strain-softening is characterised by a decline of stress with simultaneously increasing strain caused by progressive damage. In CDM this behaviour is characterised as a negative slope in the engineering stress-engineering strain diagram (see Figure 6). Strain-softening behaviour causes the tangent modulus to lose positive-definiteness which violates the material stability criterion in the sense of Hadamard [41].

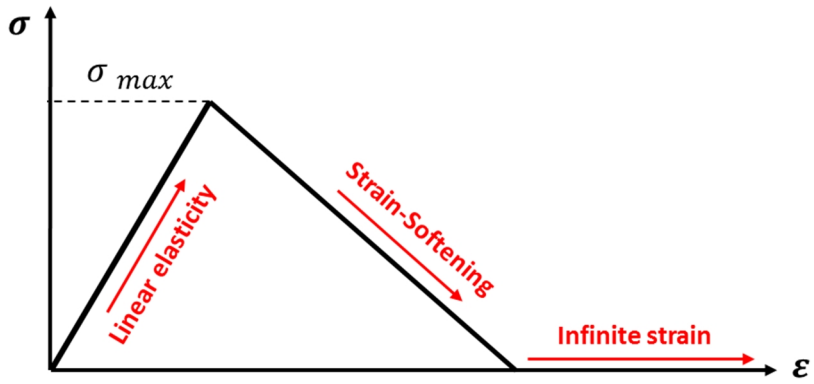

Figure 6: General stress-strain diagram for materials with strain-softening

Firstly, this chapter will provide a description of the definitions and principles used in CDM. These definitions will be the basis for the work presented in this thesis. Secondly, this chapter will focus on problems of local continua which are associated

with strain-softening behaviour. The loss of material stability and loss of uniqueness and its impact on CDM results will be discussed. The characteristic properties of a material model with strain-softening and the connected stability issues will be demonstrated analytically with a one-dimensional example of longitudinal wave propagation in a bar.

3.1 Damage Modelling

3.1.1 Definition of Damage Variables

Kachanov [56] proposed the use of a scalar damage variable first which he called 'continuity' ψ $(0 \leq \psi \leq 1)$, with $\psi = 1$ as undamaged and $\psi = 0$ as damaged configuration.

Later an alternative damage variable $\omega = 1 - \psi$ $(0 \leq \omega \leq 1)$ was proposed by Rabotnov [98], with $\omega = 0$ as undamaged and $\omega = 1$ as damaged configuration. The definition of ω is commonly used nowadays.

The general approach, see Figure 7, uses a RVE to derive an expression for damage. In this RVE damage is defined as the area of discontinuities dS_D of the surface dS intersecting the considered RVE. The RVE is designated by the surface normal n_j. The damage variable ω is scalar and represents the effective surface density of discontinuities.

$$\omega(n_j) = \frac{dS_D}{dS} \tag{3-1}$$

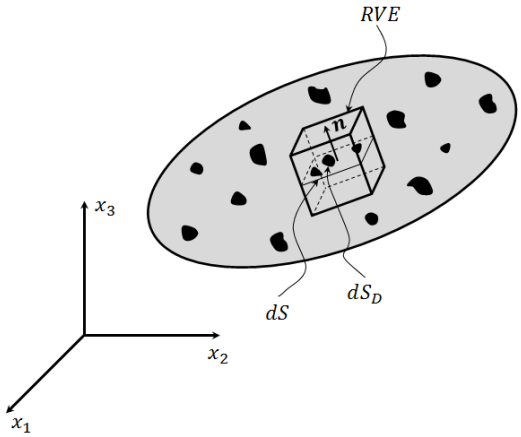

Figure 7: Damage definition

The definition of n_j might be of importance in case of anisotropic damage as damage may progress in preferred directions. However, if damage is not directional, the surface orientation is not significant and the damage process is called isotropic.

$$\omega = \frac{dS_D}{dS} \tag{3-2}$$

Due to damage the original load-carrying area is reduced by the area of discontinuities. The area remaining can be transformed into a smaller continuous area $d\tilde{S}$ which represents the effective load-carrying area.

$$d\tilde{S} = dS - dS_D \tag{3-3}$$

The transformation between damaged area and effective load-carrying area is done through the damage variable. The concept is demonstrated in Figure 8. [66]

$$d\tilde{S} = (1 - \omega)\, dS \tag{3-4}$$

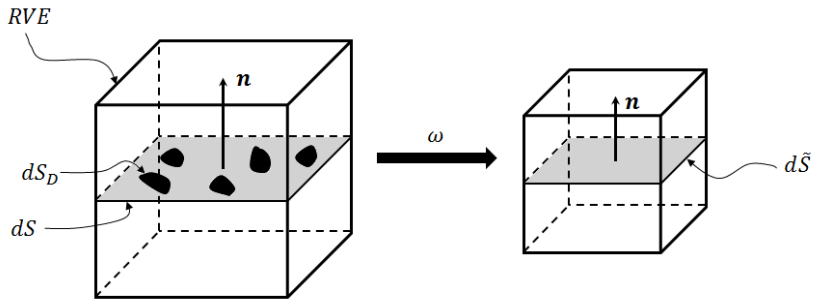

Figure 8: Transformation from damaged surface to effective load-carrying surface

In reality damage propagates in a preferred direction and damage is not isotropic. Therefore the use of a scalar damage variable is not suitable to model directional damage. If the original surface dS with the orientation n_j is transformed into a smaller area $d\tilde{S}$ with a different orientation $\tilde{n}_i$ a higher order damage tensor ω_{ij} will be required to transform the vector $n_j\, dS$ to $\tilde{n}_i d\tilde{S}$. Assuming that the shape of the considered area does not change the transformation can be done using a 2nd order damage tensor ω_{ij} which will be symmetric with three principal values. [65; 66]

$$(\delta_{ij} - \omega_{ij}) n_j\, dS = \tilde{n}_i d\tilde{S} \tag{3-5}$$

Anisotropic damage requires a representation which contains more information than the 2nd order damage tensor although ω_{ij} might be sufficient as an approximation, such as in cases of orthotropy. In case of anisotropy a reference vector ϑ_k for the geometry

should be defined in addition to the orientation vector. The transformation of the 2nd order tensor $\vartheta_i n_j \, dS$ into $\vartheta_i \tilde{n}_j d\tilde{S}$ requires a 4th order damage tensor Ω_{ijkl}. [66]

$$\left(I_{ijkl} - \Omega_{ijkl}\right)\vartheta_k n_l \, dS = \vartheta_i \tilde{n}_j d\tilde{S} \tag{3-6}$$

Chaboche [22] derived an 8th order damage tensor $\Omega_{ijklmnpq}$ by describing the mapping from the virgin stiffness tensor C_{mnpq} to the damaged stiffness tensor $\tilde{C}_{ijkl}$ through a linear transformation.

$$\tilde{C}_{ijkl} = \left(I_{ijklmnpq} - \Omega_{ijklmnpq}\right)C_{mnpq} \tag{3-7}$$

with the 8th order unit tensor

$$I_{ijklmnpq} = \frac{1}{4}\left(\delta_{im}\delta_{jn}\delta_{kp}\delta_{lq} + \delta_{im}\delta_{jn}\delta_{kq}\delta_{lp} + \delta_{in}\delta_{jm}\delta_{kp}\delta_{lq} + \delta_{in}\delta_{jm}\delta_{kq}\delta_{lp}\right) \tag{3-8}$$

Cauvin and Testa [18] state that the expression in (3-7) is the most general expression of damage possible and that it can be applied to anisotropic damage of anisotropic materials.

The description of damage enhances with increasing tensor order; however, the use of an 8th order tensor is impractical because it contains 3^8 components. Chaboche [22] stated that $\Omega_{ijklmnpq}$ can be reduced to 4th order without sacrificing quality of the damage description. Chaboche assumed a fixed principal axes system in which the directions of principal stresses and principal damage are aligned. Therefore, the damage tensor is diagonal and can be reduced to an effective order of four.

$$\Omega_{ijklmnpq} = \Omega^*_{ijkl}\delta_{Im}\delta_{Jn}\delta_{Kp}\delta_{Lq} \tag{3-9}$$

The 4th order damage tensor, which is the most general expression for anisotropic damage in an anisotropic material, is defined in (3-10). Cauvin and Testa share this opinion [18]. According to them the 8th order damage tensor reduces to 4th order when the damage tensor is symmetric in pairs of the eight indices.

$$\tilde{C}_{ijkl} = \left(I_{ijrs} - \Omega^*_{ijrs}\right)C_{rskl} \tag{3-10}$$

3.1.2 Effective Stress Concept and Mechanical Equivalence Hypotheses

The goal of CDM is the inclusion of damage effects in constitutive equations. Methods to achieve this are based on the concept of effective load-carrying area from which the

damage variable is derived. Two concepts can be used to include damage into constitutive equations: the concept of effective stress and the concept of effective strain. The former utilises a constitutive equation of the form as in (2-45). This approach is called strain-based. The latter utilises a constitutive equation of a form as in (2-65). This approach is called stress-based.

The concept of effective stress is a common approach for the definition of constitutive equations of a damaged material. The concept of effective stress is commonly used in conjunction with the hypothesis of strain equivalence or elastic energy equivalence.

In the following the notation $\mathcal{D}$ will be used if damage can be of an arbitrary even order.

3.1.2.1 Effective Stress

The CM approach considers a continuous area to carry loads. The introduction of surface and volume discontinuities into the load-carrying area violates this assumption. However, the effective stress concept is able to introduce the assumption of a homogeneous damage induced distribution of discontinuities to constitutive equations.

The idea of an effective stress $\tilde{\sigma}$ is derived from the idea of an effective load-carrying area $d\tilde{S}$. It is assumed that the Cauchy stress σ has the same consequences for a damaged configuration as the effective stress $\tilde{\sigma}$ on a configuration using an effective load-carrying area $d\tilde{S}$ (see Figure 9). The effective load-carrying area is also called virgin material.

Voyiadjis and Park [121] gave the definition of the effective stress concept as following:

> "The effective stress is defined as the stress acting on a hypothetical undamaged configuration that produces the same elastic strain or elastic strain energy as the actual state of stress acting on the current damaged configuration based on the equivalence hypothesis."

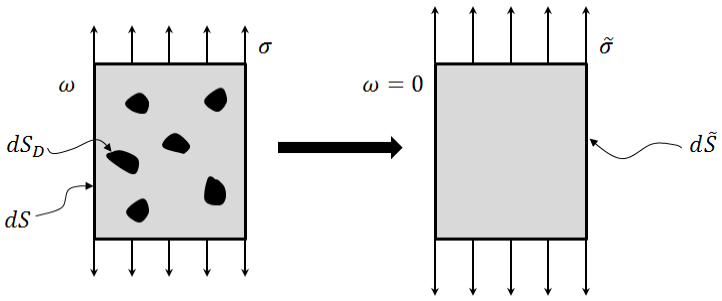

Figure 9: Effective stress concept

The mathematical expression can be easily derived from the force equilibrium of a uniaxial loading case with isotropic damage, $\sigma dS = \tilde{\sigma} d\tilde{S}$, using Equation (3-4).

$$\tilde{\sigma} = \frac{\sigma}{1-\omega} \tag{3-11}$$

The effective stress concept for the multiaxial case with isotropic damage is expressed in analogy with (3-11). The components of the effective stress tensor $\tilde{\sigma}_{ij}$ are the components of the stress tensor magnified by the factor $1/(1-\omega)$. Nonetheless, the direction of the stress tensor is not modified. Therefore, the symmetry of the stress tensor is preserved.

$$\tilde{\sigma}_{ij} = \frac{\sigma_{ij}}{1-\omega} \tag{3-12}$$

However, damage cannot be assumed to be isotropic. (3-5) defines a 2nd order tensor. It is suitable for the representation of orthotropic damage as the directions of principal stress and principal damage coincide [65]. The damage tensor will be diagonal when the principal directions of damage are considered. The diagonal entries are the eigenvalues and are called principal damage [26]. The effective stress tensor will be asymmetric [66].

$$\tilde{\sigma}_{ij} = \sigma_{ik}\left(\delta_{kj} - \omega_{kj}\right)^{-1} \tag{3-13}$$

The general transformation of the stress tensor into the effective configuration is done by a 4th order tensor which depends on a damage tensor $\mathcal{D}$ of any even order. The mapping is called damage effect tensor $M(\mathcal{D})_{ijkl}$.

$$\tilde{\sigma}_{ij} = M(\mathcal{D})_{ijkl}\sigma_{kl} \tag{3-14}$$

3.1.2.2 Equivalence Hypotheses

3.1.2.2.1 Strain Equivalence

The effective stress concept is often coupled with the hypothesis of strain equivalence to achieve a constitutive equation for the damaged material. It was stated by Lemaitre in 1971 (cited by Simo and Ju [106]):

> "The strain associated with a damaged state under the applied stress is equivalent to the strain associated with its undamaged state under the effective stress".

This means that the constitutive equation for a damaged material is derived in the same way as the general CM constitutive equation in (2-45) but the Cauchy stress is substituted by the effective stress.

$$\tilde{\sigma}_{ij} = C_{ijkl}\varepsilon_{kl} \tag{3-15}$$

According to the strain equivalence concept the strain can be expressed using the virgin and damaged stiffness tensor:

$$\varepsilon_{kl} = \tilde{\sigma}_{ij}C^{-1}_{ijkl} = \sigma_{ij}\tilde{C}^{-1}_{ijkl} \tag{3-16}$$

The link between the stiffness tensors of the damaged and virgin material can be made by using the effective stress concept in Equation (3-14):

$$\tilde{C}_{ijkl} = M(\mathcal{D})_{ijrs}C_{rskl} \tag{3-17}$$

3.1.2.2.2 Elastic Energy Equivalence

Another way of formulating constitutive equations for the damaged material is the coupling of the effective stress concept with the hypothesis of elastic energy equivalence. It was stated by Hansen and Schreyer [43] as following:

> "The elastic energy of the damaged material is the same in form as that of an undamaged material except that the stress is replaced by the effective stress."

This means that the elastic energy equation which utilises the effective stress and the virgin stiffness tensor

$$W(\tilde{\sigma}, 0) = \frac{1}{2}\tilde{\sigma}_{ij}C^{-1}_{ijkl}\tilde{\sigma}_{kl} \tag{3-18}$$

will be equivalent to the elastic energy equation which depends on the Cauchy stress and damaged stiffness tensor.

$$W(\sigma, \mathcal{D}) = \frac{1}{2}\sigma_{ij}\tilde{C}^{-1}_{ijkl}\sigma_{kl} \tag{3-19}$$

The link between the stiffness tensors of the damaged and virgin material can be made by using the effective stress concept in Equation (3-14):

$$\tilde{C}(\mathcal{D})_{ijkl} = M(\mathcal{D})^{-1}_{ijpq}C_{pqmn}M(\mathcal{D})^{-T}_{mnkl} \tag{3-20}$$

3.1.3 Symmetrisation

The concept of effective stress was discussed earlier. However, in the case of a general transformation as in (3-14), the effective stress tensor's symmetry cannot be guaranteed. A symmetrisation method for the effective stress transformation needs to be applied to ensure the subsequent analysis to be as simple as possible.

Anisotropy in engineering is mostly orthotropic or can be described with good accuracy as orthotropic. Therefore a damage tensor of 2nd order is sufficient. For this case Cordebois and Sidoroff [26] proposed two symmetrisation techniques which are commonly used in literature, such as in Hansen and Schreyer [43] and Carol et al. [17]: product-type and sum-type symmetrisation. These techniques lead to a 4th order damage effect tensor as proposed in (3-14).

The expression in (3-21) represents the product-type symmetrisation and the expression in (3-22) represents the sum-type symmetrisation of the effective stress tensor.

$$\tilde{\sigma}_{ij} = (\delta_{ik} - \omega_{ik})^{-\frac{1}{2}} \sigma_{kl} (\delta_{jl} - \omega_{jl})^{-\frac{1}{2}} \tag{3-21}$$

$$\tilde{\sigma}_{ij} = \frac{1}{2}\left[\sigma_{ik}(\delta_{kj} - \omega_{kj})^{-1} + (\delta_{jk} - \omega_{jk})^{-1}\sigma_{ki}\right] \tag{3-22}$$

The according damage effect tensors are read from (3-21) and (3-22) directly.

$$M_{ijkl} = (\delta_{ik} - \omega_{ik})^{-\frac{1}{2}} (\delta_{jl} - \omega_{jl})^{-\frac{1}{2}} \tag{3-23}$$

$$M_{ijkl} = \frac{1}{2}\left[(\delta_{kj} - \omega_{kj})^{-1} + (\delta_{jk} - \omega_{jk})^{-1}\right] \tag{3-24}$$

The expression for the damage effect tensor can be derived from either the strain-based, as done in (3-23) and (3-24), or the stress-based representation. In case of the product-type symmetrisation the damage effect tensors are equivalent: $M_{ijkl} = M_{ijkl}^{-1}$. However, equivalence of the damage effect tensor cannot be achieved for the sum-type symmetrisation: $M_{ijkl} \neq M_{ijkl}^{-1}$. Therefore the damage effect tensor in (3-23), derived from product-type symmetrisation, should be preferred. The derivation of strain- and stress-based damage effect tensors for product- and sum-type symmetrisation was demonstrated by Carol et al. [17] and is represented in Appendix A.

3.2 Local Approach to Damage

This work concerns instabilities occurring in CDM models with strain-softening. Therefore, it needs to be established how these instabilities occur and which affect they have on the solutions obtained. This subsection aims to support the understanding of characteristic strain-softening behaviour and the consequences of strain-softening on the definition of the mathematical problem and the physical results. Of special interest will be the case of dynamic strain-softening. First, an overview on longitudinal wave propagation and its physical justification will be given. Then an analytical solution of the dynamic strain-softening problem derived by Bažant and Belytschko [6] will be discussed.

3.2.1 Classification of Partial Differential Equations

PDEs are differential equations which contain two or more independent variables, such as x and y, and a dependent variable $\phi = \phi(x, y)$ and its partial derivatives. Therefore, the rate of change of a variable with respect to a continuous variable can be expressed. The order of a PDE depends on the highest derivative included.

PDEs of 2nd order are most important in this work. Therefore, it will be restricted to these. A general example of a 2nd order PDE with two independent variables is given as: [48]

$$A\frac{\partial^2\phi}{\partial x^2} + B\frac{\partial^2\phi}{\partial x\partial y} + C\frac{\partial^2\phi}{\partial y^2} + D\frac{\partial\phi}{\partial x} + E\frac{\partial\phi}{\partial y} + F\phi + G = 0 \tag{3-25}$$

The PDE is linear if $A, B, \dots G$ depend on x and y. If $G = 0$ the PDE is homogeneous.

Physical problems are governed by a number of different PDEs. The type of a linear PDE depends only on the highest order derivatives. It can be determined by analysing the roots of a quadratic equation defined by the terms of the highest order derivatives. The PDE in (3-25) will be analysed in the following way: [59]

$$Ax^2 + Bx + C = 0 \tag{3-26}$$

The solutions of (3-25) are:

$$x_{1,2} = \frac{-B \pm \sqrt{B^2 - 4AC}}{2A} \tag{3-27}$$

The type of a PDE is determined by the number of real solutions of the discriminant in (3-27). The terminology used in the classification of PDEs is taken from the classification of conic sections. [47]

elliptic	$B^2 - 4AC < 0$: no real solution exists	(3-28)
parabolic	$B^2 - 4AC = 0$: exactly one real solution exists	
hyperbolic	$B^2 - 4AC > 0$: two real solutions exists	

The classification of PDEs is strongly connected with the characteristics of a PDE. Characteristics are paths in space-time along which information propagates. Characteristics can be real or imaginary. [47]

The differential equation of the characteristics is called the characteristic equation. The characteristic equation corresponding to (3-25) is: [47; 48]

$$A\left(\frac{dy}{dx}\right)^2 + B\left(\frac{dy}{dx}\right) + C = 0 \tag{3-29}$$

The solutions of (3-29) are the roots of the quadratic equation (3-27).

$$\left(\frac{dy}{dx}\right)_{1,2} = \frac{-B \pm \sqrt{B^2 - 4AC}}{2A} \tag{3-30}$$

The discriminant in (3-30) leads to a pair of characteristics due to the ± sign. The kind of characteristics depends on the type of PDE.

elliptic	$B^2 - 4AC < 0$: imaginary characteristics	(3-31)
parabolic	$B^2 - 4AC = 0$: real and repeated characteristics	
hyperbolic	$B^2 - 4AC > 0$: real and distinct characteristics	

PDEs can be physically interpreted based on the information about their characteristics. PDEs with complex characteristics, such as elliptic PDEs, do not have time dependence and therefore no preferred paths in space-time exist. Elliptic PDEs govern equilibrium problems. If any real characteristics exist information travels along preferred paths in space-time. This means that an explicit dependence on time exists. The speed with which information travels is the speed of sound and it depends on the slope of the characteristics. Parabolic and hyperbolic PDEs have real characteristics and are called propagation problems. [47]

3.2.2 Loss of Material Stability

The development of localised deformation is caused by a physical process occurring on the material's microscale. The process is defined by the initiation, growth and interaction of cracks and voids which finally lead to complete material fracture. In this investigation a definition of localisation proposed by Rudnicki and Rice [100] is used.

> "Localization is defined as instability in the macroscopic constitutive description of inelastic deformation of the material".

The instability allows the constitutive equations of an originally homogeneous material to reach a bifurcation point and become unstable. As a consequence the deformation localises and becomes non-uniform. Outside this instability zone the material continues to be stable [100].

A material is considered to be stable and stays in equilibrium when the inner product of stress-rate $\dot{\sigma}_{ij}$ and strain-rate $\dot{\varepsilon}_{ij}$ is positive. This criterion is also called general bifurcation criterion [86], which is true as long as the stress-strain relationship of the material has a positive slope.

$$\dot{\varepsilon}_{ij}\dot{\sigma}_{ij} > 0 \tag{3-32}$$

In this section only the rate form of constitutive equations is considered to ensure a piecewise linear relationship between stress-rate and strain-rate. The relationship between stress-rate and strain-rate is established through the material tangent stiffness tensor D_{ijkl}.

$$\dot{\sigma}_{ij} = D_{ijkl}\dot{\varepsilon}_{kl} \tag{3-33}$$

Therefore, the inequality in (3-32) reads:

$$\dot{\varepsilon}_{ij}D_{ijkl}\dot{\varepsilon}_{kl} > 0 \tag{3-34}$$

The material becomes unstable when the material reaches its limiting point. This point occurs when the condition in (3-34) is violated. The condition in (3-35) is called bifurcation criterion.

$$\dot{\varepsilon}_{ij}D_{ijkl}\dot{\varepsilon}_{kl} = 0 \tag{3-35}$$

Condition (3-35) is satisfied when the tangent stiffness tensor becomes singular, i.e. is not positive-definite anymore.

$$det(D_{ijkl}) = 0 \tag{3-36}$$

3.2.3 Strain Localisation in Dynamic Problems

3.2.3.1 Description of Strain-Softening Bar as Test Problem

It is of high importance throughout this work to observe and analyse strain-softening phenomena and to evaluate different methods concerning this behaviour, such as regularisation methods at a later stage of this work. Therefore, a test method is required which allows a clear observation of characteristic properties of the strain-softening phenomenon and allows a comparison of different approaches. Additionally, the test problem should allow these comparisons in an analytical, numerical and physical sense.

An evaluation of literature showed that strain-softening phenomena and solutions to it can be examined with tensile tests [50; 79], biaxial tests [30; 123] or bending tests [12; 91] for example. These tests, however, represent normally a more advanced step of validation to compare solutions obtained for numerical strain-softening models to experimental results. These tests are more dimensional and solutions might be approximated with hand calculation but they lack the simple and clear analytical solution.

The analytical and later numerical investigation of strain-softening will be carried out by investigating longitudinal wave propagation in a bar (see illustration in Figure 10). This problem in context with local strain-softening continua was first introduced by Bažant and Belytschko [6] and became very popular in the field of strain-softening within the continuum damage mechanics framework and the investigation of regularisation methods [9; 11; 90; 92; 93; 96; 102; 109; 110].

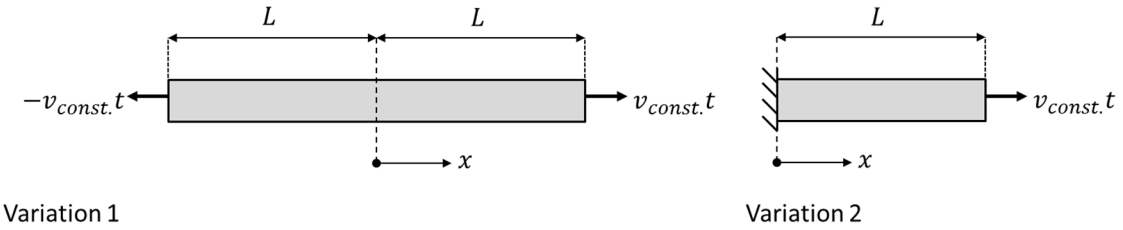

Figure 10: Strain-softening bar in two variations

Firstly, the problem is one-dimensional which simplifies the resulting strain-softening effects. It uses well-established theory of longitudinal waves which has been studied extensively over decades [39; 120] and can be applied as validation to experimental

investigations, such as the Split Hopkinson pressure or tension bar [39; 69]. The strain-softening bar has been studied in two variations. One uses the symmetric application of equal opposite tensile velocities at both ends of the bar which act in opposite direction with same magnitude [6]. The other variation is the application of a constant tensile velocity to a fully fixed bar [109]. The used variation of the strain-softening bar is not of importance as the basic idea is for both types the same. The constant velocities produce an elastic tensile stress wave which propagates away from the point of load application. In the first version the waves superpose in the centre of the bar and in the second version the tensile wave reflects at the fixed boundary. In both cases the magnitude of the tensile wave doubles instantaneously and material behaviour enters immediately the strain-softening regimen. Therefore, the time and location of strain-softening occurrence can be determined precisely using wave theory.

Secondly, the strain-softening bar has a closed-form solution which can be derived easily with longitudinal wave propagation theory. Analytical solutions to other strain-softening problems, such as biaxial tests, are rare as strain-softening is nonlinear and so they are not easily obtained. Therefore, numerical results can be easily checked for convergence and accurate predictions of issues connected to strain-softening. Using this problem it can be shown that the strain-softening problem does not depend continuously on the applied initial conditions and boundary conditions and is unstable [6].

Strain-softening will occur instantaneously upon superposition or reflection of waves. The wave speed will become imaginary as a consequence of the negative tangent stiffness associated with strain-softening. Due to this waves in the point of strain-softening transform to a standing wave and the strain-softening cross-section acts as a free boundary. This solution is the same for any considered slope of the tangent modulus in the strain-softening branch and therefore it can be shown that the strain-softening solution is discontinuous from input data [6].

Lastly, the investigation with a strain-softening bar example ensures that the deformation localisation in numerical examples is captured precisely in a single row of elements. Of course, localisation bands can be observed in two- and three dimensional FE examples too; however, the localisation in a confined band of elements cannot be guaranteed and the occurrence of diffused localisation is possible [87].

The example of a strain-softening bar as defined by Bažant and Belytschko [6] is favourable due to its simplicity and clear demonstration of characteristic properties of strain-softening. Therefore, this example will be used extensively for evaluation of analytical and numerical results in this work.

3.2.3.2 General Aspects of Wave Propagation in Bars

The theory of wave propagation is well-established in literature and it is well worth to study wave propagation as they are of high interest to structural response under impact loads, such as in aerospace industry. A good example of wave propagation is the propagation of longitudinal waves in a bar. This is a structure which is rather easy to understand, especially when it comes to concepts of stress and strain. The wave equation as an equation of motion is well-established and is valid for elastic as well as plastic material behaviour:

$$c^2 \frac{\partial^2 u}{\partial x^2} = \frac{\partial^2 u}{\partial t^2} \text{ with } c = \sqrt{\frac{E}{\rho}} \tag{3-37}$$

with the stiffness E, density ρ, longitudinal coordinate x, longitudinal displacement u and wave velocity c.

If the material behaviour is linearly elastic the material behaviour can be described by Hooke's law. The connection between the axial stress σ and the axial strain ε is established by the Young's modulus E of the material.

$$\sigma = E\varepsilon \tag{3-38}$$

with

$$\varepsilon = \frac{\partial u}{\partial x} \tag{3-39}$$

The wave equation as in (3-37) underlies certain simplifications. The material is assumed to be homogeneous and the cross-section remains parallel and plane. More importantly the stress is uniaxial which does not imply that the strain is uniaxial too. However, effects of lateral contraction are neglected in (3-37). Equation (3-37) is similar to the wave equation as it is known for strings. The difference between bars and strings lies in the physical aspect. The particle motion in a string is perpendicular to the direction of wave propagation. Therefore, waves are said to be transversal. Perpendicular motion is not possible in a bar and particles move along the direction of wave propagation. The waves are said to be longitudinal. [39]

Due to the mathematical equivalence of the wave equation for strings and bars the D'Alembert solution for the wave equation in strings can be transferred to longitudinal wave propagation.

$$u(x,t) = f(x - c_e t) + g(x + c_e t) \tag{3-40}$$

or

$$u(x,t) = f\left(t - \frac{x}{c_e}\right) + g\left(t + \frac{x}{c_e}\right) \tag{3-41}$$

The longitudinal displacement in a bar depends on the location x and time t and longitudinal waves propagate with the elastic wave speed c_e. As time t increases the displacement u will increase too. Therefore, f represents a distortion propagating in positive x-direction and g represents a distortion propagating in negative x-direction.

The functions f and g are arbitrary functions which will be determined with initial and boundary conditions and define the shape of the distortion. Von Karman and Duwez [120] developed a solution for elastic longitudinal wave propagation in a semi-infinite bar. They considered an elastic bar which extends from the location $x = 0$ to $x = -\infty$ loaded with velocity v at $x = 0$, as shown in Figure 11.

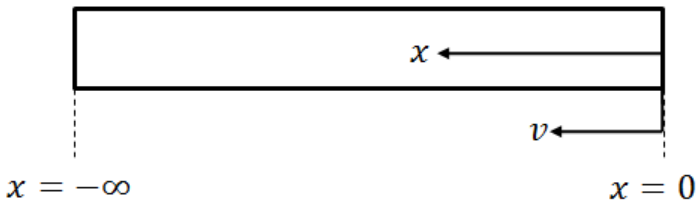

Figure 11: Semi-infinite bar subjected to velocity v

The boundary conditions for this problem for $t \geq 0$ can be easily derived as:

$$u(x = 0, t) = vt \tag{3-42}$$

$$u(x = -\infty, t) = 0$$

Due to the loading with velocity v a wave is generated which travels in the negative x-direction. Therefore, the general solution to the wave equation is restricted to:

$$u(x,t) = g\left(t + \frac{x}{c_e}\right) \tag{3-43}$$

The solution for the displacement at $x = 0$ is:

$$u(x = 0, t) = \int_0^t v(s)ds \tag{3-44}$$

An extension of (3-44) for $x \neq 0$ can be found when t is replaced by $t + (x/c_e)$. This solution will be valid for any location x and any time t.

$$u(x, t) = \int_0^{t+\frac{x}{c_e}} v(s)ds = v\left(t + \frac{x}{c_e}\right) \tag{3-45}$$

The velocity of particle motion can be easily determined with the relation

$$v(x, t) = \frac{\partial u}{\partial t} \tag{3-46}$$

Assuming that the velocity is constant in Von Karman's and Duwez's consideration, the stress profile along the bar, using Equation (3-38), will be a step wave which is rectangular in shape.

Waves produced in a semi-infinite bar will never reach a boundary; however, this is not feasible in mechanical applications as waves would interact with some kind of boundary. The two simplest boundary conditions include a fixed and a free end. It is assumed that an induced displacement pulse interacting with a fixed boundary will lead to a reflection of the incident stress pulse with doubled value. Interaction with a free boundary would lead to reflection of the stress pulse with opposite value of the original magnitude, e.g. compression is reflected as tension and tension as compression. This is called stress reversal. [39]

So far the wave considerations in a bar have been kept one-dimensional and strictly analytical. Nevertheless, the analytical considerations of longitudinal waves in bars are of physical relevance in three-dimensional space. The easiest way to introduce longitudinal stress waves in a bar is done by impacting it with another solid. The most popular experiment is the use of the Split Hopkinson pressure bar. The first apparatus for impact scenarios was used by Hopkinson [49] who exposed a bar to explosive loads or impact with bullets. Kolsky [58] adopted the idea of wave propagation in a bar and developed an apparatus where the test specimen is placed between two long steel bars, the incident and transmitter bar. This set up is nowadays termed Split Hopkinson pressure bar. In this method longitudinal waves are used to obtain dynamic material parameters, such as dynamic strength. A picture of a general set up for the Split Hopkinson pressure bar is shown in Figure 12.

During the test with the Split Hopkinson pressure bar a rectangular stress pulse is created in the incident bar through an impact with the striker bar. This loads the test specimen dynamically. During the test some of the incident waves will be reflected from the test specimen and others will be transmitted into the transmitter bar. It is assumed that the incident, reflected and transmitted strain waves ($\varepsilon_{incident}$, $\varepsilon_{reflected}$ and $\varepsilon_{transmitter}$) are recorded by the strain gauges. Displacements at the interfaces of the test specimen are called u_1 and u_2. The waves are recorded with strain gauges to both sides of the test specimen to determine dynamic material behaviour.

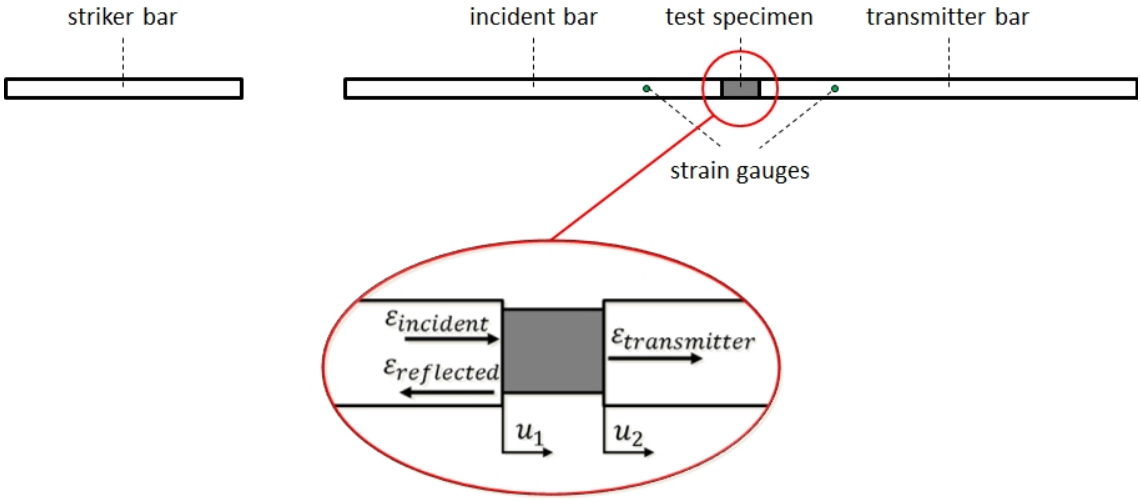

Figure 12: Set up of Split Hopkinson pressure bar

Figure 13 shows typical results for pulses recorded by the strain gauges obtained by a Split Hopkinson pressure bar experiment by Lindholm [69]. In this experiment the striker bar is made from the same material and same cross-section as the incident bar and transmitter bar. The striker bar is accelerated with a sling-shot mechanism. Using this mechanism a pressure pulse of constant amplitude (see Figure 13) and finite duration can be achieved in the incident bar. The amplitude of the pressure pulse is directly proportional to the impact velocity. When the initial compressive pulse in the incident bar reaches the specimen, a part of it is transmitted through the specimen into the transmitter bar. Another portion of the initial pressure loading is reflected from the interface between incident bar and specimen.

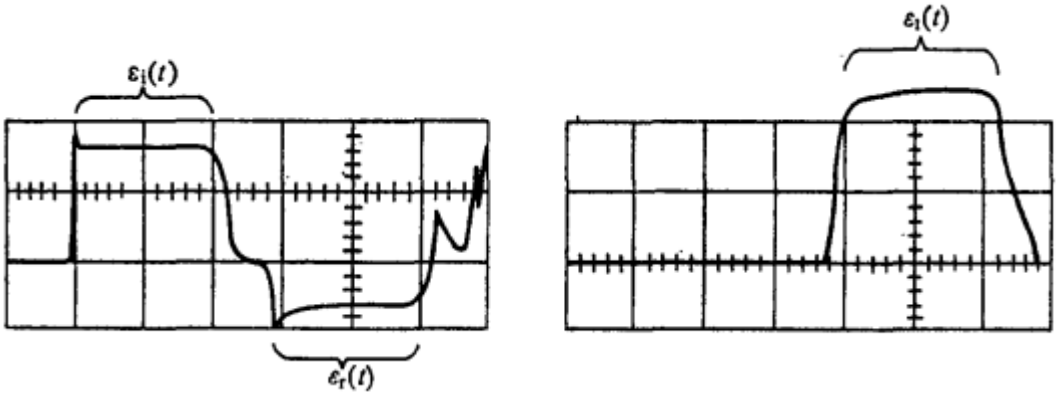

Figure 13: Typical examples of incident, reflected and transmitted strain signals recorded by strain gauges (strain over time) in a Split Hopkinson pressure bar (presented by [39], adopted from [69])

Lindholm [69] used the strain gauge recordings for the three pulses to determine the force and displacement boundary conditions at both ends of the test specimen using one-dimensional wave propagation theory.

Variations of the Split Hopkinson pressure bar are used for tensile tests. Gálvez and co-workers [34], for example, conducted a spalling test of ceramics where the transmitter bar is removed to cause tensile waves in the test specimen. Tensile waves are achieved through reflection of the initial compressive pulse on the free end of the specimen (see Figure 14). In their test compressive waves are caused in the used steel incident bar through impact, which are then transmitted into the test specimen. The compressive pulse is then reflected at the end of the test specimen and returns as tensile pulse. The tensile waves produced cause failure of the test specimen.

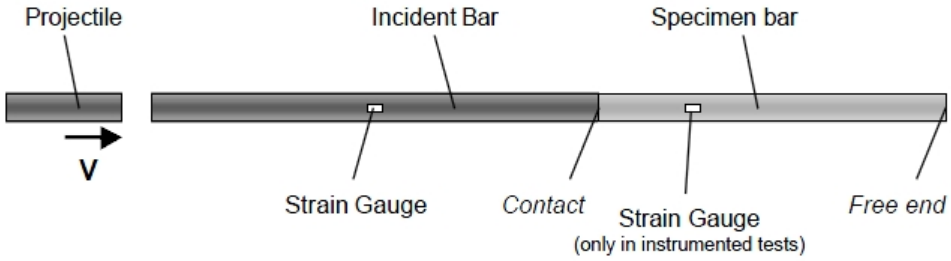

Figure 14: Spalling test of long bars [34]

3.2.3.3 Analytical Results of Wave Propagation in a Strain-Softening Bar

This section concerns the longitudinal wave propagation problem by Bažant and Belytschko [6] which will be used as example throughout this work to observe characteristic properties of the strain-softening solution. The test problem is based on one-dimensional wave propagation theory as it was introduced previously and uses therefore the well-known framework of wave propagation.

Figure 15 shows the stress-strain curve of a general softening material considered by Bažant and Belytschko [6]. The linear elastic area is shown between the points O and P. The stiffness is given by the Young's modulus E. The maximum strength f_t' is reached for the strain ε_p. The curve in the strain-softening area (area between points P and F) is given by the function $F(\varepsilon)$. The slope of this curve, $F'(\varepsilon)$, is negative for strains greater than ε_p. $F(\varepsilon)$ reaches a zero stress value for a finite strain ε or an asymptotic strain $\varepsilon \to \infty$. Unloading ($\dot{\varepsilon} < 0$) and reloading($\dot{\varepsilon} \geq 0$) is considered to be elastic and occurs parallel to the Young's modulus E of the linear elastic area.

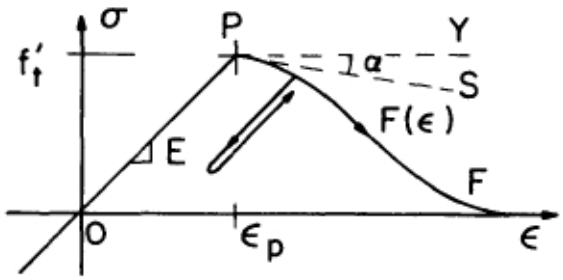

Figure 15: Material behaviour with strain-softening [6]

The strain-softening bar has a length of $2L$ and a density ρ per unit length. The bar is loaded at both ends with a constant velocity v which acts in opposite directions. Therefore, tensile waves are generated at the two ends which travel towards the centre of the bar. The longitudinal coordinate x is measured from the bar's centre. The geometry and loading conditions are illustrated in Figure 16.

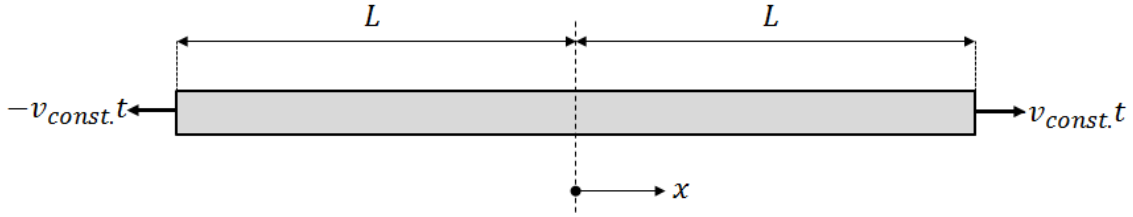

Figure 16: Geometry and loading of strain-softening bar

Two step waves are generated in the bar which travel from the edges towards the bar's centre. The two step waves of constant strain travel to the centre of the bar and meet at $x = 0$ for the time $t = L/c_e$. When the two waves meet the strain doubles instantaneously at the centre of the bar and the midsection immediately enters the strain-softening domain.

The equation of motion is the wave equation which is hyperbolic for real wave speeds. Before the onset of softening the problem is governed by the standard wave equation.

$$c_e^2 \frac{\partial^2 u}{\partial x^2} = \frac{\partial^2 u}{\partial t^2} \tag{3-47}$$

with the elastic wave speed.

$$c_e = \sqrt{\frac{E}{\rho}} \tag{3-48}$$

The longitudinal displacement function in the linear elastic domain is derived from appropriate initial and boundary conditions.

$$u(x,t) = -v\,\langle t - \frac{x+L}{c_e}\rangle + v\,\langle t + \frac{x-L}{c_e}\rangle \tag{3-49}$$

where the expressions in the brackets $\langle\cdot\rangle$ need to be positive-definite.

The related strain function is:

$$\varepsilon = \frac{\partial u}{\partial x} = \frac{v}{c_e}\left[H\left(t - \frac{x+L}{c_e}\right) + H\left(t + \frac{x-L}{c_e}\right)\right] \tag{3-50}$$

where $H(\cdot)$ is the Heaviside step function. The stress, caused by deformation, is:

$$\sigma = E\varepsilon \tag{3-51}$$

When the strain ε doubles at the bar's centre ($x = 0$) for $t = L/c_e$, two scenarios are possible. The first scenario would be that the bar remains in the linear elastic area for $L/c_e < t \leq 2L/c_e$. The second scenario would be that the bar's midsection ($x = 0$) instantaneously enters the strain-softening regime at $t = L/c_e$.

1. case: Strain $\varepsilon = v/c$ fulfils the condition $\varepsilon \leq \varepsilon_p/2$:

   In this case the assumption of linear elasticity holds even after the waves meet at the bar's midsection. At $x = 0$ for $t = L/c_e$ the strain doubles immediately but the bar remains in the linear elastic regime $(2\varepsilon \leq \varepsilon_p)$. This is valid until both waves have travelled the whole length of the bar. The solution for the transverse displacement $u(x,t)$ in Equation (3-49) holds for $t \leq 2L/c_e$.

2. case: Strain $\varepsilon = v/c$ fulfils the condition $\varepsilon_p/2 < \varepsilon \leq \varepsilon_p$:

   In this case the assumption of linear elasticity only holds for $t < L/c_e$ because at $x = 0$ the strain becomes $2\varepsilon > \varepsilon_p$ once the waves reach this point. The midsection immediately enters the strain-softening regime for $t = L/c_e$. Therefore the solution for the transverse displacement $u(x,t)$ in Equation (3-49) holds only for $t < L/c_e$.

Bažant and Belytschko [6] made three crucial assumptions for the strain-softening solution:

1. The strain-softening domain is limited to a point.
2. Strain and strain-rate in the strain-softening domain are infinite.
3. Because the strain-rate is infinite stress is considered to vanish at points of strain-softening.

The inelastic area is governed by the strain-softening domain, therefore the stress-strain curve has a negative slope: $F'(\varepsilon) < 0$. The wave speed will become imaginary due to this. Therefore, the equation of motion in the softening domain is an elliptic differential equation.

$$c^2 \frac{\partial^2 u}{\partial x^2} + \frac{\partial^2 u}{\partial t^2} = 0 \quad with \quad c^2 = \frac{F'(\varepsilon)}{\rho} \tag{3-52}$$

The mathematical problem will be ill-posed due to the change of the hyperbolic wave equation to an elliptic type, this is also called Hadamard instability [41; 99]. The solution of the strain-softening PDE will be a standing wave which cannot propagate outside the strain-softening point. Stress drops instantaneously to zero. Any parts of the bar outside $x = 0$ are still governed by the hyperbolic PDE. The elastic and strain-softening domain cannot interact with each other due to their different types of PDEs and the standing wave's inability to propagate. Therefore the strain-softening domain acts like a free boundary and tensile waves return as unloading waves instead of superposition as in the elastic case. After the occurrence of strain-softening the bar will not be able to consume further energy.

Softening is limited to an area of measure zero around $x = 0$ and a discontinuity with a displacement jump develops at $x = 0$. The difference in magnitude is $4v\langle t - L/c_e\rangle$. Strain starts to increase infinitely and stress drops to zero in the softening zone. The rest of the bar starts to unload in an elastic manner.

Strain in the softening domain can be expressed by the Dirac delta function:

$$\varepsilon = 4v\langle t - L/c_e\rangle \delta(x) \tag{3-53}$$

The solutions for the strain field outside the softening zone, $t > L/c_e$ and $x < 0$, is:

$$\varepsilon = \frac{v}{c_e}\left[H\left(t - \frac{x + L}{c_e}\right) - H\left(t - \frac{L - x}{c_e}\right) + 4\langle c_e t - L\rangle \delta(x)\right] \tag{3-54}$$

The solution in 4-7 is symmetric for $x > 0$.

The displacement function reads for $t > L/c_e$ and $x < 0$:

$$u = -v\langle t - \frac{x + L}{c_e}\rangle - v\langle t - \frac{L - x}{c_e}\rangle \tag{3-55}$$

The solutions in (3-54) and (3-55) are symmetric for $x > 0$.

The analytical solution by Bažant and Belytschko [6] was used to derive a comparison between an elastic ($\varepsilon \leq \varepsilon_p/2$) and a strain-softening ($\varepsilon_p/2 < \varepsilon \leq \varepsilon_p$) wave propagation problem. The solutions for longitudinal displacement, strain and stress are compared for the time $t = 3/4 \cdot 2L/c_e$ in Figure 17. The internal energy is plotted for the whole bar for $0 \leq t \leq 2 \cdot L/c_e$ in Figure 17.

The elastic solution represents a continuous wave propagation in a linear elastic manner after superposition of waves with no mesh-sensitivity. The results for the strain-softening solution clearly show the difficulties related to strain-softening which are the convergence to physically unreasonable results with vanishing energy dissipation. A displacement discontinuity develops after the superposition in the localisation zone at $x = 0$. This zone localises in an area with zero width. The discontinuity cannot propagate outside this zone as the type of PDEs changed to elliptic. Therefore an interaction with areas $x \neq 0$ which are governed by hyperbolic PDEs is not possible anymore. Strain reaches infinity, designated by the Dirac delta function $\delta(x)$, and cannot propagate outside the localisation zone, also called a standing wave. Simultaneously, stress drops to zero in the localisation zone. Outside the localisation zone the bar unloads in a linear elastic manner as the unloading waves travel to the bar's ends. The waves reflect from the localisation zone similar to a free boundary. After the onset of strain-softening the bar is not capable of consuming further energy (see Figure 17).

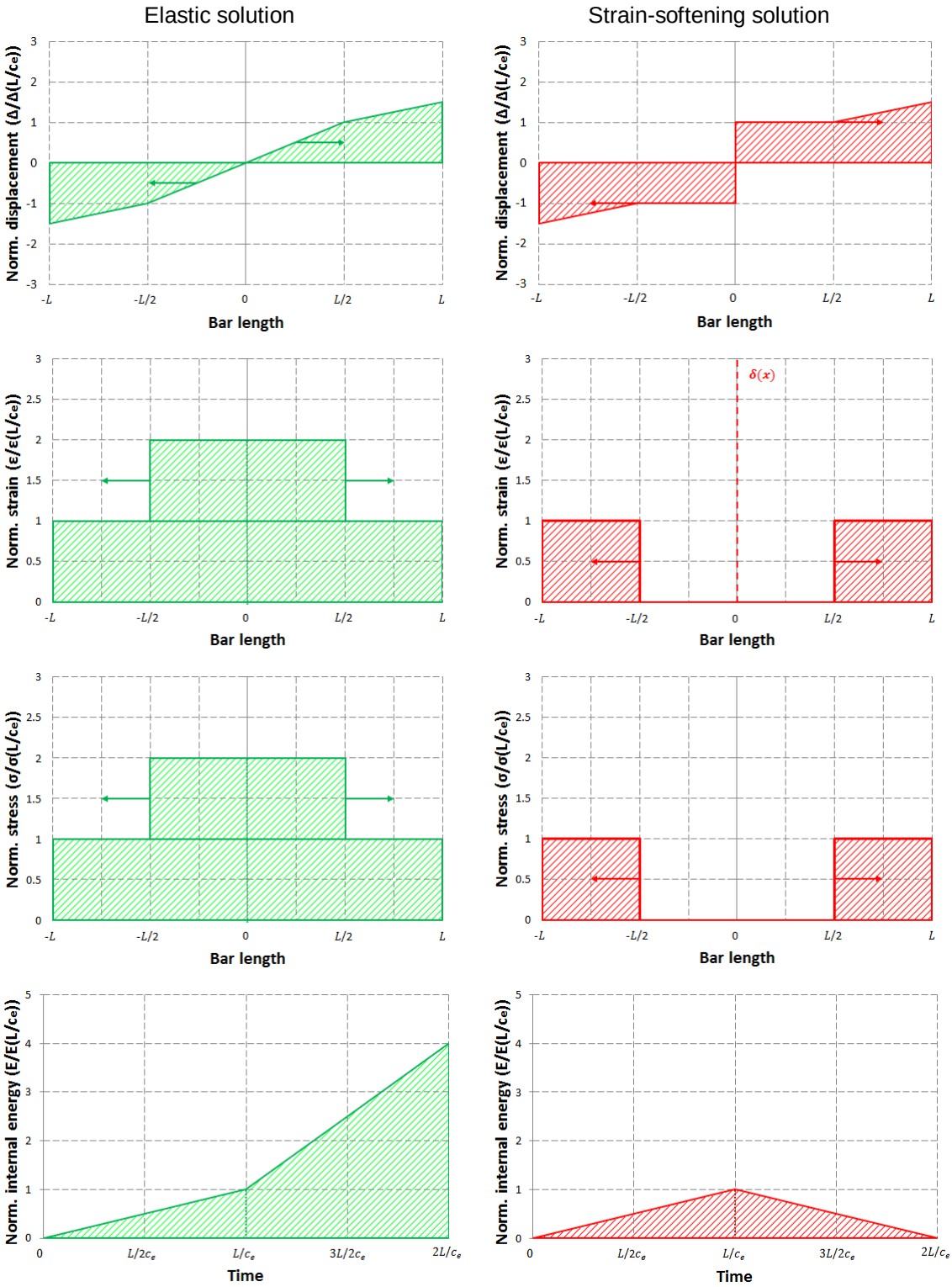

Figure 17: Analytical solution for normalised longitudinal displacement, strain and stress at $t = 3/4 \cdot 2L/c_e$, and internal energy over $0 \leq t \leq 2 \cdot L/c_e$

3.3 Summary

This chapter gave an overview on the essentials of the CDM approach. It provides a systematic framework for the analysis of damage on a material's macroscale. However, it was shown that this approach is limited if materials with strain-softening behaviour are considered.

It was shown that the consideration of damage induced strain-softening in constitutive equations violates the material stability criterion by Hadamard. The condition for the violation is that the tangent stiffness tensor becomes singular which means it is not positive-definite anymore. This is characterised as negative slope in the strain-softening stress-strain diagram. Due to this the hyperbolicity in dynamic governing equation cannot be maintained and the overall boundary value problem is ill-posed.

The characteristic features of a CDM strain-softening solution were demonstrated by considering a longitudinal wave propagation problem, namely the strain-softening bar. This problem was first described by Bažant and Belytschko [6] and has been popular in literature concerning strain-softening problems. This problem allows for an analytical solution to strain-softening through its simplicity and offers therefore an insight into strain-softening mathematics. The analytical solution obtained for the strain-softening problems carries all characteristic properties, such as consequences on the displacement, strain and stress distribution and the consequences on internal energy. It was shown that strain-softening behaviour is limited to an area with zero width. The strain in this area becomes infinite and stress vanishes. The strain-softening domain acts as a free boundary from which waves with a well-posed hyperbolic PDE reflect as unloading waves.

4 Review: Composite Material Modelling, Instabilities due to Dynamic Strain-Softening in Continuum Damage Mechanics Models and Strain-Softening Stabilisation

Firstly, this chapter aims to support the understanding of the underlying theory behind the LS-DYNA composite material models for failure and damage. Of interest are the models: MAT_022, MAT_054, MAT_055, MAT_058 and MAT_059. Firstly, common failure and damage theories will be explained. Then an evaluation of failure and damage models in LS-DYNA will be conducted using a quasi-static single element test. At the end of this all background theories are clarified and limits and merits of the available composite models are discussed.

Secondly, the consequences of strain-softening in CDM will be investigated numerically. This will be done with the longitudinal wave propagation problem, the strain-softening bar, by Bažant and Belytschko [6] which was presented in Chapter 3. In Chapter 3 an analytical solution for the strain-softening bar was presented which will allow for a comparison with FE results. The study is conducted with the composite CDM model by Matzenmiller et al. [81] which is implemented in LS-DYNA as MAT_058. It will be shown that numerical results obtained with strain-softening material models do not have a unique solution and lead to spurious mesh-sensitivity of results depending on the used spatial discretisation.

The chapter will close with an investigation of strain-softening stabilisation methods readily available in commercial FE codes, such as LS-DYNA and ABAQUS. The FE code LS-DYNA offers a keyword *MAT_NONLOCAL which can be used in conjunction with a limited number of damage models. The ABAQUS code has a “damage stabilisation” method implemented which can be used with CDM models. The properties of these methods will be investigated with the longitudinal wave propagation problem by Bažant and Belytschko [6] too as it enables the observation in change of numerical results from local to stabilised solution.

4.1 Failure and Damage Composite Models

4.1.1 Theory

Most composite theories use strength-based failure criteria. These criteria apply mostly the simplifications of a plane state of stress and homogenisation of material properties on the macroscopic level. However, a realistic modelling of composite’s mechanical

behaviour includes degeneration of material properties due to damage. This is achieved by applying the CDM method as previously explained in Chapter 3.

Figure 18 represents typical stress-strain curves for composite failure and damage theory. The curve for failure theory shows the linear elastic region up to the point at which the strength of the material is defined. Stress is set to zero instantaneously when failure occurs. The curve for damage shows a linear elastic portion too; however, before reaching the strength of the material the stress-strain relationship becomes nonlinear due to a reduction of stiffness which results from damage. After reaching the strength the slope of the stress-strain curve turns negative.

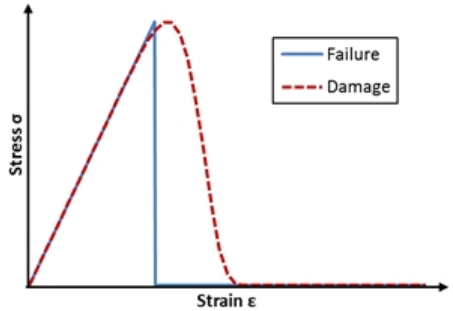

Figure 18: Representative stress-strain relationships for failure and damage theory

4.1.1.1 Failure

Failure criteria aim to distinguish a safe state of stress from the onset of failure. A number of different types and approaches were proposed for fibre reinforced composites. Nonetheless, not a single criterion is generally accepted by research or industry. This issue was addressed by "The World-Wide Failure Exercise" [46; 57]. In the following the most common composite failure criteria will be presented.

4.1.1.1.1 Background Theory

4.1.1.1.1.1 Types of Failure Criteria

Two main groups of criteria exist to predict the failure of fibre reinforced composites.

- Failure criteria without failure modes
- Failure criteria with failure modes

The first group does not distinguish between different modes of failure. The second group takes into account the heterogeneous character of composites. Therefore, failure modes are considered which depend on the characteristics of the single components of the composite.

The group without failure modes uses mathematical representations which are based on tensorial polynomials. The mathematical expressions are adjusted by curve fitting processes to experimental test data. With a single polynomial a failure surface is defined which is a function of the material's strengths defined in the principal axes system of the lamina. These principal directions are the fibre direction and the direction transverse to the fibres. Strength in stress-space is represented by the interception of the defined failure surface with the principal axes of stress. The most popular failure criterion using a single tensorial polynomial is the Tsai-Wu failure criterion [113].

The use of failure modes takes into account the heterogeneous assembly of a lamina. Two main modes are distinguished: failure of fibres and failure of the matrix. These criteria are derived from mathematical, strength-based expressions. The group of failure criteria which consider failure modes can be divided in two further categories: non-interactive and interactive failure criteria.

- Non-interactive criteria do not take into account an interaction between stress components. Individual stress components are compared with the corresponding material strength values. A common example for non-interactive failure criteria are the Maximum Stress criteria [55].
- Interactive criteria take into account the interaction between stress components. The most common criteria for fibre reinforced composites are based on the use of a polynomial. These polynomials describe a failure surface in stress-space based on the material's strength. In general, quadratic polynomials are chosen which allow curve fitting with sufficient accuracy. Commonly used criteria of this kind are the Hashin [44] and Chang-Chang [23; 24] criteria.

4.1.1.1.1.2 General Simplifications

The commonly used failure criteria stated above have certain simplifications in common:

- Plane state of stress
- Homogenisation of material properties on the macroscopic level (lamina level)
- Assumption of transverse isotropy as special case of anisotropy (for unidirectional lamina).

A plane state of stress appears in the case that one principal stress in three-dimensional space is zero. This case occurs when a free surface of a body is unloaded. This normally takes place when a structural component has one dimension

much smaller than the other two. It can be assumed that the principal stress in the direction of the smaller dimension can be neglected. The remaining two principal stresses lie in one plane and therefore the 3D problem is reduced to a plane problem. Loads are distributed uniformly over the thickness of the component and work in the considered plane. This is in particular true for components made from fibre reinforced composites which can be assumed as thin plate.

Considering the x_1x_2-plane as parallel to the plane state of stress and x_3 as direction with zero principal stress, the stress tensor for a point has the following appearance:

$$[\sigma_{ij}] = \begin{bmatrix} \sigma_{11} & \sigma_{12} & 0 \\ \sigma_{12} & \sigma_{22} & 0 \\ 0 & 0 & 0 \end{bmatrix} \tag{4-1}$$

Although the state of stress is plane, the stresses will lead to deformation in the x_3-direction due to lateral contraction. Therefore the strain tensor reads:

$$[\varepsilon_{ij}] = \begin{bmatrix} \varepsilon_{11} & \varepsilon_{12} & 0 \\ \varepsilon_{12} & \varepsilon_{22} & 0 \\ 0 & 0 & \varepsilon_{33} \end{bmatrix} \tag{4-2}$$

Composite materials are made from a combination of at least two different materials with different mechanical properties. Therefore a composite built-up is heterogeneous on the microscale. Failure criteria are used on the macroscopic lamina level. For that reason the concept of macroscopic homogeneity is applied. This means that the elastic properties of fibres and matrix are averaged over the lamina's volume.

The lamina is assumed to be a unidirectional ply. That means that all fibres of the composite are aligned in one direction. Relationships exist for this kind of ply which determine the overall elastic properties from the individual elastic properties of the fibres and matrix.

The averaging process for elastic properties is based on mathematical equations which are referred as 'Rules of Mixtures' [35]. They aim to represent the elastic properties of a lamina by taking into consideration the properties, quantity and arrangement of the constituents.

The basic assumption is the use of unidirectional lamina (see Figure 19). Material properties are directional due to the heterogeneous character of the microstructure. The mechanical properties of unidirectional laminates are highest in the longitudinal direction. The properties are at their minimum in transverse direction. Fibres are

assumed to be uniform, parallel and continuous. The connection between fibres and matrix is assumed to be ideal. If the unidirectional ply is loaded in longitudinal direction the strain in fibres and matrix is equivalent. Contraction effects are neglected.

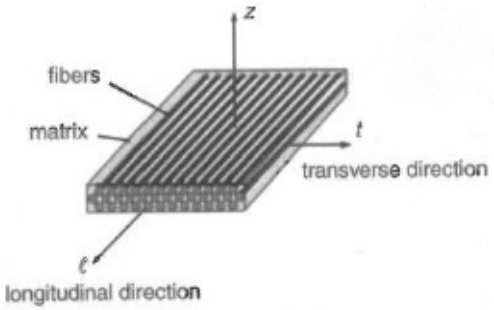

Figure 19: Built-up of unidirectional ply [35]

Due to the heterogeneous microstructure, composites are anisotropic materials. This means that the material properties depend on the considered direction; however, unidirectional composites are assumed to be transversely isotropic which is a special case of anisotropy and simplifies the material description of composites (see Equation (2-60)).

The simplification of transverse isotropy is based on the consideration of an orthotropic material (see (2-59)) which is also a special case of anisotropy. Orthotropic materials have directional elastic properties without coupling of strain and shear deformation. Orthotropy is applied if a material has three mutually perpendicular planes of rotational symmetry. A unidirectional composite possesses three mutually perpendicular planes of symmetry.

Orthotropy is always used in conjunction with a particular coordinate system. In case of unidirectional composites this is the principal axis system. Orthotropic materials are only orthotropic in their symmetry axes. Outside of this particular system orthotropic materials possess anisotropic behaviour.

For transversely isotropic materials one axis exists around which a rotation of the material does not lead to a change of the elastic properties. The plane perpendicular to this axis is called isotropic plane. All planes with other orientations possess directional properties.

In unidirectional composites the plane of transverse isotropy is relative to the axis aligned with the fibres. Figure 20 shows this concept. The unidirectional ply has rotational symmetry relative to the x_1-axis. The rotation of plane x_2x_3 around x_1 does not lead to a change of elastic properties. Therefore the x_2x_3-plane is isotropic.

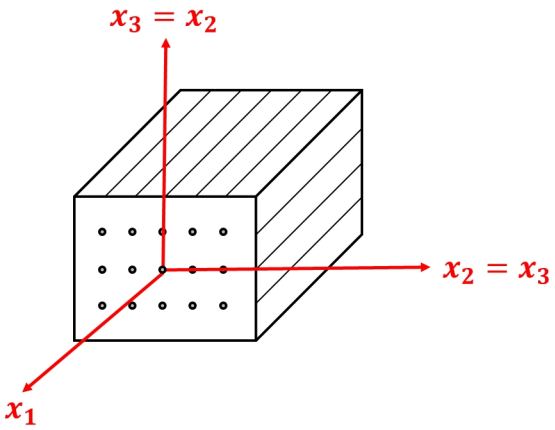

Figure 20: Transverse isotropy

The appearance of the transversely isotropic stiffness tensor has been presented in (2-60). Due to the existing isotropic plane the directional mechanical properties will reduce as follows:

$$E_2 = E_3 \tag{4-3}$$

$$G_{12} = G_{13}$$

$$\nu_{21} = \nu_{31}$$

$$\nu_{23} = \nu_{32}$$

$$G_{23} = \frac{E_2}{2(1-\nu_{23})}$$

Finally, the full elastic behaviour of a material can be expressed by five independent mechanical properties in transverse isotropy:

- Longitudinal Young's Modulus: E_1
- Transverse Young's Modulus: E_2
- In-plane Shear Modulus: G_{12}
- Poisson's ratios: ν_{21} and ν_{23}

4.1.1.1.2 Commonly used Failure Criteria

As stated earlier, failure criteria are mathematical expressions based on the concept of strength. The prediction of failure is commonly based on the plane state of stress. In this 2D assumption the following five strength values are used:

- Longitudinal tensile strength: X_t
- Longitudinal compressive strength: X_c
- Transverse tensile strength: Y_t

- Transverse compressive strength: Y_c
- In-plane shear strength (x_1x_2-plane): S

The introduction of failure criteria will be limited to the most popular criteria for fibre reinforced composites.

- Maximum stress criteria
- Tsai-Wu criterion
- Hashin criteria
- Chang-Chang criteria

A number of other criteria exist as shown by “The World-Wide Failure Exercise” [46; 57]; however, they do not compete with the popularity of the above mentioned.

4.1.1.1.2.1 Maximum Stress Criteria

The maximum stress criteria are the simplest failure mode criteria. An interaction of stress components is not taken into account. Acting stresses are simply compared with the material’s directional strength values. Failure occurs when one of the five inequalities in (4-4) to (4-8) is met. The kind of failure can be determined if the first four equations are met. Fibre failure occurs when the longitudinal principal stress σ_{11} exceeds the fibres’ strength in tension or compression. Matrix failure can be predicted when the transverse principal stress σ_{22} goes above the matrix’s strength in tension or compression. If the shear inequality occurs first, a clear prediction of the failure mode is not possible. Fibre as well as matrix failure are possible.

Longitudinal tension and compression failure:

$$\sigma_{11} \leq X_t \tag{4-4}$$

$$|\sigma_{11}| \leq X_c \tag{4-5}$$

Transverse tension and compression failure:

$$\sigma_{22} \leq Y_t \tag{4-6}$$

$$|\sigma_{22}| \leq Y_c \tag{4-7}$$

Shear failure:

$$|\sigma_{12}| \leq S \tag{4-8}$$

The maximum stress criteria can be represented by a failure surface in stress-space as shown in Figure 21. Failure stresses are assumed to be finite which leads to a closed failure surface. The failure surface is defined by constant lines parallel to the stress axis. The interception of the failure surface with the principal stress axes is understood as failure strength.

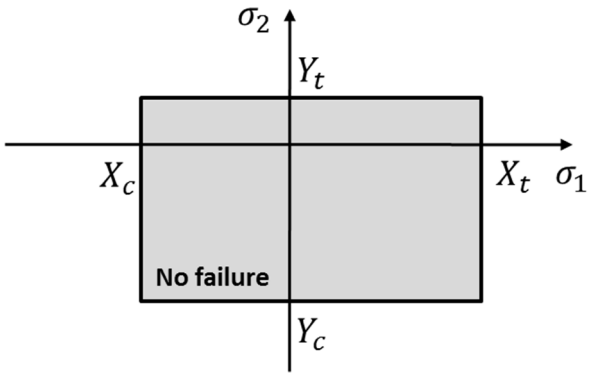

Figure 21: Failure surface of Maximum Stress criterion

4.1.1.1.2.2 Tsai-Wu Criterion

The Tsai-Wu failure criterion [113] is based on a single valued quadratic polynomial with tensorial character which was inspired by Gol'denblat's and Kopnov's [37] work: $F_i\sigma_i + F_{ij}\sigma_i\sigma_j = 1,\ \ i,j = 1,\ldots$. It is assumed that the quadratic terms will span an ellipsoidal failure surface in stress-space which is limited by the material's strengths (see Figure 22).

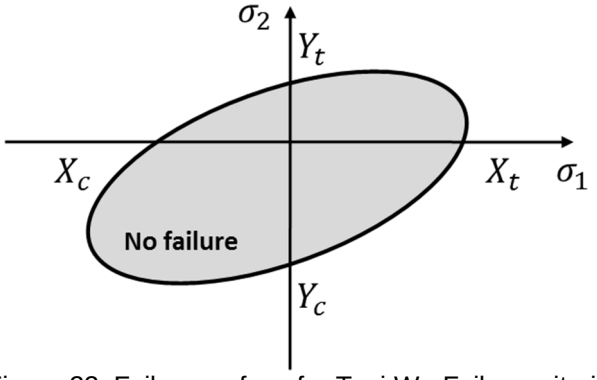

Figure 22: Failure surface for Tsai-Wu Failure criterion

The Tsai-Wu criterion is a general mathematically based failure criterion. It is characterised by its invariance and the use of symmetry properties similar to the stiffness tensor. Despite its simplicity, the Tsai-Wu failure criterion does not take into account the heterogeneous character of composites. Therefore a distinction of failure modes is not possible.

The full Tsai-Wu criterion for the orthotropic case reads:

$$F_1\sigma_{11} + F_2\sigma_{22} + F_{11}\sigma_{11}^2 + F_{22}\sigma_{22}^2 + F_{66}\sigma_{12}^2 + 2F_{12}\sigma_{11}\sigma_{22} = 1 \tag{4-9}$$

The terms F_i and F_{ij} can be expressed as following:

Longitudinal tension and compression term:

$$F_1 = \frac{1}{X_t} - \frac{1}{X_c} \tag{4-10}$$

$$F_{11} = \frac{1}{X_t X_c} \tag{4-11}$$

Transversal tension and compression term:

$$F_2 = \frac{1}{Y_t} - \frac{1}{Y_c} \tag{4-12}$$

$$F_{22} = \frac{1}{Y_t Y_c} \tag{4-13}$$

Shear term:

$$F_{66} = \frac{1}{S^2} \tag{4-14}$$

Assumption for F_{12} term:

$$F_{12} = -\frac{1}{2}\sqrt{F_{11}F_{22}} \tag{4-15}$$

4.1.1.1.2.3 Hashin Criteria

The Hashin criteria [44] are based on a quadratic polynomial to describe a closed failure surface in stress-space. Hashin takes the heterogeneous character of composites in consideration. Therefore different modes of failure are distinguished. The failure criteria are limited to unidirectional composites which allow the simplification of a transversely isotropic material. Hashin's criteria are applicable to 2D and 3D states. In the 3D state two shear strength terms need to be considered:

- Axial shear strength: S_A
- Transverse shear strength: S_T

The used polynomial depends on stress invariants I_1 to I_5 which is enforced by the existence of transverse isotropy. The polynomial chosen by Hashin is (4-16). As the polynomial has to be quadratic, invariant I_5 is neglected.

$$A_1 I_1 + B_1 I_1^2 + A_2 I_2 + B_2 I_2^2 + C_{12} I_1 I_2 + A_3 I_3 + A_4 I_4 = 1 \tag{4-16}$$

For the approach Hashin identifies two main failure modes in unidirectional composites. These are the fibre mode along the fibres and the matrix mode normal to the fibre direction. He assigns two planes to which the failure modes are restricted to occur. For fibre failure it is the x_2x_3-plane. For matrix failure the failure plane is oriented along the fibre direction.

The stress invariants in (4-16) are associated with the components of the stress tensor σ_{ij}. The constants A_i and B_i are related to the strengths of the material. Due to this Hashin derived the following failure criteria for the 3D case:

Longitudinal tension failure 3D:

$$\left(\frac{\sigma_{11}}{X_t}\right)^2 + \frac{1}{S_A^2}(\sigma_{12}^2 + \sigma_{13}^2) = 1 \tag{4-17}$$

Longitudinal compression failure 3D:

$$\sigma_{11} = -X_c \tag{4-18}$$

Transverse tension failure 3D:

$$\frac{1}{Y_t^2}(\sigma_{22} + \sigma_{33})^2 + \frac{1}{S_T^2}(\sigma_{23}^2 - \sigma_{22}\sigma_{33}) + \frac{1}{S_A^2}(\sigma_{12}^2 + \sigma_{13}^2) = 1 \tag{4-19}$$

Transverse compression failure 3D:

$$\frac{1}{Y_c}\left[\left(\frac{Y_c}{2S_T}\right)^2 - 1\right](\sigma_{22} + \sigma_{33}) + \frac{1}{4S_T^2}(\sigma_{22} + \sigma_{33})^2 + \frac{1}{S_T^2}(\sigma_{23}^2 - \sigma_{22}\sigma_{33}) + \frac{1}{S_A^2}(\sigma_{12}^2 + \sigma_{13}^2) = 1 \tag{4-20}$$

In case of plane stress conditions, just the principal stresses σ_{11} and σ_{22} and the axial shear stress σ_{12} have an influence. The failure criteria reduce to:

Longitudinal tension failure 2D:

$$\left(\frac{\sigma_{11}}{X_t}\right)^2 + \left(\frac{\sigma_{12}}{S_A}\right)^2 = 1 \tag{4-21}$$

Longitudinal compression failure 2D:

$$\sigma_{11} = -X_c \tag{4-22}$$

Transverse tension failure 2D:

$$\left(\frac{\sigma_{22}}{Y_t}\right)^2 + \left(\frac{\sigma_{12}}{S_A}\right)^2 = 1 \tag{4-23}$$

Transverse compression failure 2D:

$$\left(\frac{\sigma_{22}}{2S_T}\right)^2 + \left[\left(\frac{Y_c}{2S_T}\right)^2 - 1\right]\frac{\sigma_{22}}{Y_c} + \left(\frac{\sigma_{12}}{S_A}\right)^2 = 1 \tag{4-24}$$

4.1.1.1.2.4 Chang-Chang Criteria

The 2D failure criteria proposed by Chang and Chang [23; 24] are based on work by Hashin [44]. They account for fibre and matrix failure modes and take into consideration the interaction of stress components. The Chang-Chang criteria are limited to in-plane failure.

The Chang-Chang criteria account for nonlinearities in the relationship between shear stresses and shear strains. This is done by the introduction of the experimental

nonlinear shear stress parameter α. All criteria influenced by a shear stress term are influenced by these nonlinearities.

The implementation of the nonlinear shear stress parameter α to the failure criteria is done by the introduction of Hahn's and Tsai's shear stress-shear strain relationship [42], expressed with engineering constants.

$$\varepsilon_{12} = \left(\frac{1}{G_{12}}\right)\sigma_{12} + \alpha\sigma_{12}^3 \tag{4-25}$$

This relationship is included to the criteria by the fibre-matrix-shearing term $\bar{\tau}$:

$$\bar{\tau} = \frac{\int_0^{\varepsilon_{12}} \sigma_{12} d\varepsilon_{12}}{\int_0^{\varepsilon_{12}^u} \sigma_{12} d\varepsilon_{12}} = \frac{\frac{\sigma_{12}^2}{2G_{12}} + \frac{3}{4}\alpha\sigma_{12}^4}{\frac{S^2}{2G_{12}} + \frac{3}{4}\alpha S^4} \tag{4-26}$$

The Chang-Chang criteria for in-plane failure are:

CC1: Tensile fibre mode:

$$\sqrt{\left(\frac{\sigma_{11}}{X_t}\right)^2 + \bar{\tau}} = 1 \tag{4-27}$$

CC2: Compressive fibre mode:

$$\sqrt{\frac{\sigma_{11}}{X_c}} = 1 \tag{4-28}$$

CC3: Tensile matrix mode:

$$\sqrt{\left(\frac{\sigma_{22}}{Y_t}\right)^2 + \bar{\tau}} = 1 \tag{4-29}$$

CC4: Compressive matrix mode:

$$\sqrt{\left(\frac{\sigma_{22}}{2S}\right)^2 + \left[\left(\frac{Y_c}{2S}\right)^2 - 1\right]\frac{\sigma_{22}}{Y_c} + \bar{\tau}} = 1 \tag{4-30}$$

4.1.1.2 Damage

A CDM composite model was developed by Matzenmiller et al. [81] for anisotropic damage of composites. The damage initiates after the material exceeds the initial elastic area. The expression of damage is exponential:

$$d_i = 1 - exp\left[-\frac{1}{m_i e}\left(\frac{\varepsilon_i}{\varepsilon_{f1}}\right)^{m_i}\right] \tag{4-31}$$

with the Euler's Number e. i is an index which designates the direction of the quantity. m is the so-called strain-softening parameter which controls the development of the stress-strain relationship.

The strain at which failure initiates is expressed as following:

T1: Longitudinal threshold failure value

$$\varepsilon_{f1} = \frac{X_{t,c}}{E_1} \tag{4-32}$$

T2: Transverse threshold failure value

$$\varepsilon_{f2} = \frac{Y_{t,c}}{E_2} \tag{4-33}$$

T3: Shear threshold failure value

$$\varepsilon_{f12} = \frac{S}{G_{12}} \tag{4-34}$$

4.1.2 Composite Modelling in LS-DYNA

The LS-DYNA material models are based on well-known 2D failure and CDM models. However, a lack in confidence in the applicability of these models exists, especially for 3D applications.

Work published by the LS-DYNA User's Manual [70], the LS-DYNA support site [72], the manual on the public DYNA3D code [68] and Schweizerhof and co-workers publication [104] offer some insight into the operational mode of LS-DYNA. However, no certainty can be gained from these sources alone.

Table 4-1 summarises the considered LS-DYNA composite models with the according type of theory and element type.

Table 4-1: Summary of LS-DYNA composite material models

Material		Model behaviour		Element type	
№	Name	Failure	Damage	Shells	Solids
22	Composite Damage	✓	-	✓	✓
54	Composite Damage with Chang-Chang	✓	-	✓	-
55	Composite Damage with Tsai-Wu	✓	-	✓	-
58	Laminated Composite Fabric	-	✓	✓	-
59	Composite Failure	✓	-	✓	✓

The next subsection presents the gathered information of the composite material models in LS-DYNA. Then the identified failure and damage theories will be presented.

4.1.2.1 Summary of LS-DYNA Composite Models

4.1.2.1.1 Composite Damage (MAT_022)

The name “damage” for MAT_022 is misleading as it is a composite failure model based on the theory by Chang and Chang [23; 24]. This theory is defined for 2D cases and explains therefore the working mode for 2D elements. However, MAT_022 is implemented for 3D elements too.

This model has two main weaknesses. Firstly, Chang-Chang’s compressive failure mode is not implemented and, secondly, information about the working mode in 3D elements is not clear. However, the DYNA3D code has a material model (see MAT_022 in DYNA3D [68]) implemented which operates in a similar manner to MAT_022 in LS-DYNA. The manual states that a delamination criterion is implemented for 3D elements.

DL1: Delamination criterion MAT_022 in LS-DYNA:

$$\sqrt{\left(\frac{\sigma_{33}}{Z_t}\right)^2 + \left(\frac{\sigma_{13}}{S_{13}}\right)^2 + \left(\frac{\sigma_{23}}{S_{23}}\right)^2} = 1 \tag{4-35}$$

4.1.2.1.2 Composite Damage with Chang-Chang or with Tsai-Wu (MAT_054/055)

The theory of these closely related material models is well stated in the LS-DYNA manual. Both material models use 2D elements only and are based on the Chang-Chang theory or partly Chang-Chang theory with addition of the Tsai-Wu failure criterion for matrix failure.

The representation of the Tsai-Wu criterion in LS-DYNA is limited to tensile and compressive matrix failure:

TW1: LS-DYNA implementation of Tsai-Wu criterion

$$\sqrt{\frac{\sigma_{22}^2}{Y_t Y_c} + \left(\frac{\sigma_{12}}{S_{12}}\right)^2 + \frac{(Y_c - Y_t)\sigma_{22}}{Y_c Y_t}} = 1 \tag{4-36}$$

4.1.2.1.3 Laminated Composite Fabric (MAT_058)

This model is the only implemented composite CDM model in LS-DYNA. Unfortunately, information in the LS-DYNA User’s Manual is limited. However, Schweizerhof et al. [104] published a conference paper which presents a modification of this material model. According to Schweizerhof et al. MAT_058 is a material model based on the anisotropic damage model for fibre composites proposed by Matzenmiller et al. [81]. This model contains a softening parameter which controls the shape of the stress-

strain curve. This parameter cannot be set in the input card of MAT_058. Therefore, it must be assumed that this parameter has a constant value. The evaluation of the damage model in Section 4.1.2.2 will include an investigation of this parameter as well.

4.1.2.1.4 Composite Failure (MAT_059)

MAT_059 is a composite failure model implemented for 2D and 3D elements. Unfortunately, no reference is provided for this material model. However, the similarities with its input data and that of MAT_022 are striking. It can be assumed with confidence that the Chang-Chang theory is implemented for 2D elements as MAT_059 considers a nonlinear shear stress parameter 'ALP' which is a speciality of the Chang-Chang theory. MAT_059 differs from MAT_022 as it considers longitudinal compressive strength. This leads to the assumption that the full set of Chang-Chang failure criteria is implemented. The 3D failure theory for solids is not known but the LS-DYNA support site for composites [73] provides a link to a report by Cheng and Hallquist [25] which represents a 3D failure theory with striking similarities to the Chang-Chang failure theory. In Section 4.1.2.2 it will be evaluated if this theory by Cheng and Hallquist is implemented for 3D elements in MAT_059.

The theory by Cheng and Hallquist [25] is an extension of Chang-Chang's theory and includes eight criteria:

CH1: Longitudinal tensile failure with $\sigma_{11} > 0$:

$$\sqrt{\left(\frac{\sigma_{11}}{X_t}\right)^2 + \left(\frac{\sigma_{12}}{S_{12}}\right)^2 + \left(\frac{\sigma_{13}}{S_{13}}\right)^2} = 1 \tag{4-37}$$

CH2: Transverse tensile failure with $\sigma_{22} > 0$:

$$\sqrt{\left(\frac{\sigma_{22}}{Y_t}\right)^2 + \left(\frac{\sigma_{12}}{S_{12}}\right)^2 + \left(\frac{\sigma_{23}}{S_{23}}\right)^2} = 1 \tag{4-38}$$

CH3: Longitudinal shear failure:

$$\sqrt{\left(\frac{\sigma_{11}}{X_t}\right)^2 + \left(\frac{\sigma_{13}}{S_{13}}\right)^2} = 1 \tag{4-39}$$

CH4: Transverse shear failure:

$$\sqrt{\left(\frac{\sigma_{22}}{Y_t}\right)^2 + \left(\frac{\sigma_{23}}{S_{23}}\right)^2} = 1 \tag{4-40}$$

CH5: Delamination failure:

$$\sqrt{\left(\frac{\sigma_{33}}{Z_t}\right)^2 + \left(\frac{\sigma_{13}}{S_{13}}\right)^2 + \left(\frac{\sigma_{23}}{S_{23}}\right)^2} = 1 \tag{4-41}$$

CH6: Longitudinal compressive failure with $\sigma_{11} < 0$:

$$\sqrt{\left(\frac{\sigma_{11}}{X_c}\right)^2} = 1 \tag{4-42}$$

CH7: Transverse compressive failure with $\sigma_{22} < 0$:

$$\sqrt{\left(\frac{\sigma_{22}}{S_{12} + S_{23}}\right)^2 + \left[\left(\frac{Y_c}{S_{12} + S_{23}}\right)^2 - 1\right]\frac{\sigma_{22}}{Y_c} + \left(\frac{\sigma_{12}}{S_{12}}\right)^2 + \left(\frac{\sigma_{23}}{S_{23}}\right)^2} = 1 \tag{4-43}$$

CH8: Normal compressive failure with $\sigma_{33} < 0$:

$$\sqrt{\left(\frac{\sigma_{33}}{S_{13} + S_{23}}\right)^2 + \left[\left(\frac{Z_c}{S_{13} + S_{23}}\right)^2 - 1\right]\frac{\sigma_{33}}{Z_c} + \left(\frac{\sigma_{13}}{S_{13}}\right)^2 + \left(\frac{\sigma_{23}}{S_{23}}\right)^2} = 1 \tag{4-44}$$

4.1.2.2 LS-DYNA Composite Model Evaluation

4.1.2.2.1 Method and Setup

To enable a comparison between LS-DYNA composite material models and verify analytical results, a simple single element test is chosen. 2D (shells) and 3D (solids) elements are used; however, the chosen element type depends on the element definition of the considered material model (see Table 4-1).

The single elements have a consistent edge length of $1mm$. The elements are quasi-statically loaded with a strain-rate of $\dot{\varepsilon} = 10^{-1}\frac{1}{s}$ which results in a loading velocity of $v = 10^{-1}\frac{mm}{s}$ in the considered case. The investigated load cases are:

- tension
- compression
- shear

for three different orientations:

- 0°
- 45°
- 90°

The loading conditions of 2D elements are shown in Figure 23.

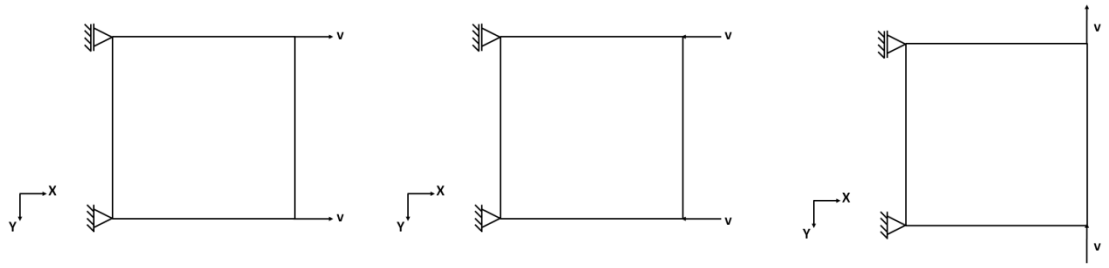

Figure 23: Loading conditions of a single 2D element: tension, compression and shear

The loading conditions of 3D elements are shown in Figure 24. The boundary conditions in the corners of one end are designated with capital letters of the restricted local direction: X,Y and Z.

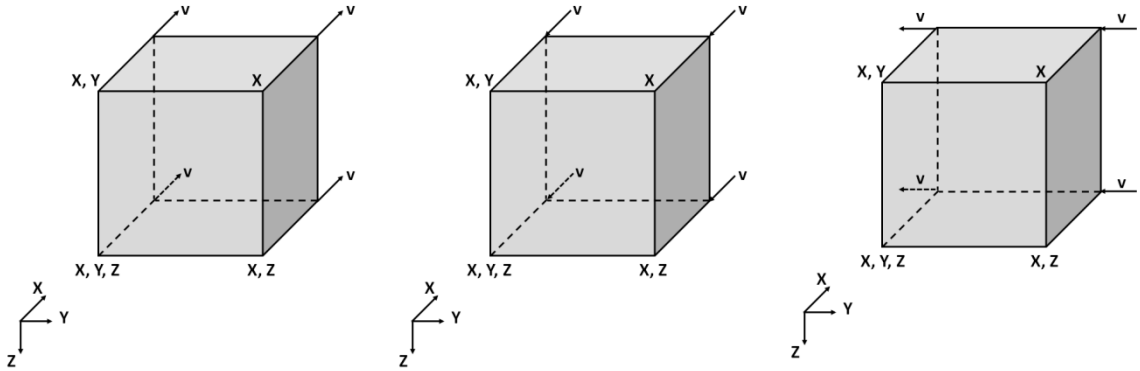

Figure 24: Loading conditions of a single 3D element: tension, compression and shear

For 2D elements five material models, three orientations and three loading cases will be investigated. This results in a total of 45 individual test cases. Overall just three simulations will be conducted. Each input file contains 15 elements, each of which tests one combination of material type and the material orientation (see Figure 25). The simulations only differ by the considered load case. This approach is more favourable than running one simulation for each test case because:

- the number of input/output files is reduced,
- changes in the LS-DYNA input files can be done easily for 18 elements at a time, and
- results of different material models and orientations can be compared easily and directly from the output files.

For 3D elements 2 material models, nine orientations (0°, 45° and 90° in the ab-, ac- and bc plane) and three loading cases (tension, compression and shear) will be investigated. This leads into 54 individual test cases. Overall just nine simulations will be conducted. Three simulations will consider all material models with three material orientations in the ab-plane, ac-plane and bc-plane. The simulations just differ in the considered load case (see Figure 26).

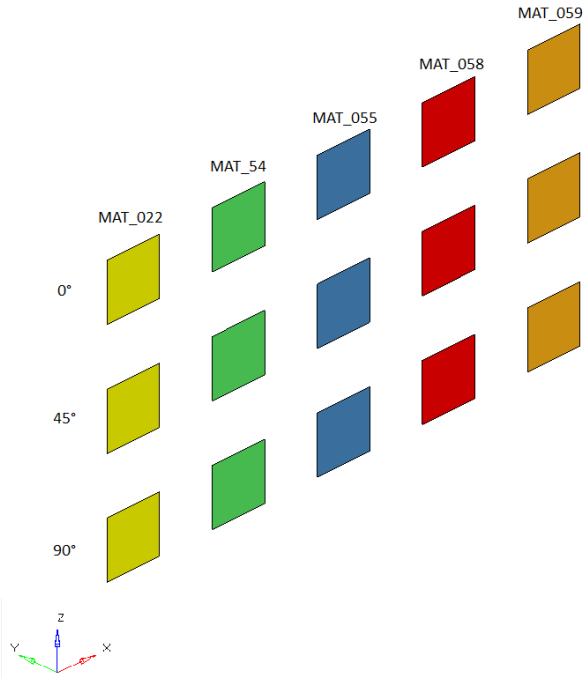

Figure 25: Example of single element tests with 2D elements

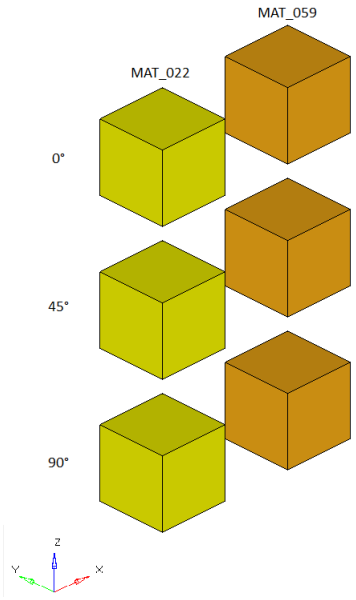

Figure 26: Example of single element tests with 3D elements

A set of input data for composites, available within the "Crashworthiness, Impact & Structural Mechanics Group" in Cranfield University, was used for the composite model evaluation and is presented in Table 4-2.

Table 4-2: Input data for composite models in LS-DYNA

Value	Sign	Magnitude	Unit
Density	ρ	$1.55 \cdot 10^{-9}$	t/mm^3
Young's modulus, a-direction	E_a	70800	MPa
Young's modulus, b-direction	E_b	42700	MPa
Young's modulus, c-direction	E_c	8000	MPa
Poisson's ratio, ba-plane	v_{ba}	0.125	–
Poisson's ratio, ca-plane	v_{ca}	0.037	–
Poisson's ratio, bc-plane	v_{bc}	0.062	–
Shear modulus, ab-plane	G_{ab}	10600	MPa
Shear modulus, ac-plane	G_{ac}	4400	MPa
Shear modulus, bc-plane	G_{bc}	2600	MPa
Longitudinal tensile strength	X_T	1119	MPa
Transverse tensile strength	Y_T	617	MPa
Normal tensile strength	Z_T	60	MPa
Longitudinal compressive strength	X_C	768	MPa
Transverse compressive strength	Y_C	463	MPa
Normal compressive strength	Z_C	30	MPa
Shear strength, ab-plane	S_{ab}	146	MPa
Transverse shear strength, ac-plane	S_{ac}	93	MPa

Value	Sign	Magnitude	Unit
Transverse shear strength, bc-plane	S_{bc}	53	MPa
Critical longitudinal tensile strain	$\varepsilon_{XT} = X_T / E_a$	+0.0158	–
Critical transverse tensile strain	$\varepsilon_{YT} = Y_T / E_b$	+0.0145	–
Critical normal tensile strain	$\varepsilon_{ZT} = Z_T / E_b$	+0.0075	–
Critical longitudinal compressive strain	$\varepsilon_{XC} = X_C / E_a$	−0.0109	–
Critical transverse compressive strain	$\varepsilon_{YC} = Y_C / E_b$	−0.0108	–
Critical normal compressive strain	$\varepsilon_{ZC} = Z_C / E_b$	−0.00375	–
Critical shear strain, ab-plane	$\varepsilon_{ab} = S_{ab} / G_{ab}$	±0.0138	–
Critical shear strain, ac-plane	$\varepsilon_{ac} = S_{ac} / G_{ac}$	±0.0211	–
Critical shear strain, bc-plane	$\varepsilon_{bc} = S_{bc} / G_{bc}$	±0.0204	–

4.1.2.2.2 Results

The results of 2D and 3D single element tests will be compared with analytical solutions for the failure and damage criteria presented in Section 4.1.1.1.2 and 4.1.2.1. These comparisons are straightforward in case of load application aligned with longitudinal, transverse and normal directions. In case of the 45°-orientations lamination theory needs to be applied to transform the state of stress into the principal axes system first to evaluate them with failure and damage criteria.

The proposed failure and damage criteria from Section 4.1.1.1.2 and 4.1.2.1 were evaluated through a comparison of LS-DYNA maximum stress results with analytical maximum strength results. As well it will be stated which criterion, if possible, determined failure.

4.1.2.2.2.1 Composite Damage (MAT_022)

MAT_022 follows the 2D failure theory of Chang-Chang in the case of 2D elements. Figure 27, Figure 29 and Figure 31 represent the results for shell elements in tension, compression and shear. It can be seen that numerical results for the maximum reached stress follow this theory well. An exception is the case of compression in longitudinal direction. MAT_022 lacks the implementation of this failure criterion completely; therefore, no failure can be detected.

Figure 28, Figure 30 and Figure 32 represent the results for 3D elements in tension, compression and shear for the ab-plane.

These tests are meant to evaluate the 3D delamination criterion mentioned in the DYNA3D manual [68]. As it can be seen the analytical results are in excellent agreement with the LS-DYNA results. Hence, it can be stated with confidence that

MAT_022 has the Chang-Chang criteria implemented plus a delamination criterion implemented for 3D elements.

Some issues should be addressed at this point. It can be seen in Figure 30 that no compressive failure occurred in longitudinal and transverse direction for 3D. The missing compressive failure was expected for longitudinal and normal direction due to missing data in the material model card. However, transverse compressive strength is a part of the MAT_022 input data.

Additionally, it should be pointed out that in-plane LS-DYNA and in-plane analytical results for shear of the 45°-orientation differ significantly for 2D and 3D elements (see Figure 31 and Figure 32). However, results are correct although different. It should be kept in mind that tensile stresses are caused in addition to shear. In cases of shear in 45°-orientation for 2D and 3D the tensile fibre criterion determines failure.

Results for tension, compression and shear in 3D for the ac- and bc-plane are presented in Appendix B for completeness. As well the accuracy of failure strength, failure strain and stiffness are compared for all 2D and 3D tests with MAT_022 in Appendix B.

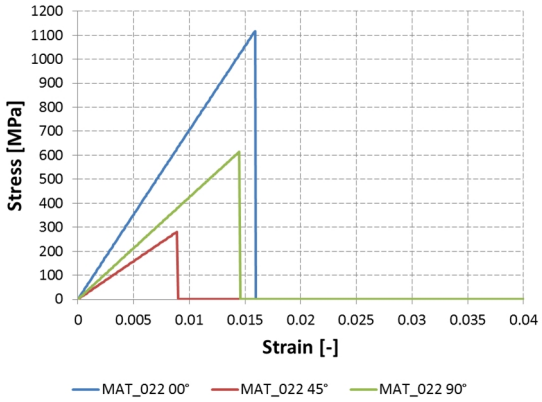

Figure 27: Single element test MAT_022: tension in 2D elements (00°, 45° and 90°)

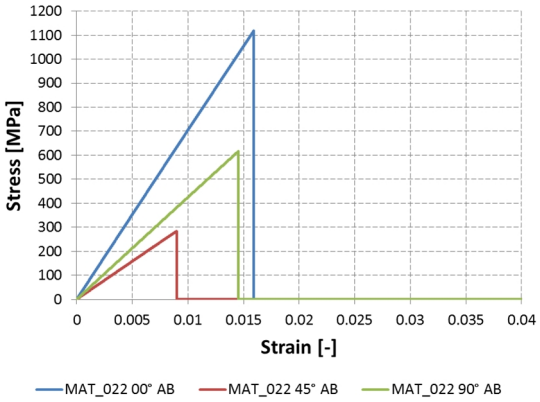

Figure 28: Single element test MAT_022: tension in ab-plane of 3D elements (00°, 45° and 90°)

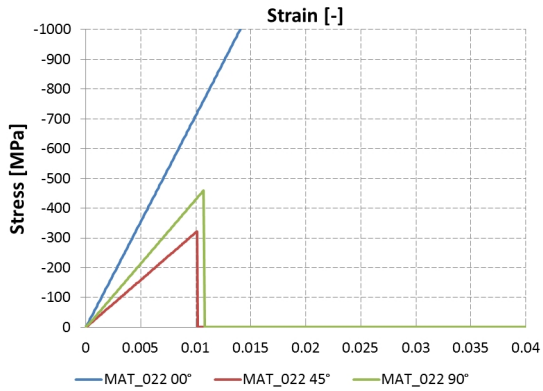

Figure 29: Single element test MAT_022: compression in 2D elements (00°, 45° and 90°)

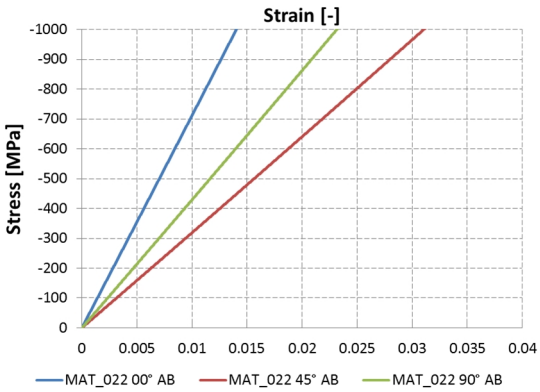

Figure 30: Single element test MAT_022: compression in ab-plane of 3D elements (00°, 45° and 90°)

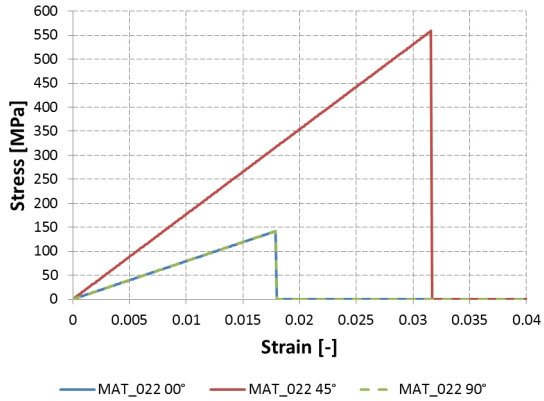

Figure 31: Single element test MAT_022: shear in 2D elements (00°, 45° and 90°)

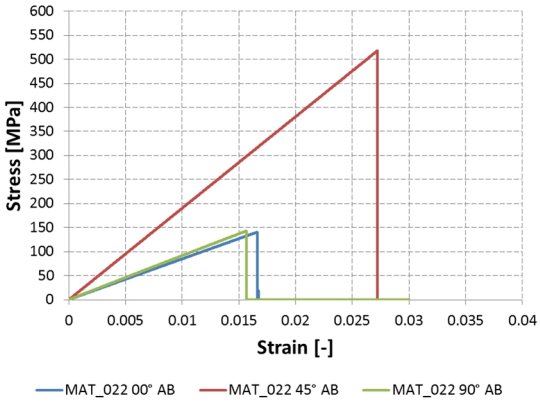

Figure 32: Single element test MAT_022: shear in ab-plane of 3D elements (00°, 45° and 90°)

4.1.2.2.2.2 Composite Damage with Chang-Chang/with Tsai-Wu (MAT_054/055)

Figure 33, Figure 35 and Figure 37 show results for material model MAT_054 in tension, compression and shear. MAT_054 only allows 2D elements and is based on the Chang-Chang failure theory. Therefore, results similar to MAT_022 for 2D (see Figure 27, Figure 29 and Figure 31) are expected. In fact, the results show excellent agreement with the Chang-Chang theory. In difference to MAT_022, compressive longitudinal failure can be determined with MAT_054 due to full implementation of the failure criteria in difference to 2D in MAT_022.

MAT_055 is closely related to MAT_054; however, it combines the Chang-Chang failure criteria with the single valued Tsai-Wu criterion for matrix failure. In consequence numerical and analytical results have many similarities with the results of MAT_054. Nonetheless, the combination of these two theories might add some difficulty in understanding how failure was determined by LS-DYNA. Figure 34, Figure

36 and Figure 38 show results for MAT_055. As it can be seen most of the results are similar to the findings of MAT_054 (see Figure 33, Figure 35 and Figure 37).

The results for 2D elements show that stress is not set to zero after reaching the material's strength except when the longitudinal tension criterion is affected. This can be controlled with the options DFAILx in MAT_054 and MAT_055 which represents failure strains.

The accuracy of failure strength, failure strain and stiffness are also compared for MAT_054 and MAT_055 tests in Appendix B.

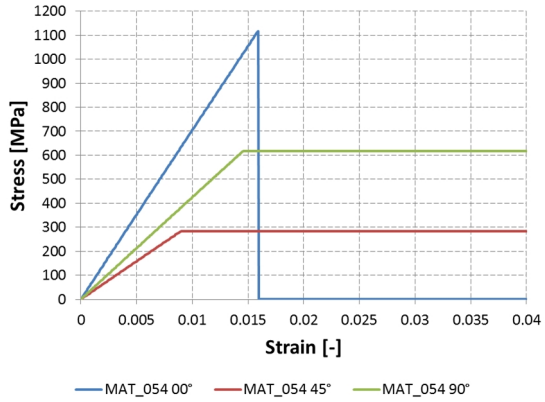

Figure 33: Single element test MAT_054: tension in 2D elements (00°, 45° and 90°)

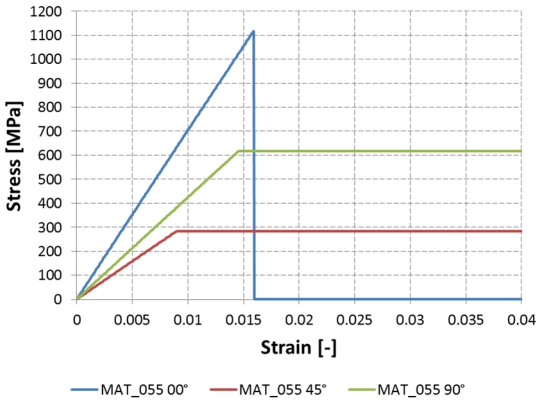

Figure 34: Single element test MAT_055: tension in 2D elements (00°, 45° and 90°)

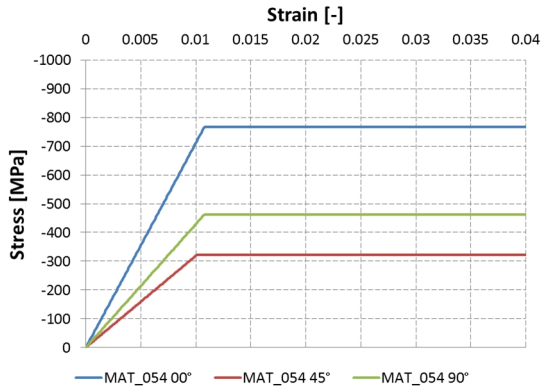

Figure 35: Single element test MAT_054: compression in 2D elements (00°, 45° and 90°)

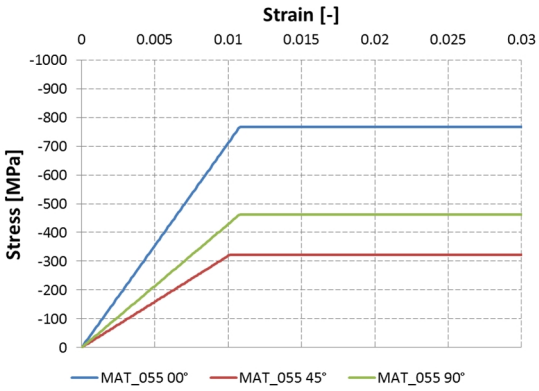

Figure 36: Single element test MAT_055: compression in 2D elements (00°, 45° and 90°)

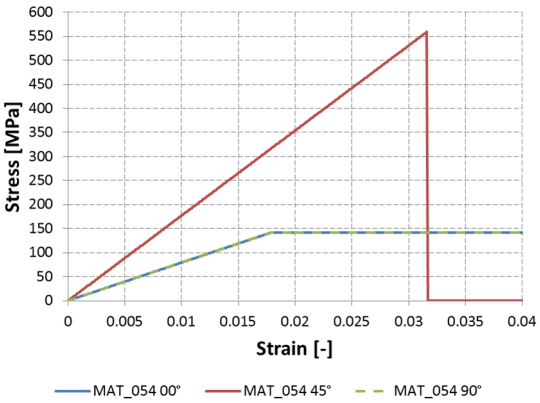

Figure 37: Single element test MAT_054: shear in 2D elements (00°, 45° and 90°)

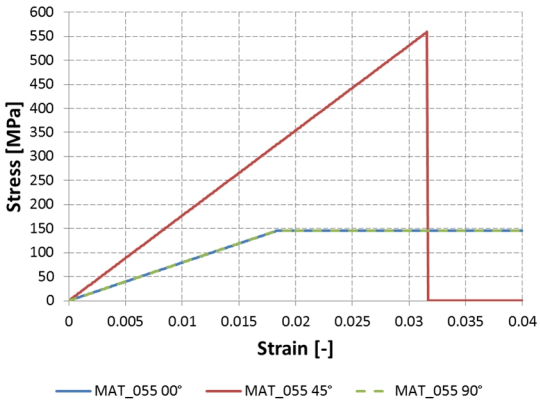

Figure 38: Single element test MAT_055: shear in 2D elements (00°, 45° and 90°)

4.1.2.2.2.3 Laminated Composite Fabric (MAT_058)

MAT_058 is a composite CDM model following the recommendations of Matzenmiller et al. [81] and, therefore, it differs strongly from the other composite material models. MAT_058 uses an exponential decay of stress after reaching maximum stress. This is supposed to represent damage. The onset of damage is determined with the failure criteria used in Matzenmiller et al.'s theory.

Figure 40 to Figure 42 show the results for tension, compression and shear for MAT_058. These values agree well with failure stresses of previous material models as the failure criteria used in the theory by Matzenmiller et al. are a modification of those used in Hashin's theory [44], and therefore are strongly related to the Chang-Chang theory.

In Matzenmiller et al.'s damage theory the shape of the damage stress-strain curve is controlled by the strain-softening parameter m. However, MAT_058 does not allow the control of this parameter. Additionally, a default setting of m is not mentioned in the manual. Figure 39 shows stress-strain curves for different values of m for longitudinal tensile loading. The comparison with the stress-strain curve by LS-DYNA shows an agreement for m = 10 which leads to a quasi-brittle behaviour suiting the needs of composites.

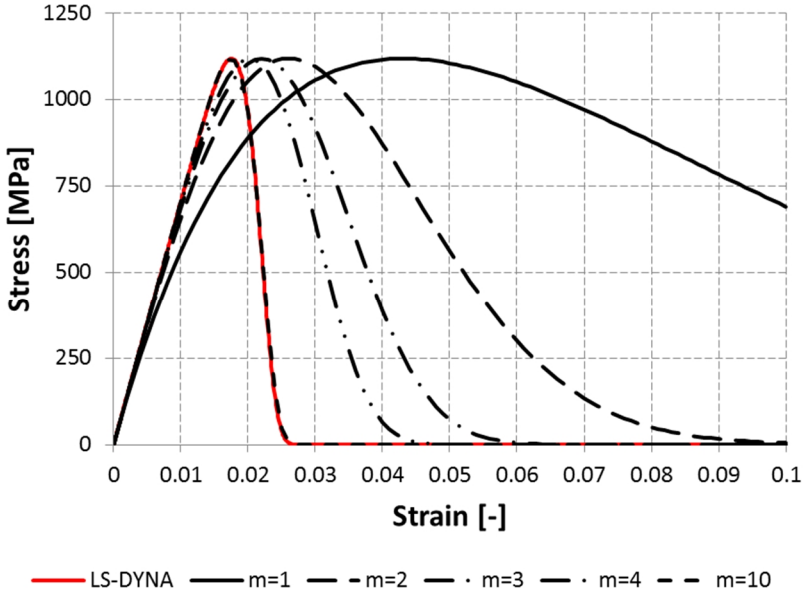

Figure 39: Tensile stress-strain relationships for different values of strain-softening parameter $'m'$

The accuracy of failure strength, failure strain and stiffness are compared for MAT_058 in Appendix B.

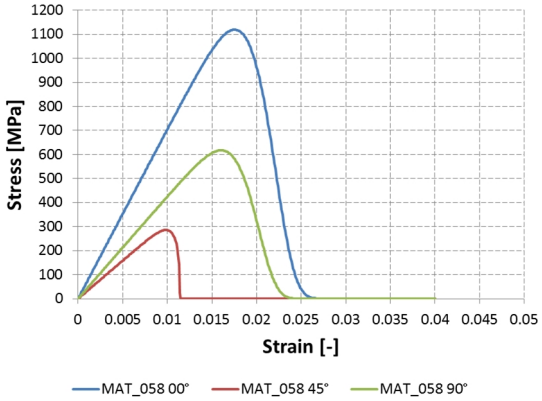

Figure 40: Single element test MAT_058: tension in 2D elements (00°, 45° and 90°)

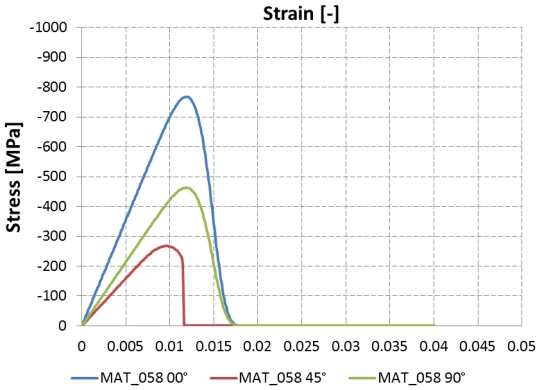

Figure 41: Single element test MAT_058: compression in 2D elements (00°, 45° and 90°)

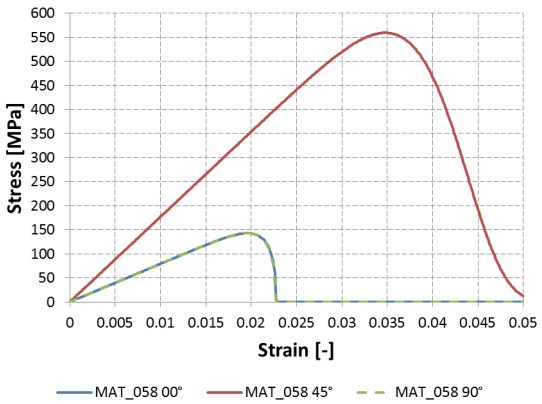

Figure 42: Single element test MAT_058:

shear in 2D elements (00°, 45° and 90°)

4.1.2.2.2.4 Composite Failure (MAT_059)

A reference to the underlying theory of MAT_059 is hard to come by but many similarities with MAT_022 exist regarding the input data. Therefore, it was assumed that MAT_022 and MAT_059 share a common theory.

Figure 43, Figure 45 and Figure 49 show results for 2D elements in tension, compression and shear conducted with MAT_059. The LS-DYNA results were compared with analytical results of the Chang-Chang failure theory. The results are in excellent agreement with results of MAT_022 with two exceptions. Firstly, MAT_059 considers the longitudinal compressive strength as input data; therefore, it can be assumed that Chang-Chang's compressive fibre mode is implemented. Secondly, compressive failure of the 45°-orientation occurs earlier in LS-DYNA simulations and analytical considerations. MAT_059 reacts solely on the shear caused in the 45°-orientation.

The results for 2D elements show that stress is not set to zero after reaching the material's failure criteria. This cannot be controlled for 2D in MAT_059.

Figure 44, Figure 46 and Figure 48 show results for the 3D single element tests in the ab-plane. The results are in excellent agreement with analytical results derived by the Cheng and Hallquist theory [25].

Results for tension, compression and shear in the ac- and bc-plane of the solid elements are presented in Appendix B. As well the accuracy of failure strength, failure strain and stiffness are compared for 2D and 3D elements of MAT_059.

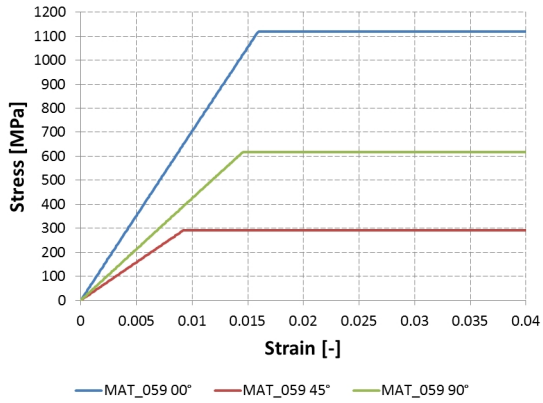

Figure 43: Single element test MAT_059: tension in 2D elements (00°, 45° and 90°)

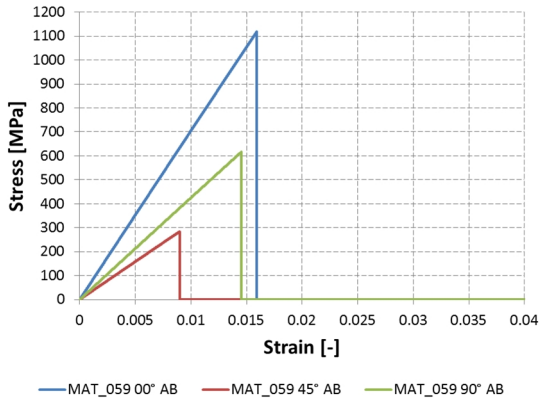

Figure 44: Single element test MAT_059: tension in ab-plane of 3D elements (00°, 45° and 90°)

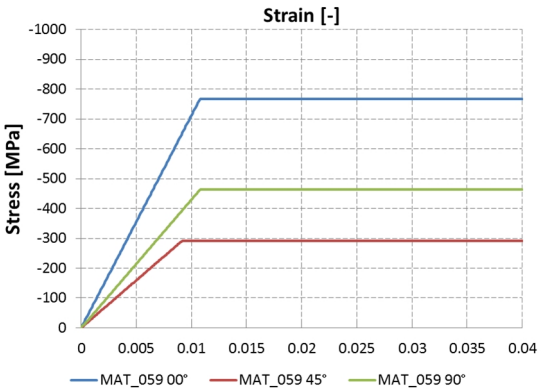

Figure 45: Single element test MAT_059: compression in 2D elements (00°, 45° and 90°)

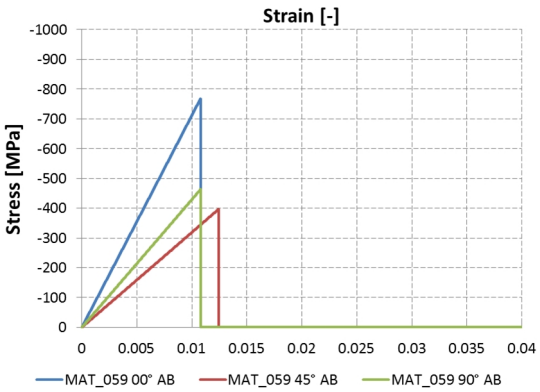

Figure 46: Single element test MAT_059: compression in ab-plane of 3D elements (00°, 45° and 90°)

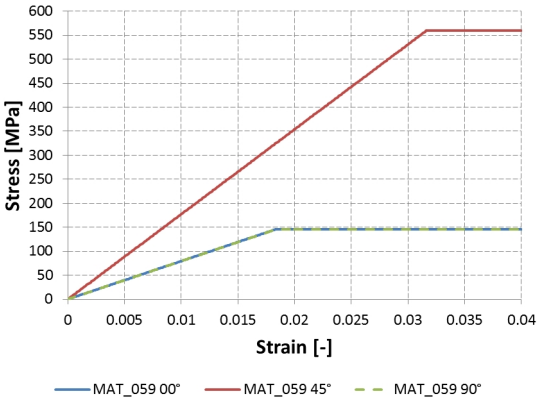

Figure 47: Single element test MAT_059: shear in 2D elements (00°, 45° and 90°)

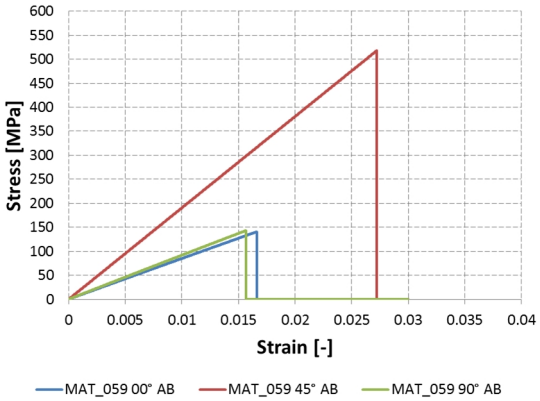

Figure 48: Single element test MAT_059: shear in ab-plane of 3D elements (00°, 45° and 90°)

4.2 Dynamic Strain-Softening

A material's strain-softening behaviour leads to mathematical difficulties and physically unreasonable results in a local continuum. Apart from this, when modelled using FE codes, it will lead to numerical instabilities which express themselves as pronounced mesh-sensitivity of results. Therefore a numerical investigation of a FE strain-softening CDM model is performed using Bažant's and Belytschko's [6] test problem of longitudinal wave propagation which was presented in Chapter 3. The material model used for the FE investigastion is the LS-DYNA's composite CDM model (MAT_058) by Matzenmiller et al. [81].

Strain-softening manifests itself in the smallest area possible which is a single point in the analytical solution (see Chapter 3, Section 3.2). In FE analysis this smallest area is defined by the chosen element size. Therefore, it is assumed that results will strongly depend on the element size.

The bar has an overall length of $2L$ = $200mm$. Different element numbers along the length of the bar are chosen to demonstrate mesh-sensitivity:

- Bar 1: 11 elements
- Bar 2: 31 elements
- Bar 3: 101 elements

The test cases are shown in Figure 49 in comparison with the theoretical setup by Bažant and Belytschko [6].

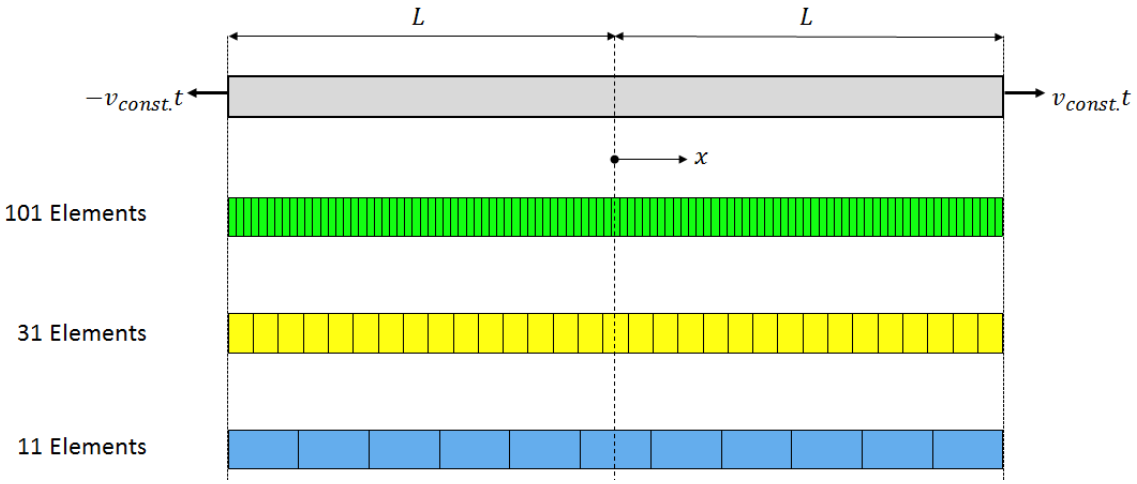

Figure 49: Strain-softening bar by Bažant and Belytschko [6] with different mesh discretisations for numerical testing of strain-softening CDM model

MAT_058 is defined for shell elements. All degrees of freedom outside the x-direction will be fully restricted to be in agreement with the 1D problem stated by Bažant and Belytschko.

MAT_058 is a composite damage model. It provides for the definition of different directional material properties. In this experiment the longitudinal material direction is aligned with the x-direction. The same composite data as used in the quasi-static single element tests (see Table 4-2) will be used. The important data for this experiment is data of the longitudinal direction and is summarised in Table 4-3:

Table 4-3: Input data for composites in longitudinal direction

Value	Sign	Magnitude	Unit
Density	ρ	$1.55 \cdot 10^{-9}$	t/mm^3
Young's modulus, a-direction	E_a	70800	MPa
Longitudinal tensile strength	X_T	1119	MPa
Critical longitudinal tensile strain	$\varepsilon_{XT} = X_T/E_a$	+0.0158	–

The elastic wave speed in longitudinal direction for the test problem is determined as:

$$c_e = \sqrt{\frac{E_a}{\rho}} = 6758507.18 \frac{mm}{s} \tag{4-45}$$

The determination time of the problem is

$$t = 2 \cdot \frac{L}{c_e} = 2.9592 \cdot 10^{-5} s \tag{4-46}$$

at which stage both waves are supposed to have travelled the whole length of the bar. The superposition of waves is supposed to happen at

$$t = \frac{L}{c_e} = 1.4796 \cdot 10^{-5} \tag{4-47}$$

The constant velocity for the elastic and strain-softening case can be determined with:

$$\varepsilon = \frac{v}{c_e} \quad with \quad \varepsilon \leq \varepsilon_p / 2 \tag{4-48}$$

$$\varepsilon = \frac{v}{c_e} \quad with \quad \frac{\varepsilon_p}{2} < \varepsilon \leq \varepsilon_p \tag{4-49}$$

The maximum loading to avoid strain-softening is:

$$v_{max} < \frac{\varepsilon_p}{2} \cdot c_e = 53392 \frac{mm}{s}$$

The minimum and maximum loading which ensures strain-softening at $x = 0$ for $t = L/c_e$ is:

$$v_{min} = \frac{\varepsilon_p}{2} \cdot c_e = 53392 \frac{mm}{s}$$

$$v_{max} = \varepsilon_p \cdot c_e = 106784 \frac{mm}{s}$$

In the following the elastic test will be run with $v_{elastic} = 3.5 \cdot 10^4 mm/s$ and the strain-softening test will be run with $v_{softening} = 7 \cdot 10^4\ mm/s$. The elastic and strain-softening solutions resulting from (4-48) and (4-49) will be compared for longitudinal displacement, strain and stress. The time $t = 3/4 \cdot 2L/c_e$ is chosen as example as the waves from the bar's edges have travelled $3/4$ of the bar's length. At this stage the area $-L/2 \leq x \leq L/2$ is governed by the strain-softening solution. The areas outside the strain-softening domain will continue to obey the elastic solution. The internal

energy will be presented for the overall bar for the full time span of the test: $0 \leq t \leq 2 \cdot L/c_e$.

Figure 50 and Figure 51 show the stress-strain curves for elastic and strain-softening tests respectively in the element located at x = 0. It is clearly visible in Figure 50 that the bar is governed by the elastic solution at all times. Figure 51 shows the typical strain-softening behaviour in the middle element with declining stress-strain branch due to softening.

Figure 52 to Figure 61 show the results for longitudinal displacement, strain and stress for the elastic and strain-softening case at $t = 3/4 \cdot 2L/c_e$. Figure 62 and Figure 63 show the results for internal energy for elastic and strain-softening between $0 \leq t \leq 2 \cdot L/c_e$. It is clear from the elastic solutions that no mesh-sensitivity exists in the elastic area and results follow the analytical solution well; however, an increase in accuracy can be observed with increasing mesh fineness. The strain-softening bars on the contrary show strong mesh-sensitivity in the strain-softening area $-L/2 \leq x \leq L/2$. It can be observed that the results follow the analytical solution increasingly accurate with increasing mesh fineness which proves the point of mesh-sensitivity. Also the area of strain-softening becomes more refined with increasing mesh fineness. The areas outside $-L/2 \leq x \leq L/2$ are still governed by the elastic solution in presence of strain-softening and do not show any mesh-sensitivity at all. The area in which damage develops (see Figure 55) becomes more refined with increasing element number and is dictated by the size of the strain-softening element. The solution for longitudinal displacement in Figure 57 shows strong mesh-sensitivity too and a convergence to the non-physical strain-softening solution with increasing element number. Bar 3 (101 elements) has a well-developed displacement jump in the middle of the bar which is stronger pronounced than for bar 1 and 2, which have a lower element number. In Figure 59 the strain displays the development of a localisation zone for all spatial discretisations; however, the localisation zone becomes sharper with decreasing element size and strain results converge to the Dirac delta function. The corresponding stress profiles are plotted in Figure 61 which show convergence to the strain-softening solution with increasing element number too. Another critical feature of strain-softening behaviour is the zero energy dissipation, displayed in Figure 63. The solution for energy dissipation approaches, with increasing element number, the non-physical solution which tends to zero.

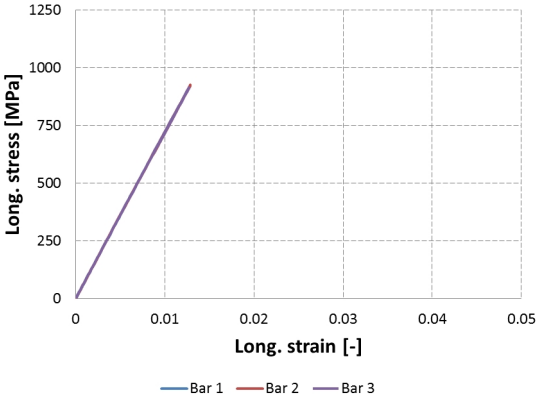

Figure 50: Numerical results for long. stress-long. strain relationship in elastic case

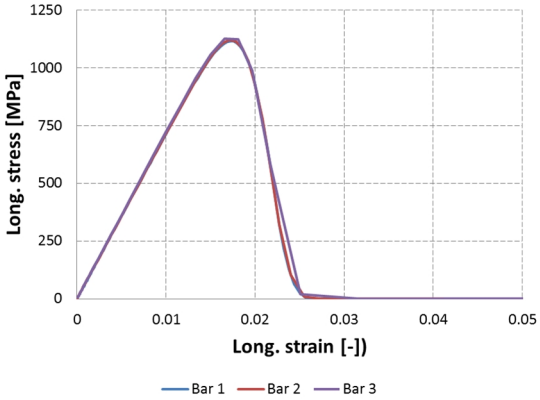

Figure 51: Numerical results for long. stress-long. strain relationship in strain-softening case

No damage

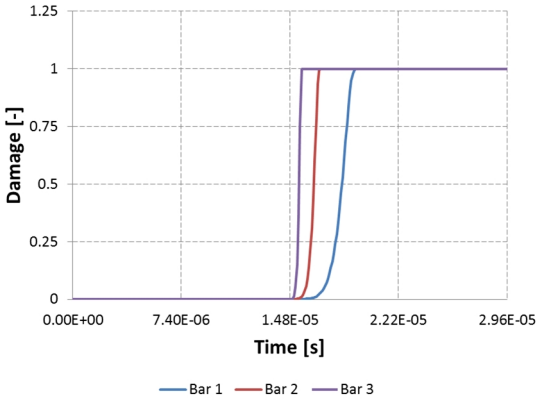

Figure 52: Numerical results for damage in softening element in elastic case

Figure 53: Numerical results for damage in softening element in strain-softening case

No damage

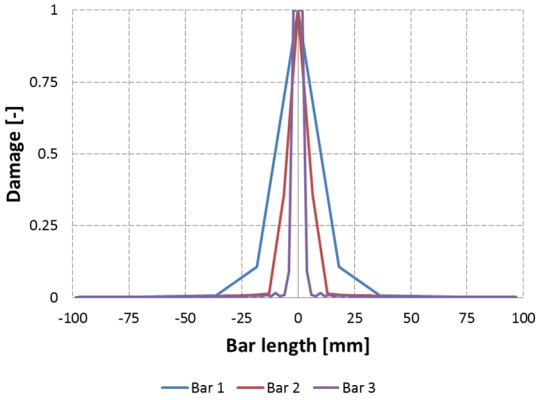

Figure 54: Numerical results for damage in elastic case at $t = 3/4 \cdot 2L/c_e$

Figure 55: Numerical results for damage in strain-softening case at $t = 3/4 \cdot 2L/c_e$

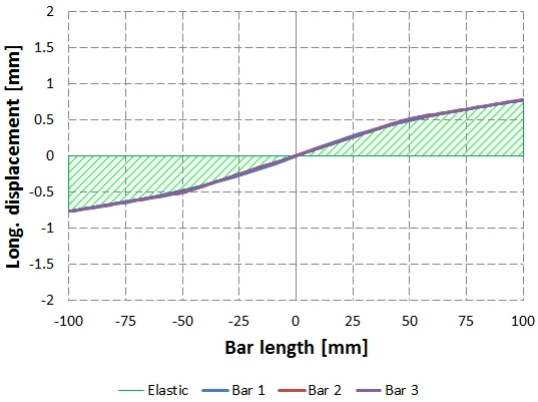

Figure 56: Numerical results for longitudinal displacement in elastic case at $t = 3/4 \cdot 2L/c_e$

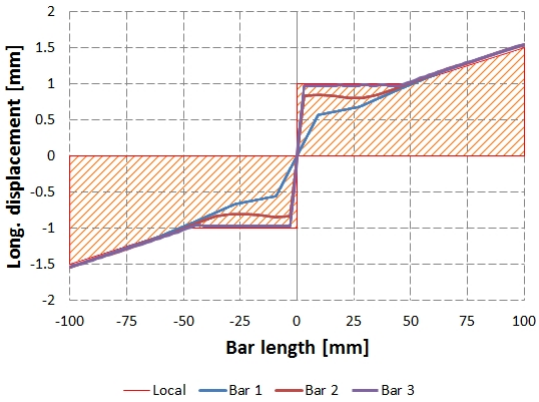

Figure 57: Numerical results for longitudinal displacement in strain-softening case at $t = 3/4 \cdot 2L/c_e$

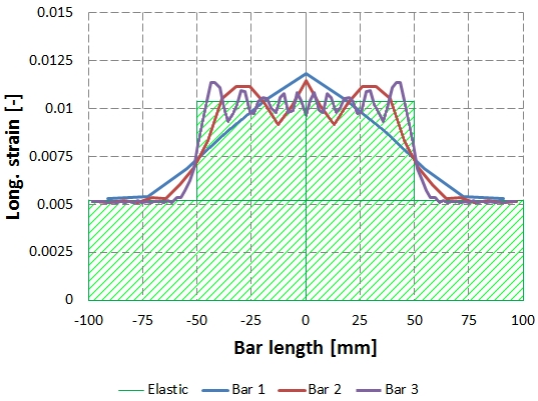

Figure 58: Numerical results for longitudinal strain in elastic case at $t = 3/4 \cdot 2L/c_e$

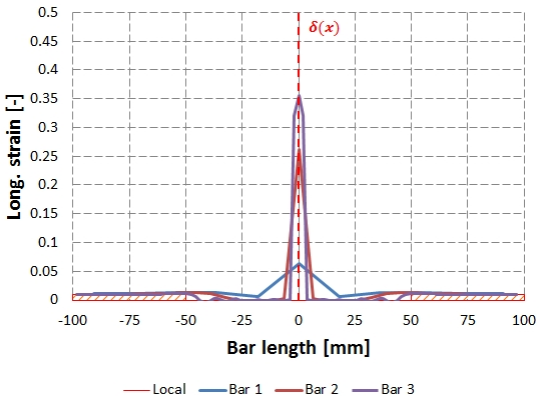

Figure 59: Numerical results for longitudinal strain in strain-softening case at $t = 3/4 \cdot 2L/c_e$

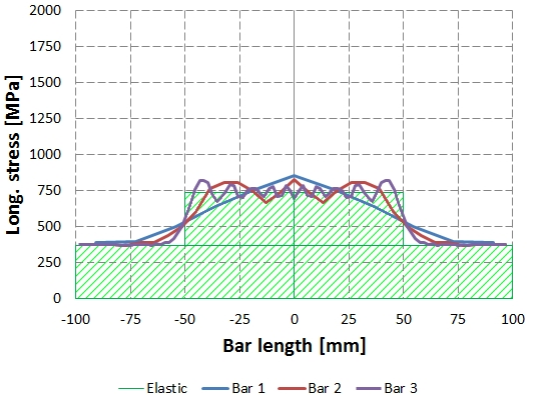

Figure 60: Numerical results for longitudinal stress in elastic case at $t = 3/4 \cdot 2L/c_e$

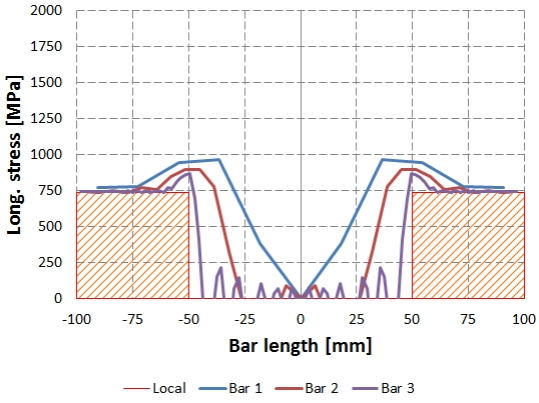

Figure 61: Numerical results for longitudinal stress in strain-softening case at $t = 3/4 \cdot 2L/c_e$

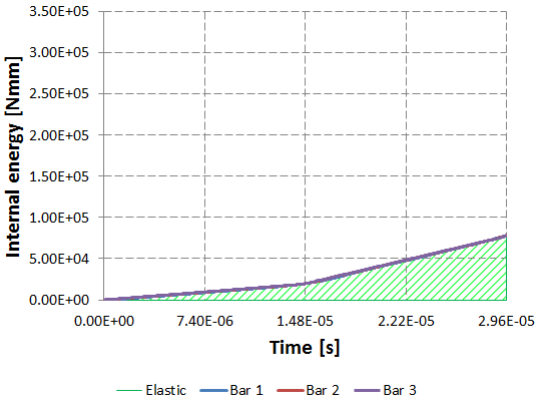

Figure 62: Numerical results for internal energy in elastic bar for $0 \leq t \leq 2 \cdot L/c_e$

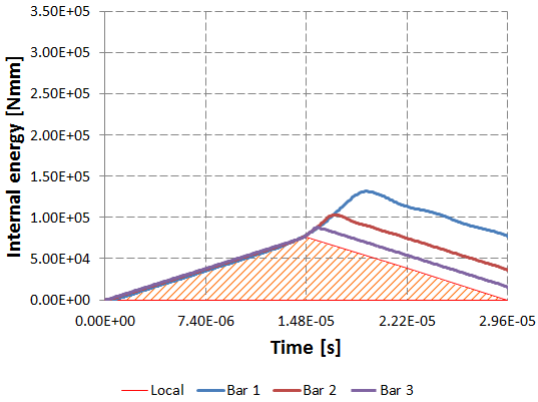

Figure 63: Numerical results for internal energy in strain-softening bar for $0 \leq t \leq 2 \cdot L/c_e$

Figure 64 shows the development of strain over time in strain-softening bar 3 which is discretised with 101 elements. It becomes clear that strain localises in the middle of the bar and grows infinitely in magnitude. The area in which strain localises is clearly refined and the area coincides with the size of a single element.

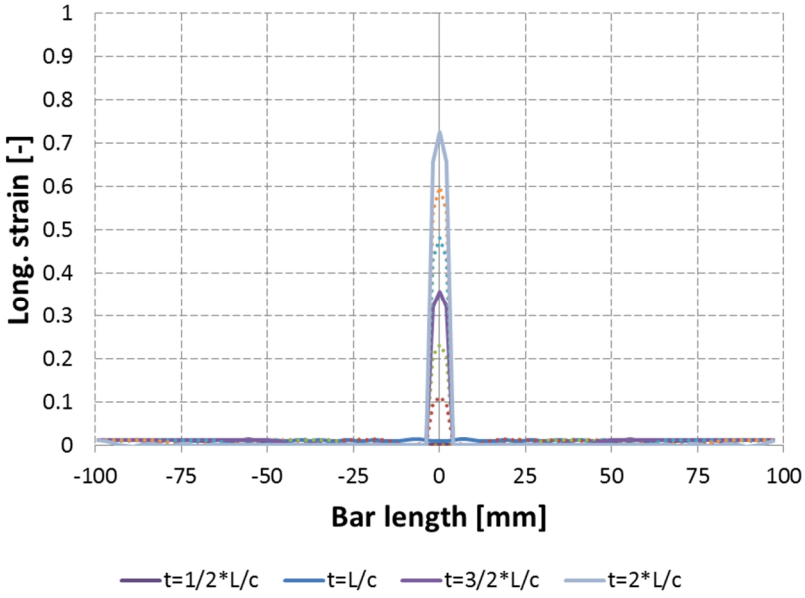

Figure 64: Numerical results for longitudinal strain in strain-softening case over the period $0 \leq t \leq 2 \cdot L/c_e$ for bar 3 (101 elements)

Figure 65 shows the relative deformation of the strain-softening element clearly. The deformation becomes more apparent with decreasing element size as for bar 3 with 101 elements. The fringe level represents the strain in the softening element at $t = 3/4 \cdot 2L/c_e$. The strain is more intense with decreasing element size although the boundary and loading conditions are equivalent for all bars. Outside the strain-softening zone the elements are unloaded.

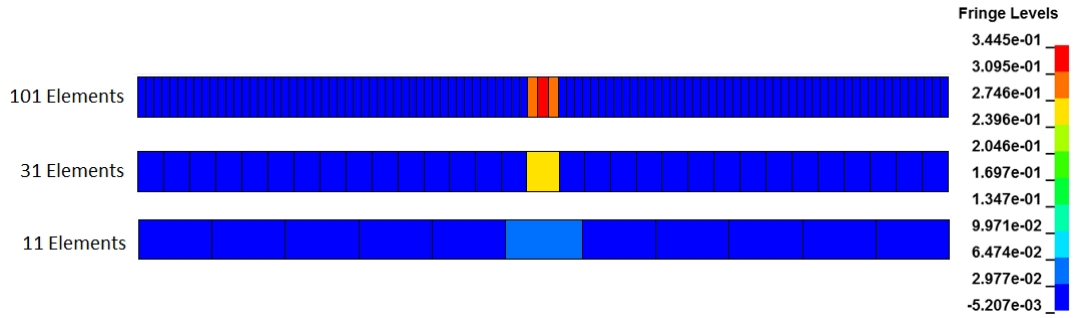

Figure 65: Strain in strain-softening element at x = 0 for t = 3/4 · 2L/c_e (fringe level: strain [-])

4.3 Strain-Softening Stabilisation

It was shown in the previous section (Section 4.2) that CDM models with strain-softening behaviour lead to numerical instabilities and that results do not converge to a unique solution. In this section numerical examples of options in LS-DYNA and ABAQUS will be investigated which appear to be nonlocal and viscous regularisation methods. LS-DYNA offers a keyword *MAT_NONLOCAL which can be used in conjunction with different CDM material models. ABAQUS offers a "damage stabilisation" option of viscous character.

The investigation will be conducted with Bažant and Belytschko's 1D wave propagation problem [6] which was presented Chapter 3. The test setup of the simulations for nonlocal stabilisation in LS-DYNA and damage stabilisation in ABAQUS are following the exact setup presented in Section 4.2.

4.3.1 Nonlocal Stabilisation

The analysis of nonlocal regularisation will be carried out with the keyword *MAT_NONLOCAL in LS-DYNA. The LS-DYNA User's Manual [70] states that *MAT_NONLOCAL is based on the nonlocal theory by Pijaudier-Cabot and Bažant [95]. Nonlocal theory applies an averaging process to damage and plastic strain values of neighbouring elements. The weighting function required to do so is stated in the LS-DYNA manual as:

$$\alpha(r) = \alpha(\|x_i - \xi_i\|) = \left[1 + \left(\frac{\|x_i - \xi_i\|}{l}\right)^p\right]^{-q} \tag{4-50}$$

The weighting function α in (4-50) depends on the spatial domain spanned by the distance between points x_i and ξ_i and the characteristic length l. Additionally, the

magnitude of the weighting function can be influenced by two exponential parameters p and q. The LS-DYNA User's Manual [70] provides typical values for the exponential parameters as the following: p = 8 and q = 2.

The characteristic length needs to be chosen in a way that integration points of neighbouring particles will be included in the weighting function (4-50). The choice of l is not straightforward. Here an approach suggested by Schwer [105] will be adopted which aims to keep the number of neighbouring integration points constant by defining the characteristic length as:

$$l = \sqrt{2} \cdot l_{element} \tag{4-51}$$

Due to the definition in (4-51) the characteristic length depends on the element length $l_{element}$ used.

The keyword *MAT_NONLOCAL will be used in conjunction with *MAT_DAMAGE_1 (MAT_104) which is a CDM model. The option $FLAG \geq 0$ activates the damage model developed by Lemaitre [65]. The effective stress is defined according to (3-11) and the evolution of damage is defined as:

$$\dot{\omega} = \begin{cases} 0 & for\ r \leq r_D \\ \dfrac{Y}{S(1-\omega)}\dot{r} & for\ r > r_D\ and\ \sigma > 0 \end{cases} \tag{4-52}$$

with the effective plastic strain r_D at which strain-softening is initiated, the strain energy release rate S and the strain energy density release rate Y.

The longitudinal wave propagation problem presented in Chapter 3 will be used as an example for the nonlocal regularisation. The same material properties (see Table 4-3) and same initial and boundary conditions are applied as in Section 4.2. The bar will be analysed with three different mesh discretisations:

- Bar 1: 11 elements
- Bar 2: 31 elements
- Bar 3: 101 elements

*MAT_DAMAGE_1 will be used the following way: r_D = 0 (default), damage material constant S = 0.54, critical damage at which elements are deleted D_c = 1. Strain-softening is enabled by using the option $FLAG$ = 1. *MAT_NONLOCAL will use the input data for the exponential parameters p = 8 and q = 2 [70] and $l = \sqrt{2} \cdot l_{element}$ as

the characteristic length suggested by Schwer [105]. Additionally, the parameters to be averaged need to be specified for nonlocal treatment. These are effective plastic strain and the damage variable in *MAT_DAMAGE_1 [70].

Figure 66 to Figure 79 present the results for the 1D problem using the local solution (*MAT_DAMAGE_1) and the nonlocal solution (*MAT_DAMAGE_1 with *MAT_NONLOCAL) at $t = 3/4 \cdot 2L/c_e$. The local solutions show the typical features of strain-softening accompanied by mesh dependence of results on the spatial discretisation. The results of bar 3 for damage and strain (see Figure 70 and Figure 72) are designated with asterisks (*). *MAT_DAMAGE_1 deletes the softening element when damage reaches the critical value D_c. This already happened for the softening element in bar 3 at $t = 3/4 \cdot 2L/c_e$. These results are designated with a single asterisk (*). Energy dissipation in the local case is presented in Figure 78 and tends to zero in the presence of strain-softening.

Figure 67 shows the stress-strain behaviour for the bars which was obtained with LS-DYNA's *MAT_NONLOCAL option. The bars apparently do not undergo strain-softening anymore and instead have a plastic behaviour. Therefore, it must be assumed that following results obtained with *MAT_NONLOCAL will not show typical strain-softening behaviour.

Figure 69 shows the development of damage in the strain-softening element over time. In comparison to the local results in Figure 68 the damage values are strongly reduced and the development over time seems to approach a similar trend for all mesh discretisation. Damage is plotted along the bar in Figure 71 for *MAT_NONLOCAL. Damage develops in all bars in an area which can be assumed to be equivalent and the magnitude of damage is similar. This is a very interesting result as damage should be confined to an area which is dictated by the characteristic length; however, the characteristic length is defined as $l = \sqrt{2} \cdot l_{element}$ and is therefore different for each bar.

The results for longitudinal displacement in Figure 73 resemble linear elastic behaviour. The results do not show a dependence on the used element size but they do not show a development of a localisation zone either due to damage which is defined by the characteristic length.

Figure 75 and Figure 77 show the strain and stress profiles achieved with *MAT_NONLOCAL. The results show an accumulation of strain and according stress in the centre of the bars and results do not seem to depend on the mesh discretisation.

Figure 79 shows the internal energy of the bars over time. All results follow the same path and do not show mesh-sensitivity. Instead the behaviour seems to be rather linear elastic.

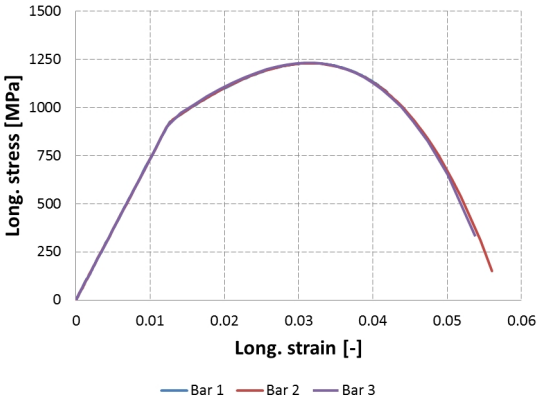

Figure 66: Numerical results for long. stress-long. strain relationship in local case

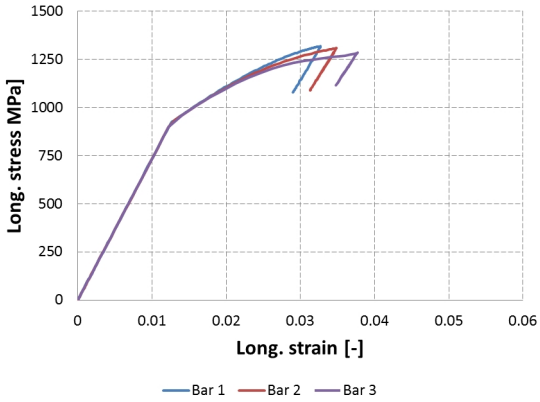

Figure 67: Numerical results for long. stress-long. strain relationship in nonlocal case

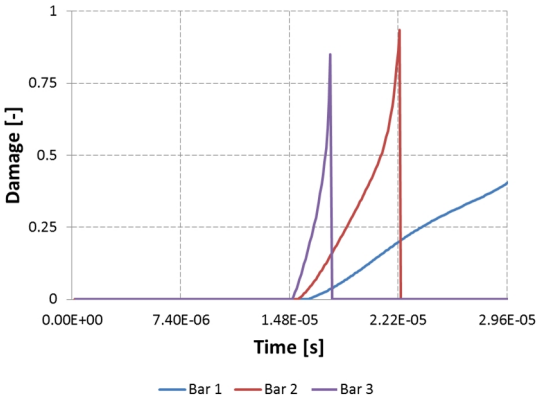

Figure 68: Numerical results for damage in softening element in local case

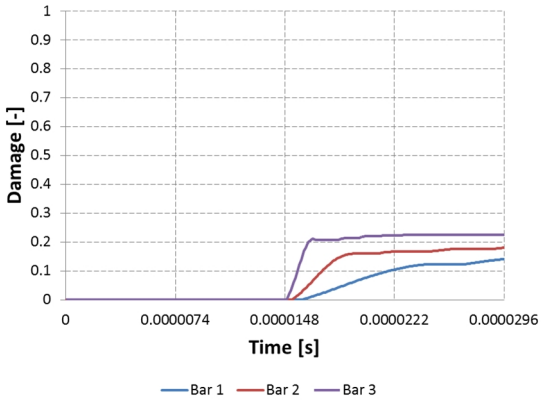

Figure 69: Numerical results for damage in softening element in nonlocal case

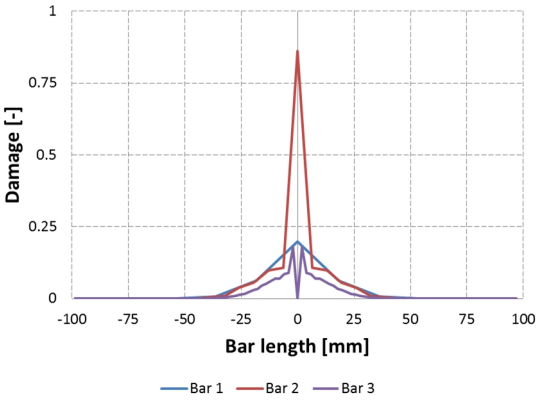

Figure 70: Numerical results for damage in

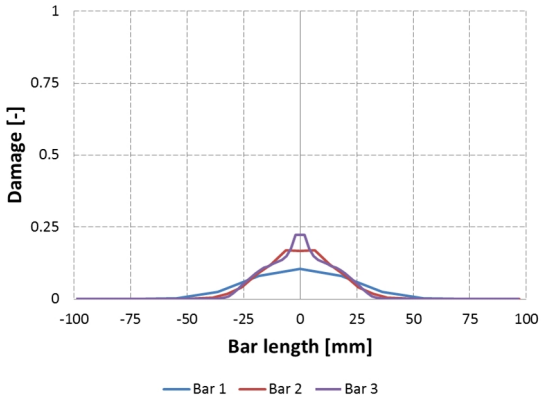

Figure 71: Numerical results for damage in

local case at $t = 3/4 \cdot 2L/c_e$

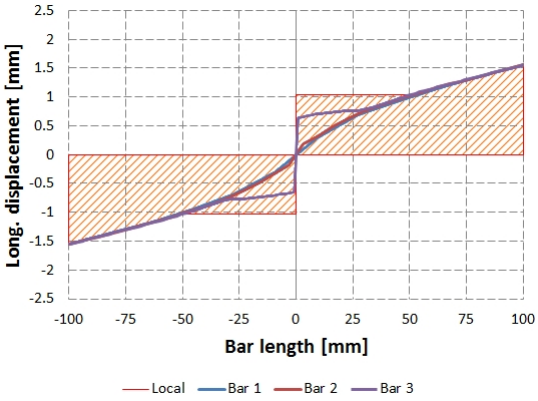

Figure 72: Numerical results for longitudinal displacement in local case at $t = 3/4 \cdot 2L/c_e$

nonlocal case at $t = 3/4 \cdot 2L/c_e$

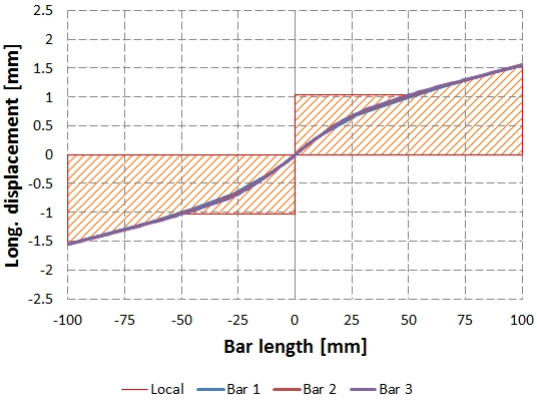

Figure 73: Numerical results for longitudinal displacement in nonlocal case at $t = 3/4 \cdot 2L/c_e$

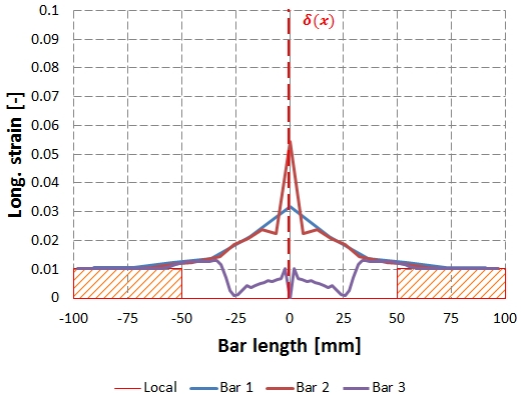

Figure 74: Numerical results for longitudinal strain in local case at $t = 3/4 \cdot 2L/c_e$

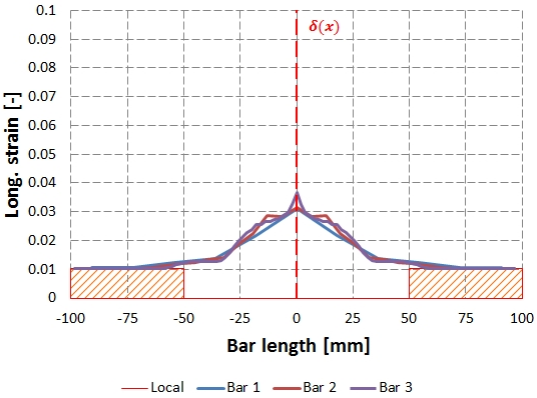

Figure 75: Numerical results for longitudinal strain in nonlocal case at $t = 3/4 \cdot 2L/c_e$

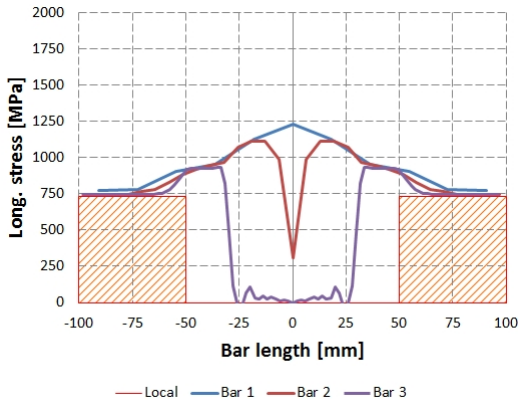

Figure 76: Numerical results for longitudinal stress in local case at $t = 3/4 \cdot 2L/c_e$

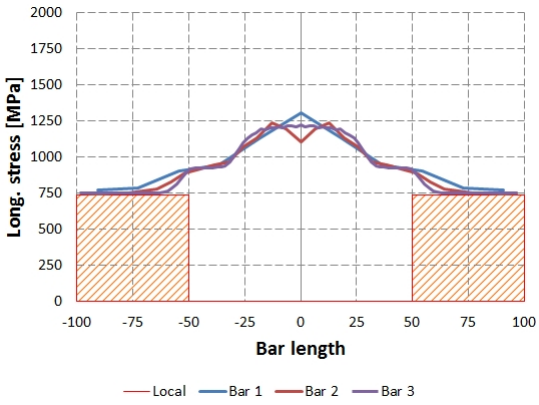

Figure 77: Numerical results for longitudinal stress in nonlocal case at $t = 3/4 \cdot 2L/c_e$

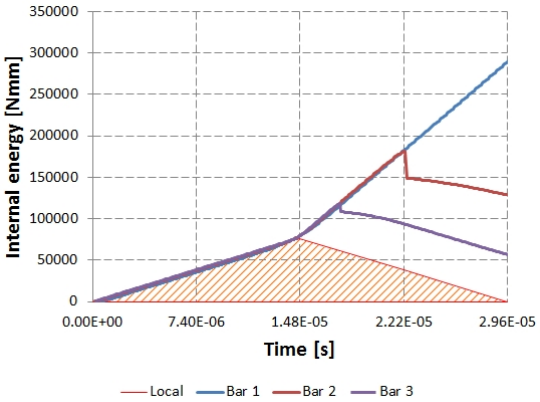

Figure 78: Numerical results for internal energy in local bar for $0 \leq t \leq 2 \cdot L/c_e$

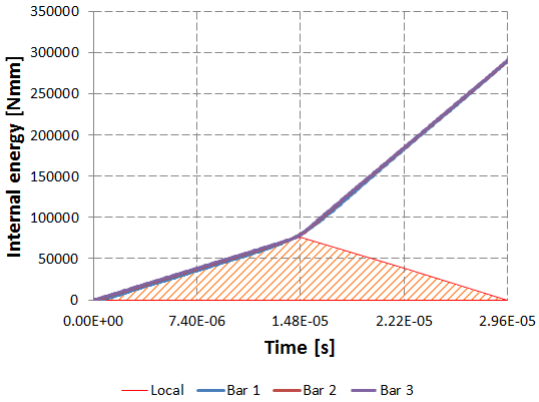

Figure 79: Numerical results for internal energy in nonlocal bar for $0 \leq t \leq 2 \cdot L/c_e$

Next the influence of a characteristic length change on results will be investigated. The bar with 101 elements will be used as example. The analysis will use three different characteristic lengths:

- Length 1: $l_1 = \sqrt{2} \cdot l_{element}$
- Length 2: $l_2 = 2 \cdot \sqrt{2} \cdot l_{element}$
- Length 3: $l_3 = 3 \cdot \sqrt{2} \cdot l_{element}$

The results for the tests with the same spatial FE discretisation and changing characteristic length are presented in Figure 80 to Figure 86. It was expected that the results would change for the bar with 101 elements in dependence of the characteristic length used; however, such dependence cannot be seen in the results. The stress-strain relationships are shown in Figure 80. They do not show any strain-softening. Instead they have a plastic material behaviour. The following results for damage, longitudinal displacement, strain, stress and internal energy can be assumed as equivalent and do not show any significant change in dependence of the used characteristic length. Apart from this the observations made for the previous experiment with *MAT_NONLOCAL are valid for the current experiment as well.

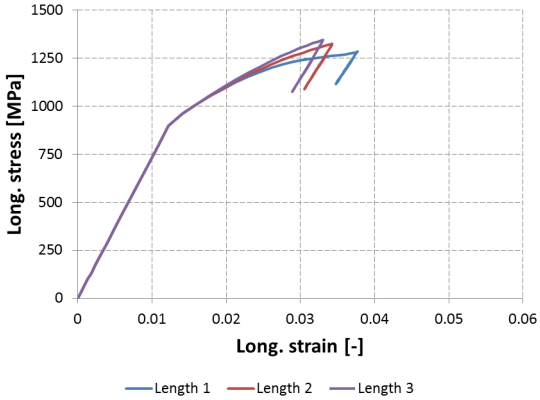

Figure 80: Numerical results for long. stress-long. strain relationship in nonlocal case with varying characteristic length

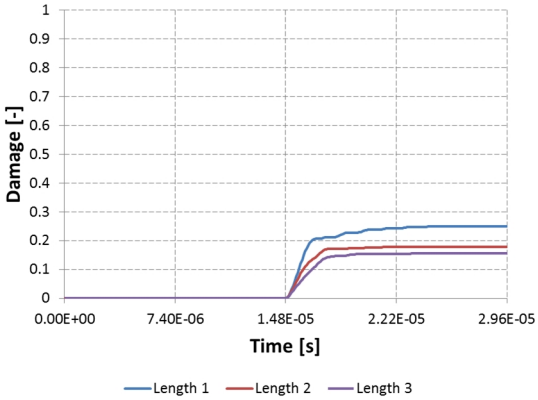

Figure 81: Numerical results for damage in softening element in nonlocal case with varying characteristic length

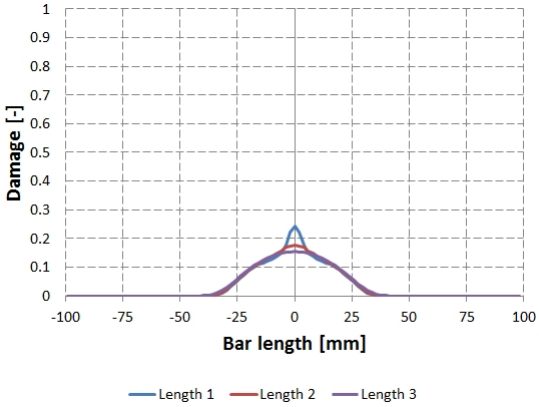

Figure 82: Numerical results for damage in nonlocal case with varying characteristic length at $t = 3/4 \cdot 2L/c_e$

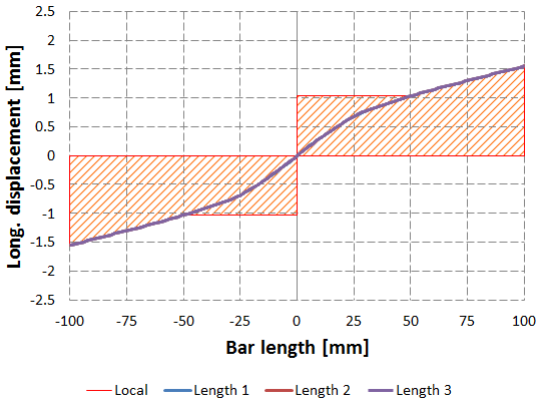

Figure 83: Numerical results for longitudinal displacement in nonlocal case with varying characteristic length at $t = 3/4 \cdot 2L/c_e$

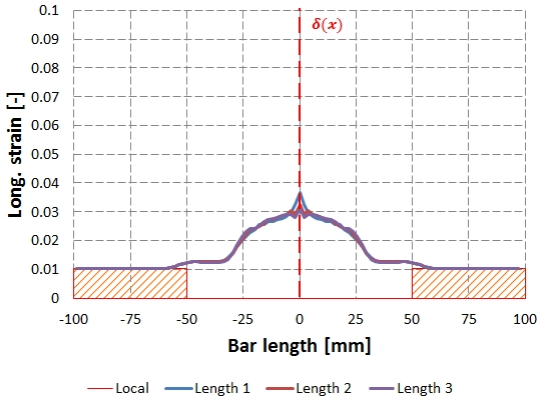

Figure 84: Numerical results for longitudinal strain in nonlocal case with varying characteristic length at $t = 3/4 \cdot 2L/c_e$

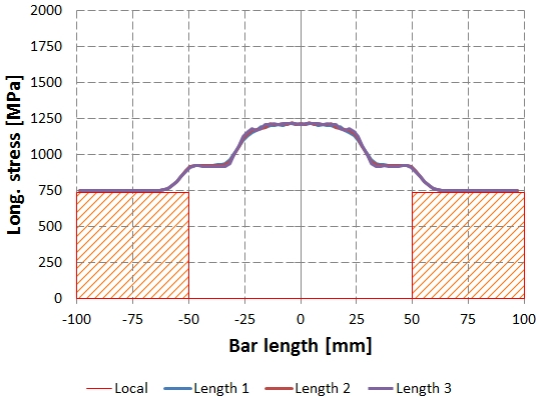

Figure 85: Numerical results for longitudinal stress in nonlocal case with varying characteristic length at $t = 3/4 \cdot 2L/c_e$

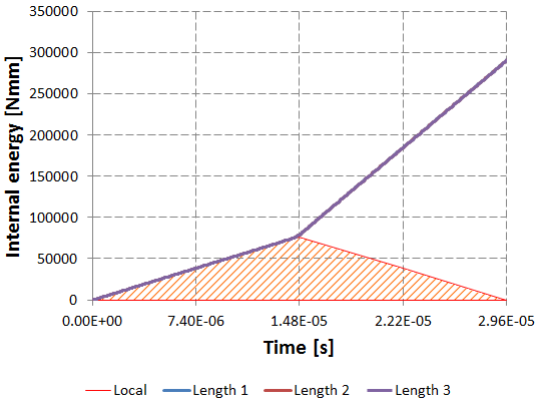

Figure 86: Numerical results for internal energy in nonlocal case with varying characteristic length for $0 \leq t \leq 2 \cdot L/c_e$

The experiments done in this subsection were meant to evaluate a readily available nonlocal regularisation method in LS-DYNA. A CDM material model (*MAT_DAMAGE_1) was chosen which undergoes strain-softening due to damage. The results showed a dependence on the spatial discretisation as expected for a strain-softening model which occurs due to the negative tangent stiffness in strain-softening.

Next, *MAT_NONLOCAL was used in conjunction with *MAT_DAMAGE_1. The LS-DYNA User's Manual [70] states that *MAT_NONLOCAL applies a nonlocal regularisation method to the strain-softening problem. In nonlocal theory a characteristic length is introduced into the constitutive equations which define an area over which strain-softening results, such as damage and effective plastic strain, are averaged. Therefore, the localisation process due to damage and the mesh-sensitivity of results can be controlled by setting an appropriate characteristic length. However, the results achieved with *MAT_NONLOCAL do not reflect this behaviour. First of all, the strain-softening area does not undergo strain-softening behaviour at all, instead the behaviour is plastic. The achieved results do not show mesh-sensitivity but they also do not show a dependence on the used characteristic length. Also a distinct damage zone, depending on the characteristic length, could not be observed. *MAT_NONLOCAL seems to achieve a stabilisation effect by manipulating the stress-strain curve (instead of averaging the damage and effective plastic strain due to strain-softening over an area defined by the characteristic length) and prevent the negative tangent stiffness from becoming negative which is a characteristic of strain-softening. Therefore, the typical strain-softening behaviour and the sensitivity of the results to the used spatial discretisation do not occur.

4.3.2 Viscous Stabilisation

The analysis of a viscous regularisation scheme will be carried out with ABAQUS. ABAQUS provides a description of failure and damage for fibre-reinforced composites [107]. In this model damage initiation is determined by the Hashin criteria (see Section 4.1). The model is a CDM model which uses the effective stress concept following the form in (3-14). The material model undergoes linear strain-softening after the initiation of damage.

ABAQUS provides a viscous regularisation method, which they call “damage stabilisation”, to solve the issue of convergence. Due to regularisation the tangent stiffness tensor is supposed to be positive for sufficiently small time increments in the softening domain. The regularisation method uses a viscous damage variable [107]:

$$\dot{\omega}_v = \frac{1}{\mu}(\omega - \omega_v) \tag{4-53}$$

In (4-53), ω is the damage variable of the rate-independent material. μ is the viscosity coefficient which describes the relaxation time of the viscous system. The choice of μ has to be smaller than the characteristic time increment to improve results. However, the choice of the viscosity coefficient is not straightforward as it needs to be chosen in a way which guaranties convergence of results to a unique solution but ensures reasonable results at the same time.

The investigation will be conducted with Bažant and Belytschko’s 1D wave propagation problem [6] which was presented Chapter 3. The bar will be analysed with three different mesh discretisations:

- Bar 1: 11 elements
- Bar 2: 31 elements
- Bar 3: 101 elements

The material properties which were used are equivalent to the ones used in Table 4-2. The damage evolution in all examples is specified by G^c, the energy dissipated due to failure. The value is set to $G_c = 500 N/mm$. The examples using the regularisation scheme have a value of $\mu = 3.5 \cdot 10^{-6}$ for the viscosity coefficient.

Figure 87 to Figure 100 compare the results of the local and viscous approach. Figure 87 compares the stress-strain curves obtained for the three examples with the local approach. All curves represent strain-softening behaviour; however, their softening

branches differ although the exact same input data was used. This is caused by the definition of G^c. G^c is equivalent for all mesh discretisations; however, it defines the energy dissipated per unit volume of an element and the size of the softening element varies for the three examples. The remaining local solutions show the typical features of strain-softening accompanied by mesh dependence of results.

Figure 88 shows the stress-strain behaviour of the three test bars after application of the viscous stabilisation scheme in ABAQUS. The curves do not show strain-softening, characterised by its softening branch with negative slope. Instead the linear elastic area continues to be valid beyond the failure strength. Therefore it must be assumed that the result obtained with ABAQUS' viscous stabilisation scheme will not show conventional regularised strain-softening behaviour.

Figure 90 shows the damage development over time for the three test bars. Damage is strongly reduced in comparison to damage in the local configuration (see Figure 89) and develops for all bars equally. Damage is plotted along the bar in Figure 92. It is again visible that damage values are strongly reduced and additionally any mesh-sensitivity of damage results is not present.

The results for longitudinal displacement, strain, stress and internal energy for the experiment with viscous stabilisation are plotted over the analytical solution for the strain-softening bar in Figure 94, Figure 96, Figure 98 and Figure 100. It can be easily seen that the results do not show any mesh-sensitivity and do not follow the non-physical results of strain-softening. Instead they show a behaviour which is close to linear elastic wave propagation. This is not surprising as the viscous stabilisation resulted in a linear elastic stress-strain relationship (see Figure 88).

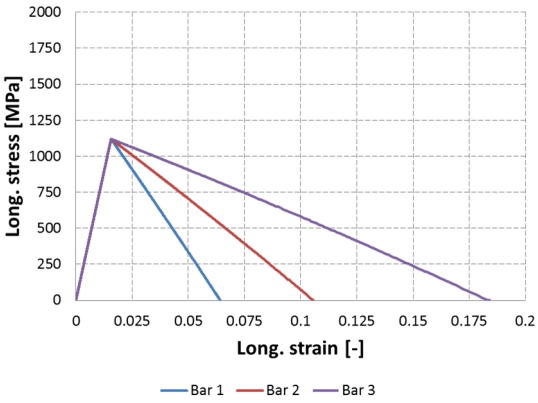

Figure 87: Numerical results for long. stress-long. strain relationship in local case

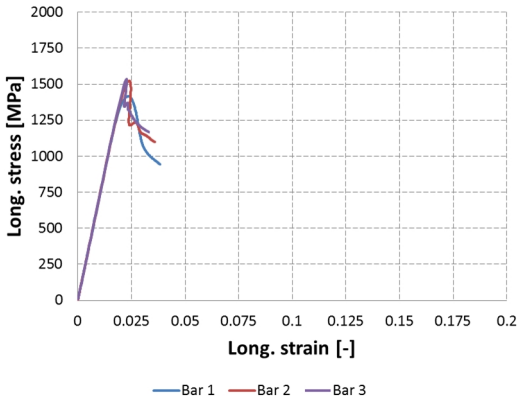

Figure 88: Numerical results for long. stress-long. strain relationship in viscous case

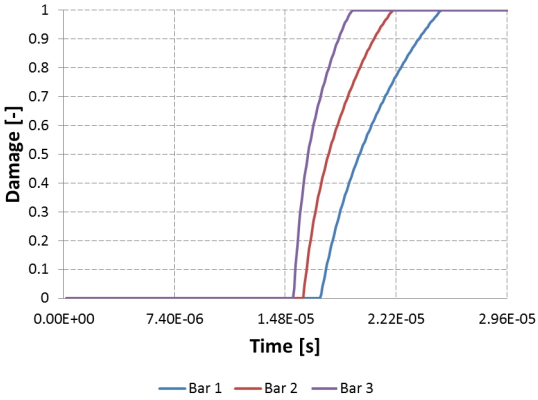

Figure 89: Numerical results for damage in softening element in local case

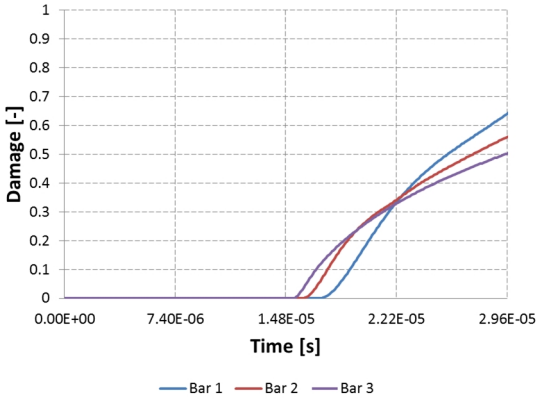

Figure 90: Numerical results for damage in softening element in viscous case

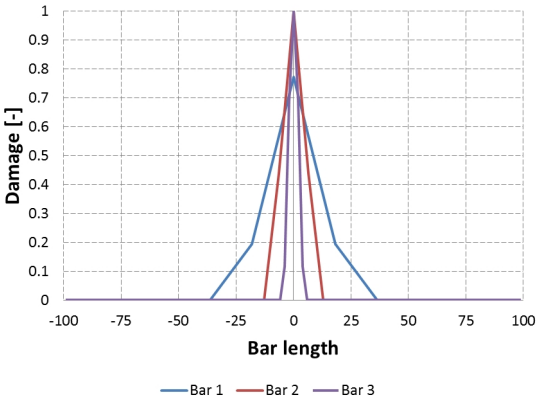

Figure 91: Numerical results for damage in local case at $t = 3/4 \cdot 2L/c_e$

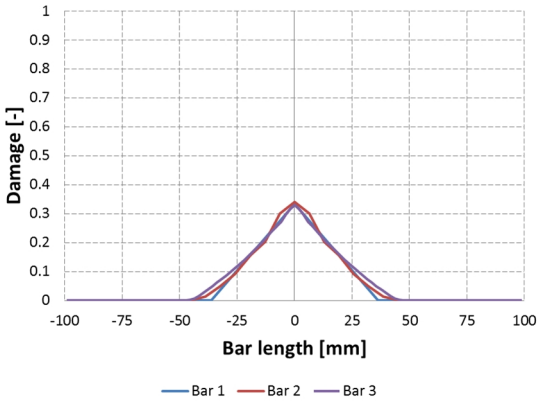

Figure 92: Numerical results for damage in viscous case at $t = 3/4 \cdot 2L/c_e$

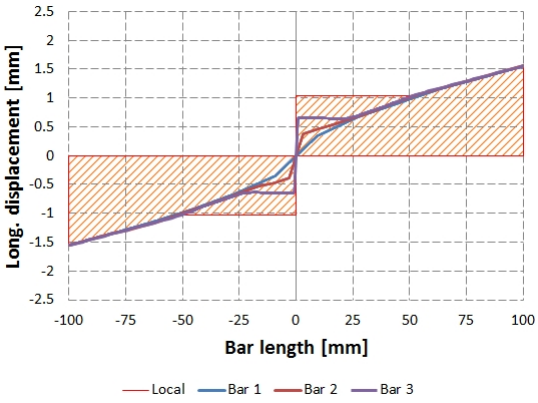

Figure 93: Numerical results for longitudinal displacement in local case at $t = 3/4 \cdot 2L/c_e$

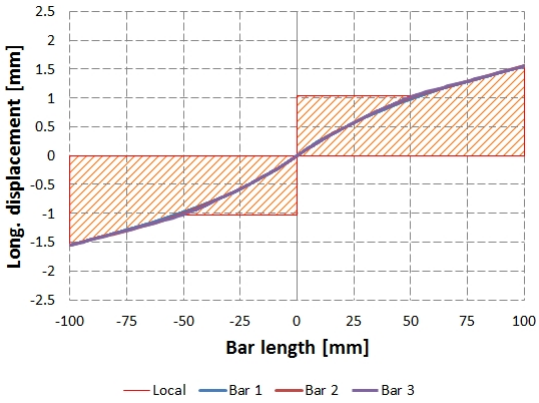

Figure 94: Numerical results for longitudinal displacement in viscous case at $t = 3/4 \cdot 2L/c_e$

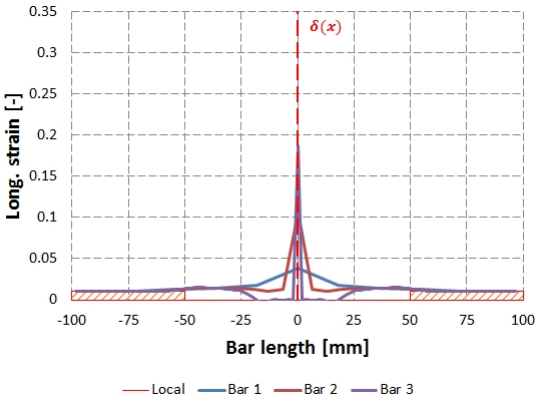

Figure 95: Numerical results for longitudinal strain in local case at $t = 3/4 \cdot 2L/c_e$

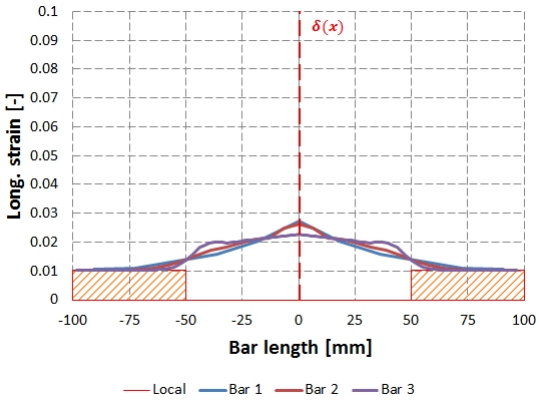

Figure 96: Numerical results for longitudinal strain in viscous case at $t = 3/4 \cdot 2L/c_e$

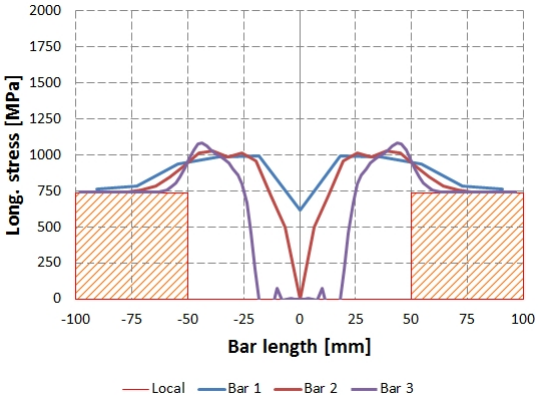

Figure 97: Numerical results for longitudinal stress in local case at $t = 3/4 \cdot 2L/c_e$

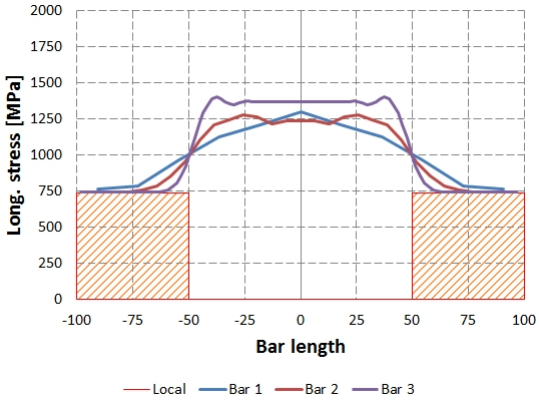

Figure 98: Numerical results for longitudinal stress in viscous case at $t = 3/4 \cdot 2L/c_e$

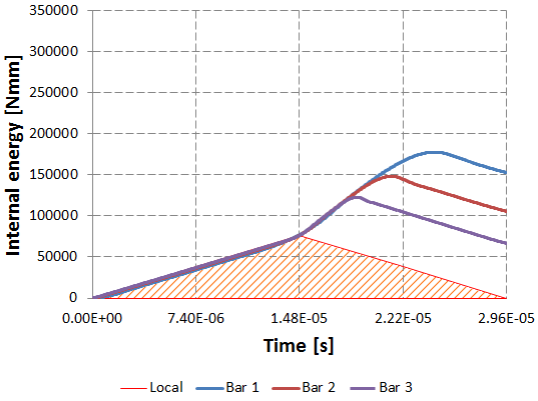

Figure 99: Numerical results for internal energy in local bar for $0 \leq t \leq 2 \cdot L/c_e$

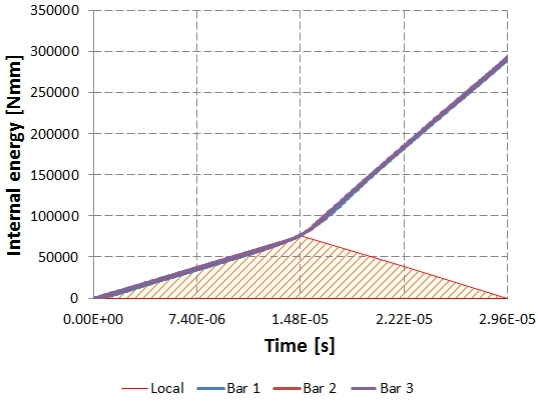

Figure 100: Numerical results for internal energy in viscous bar for $0 \leq t \leq 2 \cdot L/c_e$

Also of interest is how a change in the viscosity coefficient influences results. The bar with 101 elements will be used as an example which will be investigated with three different viscosity coefficients:

- Viscosity 1: $\eta = 10^{-6}$
- Viscosity 2: $\eta = 10^{-5}$

- Viscosity 3: $\eta = 10^{-4}$

The results are presented in Figure 101 to Figure 107. It is clear that a change in the order of magnitude of the viscosity coefficient has a great impact on the results. With increasing viscosity coefficient the stress-strain relationship approaches a linear elastic behaviour (see Figure 101). The magnitude of damage decreases with increasing viscosity parameter until it almost vanishes (see Figure 102). The width of the damaged area stays equivalent (see Figure 103) with increasing viscosity coefficient; however, the peak value of damage decreases noticeably. The longitudinal displacement only changes slightly with increasing viscosity parameter as seen in Figure 104; however, the longitudinal displacement is for all viscosity parameters similar to the displacement caused by linear elastic wave propagation. The strain profile shows dependence on the viscosity parameter too. With increasing magnitude of the viscosity parameter the peak strain in the softening elements decreases until it finally approaches a linear elastic strain distribution (see Figure 105). The stress response in the strain-softening area approaches the linear elastic wave propagation too with increasing viscosity (see Figure 106). The internal energy results in Figure 107 improve slightly by increasing the viscosity parameter; however, all results show an internal energy development which would be expected from linear elastic wave propagation.

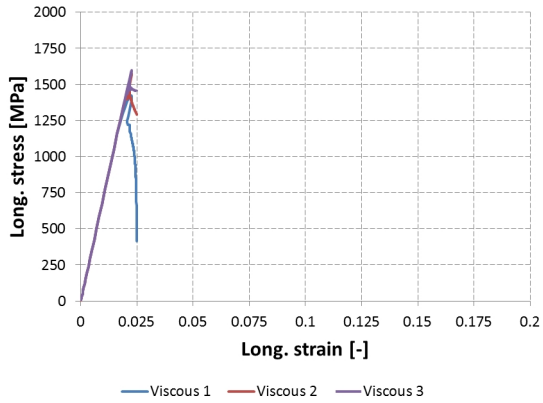

Figure 101: Numerical results for long. stress-long. strain relationship in viscous case with varying viscosity coefficient

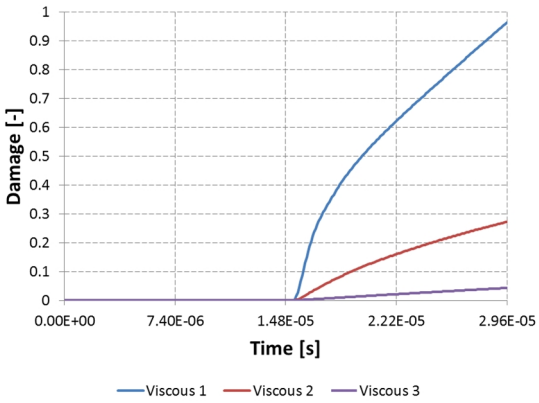

Figure 102: Numerical results for damage in softening element in viscous case with varying viscosity coefficient

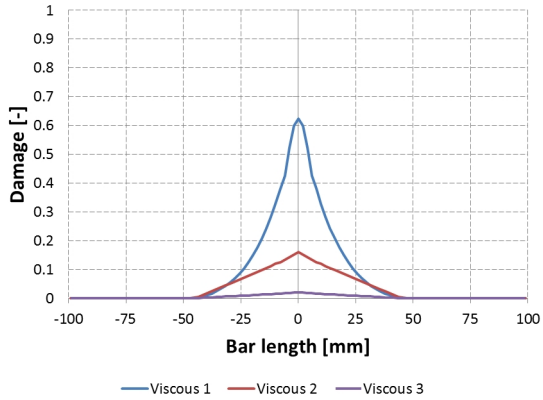

Figure 103: Numerical results for damage in viscous case with varying viscosity coefficient at $t = 3/4 \cdot 2L/c_e$

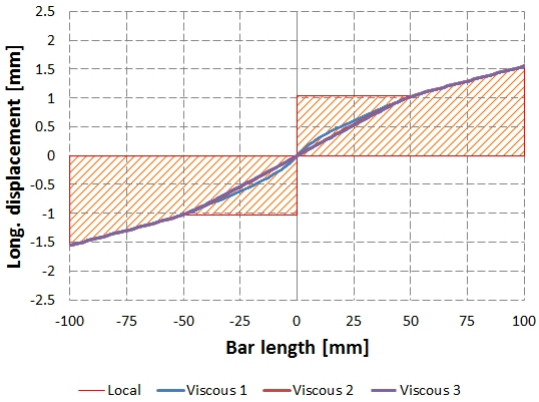

Figure 104: Numerical results for longitudinal displacement in viscous case with varying viscosity coefficient at $t = 3/4 \cdot 2L/c_e$

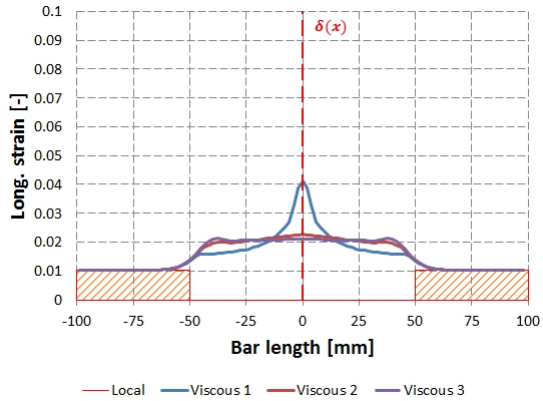

Figure 105: Numerical results for longitudinal strain in viscous case with varying viscosity coefficient at $t = 3/4 \cdot 2L/c_e$

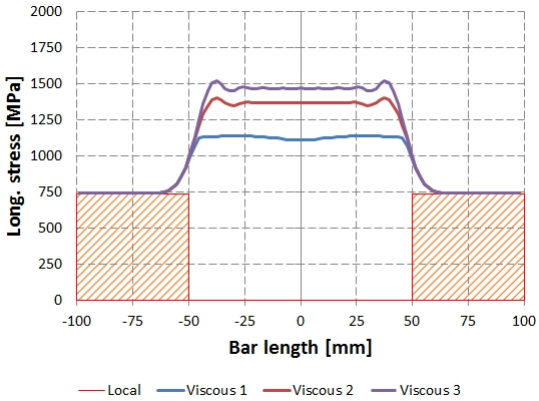

Figure 106: Numerical results for longitudinal stress in viscous case with varying viscosity coefficient at $t = 3/4 \cdot 2L/c_e$

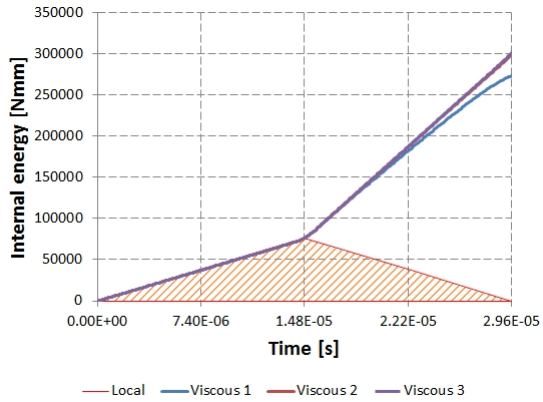

Figure 107: Numerical results for internal energy in viscous case with varying viscosity coefficient for $0 \leq t \leq 2 \cdot L/c_e$

The experiments conducted in this subsection were meant to evaluate a readily available viscous regularisation scheme in ABAQUS. A composite CDM model is available in ABAQUS which was tested first and showed strain-softening behaviour. The results showed non-physical behaviour associated with softening and results were

dependent on the chosen spatial discretisation. These problems occur due to a negative stiffness in the strain-softening domain.

In the next step the viscous regularisation scheme in ABAQUS was used in conjunction with the local composite CDM model. Viscous regularisation schemes keep the tangent stiffness tensor positive for sufficiently small time increments. Therefore, the localisation process and the mesh dependency of results can be controlled by setting an appropriate rate-sensitivity parameter. However, the regularisation scheme over-stiffens the stress-strain response in a way that keeps its behaviour linear elastic. The achieved results for damage, displacement, strain, stress and internal energy do not show mesh-sensitivity of results; however, this was expected from the stress-strain results which did not show a negative tangent stiffness. The results were similar to results which would be obtained with linear elastic wave propagation and did not show a development of a distinct localisation zone in which the size is governed by the viscous regularisation scheme.

4.4 Summary

This chapter aimed to evaluate LS-DYNA composite material models. The implemented failure theory for 3D elements was of special interest as well as the operational mode of the implemented CDM approach in MAT_058. Especially the default setting of the implemented material softening parameter m was of importance.

This study successfully evaluated the 3D failure criteria of MAT_022 and MAT_059. It was found that MAT_022 utilises a delamination criterion and MAT_059 is based on an extensions of Chang-Chang failure criteria to 3D by Cheng and Hallquist [25]. As well it was found that the capabilities of MAT_022 are limited in 2D and 3D cases in comparison to MAT_059 because failure criteria for longitudinal compression (in 2D and 3D), and transverse and normal compression (in 3D) are not implemented. MAT_059 includes the full set of failure criteria.

The 2D failure criteria MAT_054 and MAT_055 were evaluated too. It was found that their failure theory is well described in the LS-DYNA User's Manual [70] and that the implementation agrees well with the Chang-Chang criteria and the Tsai-Wu criterion.

It was possible to gain certainty about the CDM theory behind MAT_059. This model is based on an anisotropic damage model for fibrous composites by Matzenmiller et al. [81]. The maximum stress is defined by a modification of Hashin's 2D failure criteria.

The degeneration of strengths is described with an exponential damage law. The shape of the stress-strain curve of MAT_059 is dominated by a softening parameter m. This parameter is hardwired in MAT_059 with a value of m = 10 which correlates to a brittle material behaviour.

Table 4-4 summarises the above stated failure and damage theories identified for the composite material models implemented in LS-DYNA.

Table 4-4: Summary of implemented failure and damage theory in LS-DYNA composite models MAT_022, MAT_054/055 and MAT_059

Material №	**Model behaviour**		**2D**			**3D**	
	Failure	Damage	Matzenmiller et al. [81]	Chang-Chang [23; 24]	Tsai-Wu [113]	Delam. criterion [68]	Cheng and Hallquist [25]
22	✓	-	-	✓	-	✓	-
54	✓	-	-	✓	-	-	-
55	✓	-	-	✓	✓	-	-
58	-	✓	✓	-	-	-	-
59	✓	-	-	✓	-	-	✓

In a next step numerical results for CDM models with strain-softening were evaluated. The example of longitudinal wave propagation in a bar, first introduced by Bažant and Belytschko [6] in the context of strain-softening, was evaluated. This example allowed the comparison of numerical results to the analytical solution obtained for the same problem in Chapter 3. The anisotropic CDM model by [81], which is implemented as MAT_058 in the commercial code LS-DYNA, was used for the investigation. It was shown that strain-softening leads to severe numerical instabilities which result in spurious mesh-sensitivity of results and non-physical results. The results obtained for displacement, strain, stress and internal energy followed well the analytical predictions made by [6].

Lastly, readily available strain-softening stabilisation schemes in LS-DYNA an ABAQUS were tested. These models address numerical instabilities and non-physical results due to a negative tangent stiffness during strain-softening. It was expected that the regularisation schemes would remove mesh-sensitivity due to strain-softening and would lead to a confined area of damage evolution. The results obtained with the nonlocal and viscous methods were not sensitive to the spatial discretisation; however, the methods prevented the stress-strain behaviour from strain-softening in the first place. The nonlocal option in LS-DYNA kept a plastic material behaviour and the viscous regularisation scheme in ABAQUS over stiffened the material behaviour.

5 Regularisation Methods

Strain localisation due to damage is for engineering materials a process leading ultimately to failure which cannot be neglected. Therefore, there is high demand for computational methods which are able to model strain localisation properly in a physical and mathematical sense. However, the correct modelling of the strain localisation zone proved to be cumbersome as it was shown in Chapter 3 and 4.

Generally, mechanical behaviour of solids is investigated within the continuum mechanics framework which considers a continuous displacement field on the macroscopic scale; however, strain-softening is associated with a discontinuous displacement field. There are two main branches dealing with these discontinuities: the discrete approach and the continuum approach. The discrete methods are related to fracture mechanics. The area with discontinuities is modelled by special constitutive equations capturing the jump in the displacement field while the rest of the material is modelled with standard continuum constitutive equations. A common example of discrete methods is the cohesive method. The continuum approach applies the concept of stress and strain to all parts, with or without discontinuities. The representation of the discontinuity is achieved either by applying methods in which the strain localisation zone is defined by specialised constitutive equations or by a characteristic length which keeps the boundary value problem stable. Typical examples for the group of continuum approaches are the smeared crack method, Gurson model, nonlocal integral regularisation, gradient-enhanced regularisation and viscous regularisation.

This chapter will start with a review on cohesive method, smeared crack method and Gurson damage model. However, this is intended as an overview only as these methods do not address the issue of an ill-posed boundary value problem due to strain-softening, which is the focus of this work.

Then regularisation methods, which deal with the ill-posed boundary value problem, namely nonlocal, gradient-enhanced and viscous method, will be reviewed. These methods introduce higher-order terms of space and time into constitutive equations which maintain a well-posed boundary value problem. This property of regularisation properties is of interest in this work. Therefore, regularisation methods will be dealt with in more detail. In this the focus lies on the influence of higher-order terms on the boundary value problem.

5.1 Overview of Computational Methods Addressing Strain-Softening

5.1.1 Cohesive Method

The first theories regarding the cohesive method reach back five decades ago when Barenblatt [4] introduced the concept of a cohesive force for cracks in brittle solids. Another method now regarded as cohesive method is the strip yield zone model by Dugdale [32] in which he investigated the size of plastic zones near crack tips in steel sheets. The cohesive method as it is known now and was brought into connection with FE was first described by Hillerborg et al. [45] in 1976. This work is based on Barenblatt's work and utilises the concept of cohesive traction and fracture energy during the crack opening process.

The discrete cohesive zone approach aims to combine fracture mechanics with FE modelling. The idea is that strain-softening is confined to an area which is much smaller than the rest of the structure and therefore the strain-softening area can be simplified as a crack. In this method the process of failure is confined in a zone which is modelled with interface elements, the cohesive zone, connected to a crack tip. The cohesive elements are of vanishing thickness and are modelled using cohesive constitutive laws which relate the so-called cohesive traction to the fracture displacement. The cohesive traction prevents the crack opening as long as the ultimate strength of the material has not been reached. Once the ultimate strength of the material is reached the cohesive traction will gradually decrease and will allow the crack to grow. The vanishing of the cohesive traction coincides with fracture. The cohesive zone is embedded between continuum elements and defines the fracture path. Elements embedding the cohesive zone are modelled with standard continuum constitutive laws.

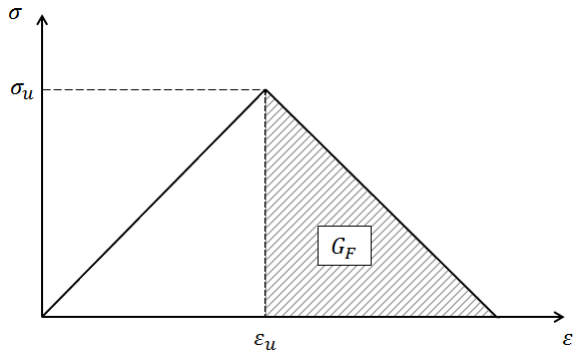

Figure 108: Constitutive law of cohesive method

Two assumptions are necessary for the cohesive method. Firstly, fracture in the cohesive zone does not start until the ultimate strength f_t of the material is reached. Secondly, after f_t is reached the material is damaged but is still capable of transferring stresses. The stresses in the damage process decreases with increasing crack opening displacement and the separation work G_c, also called fracture energy, needed to open the crack is defined by the area under the stress-strain diagram (see Figure 108).

$$G_c = \int \sigma du \tag{5-1}$$

with σ being the stress and u the relative displacement in the fracture zone.

The cohesive method has been applied successfully to investigate the material failure in softening materials. In these models the nonlinear softening behaviour is restricted to a narrow area modelled with cohesive elements. The cohesive method is capable of modelling the failing of a material in a physically manner as a sizing effect is considered for the crack zone. However, the path of crack propagation and occurrence of the displacement discontinuity needs to be known beforehand. Another drawback is that these methods are computationally costly [38].

5.1.2 Smeared Crack Method

The smeared crack method, which is related to the cohesive method, was proposed by Bažant and Oh [8]. However, it takes the cohesive method from a discrete method to a continuum method by continuously distributing (smearing) the fracture energy G_c over a band which has the width of a finite element. The width of the element represents the localisation zone of the crack.

$$G_c = \int \int \sigma d\varepsilon\,(x) dx \tag{5-2}$$

with x being the coordinate which is orthogonal to the crack.

The width of a smeared crack element is designated with w. w can be used to define the fracture energy by means of the energy dissipation per unit volume g_c.

$$G_c = w g_c \tag{5-3}$$

with

$$g_c = \int \sigma d\varepsilon \tag{5-4}$$

The element length w acts as the characteristic length of the crack. The characteristic length leads to the convergence of results even in the strain-softening area, making it insensitive to the spatial discretisation.

It has been shown that the smeared crack method achieves convergence of results, insensitive to the mesh discretisation, and results are physical [27; 28]. However, there are concerns regarding the objectivity of results due to the problem of mesh refinement. If the size of the crack zone is estimated wrong the energy dissipated will be wrong and with this the results will be without physical relevance. Another issue with this method is that the ill-posedness of the boundary value problem due to strain-softening is not addressed.

5.1.3 Gurson Model

The Gurson model [40; 84; 115-117] is a micromechanically motivated damage model first introduced by Gurson [40], and further developed by Needleman and Tvergaard [84] to the Gurson-Tvergaard-Needleman (GTN) model, for modelling ductile porous materials. The model considers the nucleation, coalescence and growth of voids as influence on the constitutive material behaviour, and builds therefore a bridge between continuum description and micromechanical damage behaviour. The Gurson model considers macromechanical strain-softening material behaviour as a consequence of increasing porosity in a material.

The Gurson model incorporates a homogenisation method to derive a pressure dependent yield function ϕ from a void in a continuum which links micromechanical void nucleation and growth with the macromechanical plasticity. In this the void volume fraction f is used as damage parameter.

$$\phi = \frac{\sigma_{eq}^2}{\sigma_0^2} + 2f^* cosh\left(\frac{3\sigma_m}{2\sigma_0}\right) - \left(1 + \left(f^{*2}\right)\right) = 0 \tag{5-5}$$

in which σ_{eq} is the macroscopic equivalent Von Mises stress, σ_0 is the microscopic yield stress of the undamaged material and σ_m is the macroscopic mean normal stress.

f^* is a function depending on the void growth fraction f. f^*, introduced by Tvergaard and Needleman [117], is used to take into account the loss of load-carrying capacity due to void coalescence.

$$f^*(f) = \begin{cases} f & , \quad for \quad f \leq f_c \\ f_c + \dfrac{f_u^* - f_c}{f_F - f_c}(f - f_c) & , \quad for \quad f > f_c \end{cases} \tag{5-6}$$

in which f_c is the critical void fraction for the onset of void coalescence which accelerates the increase of the void fraction, f_F is marking the void fraction at failure and f_u^* is the ultimate value of the damage parameter.

The macroscopic plastic strain is found in dependence on the yield function:

$$\varepsilon_{pl} = \dot{\lambda}\frac{\partial \phi}{\partial \sigma} \tag{5-7}$$

where $\dot{\lambda}$ is the Lagrange multiplier.

The rate of increase for the void fraction in the Gurson model depends on the growth of voids as well as on the nucleation of voids. The nucleation is determined by plastic strain experienced by the material.

$$\dot{f} = \dot{f}_{growth} + \dot{f}_{nucleation} \tag{5-8}$$

The Gurson model builds the bridge between the microstructure and constitutive equation which is missing in many CDM models; however, the inclusion of void fraction in the Gurson model leads finally to strain-softening. The implementation of this model in numerical codes will eventually lead to a loss of material stability and leaves the boundary value problem ill-posed. Therefore spurious mesh-sensitivity will occur in numerical simulations.

5.2 Regularisation Methods

5.2.1 Nonlocal Regularisation

In local theory stress only depends on the deformation history of a single point x_i. Nonlocal theory considers additionally the influence of the deformation of surrounding points ξ_i in a RVE. This is done by substituting the local variable $\eta(x_i)$ by a weighted average $\bar{\eta}(x_i)$ of the variable within the point's spatial neighbourhood.

Two main groups of nonlocal theory exists: integral methods [10; 52; 108] and gradient-enhanced methods [54; 93].

5.2.1.1 Integral Method

In nonlocal damage theory a local variable is substituted by a weighted average of the state variables over a point's spatial neighbourhood. The elastic area of the material behaviour is still treated as local and the averaging procedure just applies to variables which contribute to strain-softening [10]. The mathematical model introduces a so-called localisation limiter to restrain the softening region to a finite size [108]. The transformation rule to transform a local field $\eta(x_i)$ into a nonlocal field $\bar{\eta}(x_i)$ is:

$$\bar{\eta}(x_i) = \int_V \alpha(x_i, \xi_i)\eta(\xi_i)\, d\xi_i \tag{5-9}$$

$\alpha(x_i, \xi_i)$ represents a weighting function which determines the average of a local state variable in the spatial domain V. It only depends on the distance between the points x_i and ξ_i. x_i is called the "receiver" point and ξ_i the "source" point [53] (see Figure 109). Using this concept the weighting function will reduce smoothly with decreasing distance to x_i.

$$r = \|x_i - \xi_i\| \tag{5-10}$$

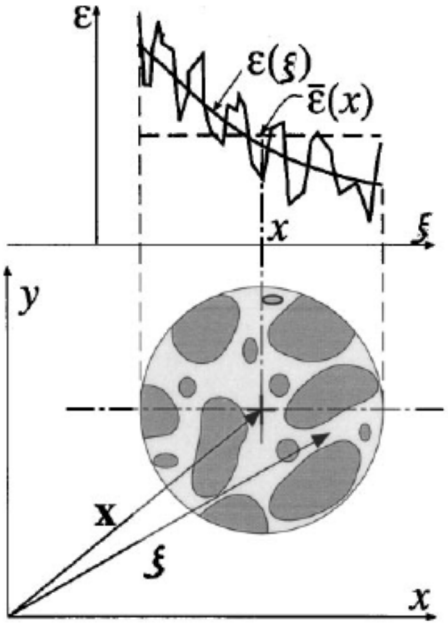

Figure 109: RVE for averaging technique and strain averaging over RVE [7]

The averaging procedure is defined by the distance l between the local point and its surrounding. This distance is called the internal length. It is understood as a material

property which defines the size of heterogeneities on the microscale. The averaging function $\alpha(x_i, \xi_i)$ can be expressed by the Gaussian function or a quartic function. The Gauss function is used in general and reads:

$$\alpha(r) = \alpha(\|x_i - \xi_i\|) = \frac{1}{(2\pi)^{3/2} l^3} exp\left(-\frac{r^2}{2l^2}\right) \tag{5-11}$$

The Gaussian function allows the interaction between any possible points as no interaction radius is defined ("unbounded support"). Therefore, the interaction radius can be assumed to be infinite. The exponential function in (5-11) will decrease rapidly for values $r > 2l$, thus the weighting function is set to zero in these cases.

5.2.1.2 Gradient-Enhanced Method

The gradient enhanced theory is derived as an approximation of the nonlocal integral theory. It uses differential operators instead of weighted spatial averages.

Two classes of gradient-enhanced methods are distinguished: explicit [89; 93] and implicit [92; 93].

- Explicit models: Gradients of local variables are introduced in governing equations directly. Therefore the stress response depends on the material point and its vicinity. However, the vicinity can be small.
- Implicit models: Higher-order differential terms are not introduced in governing equations directly. The differential operators are not applied to the local variables, they rather define a nonlocal field.

5.2.1.2.1 Explicit models

The gradient-enhanced method expands the local variable $\eta(x_i)$ in the weighted average in (5-9) through a Taylor expansion. Therefore, a link between nonlocal and gradient-enhanced theory is established. The expansion is combined with the Gauss distribution in (5-11) and odd terms are dropped. The expression for the nonlocal variable $\bar{\eta}(x_i)$ reads:

$$\bar{\eta}(x_i) = \eta(x_i) + c\nabla^2\eta(x_i) + d\nabla^4\eta(x_i) + \cdots \tag{5-12}$$

Terms higher than two are neglected. The term c in (5-12) is determined by the weighting function as $c = 1/2 \cdot l^2$.

$$\bar{\eta}(x_i) = \eta(x_i) + c\nabla^2\eta(x_i) \tag{5-13}$$

Although the second gradient introduces a spatial interaction to constitutive models, the 2nd order derivative is still a local measure. Hence, the explicit gradient formulation is local in a mathematical sense.

(5-13) depends on a 2nd order derivative which alters the order of the equation of motion. Therefore an extra boundary conditions needs to be provided. The simplest way to do so is to use the natural boundary conditions: [92; 93]

$$\frac{\partial \overline{\eta}}{\partial n} \equiv n_i \frac{\partial \overline{\eta}}{\partial x_i} = 0 \tag{5-14}$$

5.2.1.2.2 Implicit models

The implicit expression is based on the explicit gradient-enhanced model in (5-13). (5-13) is differentiated with respect to x and rearranged with respect to the local variable $\eta(x_i)$. Terms higher than order two are neglected.

$$\eta(x_i) = \bar{\eta}(x_i) - c\nabla^2\bar{\eta}(x_i) \tag{5-15}$$

Constitutive models including (5-15) depend now on nonlocal measures. As it was the case for the explicit expression, an additional boundary condition needs to be applied (see Equation (5-14)).

5.2.2 Viscous Regularisation

The viscous regularisation method is entirely different to the nonlocal regularisation because higher-order time derivatives, called rate-effects, are included to constitutive equations. These rate-effects account for the increased strain-rate during failure.

$$\sigma = f(\varepsilon_{cr}) + m\dot{\varepsilon}_{cr} \tag{5-16}$$

(5-16) represents the connection of a crack model with rate-effects [109]. Rate-effects are only applied to the crack strain ε_{cr} and m defines the rate-sensitivity of the material on ε_{cr}. $f(\varepsilon_{cr})$ is the material's softening function.

According to Sluys and de Borst [109] viscous regularisation introduces implicitly an internal length scale l. The internal length scale is derived from the damping coefficient α of the system. Sluys and de Borst investigate the dependence of α on the angular frequency ω of the system. They discovered that α reaches a limiting value l^{-1} which represents the internal length scale.

$$\lim_{\omega \to \infty} \alpha(\omega) = l^{-1} \quad with \quad l = \frac{2mc_e}{E} \tag{5-17}$$

where E is the Young's modulus and c_e is the elastic speed of sound.

The viscous regularisation method accounts for the increased strain-rate in the localisation zone. The regularisation effect is based on the viscous model's capability to smooth the transition between elastic and inelastic behaviour and keep the tangent stiffness tensor positive for sufficiently small time increments.

5.3 Influence of Regularisation Methods on the Type of PDEs

This subsection aims to show the effect of regularisation methods on the type of PDEs in contrast to a local constitutive model. The PDEs in regularised dynamic problems are supposed to stay hyperbolic in the strain-softening domain to ensure a well-posed boundary value problem.

The case of longitudinal wave propagation is chosen as an example for dynamic loading (as presented in Chapter 3). Solutions for the local and nonlocal continua were discussed by Peerlings and co-workers in [89; 90; 92]. The application of viscous regularisation in a 1D tension case was demonstrated by Sluys and de Borst [109].

The constitutive equation for quasibrittle damage includes the damage variable ω.

$$\sigma = (1 - \omega) E \varepsilon \tag{5-18}$$

The equation of motion for the dynamic problem is the wave equation. It reads for a 1D bar wave propagation problem:

$$\frac{\partial \sigma}{\partial x} = \rho \frac{\partial v}{\partial t} \tag{5-19}$$

The axial stress is described by σ (in x-direction), ρ is the material density and v is the velocity.

A kinematic equation is needed to establish a relationship between strain and displacement. Expressed in rate format the kinematic equation reads:

$$\frac{\partial \varepsilon}{\partial t} - \frac{\partial v}{\partial x} = 0 \tag{5-20}$$

Figure 14 shows a qualitative representation of a linear strain-softening law. κ is a history variable which represents deformation history. The strain equal to κ_i denotes the limit of the linear elastic region. κ_c denotes the point at which the material losses its complete load-carrying capability.

$$D = \begin{cases} \frac{\kappa_c}{\kappa}\frac{\kappa - \kappa_i}{\kappa_c - \kappa_i} & if\ \kappa_i < \kappa \leq \kappa_c \\ 1 & if\ \kappa \geq \kappa_c \end{cases} \tag{5-21}$$

with the tangent modulus

$$\frac{\partial \sigma}{\partial \varepsilon} = E\left(1 - D - \frac{\partial D}{\partial \kappa}\varepsilon\right) = -\frac{E\kappa_i}{\kappa_c - \kappa_i} \tag{5-22}$$

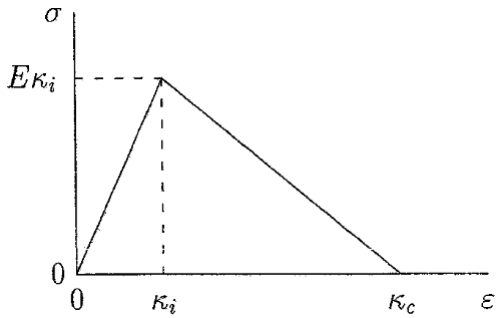

Figure 110: Local damage stress-strain relationship [89]

The combination of the wave equation (5-19) and the kinematic relation (5-20) leads to a system of PDEs. Further analysis in terms of eigenvalues gives information about the type of the PDEs. In a dynamic problem the PDEs need to be hyperbolic to obtain a well-posed boundary value problem.

Further investigation of the equation of motion gives important information about the wave propagation behaviour in the softening zone. For the solution of the equation of motion a single harmonic wave is assumed. $\underline{\hat{u}}$ is the amplitude, k is the wave number and c the phase velocity.

$$\delta \underline{u} = \underline{\hat{u}} exp(ik(x - ct)) \tag{5-23}$$

Wave propagation will be dispersive when the phase velocity c depends on the wave number k. A dispersive wave speed is needed to enable a transformation of loading waves in the strain-softening zone.

5.3.1 Local Method

A scalar valued loading function f needs to be defined when a damage model is used. This function can have values equal or smaller than zero. A value of zero defines the materials elastic limit and is needed for damage to propagate.

$$f(\varepsilon, \kappa) = \varepsilon - \kappa \tag{5-24}$$

The damage criterion is defined by the Kuhn-Tucker conditions:

$$f\dot{\kappa} = 0, \qquad f \leq 0, \qquad \dot{\kappa} \geq 0 \tag{5-25}$$

A substitution of (5-18) in the wave equation (5-19) leads to:

$$\left(1 - \omega - \frac{\partial \omega}{\partial \kappa}\varepsilon\right)\frac{\partial \varepsilon}{\partial x} - \frac{1}{c_e^2}\frac{\partial v}{\partial t} = 0 \tag{5-26}$$

A combination of (5-26) with the kinematic relation in (5-20) leads to a system of PDEs which can be investigated in terms of its eigenvalues.

$$\begin{pmatrix} -\frac{1}{c_e^2}\frac{\partial v}{\partial t} \\ \frac{\partial \varepsilon}{\partial t} \end{pmatrix} + \begin{pmatrix} \left(1 - \omega - \frac{\partial \omega}{\partial \kappa}\varepsilon\right)\frac{\partial \varepsilon}{\partial x} \\ -\frac{\partial v}{\partial x} \end{pmatrix} = \begin{pmatrix} 0 \\ 0 \end{pmatrix} \tag{5-27}$$

The variables for velocity and strain are combined in vector form:

$$\underline{u} = \begin{pmatrix} v \\ \varepsilon \end{pmatrix} \tag{5-28}$$

Therefore, the equation of motion (5-27) can be expressed as in (5-29). This system of PDEs is nonlinear. As a linear softening law has been used, the system of PDEs can be assumed to be linear.

$$\underline{\underline{P}}(\underline{u})\frac{\partial \underline{u}}{\partial t} + \underline{\underline{Q}}(\underline{u})\frac{\partial \underline{u}}{\partial x} = \underline{r}(\underline{u}) \tag{5-29}$$

with

$$\underline{\underline{P}}(\underline{u}) = \begin{pmatrix} -\frac{1}{c_e^2} & 0 \\ 0 & 1 \end{pmatrix}$$

$$\underline{\underline{Q}}(\underline{u}) = \begin{pmatrix} 0 & 1 - \omega - \frac{\partial \omega}{\partial \kappa}\varepsilon \\ -1 & 0 \end{pmatrix}$$

$$\underline{r}(\underline{u}) = \begin{pmatrix} 0 \\ 0 \end{pmatrix}$$

To define the type of the PDE in (5-29) the eigenproblem, defined in (5-30), needs to be solved. The eigenvalues $\lambda_{1,2}$ of the system define the characteristic directions in the space-time coordinates.

$$\underline{w}\left(\underline{\underline{P}} - \lambda \underline{\underline{Q}}\right) = \underline{0} \tag{5-30}$$

The local model has two imaginary eigenvalues λ and the slope of the characteristic lines is defined by $\frac{dx}{dt} = \frac{1}{\lambda}$:

$$\lambda_{1,2} = \pm \frac{1}{c_e \sqrt{1 - \omega - \frac{\partial \omega}{\partial \kappa} \varepsilon}} \tag{5-31}$$

In case of the local softening continuum the two eigenvalues are imaginary. Therefore, the set of PDEs has an elliptic type. Outside the softening domain damage is not progressing which means that $\frac{\partial \omega}{\partial \kappa} \varepsilon$ is zero in (5-31). Hence, the domains outside the softening zone stay hyperbolic and the overall boundary value problem is ill-posed. In case of $\omega = 1$ outside the softening zone the PDEs have a parabolic type [89]. An analysis of this problem is not performed because $\omega = 1$ coincides with complete fracture of the material.

The equation of motion in (5-29) is normally nonlinear. It is common to linearize it to enable explicit solutions. Deformation is assumed to be infinitesimal small and the equation of motion can be assumed homogeneous. The homogeneous equilibrium is defined by ε_0, ω_0 and σ_0.

$$\delta \underline{u} = \underline{u} - \underline{u}_0 \tag{5-32}$$

$$\underline{\underline{P}}(\underline{u}_0) \frac{\partial(\delta \underline{u})}{\partial t} + \underline{\underline{Q}}(\underline{u}_0) \frac{\partial(\delta \underline{u})}{\partial x} - \left(\frac{\partial \underline{r}}{\partial \underline{u}}\right)_0 \delta \underline{u} = 0 \tag{5-33}$$

From (5-32) and (5-23) it follows:

$$\underline{\hat{u}} \exp\big(ik(x - ct)\big) \left(-ikc \underline{\underline{P}}(\underline{u}_0) + ik \underline{\underline{Q}}(\underline{u}_0) - \underbrace{\left(\frac{\partial \underline{r}}{\partial \underline{u}}\right)_0}_{=0} \right) = 0 \tag{5-34}$$

To find a non-trivial solution the determinant of the system needs to be zero. From this the phase velocity of the wave can be determined.

$$det\left(-ikc\underline{\underline{P}}(\underline{u}_0) + ik\underline{\underline{Q}}(\underline{u}_0)\right) = 0 \tag{5-35}$$

$$\Rightarrow\ c = c_e\sqrt{1-\omega_0-\left(\frac{\partial\omega}{\partial\kappa}\right)_0\varepsilon_0} \tag{5-36}$$

The wave velocity for the local softening continuum is imaginary for any wave number because it is non-dispersive. Therefore loading waves cannot propagate in the softening zone and the perturbation $\delta\underline{u}$ can grow.

5.3.2 Nonlocal Regularisation Methods

5.3.2.1 Integral Method

Damage evolution in a nonlocal integral continuum depends on the deformation at a point and on the vicinity of this point. Therefore a weighted average of the local strain is applied to the damage evolution.

$$\overline{\varepsilon} = \varepsilon\, exp\left(-\frac{1}{2}k^2l^2\right) \tag{5-37}$$

The evolution of the history variable depends on the weighted average of strain:

$$\dot{\kappa}(\overline{\varepsilon}-\kappa) = 0, \qquad \overline{\varepsilon}-\kappa \le 0, \qquad \dot{\kappa} \ge 0 \tag{5-38}$$

The inclusion of the weighted average in the constitutive equation (5-18) and wave equation (5-19) leads to:

$$(1-\omega)\frac{\partial\varepsilon}{\partial x} - \frac{\partial\omega}{\partial\kappa}\varepsilon\frac{\partial\varepsilon}{\partial x}exp\left(-\frac{1}{2}k^2l^2\right) - \frac{1}{c_e^2}\frac{\partial v}{\partial t} = 0 \tag{5-39}$$

A combination of (5-39) with the kinematic relation in (5-20) leads to a system of PDEs:

$$\begin{pmatrix} -\dfrac{1}{c_e^2}\dfrac{\partial v}{\partial t} \\ \dfrac{\partial\varepsilon}{\partial t} \end{pmatrix} + \begin{pmatrix} (1-\omega)\dfrac{\partial\varepsilon}{\partial x} - \varepsilon\dfrac{\partial\omega}{\partial\kappa}\dfrac{\partial\varepsilon}{\partial x}e^{-\frac{1}{2}k^2l^2} \\ -\dfrac{\partial v}{\partial x} \end{pmatrix} = \begin{pmatrix} 0 \\ 0 \end{pmatrix} \tag{5-40}$$

The variables for velocity and strain are combined in vector form:

$$\underline{u} = \begin{pmatrix} v \\ \varepsilon \end{pmatrix} \tag{5-41}$$

The equation of motion can be summarised as follows:

$$\underline{\underline{P}}(\underline{u})\frac{\partial \underline{u}}{\partial t} + \underline{\underline{Q}}(\underline{u})\frac{\partial \underline{u}}{\partial x} = \underline{r}(\underline{u}) \tag{5-42}$$

with

$$\underline{\underline{P}}(\underline{u}) = \begin{pmatrix} -\frac{1}{c_e^2} & 0 \\ 0 & 1 \end{pmatrix}$$

$$\underline{\underline{Q}}(\underline{u}) = \begin{pmatrix} 0 & -\varepsilon\frac{\partial \omega}{\partial \kappa}e^{-\frac{1}{2}k^2l^2} \\ -1 & 0 \end{pmatrix}$$

The system has two real linear independent eigenvalues. The system of PDEs stays hyperbolic with a dispersive phase velocity, even in the softening zone.

$$\lambda_{1,2} = \frac{\pm 1}{c_e\sqrt{1-\omega-\varepsilon\frac{\partial \omega}{\partial \kappa}exp\left(-\frac{1}{2}k^2l^2\right)}} \tag{5-43}$$

$$c = c_e\sqrt{1-\omega-\varepsilon\frac{\partial \omega}{\partial \kappa}exp\left(-\frac{1}{2}k^2l^2\right)} \tag{5-44}$$

The non-trivial solution of the problem leads to a dispersive velocity which stays real as long as the wave number k does not go under the critical wave number k_c.

$$k_c = \frac{1}{l}\sqrt{2ln\left(\frac{\left(\frac{\partial \omega}{\partial \kappa}\right)\varepsilon}{1-\varepsilon}\right)} \tag{5-45}$$

5.3.2.2 Gradient-Enhanced Method

5.3.2.2.1 Explicit

The differential equation in (5-46) represents the explicit enrichment of the constitutive equations with higher-order gradient terms of the strain.

$$\bar{\varepsilon} = \varepsilon + \frac{1}{2}l^2\frac{\partial^2 \varepsilon}{\partial x^2} \tag{5-46}$$

The evolution of the history variable is an explicit function of the nonlocal strain $\bar{\varepsilon}$. The 2nd order derivative will be a local measure.

$$\dot{\kappa}(\bar{\varepsilon} - \kappa) = 0, \qquad \bar{\varepsilon} - \kappa \leq 0, \qquad \dot{\kappa} \geq 0 \tag{5-47}$$

The inclusion of the enrichment in the constitutive equation (5-18) and wave equation (5-19) leads to:

$$(1-\omega)\frac{\partial \varepsilon}{\partial x} - \frac{\partial \omega}{\partial \kappa}\varepsilon\frac{\partial \bar{\varepsilon}}{\partial x} - \frac{1}{c_e^2}\frac{\partial v}{\partial t} = 0 \tag{5-48}$$

The definition of the gradient-enrichment is split to enable an analysis of the equation of motion.

$$\bar{\varepsilon} = \varepsilon + \frac{1}{2}l^2\frac{\partial^2 \varepsilon}{\partial x^2} \tag{5-49}$$

with

$$p = \frac{\partial \varepsilon}{\partial x} \tag{5-50}$$

and

$$\bar{\varepsilon} - \varepsilon = \frac{1}{2}l^2\frac{\partial^2 \varepsilon}{\partial x^2} \tag{5-51}$$

The combination of (5-48), (5-50), (5-51) and the kinematic equation (5-20) leads to the following system of PDEs:

$$\begin{pmatrix} -\frac{1}{c_e^2}\frac{\partial v}{\partial t} \\ \frac{\partial \varepsilon}{\partial t} \\ 0 \\ 0 \end{pmatrix} + \begin{pmatrix} (1-\omega)\frac{\partial \varepsilon}{\partial x} - \varepsilon\frac{\partial \omega}{\partial \kappa}\frac{\partial \bar{\varepsilon}}{\partial x} \\ -\frac{\partial v}{\partial x} \\ \frac{1}{2}l^2\frac{\partial \varepsilon}{\partial x} \\ \frac{\partial \varepsilon}{\partial x} \end{pmatrix} = \begin{pmatrix} 0 \\ 0 \\ \bar{\varepsilon} - \varepsilon \\ p \end{pmatrix} \tag{5-52}$$

The variables for velocity, strain, nonlocal strain and strain derivative are combined in vector form:

$$\underline{u} = \begin{pmatrix} v \\ \varepsilon \\ \bar{\varepsilon} \\ p \end{pmatrix} \tag{5-53}$$

Therefore, the equation of motion can be summarised in the same way as the local equation of motion.

$$\underline{\underline{P}}(\underline{u})\frac{\partial \underline{u}}{\partial t} + \underline{\underline{Q}}(\underline{u})\frac{\partial \underline{u}}{\partial x} = \underline{r}(\underline{u}) \tag{5-54}$$

with

$$\underline{\underline{P}}(\underline{u}) = \begin{pmatrix} -\frac{1}{c_e^2} & 0 & 0 & 0 \\ 0 & 1 & 0 & 0 \\ 0 & 0 & 0 & 0 \\ 0 & 0 & 0 & 0 \end{pmatrix}$$

$$\underline{\underline{Q}}(\underline{u}) = \begin{pmatrix} 0 & 1-\omega & -\frac{\partial D\omega}{\partial \kappa}\varepsilon & 0 \\ -1 & 0 & 0 & 0 \\ 0 & 0 & 0 & \frac{1}{2}l^2 \\ 0 & 1 & 0 & 0 \end{pmatrix}$$

$$\underline{r}(\underline{u}) = \begin{pmatrix} 0 \\ 0 \\ \bar{\varepsilon} - \varepsilon \\ p \end{pmatrix}$$

The system has two real linear independent eigenvalues. The system of PDEs stays hyperbolic with a dispersive phase velocity, even in the softening zone.

$$\lambda_{1,2,3,4} = \sqrt[4]{0} \tag{5-55}$$

$$c = c_e\sqrt{1-\omega-\left(\frac{\partial \omega}{\partial \kappa}\right)\varepsilon\left(1-\frac{1}{2}l^2k^2\right)} \tag{5-56}$$

The non-trivial solution of the problem leads to a dispersive velocity which stays real as long as the wave number k does not go under the critical wave number k_c.

$$k_c = \frac{1}{l}\sqrt{2\left(1-\frac{1-\omega}{\left(\frac{\partial \omega}{\partial \kappa}\right)\varepsilon}\right)} \tag{5-57}$$

5.3.2.2.2 Implicit

The differential equation in (5-58) represents the implicit enrichment of the constitutive equations with higher gradient terms of strain.

$$\varepsilon = \overline{\varepsilon} - \frac{1}{2} l^2 \frac{\partial^2 \overline{\varepsilon}}{\partial x^2} \tag{5-58}$$

The Kuhn-Tucker relations are expressed in dependence on the nonlocal strain:

$$\dot{\kappa}(\overline{\varepsilon} - \kappa) = 0, \qquad \overline{\varepsilon} - \kappa \leq 0, \qquad \dot{\kappa} \geq 0 \tag{5-59}$$

The inclusion of the enrichment in the constitutive equation (5-18) and wave equation (5-19) leads to:

$$(1 - \omega) \frac{\partial \varepsilon}{\partial x} - \frac{\partial \omega}{\partial \kappa} \varepsilon \frac{\partial \varepsilon}{\partial x} - \frac{1}{c_e^2} \frac{\partial v}{\partial t} = 0 \tag{5-60}$$

The definition of the implicit gradient enrichment is split to enable an analysis of the equation of motion.

$$\varepsilon = \overline{\varepsilon} - \frac{1}{2} l^2 \frac{\partial^2 \overline{\varepsilon}}{\partial x^2} \tag{5-61}$$

with

$$q = \frac{\partial \overline{\varepsilon}}{\partial x} \tag{5-62}$$

and

$$\overline{\varepsilon} - \varepsilon = \frac{1}{2} l^2 \frac{\partial^2 \varepsilon}{\partial x^2} \tag{5-63}$$

The combination of (5-60), (5-62), (5-63) and the kinematic equation (5-20) leads to a system of PDEs.

$$\begin{pmatrix} -\frac{1}{c_e^2} \frac{\partial v}{\partial t} \\ \frac{\partial \varepsilon}{\partial t} \\ 0 \\ 0 \end{pmatrix} + \begin{pmatrix} (1 - \omega) \frac{\partial \varepsilon}{\partial x} - \varepsilon \frac{\partial \omega}{\partial \kappa} \frac{\partial \varepsilon}{\partial x} \\ -\frac{\partial v}{\partial x} \\ \frac{1}{2} l^2 \frac{\partial \overline{\varepsilon}}{\partial x} \\ \frac{\partial \overline{\varepsilon}}{\partial x} \end{pmatrix} = \begin{pmatrix} 0 \\ 0 \\ \overline{\varepsilon} - \tilde{\varepsilon} \\ q \end{pmatrix} \tag{5-64}$$

The variables for velocity, strain, nonlocal strain and strain derivative are combined in vector form:

$$\underline{u} = \begin{pmatrix} v \\ \varepsilon \\ \overline{\varepsilon} \\ q \end{pmatrix} \tag{5-65}$$

Therefore the equation of motion can be summarised in the same way as the local equation of motion.

$$\underline{\underline{P}}(\underline{u})\frac{\partial \underline{u}}{\partial t} + \underline{\underline{Q}}(\underline{u})\frac{\partial \underline{u}}{\partial x} = \underline{r}(\underline{u}) \tag{5-66}$$

with

$$\underline{\underline{P}}(\underline{u}) = \begin{pmatrix} -\frac{1}{c_e^2} & 0 & 0 & 0 \\ 0 & 1 & 0 & 0 \\ 0 & 0 & 0 & 0 \\ 0 & 0 & 0 & 0 \end{pmatrix}$$

$$\underline{\underline{Q}}(\underline{u}) = \begin{pmatrix} 0 & 1-\omega & -\frac{\partial \omega}{\partial \kappa}\varepsilon & 0 \\ -1 & 0 & 0 & 0 \\ 0 & 0 & 0 & \frac{1}{2}l^2 \\ 0 & 0 & 1 & 0 \end{pmatrix}$$

$$\underline{r}(\underline{u}) = \begin{pmatrix} 0 \\ 0 \\ \overline{\varepsilon} - \tilde{\varepsilon} \\ q \end{pmatrix}$$

The system has two real linear independent eigenvalues. The system of PDEs stays hyperbolic with a dispersive phase velocity, even in the softening zone.

$$\lambda_{1,2} = \frac{\pm 1}{c_e\sqrt{1-D}} \quad and \quad \lambda_{3,4} = 0 \tag{5-67}$$

$$c = c_e\sqrt{1-\omega-\frac{\left(\frac{\partial \omega}{\partial \kappa}\right)\varepsilon}{\left(1-\frac{1}{2}l^2i^2k^2\right)}} \tag{5-68}$$

The non-trivial solution of the problem leads to a dispersive velocity which stays real as long as the wave number k does not go under the critical wave number k_c.

$$k_c = \frac{1}{l}\sqrt{2\left(\frac{\left(\frac{\partial\omega}{\partial\kappa}\right)\varepsilon}{1-\omega}-1\right)} \tag{5-69}$$

5.3.3 Viscous Regularisation Method

Sluys and de Borst [109] chose a crack model (see (5-16)) for the demonstration of viscous regularisation. The softening function $f(\varepsilon_{cr})$ is linear: $f(\varepsilon_{cr}) = f_t + h\varepsilon_{cr}$. f_t is the static yield strength and h the softening modulus. The constitutive equation for the viscous regularisation reads:

$$\sigma = f_t + h\varepsilon_{cr} + m\dot{\varepsilon}_{cr} \tag{5-70}$$

A combination of (5-70) with the kinematic relation $\varepsilon = \partial u/\partial x$, the strain-rate $\dot{\varepsilon}_{cr} = \dot{\varepsilon} - \dot{\varepsilon}_e$ and Hooke's law $\varepsilon_e = \sigma/E$, differentiation with respect to x and substitution in the wave equation (5-19) leads to a 3rd order PDE which describes the 1D softening bar under dynamic loading.

$$m\left(\frac{1}{c_e^2}\frac{\partial^3 u}{\partial t^3} - \frac{\partial^3 u}{\partial x^2 \partial t}\right) - h\frac{\partial^2 u}{\partial x^2} + \frac{(E+h)}{c_e^2}\frac{\partial^2 u}{\partial t^2} = 0 \tag{5-71}$$

The determination of the type of the 3rd order PDE in (5-71) is based on the characteristics of the wave equation. Characteristics of a PDE are based on the highest order terms in the equation. Therefore only the 3rd order terms in (5-71) are of interest.

A 3rd order differential equation in two independent variables can be expressed as follows: [33]

$$Au_{xxx} + Bu_{xxy} + Cu_{xyy} + Du_{yyy} = F(x, y, u, u_x, u_y, u_{xx}, u_{xy}, u_{yy}) \tag{5-72}$$

The characteristics of (5-72) can be determined from:

$$A\lambda^3 + B\lambda^2 + C\lambda + D = 0 \tag{5-73}$$

with

$$\lambda = \frac{dy}{dx} \tag{5-74}$$

According to this the system of PDEs in (5-71) has two real eigenvalues and stays hyperbolic in the softening zone.

$$\lambda_{1,2} = \pm \frac{1}{c_e} \tag{5-75}$$

The wave propagation is dispersive in the viscous strain-softening bar. Sluys and de Borst [110; 110] found the solution for the wave number k to be:[1]

$$k^2 = \frac{\rho\omega^2}{2E}\left(\frac{(m^2\omega^2 + h^2 + Eh) + \sqrt{(m^2\omega^2 + h^2 + Eh)^2 + (mE\omega)^2}}{m^2\omega^2 + h^2}\right) \tag{5-76}$$

ω is the angular frequency. The phase velocity c in the viscous bar is a function of ω:

$$c = \frac{\omega}{k} \tag{5-77}$$

5.3.4 Comparison of Regularisation Methods

It was shown in the previous sections that regularisation methods are able to keep the wave speed real and therefore to keep the mathematical problem stable. The results for the definition of phase velocities in local and regularised continua are summarised in Table 5-1.

Table 5-1: Comparison of phase velocity for different local and regularised continua

Continuum description	Phase velocity in softening domain	Dispersive	Type of PDEs
Local	$c = c_e\sqrt{1 - \omega - \left(\frac{\partial\omega}{\partial\varepsilon}\right)\varepsilon}$	No	elliptic
Nonlocal integral	$c = c_e\sqrt{1 - \omega - \varepsilon\frac{\partial\omega}{\partial\varepsilon}exp\left(-\frac{1}{2}k^2l^2\right)}$	Yes	hyperbolic
Gradient-enhanced (explicit)	$c = c_e\sqrt{1 - \omega - \left(\frac{\partial\omega}{\partial\varepsilon}\right)\varepsilon\left(1 - \frac{1}{2}l^2k^2\right)}$	Yes	hyperbolic
Gradient-enhanced (implicit)	$c = c_e\sqrt{1 - \omega - \frac{\left(\frac{\partial\omega}{\partial\varepsilon}\right)\varepsilon}{\left(1 + \frac{1}{2}l^2k^2\right)}}$	Yes	hyperbolic
Viscous	$c \approx c_e$	Yes	hyperbolic

[1] The equation for k is stated differently in [109]. This is due to an incorrect '-' sign. The correct expression is stated in Equation (5-76).

The different regularisation methods will be compared for the following example used by Peerlings and co-workers [89; 90] and Sluys and de Borst [109; 110]: The elastic wave speed is set to 1000 m/s and softening starts for $\varepsilon = \kappa_i$. The Young's Modulus E is 20000MPa. The nonlocal models use as limiting strain for the linear elastic area κ_i = 0.0001 and as critical strain κ_c = 0.0125. The internal length is $l = \sqrt{2}mm$. The rate-sensitivity of the viscous model is set to m = 0.2Ns/mm^2. The softening modulus is h = $-5000N/mm^2$.

Figure 111 shows a comparison of the phase velocity and wave number for all used regularisation methods. The phase velocity is dispersive for all methods.

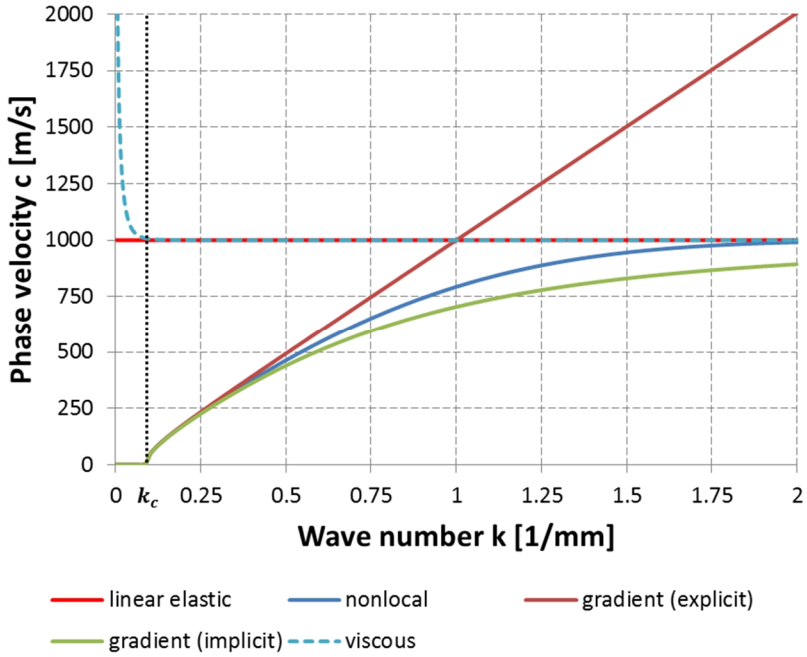

Figure 111: Comparison of phase velocity over wave number for different regularisation methods

The nonlocal models have identical results for small wave numbers. The critical wave number k_c is identical for the peak stress at κ_i. The wave speed below this critical value is imaginary and waves cannot propagate. The phase velocities diverge with increasing wave number. The nonlocal integral and the implicit gradient curve converge asymptotically to the linear elastic wave speed with increasing wave number. Therefore the phase velocities are bounded to the elastic wave speed of the material. The explicit gradient model behaves differently. The phase velocity is not bounded to the linear elastic wave velocity. With increasing wave number waves can propagate with an infinite wave speed which is physically unrealistic. Hence, the explicit gradient model does not seem to be suited for dynamic problems.

Waves in the softening zone in the viscous model behave similar to linear elastic waves. The phase velocity becomes infinite for very small wave numbers. This is not meaningful in a physical sense. It can be concluded that the regularisation effect is vanishing for very small wave numbers. The phase velocity is equal to the linear elastic wave speed for higher wave numbers.

Figure 112 and Figure 113 show the dispersion relationship $\omega = c \cdot k$ for the considered regularisation methods. All methods behave similar or nearly equivalent to the elastic wave speed except for the explicit gradient method. However, all regularisation methods seem to be inadequate for small wave numbers ($k < k_c$).

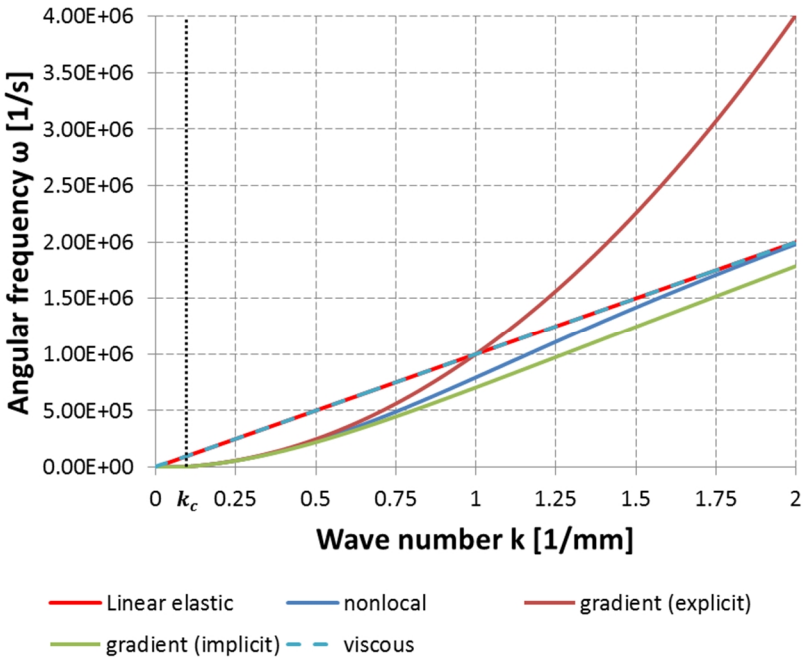

Figure 112: Dispersion relationship for different regularisation methods ($0 \leq k \leq 2$)

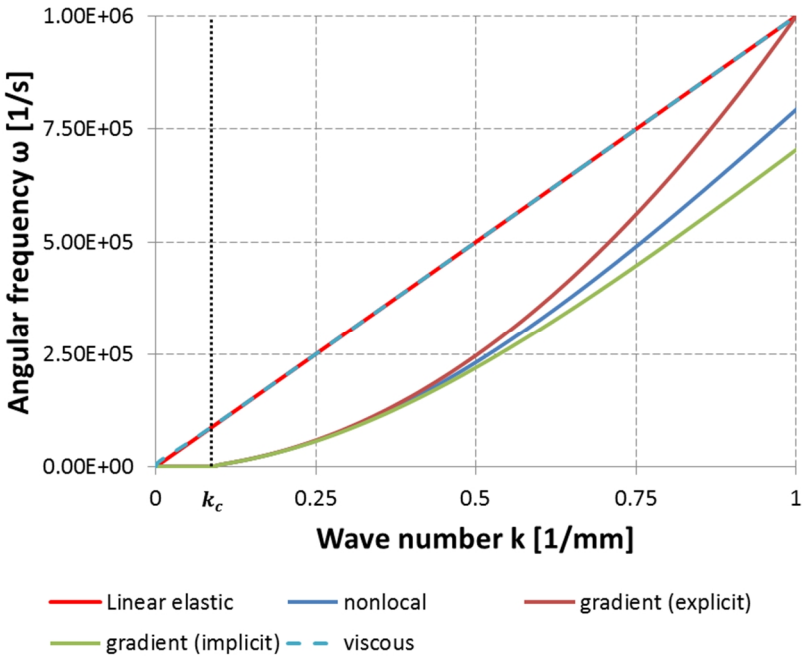

Figure 113: Dispersion relationship for different regularisation methods ($0 \leq k \leq 1$)

The dispersive relationship for the viscous regularisation is shown in more detail in Figure 114. Waves behave nearly similar to the elastic wave speed as shown in Figure 113. However, if k becomes nearly zero, as in static behaviour, the phase velocity will be infinite.

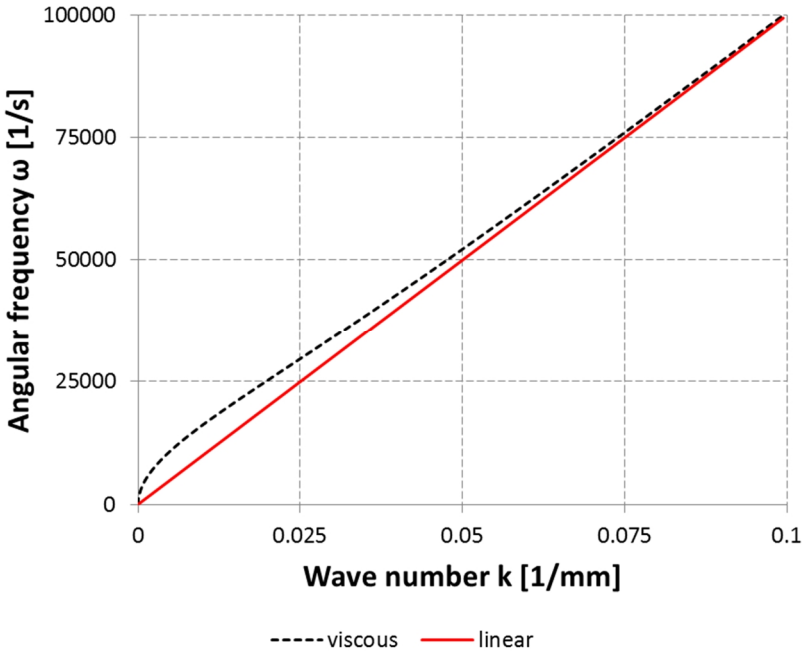

Figure 114: Dispersion relationship for a bar under viscous condition

5.4 Summary

The aim of this chapter was to investigate available regularisation methods which are able to keep the boundary value problem well-posed and remove mesh-sensitivity by introducing an internal length to constitutive equations.

The main branches of regularisation methods, nonlocal and viscous approach, were investigated in detail. The underlying theory was explained first and then it was shown with simple wave propagation assumptions that these methods keep the PDEs hyperbolic in the strain-softening domain. It was found that all methods, except for the nonlocal approach with explicit gradient-enhancement, are able to keep PDEs hyperbolic in dynamic problems and enable a continuous wave propagation with a wave speed similar to the linear elastic one in the localisation zone.

Although regularisation methods are able to overcome mathematical, physical and numerical issues associated with strain-softening, the user of these methods has to face the challenge of choosing an appropriate characteristic length in nonlocal methods and an appropriate viscosity coefficient in viscous methods. These choices are not straightforward and depend on a balance between convergence of results and real material behaviour.

6 SPH as Nonlocal Method

It is well-established by research that the use of a conventional CDM model with strain-softening has an ill-posed boundary value problem leading to non-physical results and suffers from mesh-sensitivity in numerical considerations. This has also been demonstrated in the previous Chapters 3 and 4.

The maintenance of a well-posed boundary value problem is crucial for a stable and mesh-independent numerical CDM model with strain-softening. The group of regularisation methods, which are nonlocal integral, gradient-enhanced and viscous method, are established solutions to the instability issues of conventional strain-softening models able to maintain a well-posed boundary value problem and confine damage to a finite area as observed in real materials. The effectiveness of these methods has been well-established over recent decades and much research effort has been done in this field.

Research has been focused strongly on the investigation and further development of regularisation methods over decades and regularisation methods are presented as only option to deal with an ill-posed boundary value problem due to strain-softening. The scope of this work is to investigate other ways of dealing with the issue of an instable boundary value problem and add therefore more options to modelling of strain-softening behaviour in CDM models.

First the Smoothed particle hydrodynamics (SPH) method is investigated with regards to strain-softening behaviour. SPH is a meshless particle method. The interaction of particles is defined by a weighting (smoothing) function, where the smoothing length (size of the smoothing function domain) defines the range of influence [119]. It is presumed here that this property makes SPH by nature a nonlocal method capable of overcoming difficulties due to strain-softening without any additional regularisation measures. SPH itself is not a regularisation method although it will be shown that it has nonlocal properties. The use of SPH in improving the nature of the boundary value problem in the presence of strain-softening has not been addressed in literature previously. Therefore, the characteristic properties of SPH for CDM models with strain-softening will be observed and quantified in this chapter. First, the main aspects making SPH a nonlocal method will be pointed out. Then a numerical study using the in-house SPH code MCM (“Meshless Continuum Mechanics” code) will be conducted. The investigation is done by considering the simple longitudinal wave propagation

problem defined by Bažant and Belytschko [6]. This example was used in Chapter 3 and Chapter 4 already to show analytical and numerical instabilities caused by standard CDM models with strain-softening. Therefore, the changes to the solution achieved through the nonlocal character of SPH can be observed.

6.1 Main Aspects of the SPH Method

Smoothed Particle Hydrodynamics (SPH) is a meshless, Lagrangian particle method where the motion of a continuum is described by the movement of a finite number of discrete particles which are used in the spatial discretisation of the state variables. Instead of a grid, SPH uses kernel interpolation to approximate the field variables at any point in a domain. For instance, an estimate of the value of a function $f(\boldsymbol{x})$ at the location $\boldsymbol{x}$ is given in a continuous form by an integral of the product of the function and a kernel (weighting) function $W(|\boldsymbol{x}-\boldsymbol{x}'|,h)$:

$$\langle f(\boldsymbol{x})\rangle = \int_{\Omega} f(\boldsymbol{x}')W(|\boldsymbol{x}-\boldsymbol{x}'|,h)d\boldsymbol{x}' \tag{6-1}$$

where the angle brackets $\langle\cdot\rangle$ denote a kernel approximation.

h is a parameter that defines the size of the kernel support known as the smoothing length.

$\boldsymbol{x}'$ is the new independent variable.

The kernel function usually has the following properties:

- Compact support, which means that it is zero everywhere but on a finite domain. In conventional SPH this domain is taken to be all points within twice the smoothing length, h, of the centre:

$$W(|\boldsymbol{x}-\boldsymbol{x}'|,h) = 0 \quad for \quad |\boldsymbol{x}-\boldsymbol{x}'| \geq 2h \tag{6-2}$$

- Normalised:

$$\int_{\Omega} W(|\boldsymbol{x}-\boldsymbol{x}'|,h)d\boldsymbol{x}' = 1 \tag{6-3}$$

These requirements, formulated by [76], ensure that the kernel function reduces to the Dirac delta function when h tends to zero:

$$\lim_{h\to 0} W(|\boldsymbol{x}-\boldsymbol{x}'|,h) = \delta(|\boldsymbol{x}-\boldsymbol{x}'|,h) \tag{6-4}$$

And therefore, it follows that:

$$\lim_{h\to 0}\langle f(\boldsymbol{x})\rangle = f(\boldsymbol{x}) \tag{6-5}$$

If the function $f(\boldsymbol{x})$ is only known at N discrete points, the integral of equation (6-1) can be approximated by a summation:

$$\begin{aligned} f_I &= f(\boldsymbol{x}_I) \\ &\approx \langle f(\boldsymbol{x}_I)\rangle = \int_{\Omega} f(\boldsymbol{x}')W(|\boldsymbol{x}-\boldsymbol{x}'|,h)d\Omega \approx \sum_{J=1}^{N}\frac{m_J}{\rho_J}f(\boldsymbol{x}_J)W\left(|\boldsymbol{x}_I-\boldsymbol{x}_J|,h\right) \end{aligned} \tag{6-6}$$

In the above equation, the subscript I and J denote particle numbers, m_J and ρ_J the mass and the density of particle J, N the number of neighbours of particle I (number of particles that interact with particle I, i.e. the support of the kernel), m_J/ρ_J is the volume associated to the point or particle J and $W_{IJ} = W\left(|\boldsymbol{x}_I-\boldsymbol{x}_J|,h\right)$.

In SPH literature, the term particles is misleading as these particles in fact have to be thought of as interpolation points rather than mass elements.

Equation (6-6) constitutes the basis of the SPH method. The value of a variable at a particle, denoted by superscript I, is calculated by summing the contributions from a set of neighbouring particles (see Figure 115), denoted by superscript J and for which the kernel function is not zero:

$$\langle f(\boldsymbol{x}_I)\rangle = \sum_{J}\frac{m_J}{\rho_J}f(\boldsymbol{x}_J)W\left(|\boldsymbol{x}_I-\boldsymbol{x}_J|,h\right) \tag{6-7}$$

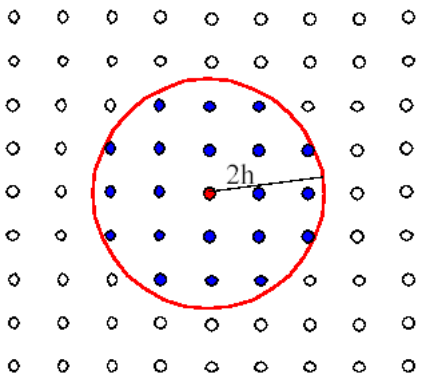

Figure 115: Set of neighbouring particles

Using basic properties of the kernel approximation it is not difficult to show that a discrete form of the spatial derivative approximation is:

$$\langle \nabla f(\boldsymbol{x}_I) \rangle = \sum_J \frac{m_J}{\rho_J} f(\boldsymbol{x}_J) \left[\nabla W\left(\left| \boldsymbol{x}_I - \boldsymbol{x}_J \right|, h \right) \right] \tag{6-8}$$

The SPH approximations of field variables and their spatial derivatives represent weighted averages over the kernel function domain or in its discrete form over a number of neighbours for a given particle I. The kernel function is the weighting function. This is the property of SPH that gives the method a nonlocal nature.

In SPH the stress and velocity fields are smoothed according to the used weighting function which makes it a nonlocal method. The discretisation used in SPH for conservation equations of mass, momentum and energy are given below. For the detailed derivations see Vignjevic et al. [118].

$$\langle \frac{D\rho_I}{Dt} \rangle = \rho_I \sum_{J=1}^{N} \frac{m^J}{\rho^J} (\boldsymbol{v}_J - \boldsymbol{v}_I) \nabla W\left(\left| \boldsymbol{x}_I - \boldsymbol{x}_J \right|, h \right) \tag{6-9}$$

$$\langle \frac{Dv_I}{Dt} \rangle = \sum_J \frac{m_J}{\rho_J} (\boldsymbol{v}_J - \boldsymbol{v}_I)(\boldsymbol{v}_R \cdot \nabla W_{IJ}) - \sum_{J=1}^{N} m_J \left(\frac{\sigma_J}{\rho_J^2} + \frac{\sigma_I}{\rho_I^2} \right) \nabla W\left(\left| \boldsymbol{x}_I - \boldsymbol{x}_J \right|, h \right) \tag{6-10}$$

$$\langle \frac{DE_J}{Dt} \rangle = -\frac{\sigma_I}{\rho_I} \sum_{J=1}^{N} m_J (\boldsymbol{v}_J - \boldsymbol{v}_I) \nabla W\left(\left| \boldsymbol{x}_I - \boldsymbol{x}_J \right|, h \right) \tag{6-11}$$

In addition for each particle a constitutive equation describing material behaviour has to be integrated. The SPH method does not require the definition of connectivity between particles. Instead it is only needed to define the initial distribution of particles within the domain of interest.

6.2 Numerical MCM Experiments

6.2.1 Material Model

The used CDM model has an isotropic material behaviour with isotropic damage. The damage behaviour is assumed to be linear which leads to a linear strain-softening branch after the onset of damage. The general stress-strain behaviour is displayed in Figure 116.

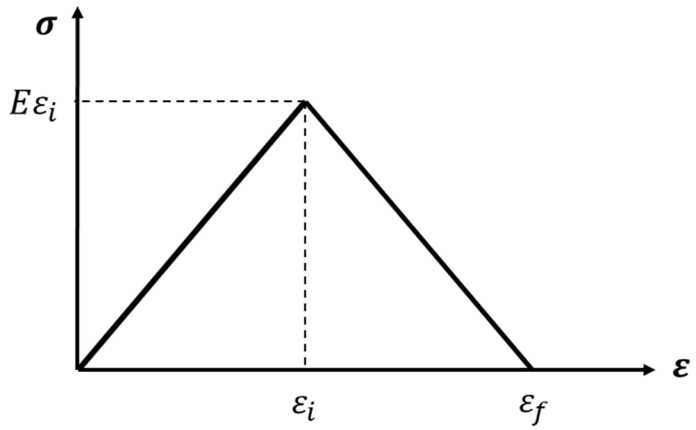

Figure 116: Material model with strain-softening

The onset of strain-softening occurs when strain reaches the initiation failure strain ε_i. Stress reaches its maximum for this strain. Stress will vanish gradually after the onset of strain-softening until it reaches zero for the critical failure strain ε_f.

The constitutive equations for the used CDM model are established by using the strain equivalence hypothesis. The definition of the damaged stiffness tensor $\tilde{C}_{ijkl}$ is then established by the virgin stiffness tensor C_{ijkl} and damage variable ω. The damage variable will be scalar due to the isotropic nature of the material behaviour and damage.

$$\tilde{C}_{ijkl} = (1-\omega)C_{ijkl} \tag{6-12}$$

The damage variable can be easily derived from a 1D example shown in Figure 117. In this picture E is the Young's modulus and defines the linear elastic behaviour. The softening branch is defined by E_t which is the tangent stiffness. Points of the softening branch and with this the damage variable can be determined with the secant stiffness $\tilde{E}$. In the case of linear elastic material behaviour the secant stiffness is equivalent to the Young's modulus. ε_i and ε_f are the initiation and critical failure strains. ε^* denotes the current strain.

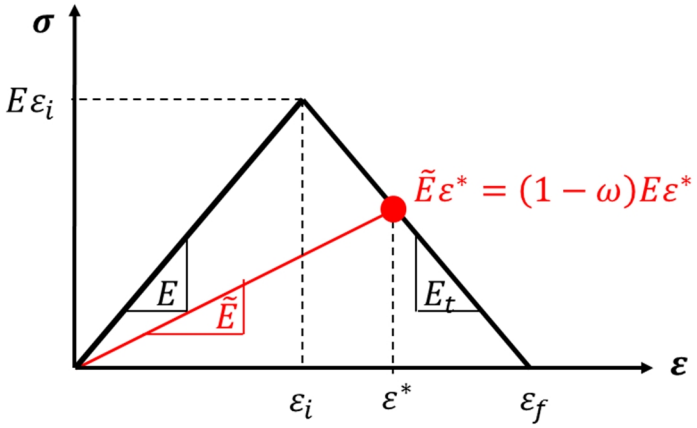

Figure 117: Determination of scalar damage variable of linear strain-softening model

The secant stiffness can be defined in terms of the Young's modulus and the damage variable:

$$\tilde{E} = (1-\omega)E \tag{6-13}$$

The tangent stiffness describes the slope of the strain-softening branch.

$$E_t = \frac{-E\varepsilon_i}{\varepsilon_f - \varepsilon_i} \tag{6-14}$$

A point on the softening branch is defined as:

$$\tilde{E}\varepsilon^* = (1-\omega)E\varepsilon^* = E_t(\varepsilon^* - \varepsilon_f) = \frac{-E\varepsilon_i}{\varepsilon_f - \varepsilon_i}(\varepsilon^* - \varepsilon_f) \tag{6-15}$$

Therefore the damage variable is determined with:

$$\omega = \frac{\varepsilon_f}{\varepsilon^*}\left(\frac{\varepsilon^* - \varepsilon_i}{\varepsilon_f - \varepsilon_i}\right) \tag{6-16}$$

6.2.2 Test Setup

The investigation of strain-softening behaviour will be conducted using Bažant and Belytschko's [6] strain-softening problem as presented in Chapter 3. The bar has an overall length of $2l$ = 200mm and a squared cross-section with 10mm edge length. The origin of the coordinate system lies in the centre of the bar which is located at x = 0. The longitudinal direction is denoted with x. All degrees of freedom except for the longitudinal direction are restricted in order to ensure uniaxial strain conditions.

The input data used is presented in Table 6-1. Apart from general material properties as density, Poisson's ratio and Young's modulus only the initiation and critical failure

strains need to be defined. The maximum strength and damage behaviour follow from the definitions of these strains.

Table 6-1: Input data for isotropic CDM model with linear strain-softening in MCM

Value	Sign	Magnitude	Unit
Density	ρ	$1.55 \cdot 10^{-9}$	t/mm^3
Young's modulus	E	70800	MPa
Poisson's ratio	v	0.125	–
Initial failure strain	ε_i	0.018	–
Critical failure strain	ε_f	0.036	–

Due to Equation (3-48) the elastic wave speed can be determined as c_e = 6758507.18mm/s. Therefore the minimum applied velocity has to be v_{min} = $\frac{\varepsilon_f}{2} \cdot c_e$. and the maximum velocity has to be v_{max} = $\varepsilon_f \cdot c_e$. A tensile loading of $v_{const.}$ = $7 \cdot 10^4 mm/s$ will be used.

It is known that the strain-softening behaviour leads to results dependent on the mesh discretisation in FE method. It is assumed that this dependence does not occur in SPH method because of its nonlocal character. To investigate the behaviour of SPH (total Lagrange form used) the wave propagation problem by Bažant and Belytschko [6] is used. The bar will be investigated with three different interparticle distances as shown in Figure 118:

- Δp = 200mm/101
- Δp = 200mm/151
- Δp = 200mm/201

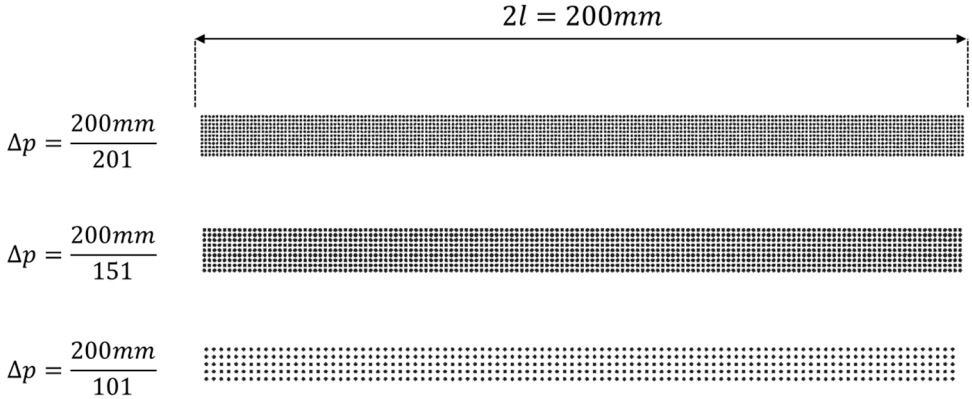

Figure 118: Particle discretisation in SPH (MCM) of strain-softening bar

The strain-softening behaviour cannot be influenced in FE; however, this is different in SPH due to the use of a weighted average to determine the particle interaction. The weighted average is influenced by the smoothing length h, defined as:

$$h = \lambda \cdot \Delta p \tag{6-17}$$

Δp represents the interparticle spacing in SPH and λ is a factor which relates the interparticle spacing to the smoothing length. The smoothing length in conjunction with the kernel function defines the range over which the properties of the particles are smoothed. This range has a radius of $2h$ and an overall width of $4h$ in SPH.

The use of the weighting function gives SPH a nonlocal character and the weighting function can be controlled by the user by defining the smoothing length. Therefore, the user can control the localisation process by choosing an appropriate smoothing length.

The influence of the smoothing length on results will be investigated with three different experiments which are summarised in Table 6-2.

The first experiment investigates the influence of the smoothing length on different particle discretisations. λ will be 1.3 which adjusts the smoothing length to the chosen interparticle distances Δp. In this case h defines a finite number of neighbours for a particle which will be equivalent for all used Δp. Particles are supposed to be neighbours if they lie within a spherical domain of radius $2h$. As a consequence results are assumed to be dependent on the chosen interparticle distance during strain-softening similar to the dependence of results on the spatial discretisation in FE.

The second experiment will assume a fixed interparticle distance (here: Δp = $200mm/201$) and a variation of λ. λ will have values of 1.25, 2.25 and 3.25 which increases the number of neighbouring particles. It is expected for this experiment that the effects of strain-softening will be averaged over an increasing area as the number of neighbours is increased. The number of neighbours is determined by the radius $2h$. Therefore, the test with λ = 1.25 will result in a damage zone of 5 particles, λ = 2.25 will result in a damage zone of 9 particles and λ = 3.25 will result in a damage zone of 13 particles. This experiment will show that the strain-softening process can be indeed controlled by the user by changing the smoothing length.

The third experiment will apply a fixed physical length of h = $2.5mm$ to different interparticle distances. The factor λ and with this the number of neighbouring particles will change accordingly to Δp. However, strain-softening effects will be smoothed over an area equivalent in physical size for all used interparticle distances. This will remove any sensitivity of results on the used particle discretisation and strain-softening effects will occur over an area with finite size which can be controlled by the user.

Table 6-2: Summary of conditions for SPH Experiment 1, 2 and 3 in MCM

Interparticle distance Δp [mm]	Support domain factor λ [-]	Physical smoothing length ($h = \lambda \cdot \Delta p$) [mm]	Particles through thickness (y- and z-direction)	Particles through length	Absolute number of particles
Experiment 1: Influence of interparticle distance					
200/101	1.3	260/101	5	101	2525
200/151		260/151	9	151	12231
200/201		260/201	11	201	24321
Experiment 2: Influence of averaging over several neighbouring particles					
200/201	1.25	250/201	11	201	24321
	2.25	150/67			
	3.25	650/201			
Experiment 3: Influence of constant smoothing length					
200/101	1.2625	2.5	5	101	2525
200/151	1.8875		9	151	12231
200/201	2.5125		11	201	24321

Failure will occur in SPH when damage reaches a value of one: $\omega = 1$. As a consequence of failure free surfaces are formed. This means that particles in this area are not numerically connected anymore and cannot interact with each other except for the material across this new formed boundary. This is equivalent to fracture in a real material. In this case stress will drop to zero and a release wave in the form of a compressive wave will occur.

6.2.3 Results: Strain-Softening in SPH (MCM)

The tests with SPH aim to investigate the influence of a nonlocal solution on the strain-softening problem. The localisation process in SPH can be controlled by the user by adjusting the smoothing length h.

The tests are conducted using Bažant and Belytschko's strain-softening experiment [6]. The solutions for longitudinal displacement, strain and stress will be presented along the bar for $t = 2/3 \cdot L/c_e$. The results are taken along the particles which lie in the middle of the bar.

6.2.3.1.1 Experiment 1

Experiment 1 investigates the behaviour of SPH in the presence of strain-softening behaviour for different interparticle distances Δp. The smoothing length is defined in each case as $h = 1.3 \cdot \Delta p$. Due to this the physical smoothing length will be different for all bars; however, due to the scaling factor $\lambda = 1.3$ the same number of neighbouring

particles will be in the range of influence. Therefore, it is expected that the SPH results of experiment 1 show a sensitivity of results due to the used interparticle distance.

Figure 120 shows the stress-strain curves for the three used particle discretisations in the middle particle of the bar. It is obvious that all bars undergo linear strain-softening behaviour.

Figure 121 shows the development of damage in the midsection of the bar. As expected, damage does not appear in a single particle alone. Instead damage is averaged over a number of particles which is defined by the radius $2h$. This makes a total of 5 particles which are the central particle plus a set of two particles to each side. It can be seen that the width of the damaged area depends on the chosen interparticle distance as the smoothing length is a function of Δp.

Figure 122, Figure 123 and Figure 124 show the profiles of longitudinal displacement, strain and stress plotted along the bar's length for the three interparticle distances. They are plotted along the analytical local strain-softening solution. At first it appears that these results show the non-physical localisation behaviour in the softening particle. However, this is not true as the damage areas have already failed and formed free surfaces (see Figure 119). The bond between particles is broken and they move apart. This leads to the displacement and strain profile in Figure 122 and Figure 123. After failure stress drops to zero and a release wave travels towards the ends of the bar (see Figure 124).

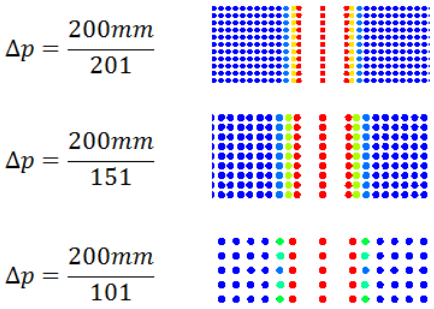

Figure 119: Formation of free surfaces after failure (SPH experiment 1)

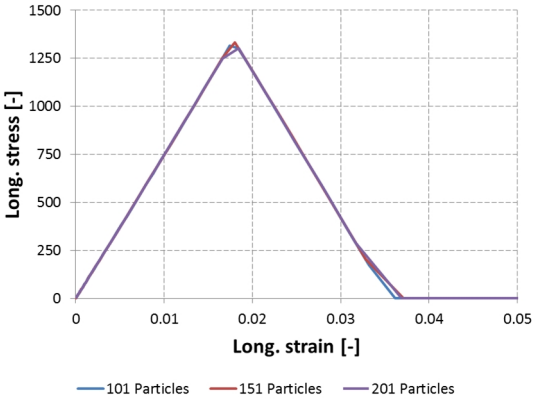

Figure 120: Numerical results for long. stress-long. strain relationship in SPH (experiment 1) with varying interparticle distance

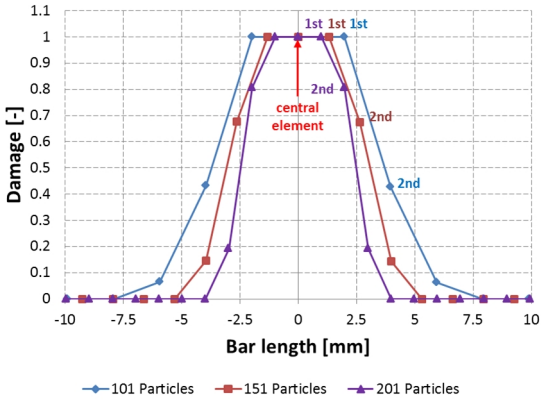

Figure 121: Numerical results for damage in SPH (experiment 1) with varying interparticle distance at $t = 3/4 \cdot 2L/c_e$

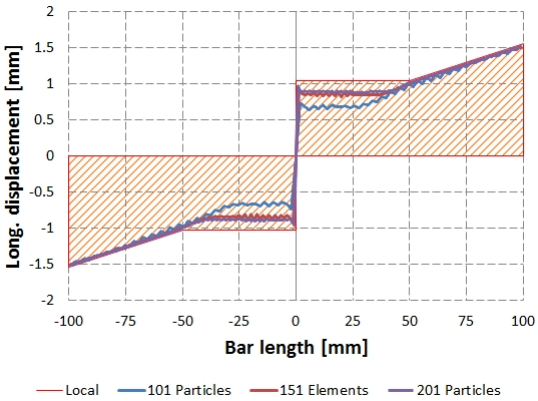

Figure 122: Numerical results for longitudinal displacement in SPH (experiment 1) with varying interparticle distance at $t = 3/4 \cdot 2L/c_e$

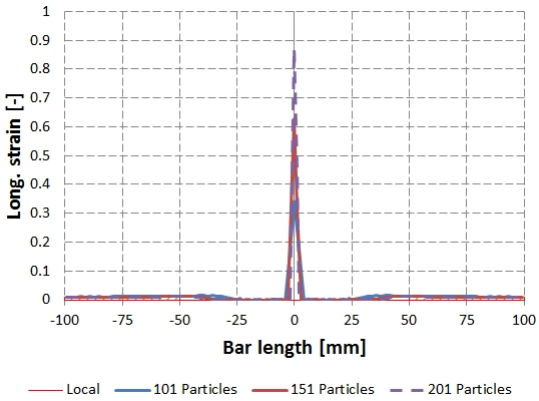

Figure 123: Numerical results for longitudinal strain in SPH (experiment 1) with varying interparticle distance at $t = 3/4 \cdot 2L/c_e$

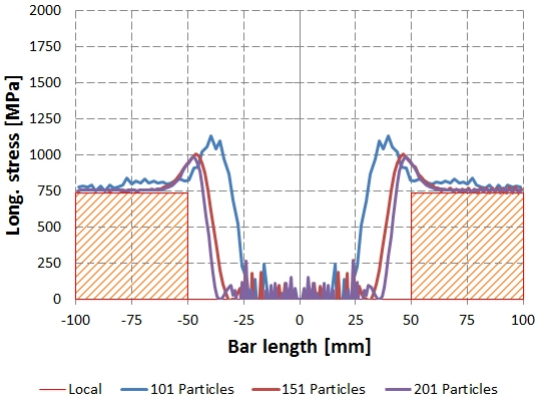

Figure 124: Numerical results for longitudinal stress in SPH (experiment 1) with varying interparticle distance at $t = 3/4 \cdot 2L/c_e$

Figure 125 shows a graphical representation of the damage zone just before failure. It can be seen that damage is averaged over 5 particles along the length of the bar. This number is constant for all Δp. It can be seen consequently that the width of the damage zone depends on the chosen interparticle distance. As the interaction radius is $2h$ the

damage zone extends over an area $4h$ and is the largest for the interparticle distance Δp = 200mm/101.

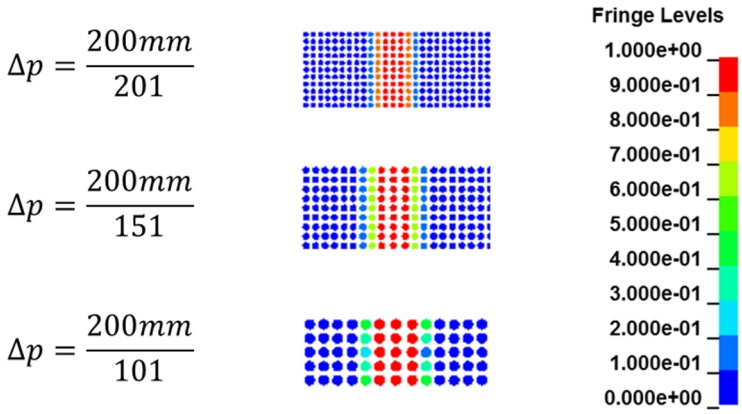

Figure 125: Localisation of damage within a radius $2h$ (h = 1.3 · Δp) around the strain-softening particle before failure (fringe level: damage [-])

6.2.3.1.2 Experiment 2

Experiment 2 is concerned with the impact on results when the smoothing length is increased for a constant interparticle distance. The bar with the interparticle distance Δp = 200mm/201 is used as an example and the smoothing length is defined by the factor λ with λ = 1.25, 2.25 and 3.25. The three factors λ lead to three smoothing lengths which differentiate clearly in size. It is expected that the number of particles with damage will rise from 5 to 9 and 13 with increasing λ.

Again the particles in the centre of the bar clearly undergo strain-softening as it can be seen from the stress-strain curves in Figure 127.

Figure 128 shows the development of damage in the midsection of the bar. It can be seen that the increase of the smoothing length indeed has a great impact on the size of the damage zone. The radius of the damage zone is $2h$ and with each increase of the smoothing length the radius $2h$ envelopes two more rows of particles with considerable damage values.

Figure 129, Figure 130 and Figure 131 show the profiles of longitudinal displacement, strain and stress plotted along the bar's length for the three interparticle distances. They are plotted along the analytical local strain-softening solution. Similar to experiment 1 it appears that the solutions follow the local strain-softening solution with the formation of a localisation band in the softening particle. However, this is caused by the formation of free surfaces due to failure (see Figure 126). The results for displacement and strain improve slightly with increasing smoothing length. Figure 129 shows that the displacement jump decreases as the number of free surfaces increases.

Therefore, the effect is smoothed out with increasing smoothing length. Stress vanishes after the occurrence of free surfaces as expected.

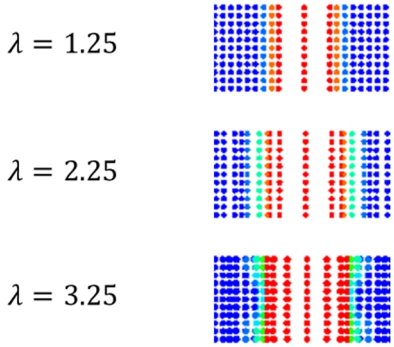

Figure 126: Formation of free surfaces after failure (SPH experiment 2)

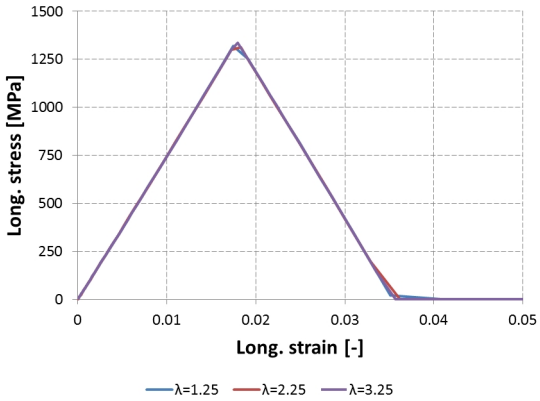

Figure 127: Numerical results for long. stress-long. strain relationship in SPH (experiment 2) with varying interparticle distance

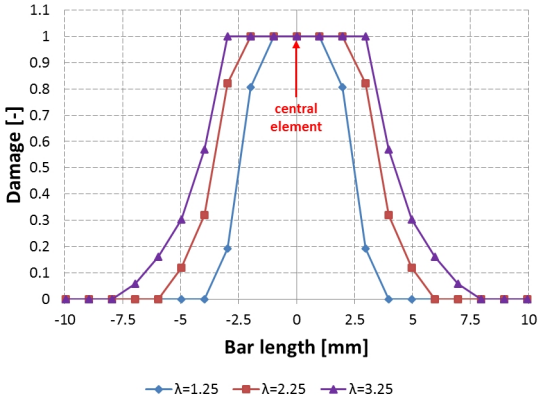

Figure 128: Numerical results for damage in SPH (experiment 2) with varying interparticle distance at $t = 3/4 \cdot 2L/c_e$

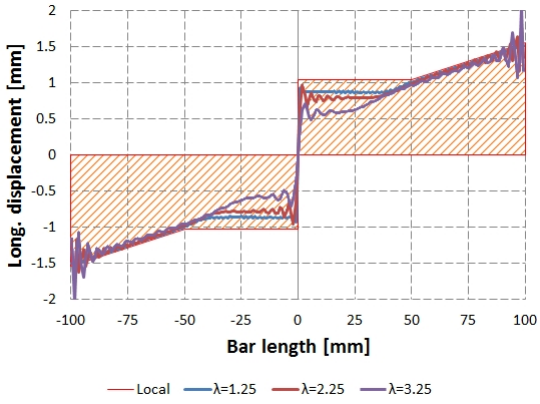

Figure 129: Numerical results for longitudinal displacement in SPH (experiment 2) with varying interparticle distance at $t = 3/4 \cdot 2L/c_e$

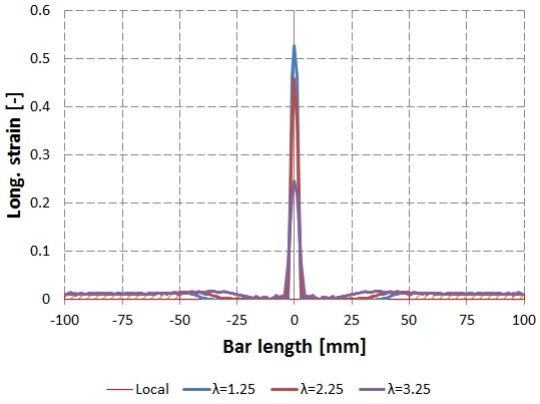

Figure 130: Numerical results for longitudinal strain in SPH (experiment 2) with varying interparticle distance at $t = 3/4 \cdot 2L/c_e$

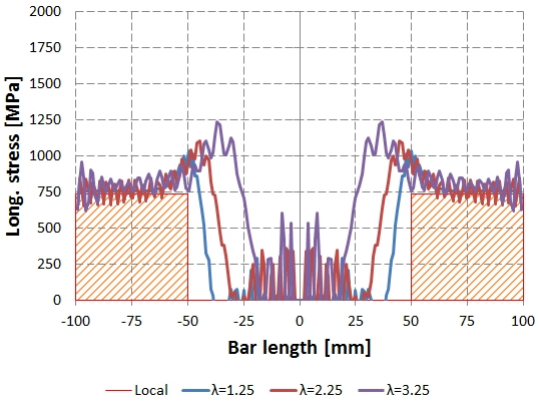

Figure 131: Numerical results for longitudinal stress in SPH (experiment 2) with varying interparticle distance at $t = 3/4 \cdot 2L/c_e$

Figure 132 shows the graphical representation of the damage zone just before failure for experiment 2. The bars have an equivalent interparticle distance $\Delta p = 200mm/201$. However, the factor relating Δp with the smoothing length is varied in a way that the number of neighbouring particles is increased. Indeed it can be seen that this happens when the radius $2h$ increases with increasing λ. Therefore, the size of the damage zone increases.

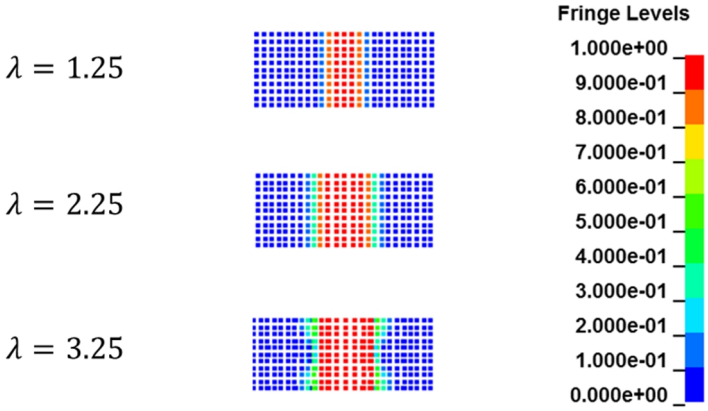

Figure 132: Localisation of damage within a radius $2h$ ($h = \lambda \cdot 200mm/201$) around the strain-softening particle before failure (fringe level: damage [-])

6.2.3.1.3 Experiment 3

Experiment 3 investigates the behaviour of SPH for different interparticle distances subjected to a fixed physical smoothing length $h = 2.5mm$. Due to the fixed smoothing length properties will be smoothed over a finite range defined by h. It is expected that the number of neighbouring particles will change according to the used interparticle distance; however, results should be independent of the interparticle distance due to the fixed smoothing length. The area of smoothed properties will have a radius of $2h = 5mm$ and overall width of $4h = 10mm$.

Figure 181 shows the stress-strain curves for the three example bars used. It is obvious that all bars undergo linear strain-softening behaviour.

Figure 136 shows the development of damage in the midsection of the bar. Also three different interparticle distances are used and the results show no dependence on Δp. It is already obvious from these results that SPH works effectively as a nonlocal regularisation method able to remove dependence on the chosen particle discretisation and is able to limit the strain-softening area to a finite size which can be controlled by the SPH user.

Other results, such as longitudinal displacement, strain and stress, as shown in Figure 136, Figure 137 and Figure 138, are equivalent as well and do not show dependence of results on the chosen discretisation. The development of a distinct displacement difference in Figure 136 and strain in Figure 137 are not caused by deformation localisation. Instead the particles failed and formed free surfaces as shown in Figure 133. The effects of failure are smoothed out over an increasing number of particles with increasing interparticle distance in this experiment. Therefore, the fracture zone in Figure 133 has an equivalent size for all interparticle distances and the displacement and strain results in Figure 136 and Figure 137 are equivalent. The stress drops to zero and vanishes after the onset of damage.

$\Delta p = \frac{200mm}{201}$

$\Delta p = \frac{200mm}{151}$

$\Delta p = \frac{200mm}{101}$

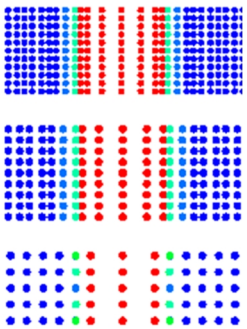

Figure 133: Formation of free surfaces after failure (SPH experiment 3)

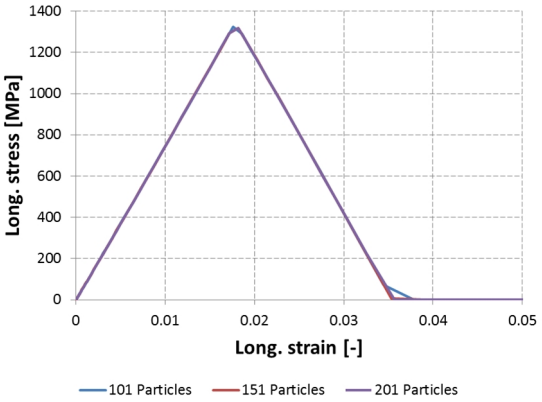

Figure 134: Numerical results for long. stress-long. strain relationship in SPH (experiment 3) with varying interparticle distance

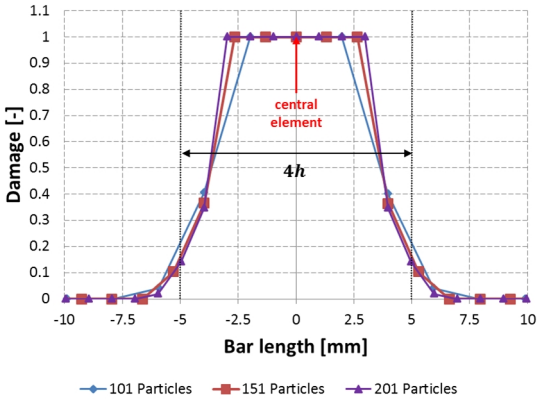

Figure 135: Numerical results for damage in SPH (experiment 3) with varying interparticle distance at $t = 3/4 \cdot 2L/c_e$

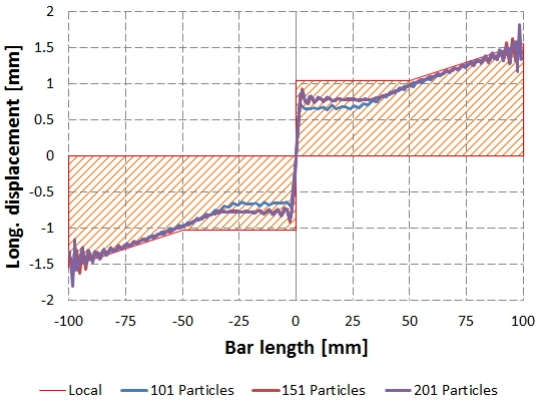

Figure 136: Numerical results for longitudinal displacement in SPH (experiment 3) with varying interparticle distance at $t = 3/4 \cdot 2L/c_e$

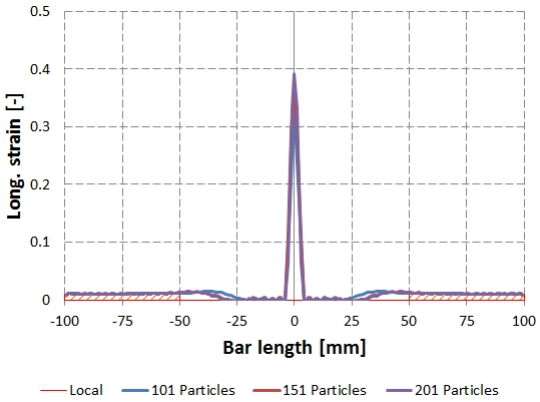

Figure 137: Numerical results for longitudinal strain in SPH (experiment 3) with varying interparticle distance at $t = 3/4 \cdot 2L/c_e$

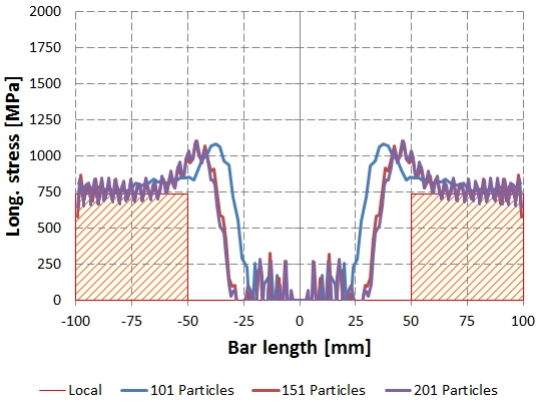

Figure 138: Numerical results for longitudinal stress in SPH (experiment 3) with varying interparticle distance at $t = 3/4 \cdot 2L/c_e$

Finally, the physical size of the damage area is compared graphically in Figure 186 for the fixed physical size of the smoothing length and the three interparticle distance

values used. Depending on the chosen discretisation the number of damage influenced particles varies; however, the physical size of the damage zone is equivalent for all used discretisations. The area has the finite size $4h$ = 10mm.

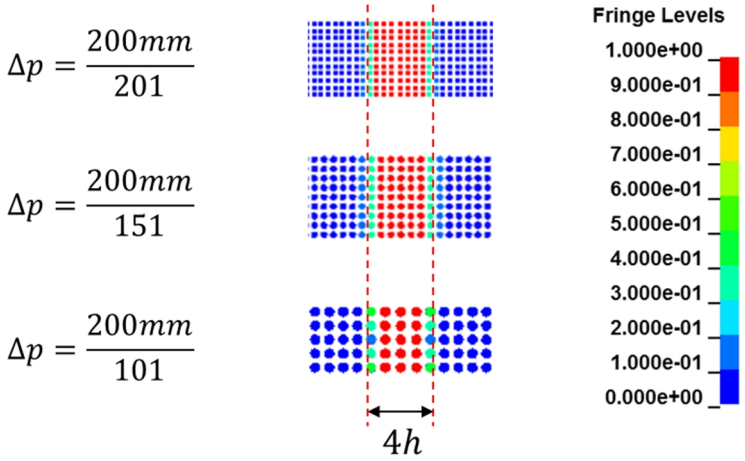

Figure 139: Localisation of damage within a radius of $2h$ (h = 2.5mm) around the strain-softening particle limiting the damage area to a finite size of $4h$ independently of the used interparticle distance Δp before failure (fringe level: damage [-])

6.3 Summary

The aim of this work is to investigate methods other than regularisation methods to keep the boundary value problem well-posed in the presence of strain-softening. The study of the meshless SPH method set out to observe and quantify nonlocal properties of SPH. The particle connectivity in SPH is established by using weighted averages of field variable over a range of particles. The domain over which averaging happens can be controlled by the user. It was presumed in this work that this property makes SPH a nonlocal method by nature.

The investigation of SPH in this chapter has shown that SPH has indeed nonlocal properties and leads to reasonable results with finite damage area. The nonlocal character in SPH is not coming from the material model, such as in regularisation methods. Therefore, the strain-softening material model does not need to be altered. The nonlocal property comes from the use of a weighting function applied to establish SPH particle connectivity, called smoothing function, which is similar to averaging functions used in nonlocal theory. The smoothing function and with this the area of particle interaction is controlled by the smoothing length h which is controlled by the user. The influence of the smoothing length on the strain-softening process was investigated with the example of longitudinal wave propagation as described by Bažant and Belytschko [6]. For the investigation a simple isotropic CDM model with linear strain-softening branch was implemented in the Cranfield SOE in-house SPH code

MCM ("Meshless Continuum Mechanics"). The following SPH experiments were conducted:

- The first experiment investigated the influence of the smoothing length h ($h = \lambda \cdot \Delta p$) on different interparticle distances Δp when the smoothing length depends on the particle distance by a factor of λ = 1.3. It was found that strain-softening effects are averaged over a finite number of neighbouring particles. The number of neighbours is defined by the radius $2h$. Therefore, the results were dependent on the interparticle distance used.
- The second experiment assumed a constant interparticle distance but a change of the factor λ (λ = 1.25, 2.25 and 3.25). Due to the change of λ the smoothing length for the three experiments varied considerably in size. It was found that changing the smoothing length has a big impact on the results obtained. The radius of influence $2h$ increases with the factor λ and includes a rising number of neighbouring particles. This experiment showed that the area influenced by damage can be controlled through h.
- The third experiment applied a fixed physical smoothing length to different interparticle distances. It was expected that strain-softening effects would be smoothed over the fixed area $4h$ and that results would be independent of the used interparticle discretisation. The application of a fixed smoothing length h leads to different factors λ depending on the interparticle distance Δp. However, the physical size of the damage area was the same for all interparticle distances. The results for damage, displacement, strain and stress were equivalent too. The experiment showed that the dependence of results on the interparticle distance can be removed successfully by fixing the smoothing length and with this the radius of influence $2h$.

It was shown that SPH is an effective nonlocal method and does not suffer from the same instabilities as conventional FE CDM models. Sensitivity of results on the spatial discretisation can be removed in SPH by adjusting the smoothing length appropriately and without changing the underlying constitutive material model. Therefore, the strain-softening process can be controlled by the user.

7 Equivalent Damage Force Approach as Solution to Strain-Softening Instabilities

It has been well-established in literature, e.g. by Pijaudier-Cabot and Bažant [96], Sluys and de Borst [110], Rice [99] and Neilsen and Schreyer [86], that strain-softening CDM models lead to an ill-posed boundary value problem (which was shown in Chapter 3, Section 3.2) and leads to numerical instabilities with pronounced mesh-sensitivity of results to the chosen mesh discretisation and non-physical results (which was shown in Chapter 4, Section 4.2).

Regularisation methods emerged as group of methods which is able to remedy issues due to strain-softening. They use higher-order terms of space and time to introduce a length scale parameter, implicitly or explicitly, into constitutive equations which keeps the boundary value problem well-posed and confines damage to a finite size. Considerable research into regularisation methods, namely nonlocal, gradient-enhanced and viscous methods, has been made for well over two decades, such as by Bažant [7; 9], Aifantis [2; 3], Needleman [83; 109], Pijaudier-Cabot [95; 96], Sluys [109; 110] and de Borst [28; 29] to name just a few.

Research in maintaining the well-posed character of the boundary value problem has been focused strongly on the group of regularisation methods. It is found by the author of this work that research on maintaining the boundary value problem, other than regularisation methods, is hardly existent or at least underrepresented. Therefore, this chapter will be concerned with developing a different and new approach. In this new approach, which will be called the “Equivalent damage force” approach, damage is modelled as body force in the equation of motion. This approach will be presented in this thesis for the first time and therefore represents a contribution to knowledge. This will be first explained with an analytical one-dimensional problem and then implemented for an isotropic material with scalar damage variable in DYNA3D. It will be first evaluated for the longitudinal wave propagation problem by Bažant and Belytschko [6] to observe the change from the characteristic strain-softening solution to the solution with the “Equivalent damage force” approach. A second validation example is the modelling of a notched concrete specimen under uniaxial tension. This second test is conducted to compare results with the “Equivalent damage force” approach against experimental results as well as against numerical results of a conventional and well-established regularisation method. These two validation steps are necessary to draw

conclusions about the limits and merits of the “Equivalent damage force” approach in its present form.

Isotropy is the simplest material behaviour; however, many engineering materials, such as composites, have a more complex material behaviour. Therefore, the “Equivalent damage force” approach is extended to orthotropy. It will be shown in this chapter that the application of the “Equivalent damage force” approach to orthotropy requires the definition of a symmetric and positive-definite 8^{th} order damage tensor. The use of 8^{th} order tensor quantities is not common due to its complexity. Therefore, the derivation of the symmetric and positive-definite 8^{th} order tensor is a contribution to knowledge itself.

7.1 “Equivalent Damage Force” Concept

The motivation for the development of the “Equivalent damage force” approach is the lack of alternatives to regularisation methods in dealing with an ill-posed boundary value problem. Regularisation methods have been investigated and applied by a multitude of researches over recent decades [2; 3; 7; 10; 28; 29; 83; 95; 96; 109; 110] to address analytical and numerical instability issues in CDM models with strain-softening. Regularisation methods have been proven to be effective and the high number of publications in this field shows the popularity of these methods. It is not the author’s intention to rival these well-established methods. The purpose is rather to show that other approaches tackling analytical and numerical instabilities may exist and that novelty in this field is still possible.

The idea for the “Equivalent damage force” approach is developed from observations made in Chapter 5 (Section 5.3.1). There it was shown that the consideration of damage (leading to a negative tangent stiffness) in the homogeneous part of the equation of motion leads to an imaginary wave speed in dynamic problems and PDEs change their type from hyperbolic to elliptic. In Chapter 3 (Section 3.2.1) it was stated that the type of a PDE is determined by its homogeneous parts and that inhomogeneous parts do not influence its type but are considered in the particular solution. It is presumed here that the conservation of a hyperbolic PDE type and well-posed boundary value problem can be achieved by modelling damage as a body force as this represents an inhomogeneous part of the equation of motion. In this way the damage influence will be isolated from the homogeneous part of the equation of motion, which is the part influencing the type of PDEs. If this isolation of damage is done the material stability criterion would not be violated and the original character of

the equation of motion, namely the hyperbolic character in dynamic problems, will be preserved at all times and wave propagation in a linear elastic fashion will be possible. Consequently, the boundary value problem will be well-posed in the presence of strain-softening.

The introduction of the “Equivalent damage force” approach will be given through a one-dimensional example of the wave equation as dynamic equation of motion. The consideration of one-dimension is used for simplicity; however, it is fully capable of introducing the concept of an “Equivalent damage force”.

First the linear elastic wave equation without consideration of damage will be investigated.

$$\frac{\partial \sigma}{\partial x} = \rho \frac{\partial v}{\partial t} \tag{7-1}$$

where x is the only space dimension, t is the time of the problem, σ is the axial stress (in x-direction), ρ is the material density and v the particle velocity.

If material behaviour is considered to be linear elastic the axial stress can be expressed with Hooke’s law in which the connection between axial stress σ and axial strain ε is established through the Young’s modulus E.

$$\sigma = E\varepsilon = E \frac{\partial u}{\partial x} \tag{7-2}$$

The speed with which waves propagate in an elastic one-dimensional medium depends on the density ρ and Young’s modulus E of the material.

$$c_e = \sqrt{\frac{E}{\rho}} \tag{7-3}$$

The particle velocity can be expressed as the rate change of the longitudinal position of a particle.

$$v = \frac{\partial u}{\partial t} \tag{7-4}$$

The definition of elastic stress, elastic wave speed and particle velocity can be substituted in (7-1) and lead to another well-known expression of the one-dimensional wave equation.

$$\frac{\partial^2 u}{\partial x^2} - \frac{1}{c_e^2}\frac{\partial^2 u}{\partial t^2} = 0 \tag{7-5}$$

The linear elastic wave equation is a 2nd order PDE for which the type of the PDE can be determined by analysing its eigenvalues (see Chapter 3, Section 3.2.1). In case of the linear elastic wave equation the eigenvalues are well-known and can be read from (7-5) directly.

$$\lambda_{1,2} = \pm\frac{1}{c_e} \tag{7-6}$$

The linear elastic wave equation has two real and distinct eigenvalues and is therefore a hyperbolic PDE.

In a next step the wave equation is investigated with the inclusion of damage but without the application of the "Equivalent damage force" concept. The stress used in the equation of motion is the true stress σ. The true stress is expressed with the effective stress concept introduced in Chapter 3. For the case of uniaxial stress with isotropic damage it reads:

$$\tilde{\sigma} = \frac{\sigma}{1-\omega} \tag{7-7}$$

The effective stress can be expressed in terms of the Young's modulus E and uniaxial strain ε.

$$\sigma = (1-\omega)E\varepsilon \tag{7-8}$$

The substitution of the constitutive equation in (7-8) into the wave equation leads to:

$$\frac{\partial}{\partial x}\big((1-\omega)E\varepsilon\big) - \frac{E}{c_e^2}\frac{\partial^2 u}{\partial t^2} = 0 \tag{7-9}$$

It is assumed that damage is evolving with increasing deformation. Therefore, the chain rule needs to be applied to (7-9). κ is a history variable which represents deformation history and is equivalent to strain ε (see Chapter 5, Section 5.3).

$$\frac{\partial \varepsilon}{\partial x}E\left(1-\omega-\frac{\partial \omega}{\partial \kappa}\varepsilon\right) - \frac{E}{c_e^2}\frac{\partial^2 u}{\partial t^2} = 0 \tag{7-10}$$

The damage influenced part in (7-10) represents the tangent modulus of the strain-softening branch.

$$E_t = \left(\frac{\partial \sigma}{\partial \varepsilon}\right)_t < 0 \tag{7-11}$$

$$\left(\frac{\partial \sigma}{\partial \varepsilon}\right)_t = E\left(1 - \omega - \frac{\partial \omega}{\partial \kappa}\varepsilon\right) \tag{7-12}$$

The eigenvalues of (7-10) can be determined easily. The equation of motion with general damage has two distinct eigenvalues which are imaginary. Therefore, the wave equation under influence of damage has an imaginary wave speed and an elliptic PDE type.

$$\lambda_{1,2} = \pm \frac{1}{c_e\sqrt{1 - \omega - \frac{\partial \omega}{\partial \kappa}\varepsilon}} \tag{7-13}$$

So far it was assumed that the equation of motion does not take into consideration the influence of a body force and had only homogeneous parts. Equation (7-14) represents the standard equation of motion with the influence of a body force.

$$\frac{\partial^2 u}{\partial x^2} - \frac{1}{c_e^2}\frac{\partial^2 u}{\partial t^2} = f(x,t) \tag{7-14}$$

The body force $f(x,t)$ is an inhomogeneous part of the equation of motion and is not taken into consideration for the determination of eigenvalues of a PDE. Therefore, the eigenvalues for (7-14) are equivalent to the eigenvalues of the linear elastic wave equation, which are two real and distinct eigenvalues.

$$\lambda_{1,2} = \pm \frac{1}{c_e} \tag{7-15}$$

This way the wave equation under consideration of a body force is still hyperbolic in type and maintains the wave propagation properties of the linear elastic form. The body force as the inhomogeneous part of the equation of motion becomes part of the particular solution.

The feature of a body force being an inhomogeneous part of the equation of motion does not change the hyperbolic type of the PDE. This is of high interest in this work. It was shown in (7-10) and (7-13) that the inclusion of damage leads to imaginary eigenvalues of the equation of motion. The type of PDE would be elliptic and a well-posed boundary value problem could not be achieved. This is avoided when the

damage influenced parts are made a body force in which evolution of the body force is defined through the deformation history variable κ.

$$\frac{\partial \varepsilon}{\partial x} E - \frac{1}{c_e^2} \frac{\partial^2 u}{\partial t^2} E = \frac{\partial}{\partial x} (E \varepsilon \omega) \tag{7-16}$$

$$\frac{\partial \varepsilon}{\partial x} E - \frac{1}{c_e^2} \frac{\partial^2 u}{\partial t^2} E = \frac{\partial \varepsilon}{\partial x} \left(\omega + \frac{\partial \omega}{\partial \kappa} \varepsilon \right) E$$

Equation (7-16) represents damage influenced terms as a body force in the wave equation. Due to this the hyperbolicity of the governing equations is preserved and wave propagation in its original linear elastic fashion will be possible.

It should be noted that the expression in (7-16) has equivalent terms to the local expression in (7-10) and does not change the properties of the original CDM material model itself; however, (7-16) does not encounter the same analytical instability issues as (7-10). It can be assumed here with confidence that the approach of the “Equivalent damage force” will remove the issue of spurious mesh-sensitivity in numerical simulations too as these are caused by the loss of well-posedness of the governing equations. The idea of an “Equivalent damage force” has not been presented in literature yet and was first developed in this chapter.

The aim of this work is to remove analytical and numerical issues of strain-softening continua with a method different to regularisation methods. This was achieved here as modelling damage as a body force does not require the introduction of higher-order terms. However, it should be noted that the introduction of higher-order terms in regularisation methods does not only serve the purpose of maintaining a well-posed boundary value problem. The introduction of additional terms also includes a length scale parameter which dictates the area in which damage develops and with which localisation of damage in a finite size is modelled. This was previously shown in Chapter 6 where SPH was quantified as a nonlocal method and is reflective of the observed behaviour of real materials. In the “Equivalent damage force” approach the development of damage will depend on the development of the state variable strain. Therefore, damage will depend on the strain profile in the considered area. As a consequence the width of the localisation area in the “Equivalent damage force” approach will depend on the applied softening branch.

This section presented the explanation of the “Equivalent damage force” approach with one-dimensional considerations. Nevertheless, this can be applied in a straightforward

manner for isotropic CDM models with a scalar damage variable because a clear separation of damage can be achieved. This separation is less obvious for orthotropic material models with a tensorial damage variable but will be further developed in the course of this chapter.

7.2 Validation of “Equivalent damage force” Concept

The “Equivalent damage force” approach is a new concept to maintain the well-posed boundary value problem while strain-softening behaviour. Therefore, it requires numerical investigation to determine its characteristic behaviour in the strain-softening domain and needs to be compared to results of conventional methods, such as regularisation methods. Following these evaluation conclusions can be drawn regarding the capabilities and limitations of the “Equivalent damage force” approach.

The first evaluation of the “Equivalent damage force” approach should enable a clear demonstration of changed behaviour in the strain-softening domain in comparison to a standard local CDM approach. This can be achieved by using the strain-softening bar example of Bažant and Belytschko [6]. This example is a longitudinal wave propagation problem for which the time and location of strain-softening initiation is well-known as well as its characteristic strain-softening solution for conventional CDM models (see Chapter 3, Section 3.2.3 for analytical considerations and Chapter 4, Section 4.2 for numerical investigation).

A second evaluation is required to establish the suitability and limitations of the “Equivalent damage force” approach to engineering applications. Therefore, results for the “Equivalent damage force” approach need to be compared for a real physical experiment and well-established conventional FE methods for dealing with strain-softening instabilities in CDM models, such as regularisation methods. To achieve this a tension test of a concrete specimen is chosen for which experimental results could be obtained from literature and for which FE results with regularisation methods by other researchers exist.

7.2.1 Isotropic Material Model with Linear Strain-Softening

The evaluation of the “Equivalent damage force” approach will be carried out with an isotropic CDM model with linear strain-softening branch. This model in its conventional local form as well as in its modified form, in the sense of the “Equivalent damage force” approach, were implemented in the public FE code DYNA3D. These two models are

essentially the same except for the treatment of damage in the equation of motion. Therefore, the change in characteristic properties of the solutions obtained can be observed clearly.

The stress-strain diagram for the isotropic damage material with linear softening law is shown in Figure 140.

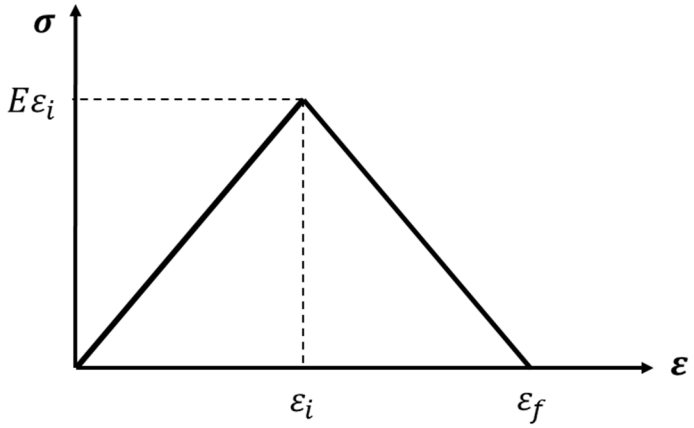

Figure 140: Material behaviour of simplified material model with strain-softening in DYNA3D

The onset of strain-softening is determined when the initiation strain ε_i for strain-softening is reached:

$$\varepsilon_i = \frac{\sigma_0}{E} \tag{7-17}$$

where σ_0 is the initial yield strength and E the Young's modulus. Stress vanishes linearly after initiation of damage until the critical failure strain ε_f is reached.

It is desired to express the isotropic damage variable ω in terms of the values of initial failure and critical failure strain. A clarification of this approach is given in Figure 141.

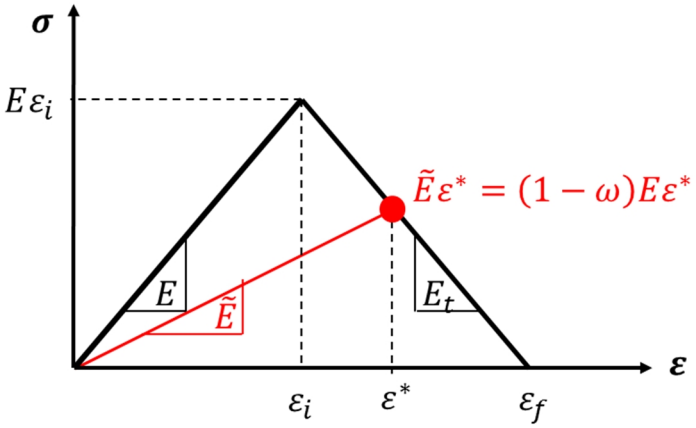

Figure 141: Determination of damage variable from simplified model with linear strain-softening

The initial yield strength is expressed in terms of the Young's modulus and the initial failure strain: $\sigma_0 = E\varepsilon_i$. E_t is the tangent stiffness of the strain-softening branch and $\tilde{E}$ is the secant stiffness of the damaged material. Points on the softening branch and therefore the damage variable can be determined with the help of the secant stiffness. The secant stiffness is defined in terms of the Young's modulus E:

$$\tilde{E} = (1 - \omega)E \tag{7-18}$$

Using the previous definitions the damage variable can be defined in terms of ε_i and ε_f. The tangent modulus is the slope of the strain-softening branch and is therefore defined as:

$$E_t = \frac{-E\varepsilon_i}{\varepsilon_f - \varepsilon_i} \tag{7-19}$$

A point on the softening branch is defined as:

$$\tilde{E}\varepsilon^* = (1 - \omega)E\varepsilon^* = E_t(\varepsilon^* - \varepsilon_f) = \frac{-E\varepsilon_i}{\varepsilon_f - \varepsilon_i}(\varepsilon^* - \varepsilon_f) \tag{7-20}$$

Therefore the damage variable is determined with:

$$\omega = \frac{\varepsilon_f}{\varepsilon^*}\left(\frac{\varepsilon^* - \varepsilon_i}{\varepsilon_f - \varepsilon_i}\right) \tag{7-21}$$

7.2.2 Validation Problems

7.2.2.1 Validation Problem 1: Strain-Softening Bar

The first validation example is the strain-softening bar by Bažant and Belytschko [6]. This model has been presented at several stages of this work, such as showing analytically and numerically the problems connected to strain-softening (see Chapter 3, Section 3.2.3 and Chapter 4, Section 4.2), evaluating strain-softening stabilisation models in readily available FE software (see Chapter 4, Section 4.3) and quantifying the nonlocal properties of SPH (see Chapter 6, Section 6.2.3). It will be used for a first evaluation of the "Equivalent damage force" approach as this example clearly demonstrates characteristic properties of CDM models with strain-softening and allows an easy accessible comparison of different methods. Therefore, the change of results in the strain-softening domain for treatment of damage as body force can be easily observed.

A uniaxial bar as described by Bažant and Belytschko [6] in their analytical approach to the softening problem will be used to investigate the behaviour of the simplified strain-softening model. The experiment has been previously described in Chapter 3. The bar has an overall length of $2L$ = 200mm and squared cross-section of 10mm edge length. The origin of the coordinate system lies in the centre of the bar (x = 0). The longitudinal direction is denoted with x. All degrees of freedom except for the longitudinal direction are restricted in order to ensure uniaxial strain conditions. The bar is loaded at both ends with a constant velocity v which causes waves of constant stress and strain in the bar. The general setup of the strain-softening bar is shown in Figure 142.

The following input data is used:

Table 7-1: Input data for isotropic strain-softening model

Value	Sign	Magnitude	Unit
Density	ρ	$1.55 \cdot 10^{-9}$	t/mm^3
Young's Modulus	E	70800	MPa
Poisson's ratio	v	0.125	–
Initiation failure strain	ε_i	0.018	–
Failure strain	ε_f	0.036	–
Softening modulus	E_t	−70800	MPa

The numerical experiments are designed in a way that strain-softening occurs when the loading waves meet in the centre of the bar. Hence, the bar responds elastically for $t < L/c_e$. The softening solution will be valid for $t \geq L/c_e$. The determination time of the problem is $t = 2 \cdot L/c_e$ at which the waves have travelled the whole length of the bar.

Strain-softening occurs instantaneously at x = 0 when both loading waves meet. The magnitude of the constant velocity v in the elastic area has to follow Bažant's and Belytschko's [6] solution:

$$\frac{\varepsilon_f}{2} \leq \frac{v}{c_e} < \varepsilon_f$$

Due to $c_e = \sqrt{E/\rho}$ the elastic wave speed can be determined as c_e = 6758507.18mm/s. Therefore the minimum applied velocity has to be $v_{min} = \frac{\varepsilon_f}{2} \cdot c_e$. and the maximum velocity has to be $v_{max} = \varepsilon_f \cdot c_e$. A tensile loading of $v_{const.} = 7 \cdot 10^4 mm/s$ will be used.

Strain-softening experiments in FE will be done with different mesh discretisations to investigate mesh-sensitivity. The setup is shown in Figure 142. Solid elements will be

used and the element size is consistent throughout the bar. The following discretisations were chosen:

- Bar 1: 11 elements
- Bar 2: 31 elements
- Bar 3: 51 elements
- Bar 4: 101 elements

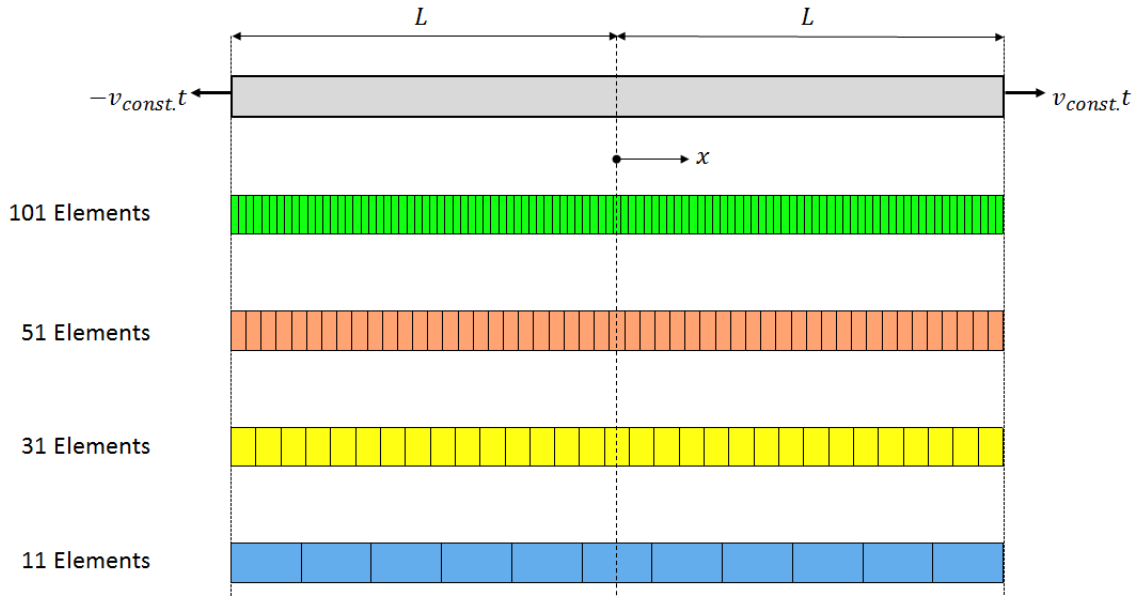

Figure 142: Strain-softening bar by Bažant and Belytschko [6] with different mesh discretisations for numerical testing of modified strain-softening CDM model

In the following the conventional and modified strain-softening solutions will be compared for longitudinal displacement, strain and stress. The time $t = 3/4 \cdot 2L/c_e$ is chosen as example as the waves from the bar's edges have travelled 3/4 of the bar's length. At this stage the area $-L/2 \leq x \leq L/2$ is governed by the strain-softening solution. The areas outside the strain-softening area still obey the elastic solution. The internal energy will be presented for the overall bar for the full time span of the test $0 \leq t \leq 2L/c_e$.

Figure 143 and Figure 144 show the stress-strain curves for conventional and modified strain-softening tests respectively in the element located at $x = 0$. The typical strain-softening behaviour in the middle element is clearly visible in Figure 143. Figure 144 shows the stress-strain behaviour of the central element for the modified strain-softening model in which the damage influence is introduced as body force. It is clearly visible that all spatial discretisation undergo strain-softening. Softening starts for the defined initiation strain and stress reaches zero for the assigned failure strain. All curves show an instability right after the onset of strain-softening. This is especially

obvious for bar 4 with the finest spatial discretisation. The stress-strain behaviour seems to follow an unloading path first before it continues the softening branch.

Figure 145, Figure 147 and Figure 149 show the development of damage in the softening element and along the bar in the conventional strain-softening case. It is visible from Figure 145 and Figure 147 that damage evolution starts for the defined strain-softening initiation strain ε_i and reaches its maximum value for ε_f and starts at the time $t = L/c_e$. The area along the bar in which damage accumulates is governed by the size of the single element at $x = 0$. Elements outside the strain-softening domain are not affected by damage.

It is visible from Figure 146 for the modified model, as in the conventional strain-softening bar, that the damage development starts when the initiation strain ε_i is reached and reaches an value of one for the failure strain ε_f. The curves can be said to be equivalent with the curves for the conventional model in Figure 145. However, all curves of damage over longitudinal strain show an instability which occurs for all bars at a damage value $\omega \approx 0.35$ before damage continues to grow. This instability corresponds with the instability observed in the stress-strain diagrams in Figure 144. Figure 146 shows the development of damage in the softening element over time. Damage is initiated for $t = L/c_e$, also with a small time delay depending on the spatial discretisation. The damage development reaches a plateau for the value $\omega \approx 0.35$ before it continues to grow. This occurrence of this plateau coincides with the instability previously observed. Figure 150 shows the development of damage along the bar for $t = 3/4 \cdot 2L/c_e$. The most important observation is that the area of damage is no longer confined by the size of the softening element. Instead damage develops in a number of elements which span an equivalent size for all spatial discretisations except for bar 4. It can be seen also that the magnitude of damage in the bars with course element discretisation, especially bar 1, lag behind the bars with finer spatial discretisation. This is especially visible for the damage value in the softening element. The value for bar 1 is only one third of the value for bar 4, which has already reached the maximum damage value $\omega = 1$.

Figure 151, Figure 153 and Figure 155 show the results for longitudinal displacement, strain and stress for the conventional strain-softening case at $t = 3/4 \cdot 2L/c_e$. Figure 157 shows the results for internal energy for the conventional strain-softening between $0 \leq t \leq 2L/c_e$. The results show a strong dependence on the chosen mesh

discretisation in the strain-softening area $-L/2 \leq x \leq L/2$ which is characteristic for conventional strain-softening. It can be observed that the results follow the analytical solution increasingly accurate with increasing mesh fineness. Also the area of strain-softening becomes more refined with increasing mesh fineness.

Figure 152 shows the longitudinal displacement for the modified model. In difference to the results of the conventional strain-softening model (see Figure 151), all bars show a consistent development of deformation. It is most important to notice that deformation is not localised in a single element and, therefore, the characteristic displacement discontinuity for strain-softening does not occur. A dependence of the displacement results on the used discretisation does not appear also. It can be noticed that the results in the area $-L/2 \leq x \leq L/2$, governed by the softening solution, are fluctuating around a mean value. It is assumed that this is associated with the instability occurring earlier.

Figure 154 show the strain profiles for the experiments with the modified strain-softening material model. These results distinguish clearly from the strain profiles of the conventional model in Figure 153. Most noticeable is that strain is not accumulated in a single element anymore and does not grow infinitely. Instead strain drops to zero when the maximum damage value is reached and the bars start to unload. It can be seen that the profiles for bar 1 and 2 have not dropped to zero at this point in time; however, damage has not developed its full magnitude for this bars as it can be seen in Figure 150. But in bar 1 and 2 it can been seen clearly too that strain does not localise and therefore waves still propagate.

Figure 156 shows the stress profiles corresponding to Figure 154. Stress vanishes when the elements have reached maximum damage and strain vanishes. After the occurrence of full damage, ω = 1, the bar unloads. Stress has not vanished for bar 1 and 2 with course spatial discretisations. However, these bars have not reached maximum damage at the considered point in time and strain has not vanished either.

Figure 158 shows the consumption of energy in the strain-softening bars for the modified models. It is clear that the bars can consume further energy even in the strain-softening zone. The vanishing internal energy during strain-softening was one of the most crucial difficulties in conventional strain-softening models. Also the results follow a common path, fluctuations in results are observed.

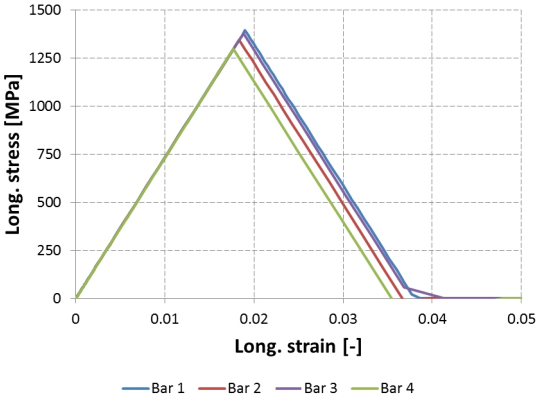

Figure 143: Numerical results for long. stress-long. strain relationship in conventional strain-softening case

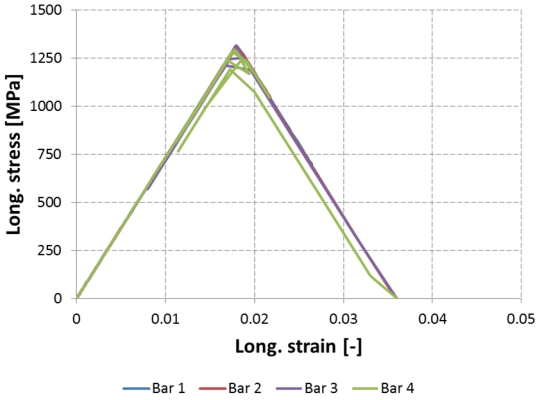

Figure 144: Numerical results for long. stress-long. strain relationship in modified strain-softening case

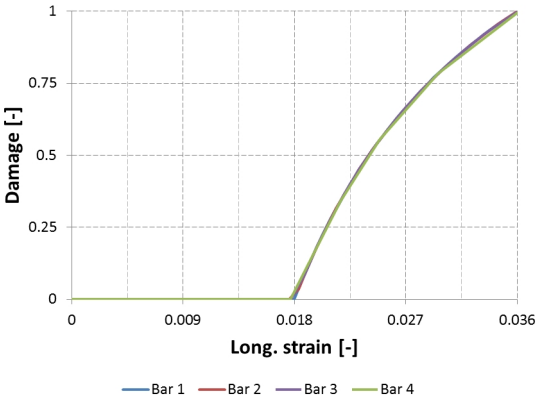

Figure 145: Numerical results for damage in softening element in conventional strain-softening case as function of strain

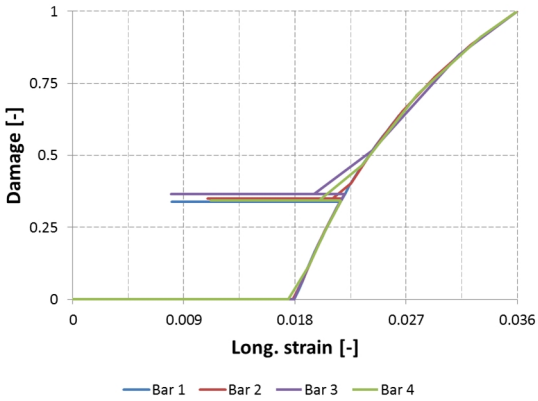

Figure 146: Numerical results for damage in softening element in modified strain-softening case as function of strain

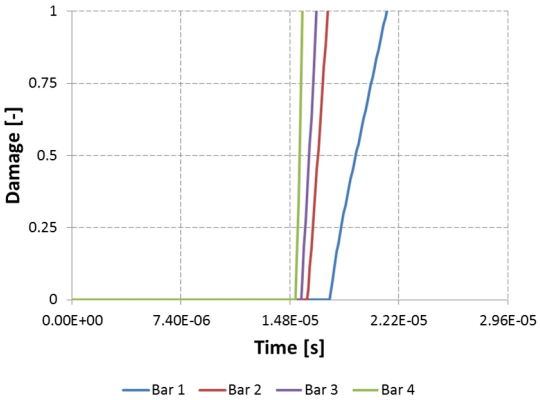

Figure 147: Numerical results for damage in softening element in conventional strain-softening case

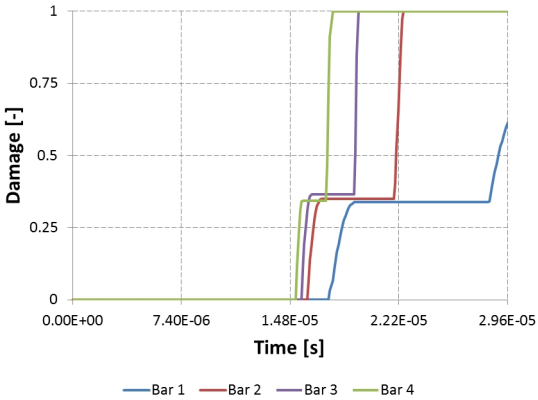

Figure 148: Numerical results for damage in softening element in modified strain-softening case

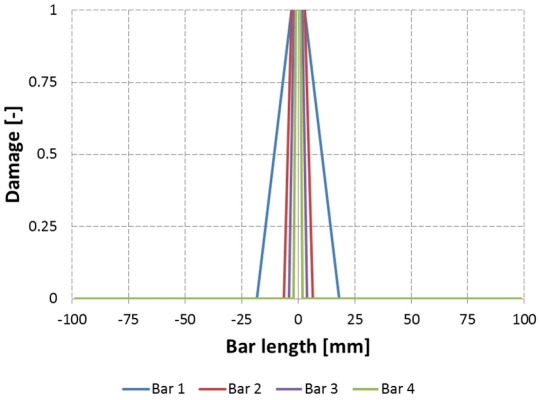

Figure 149: Numerical results for damage in conventional strain-softening case at $t = 3/4 \cdot 2L/c_e$

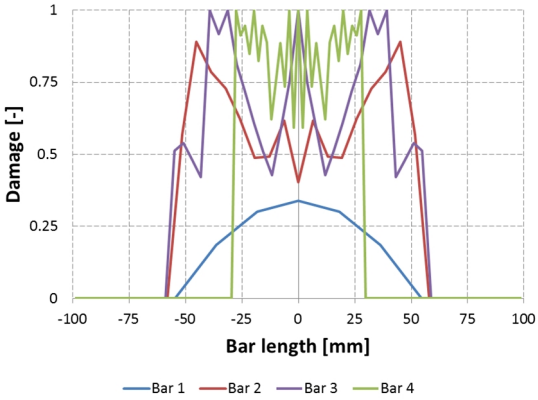

Figure 150: Numerical results for damage in modified strain-softening case at $t = 3/4 \cdot 2L/c_e$

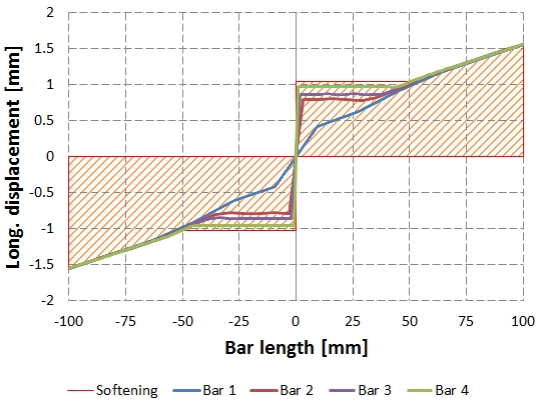

Figure 151: Numerical results for longitudinal displacement in conventional strain-softening case at $t = 3/4 \cdot 2L/c_e$

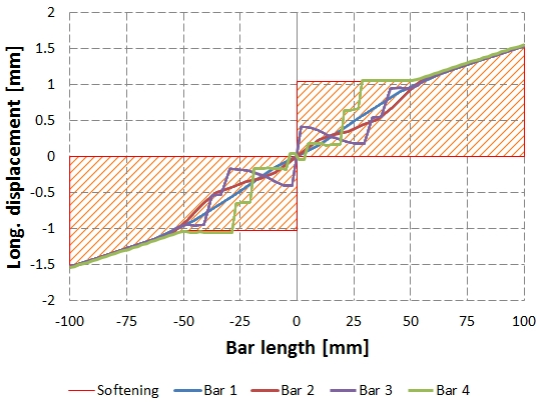

Figure 152: Numerical results for longitudinal displacement in modified strain-softening case at $t = 3/4 \cdot 2L/c_e$

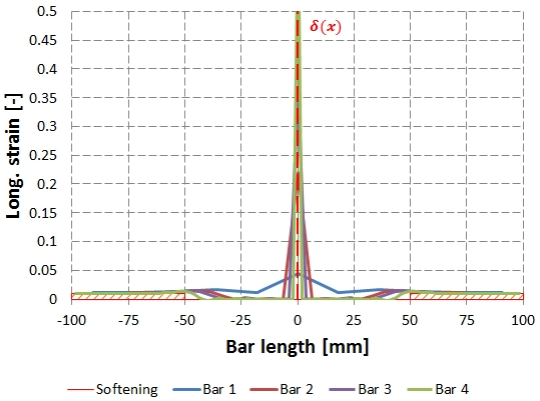

Figure 153: Numerical results for longitudinal strain in conventional strain-softening case at $t = 3/4 \cdot 2L/c_e$

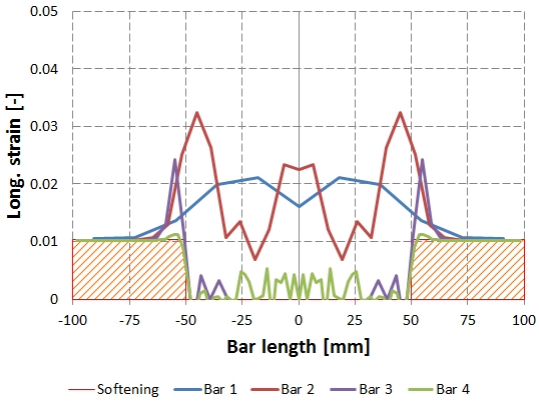

Figure 154: Numerical results for longitudinal strain in modified strain-softening case at $t = 3/4 \cdot 2L/c_e$

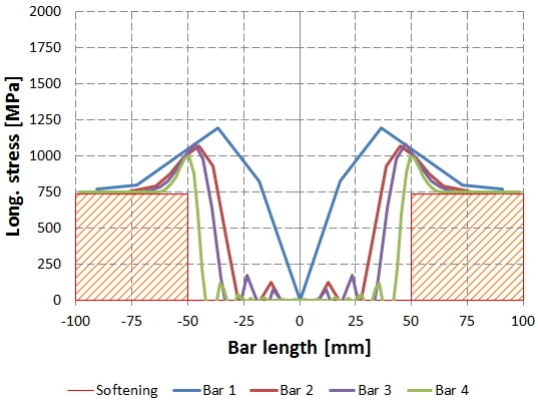

Figure 155: Numerical results for longitudinal stress in conventional strain-softening case at $t = 3/4 \cdot 2L/c_e$

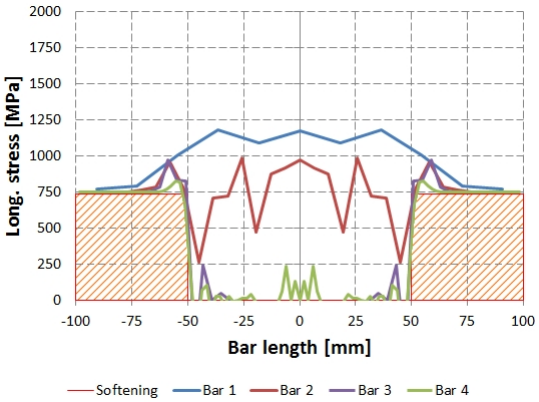

Figure 156: Numerical results for longitudinal stress in modified strain-softening case at $t = 3/4 \cdot 2L/c_e$

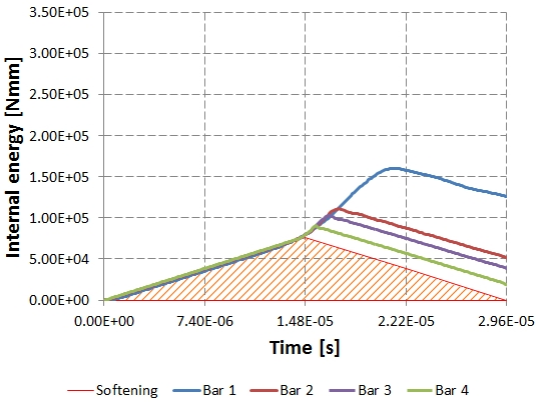

Figure 157: Numerical results for internal energy in conventional strain-softening bar for $0 \leq t \leq 2 \cdot L/c_e$

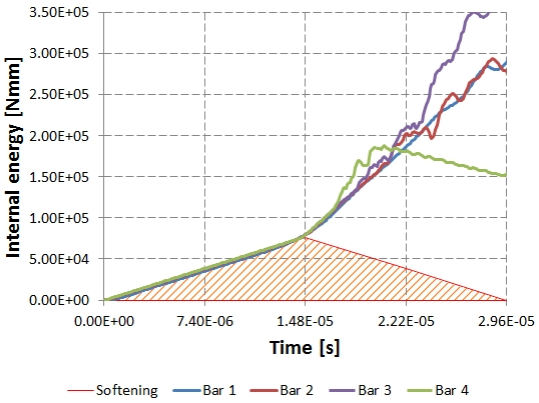

Figure 158: Numerical results for internal energy in modified strain-softening bar for $0 \leq t \leq 2 \cdot L/c_e$

The aim of the introduction of an “Equivalent damage force” was to maintain a well-posed boundary value problem and prevent mesh-sensitivity of numerical results in the presence of strain-softening. In the presented numerical results is was shown that the exclusion of damage influenced terms from the homogeneous parts of PDEs and its introduction as “Equivalent damage force” indeed prevent these unwanted features of strain-softening. Wave propagation in linear elastic fashion is still possible and results converge to a unique solution.

The numerical results of the modified strain-softening model showed instabilities in the development of damage. Additionally, it was observed that results in the domain influenced by strain-softening undergo fluctuation. The origin of these instabilities is currently not known but it is assumed that they are caused by an implementation error. The problem will be further investigated but were not scope of this work.

7.2.2.2 Validation Problem 2: Concrete Tension Test

So far numerical investigations have been kept one-dimensional with the strain-softening bar example by Bažant and Belytschko [6]. This was done to show the main characteristic of the “Equivalent damage force” approach to strain-softening. However, it is required to compare the solution obtained with more conventional material models, such as results for regularisation methods, and experimental results to draw conclusions about suitability and limitations of the “Equivalent damage force” approach in its current form.

The investigation of damage in a double notched concrete specimen under uniaxial tension was chosen as test problem. This problem was originally investigated by Hordijk [50] experimentally and was picked by other researchers as an example for the evaluation of nonlocal integral FE methods [12; 79] and the gradient-enhanced method [91]. Therefore, experimental evidence and a basis for comparison with conventional FE methods is given.

The experimental static softening studies for tension in concrete by Hordijk [50] will be used as reference study here. He performed deformation-controlled uniaxial tension tests of concrete specimens with cross-sectional area $60mm \cdot 50mm$ and variable length (L = $50mm, 125mm$ and $250mm$). A low loading rate of $0.08\mu m/s$ was applied incrementally to avoid abrupt failure of concrete. The material data of the concrete specimens were given with Young’s modulus E = $18000MPa$ and Poisson’s ratio ν = 0.2. A geometric imperfection of two notches, $5mm$ by $5mm$ area, at half-length was incorporated to trigger failure of the concrete specimens in the midsection. Both ends of the concrete specimens were glued to loading platens to apply uniaxial tension. One loading platen was fixed and the other platen was loaded with a hydraulic rig. It was ensured that the loading platens stayed parallel at all times to enable a uniform and symmetric crack opening in the centre of the concrete specimen. The average deformation over the failure zone was measured with four pairs of extensometers which have a gauge length of l_{gauge} = $35mm$. A schematic representation of the test rig and placement of extensometers used by Hordijk [50] is shown in Figure 159.

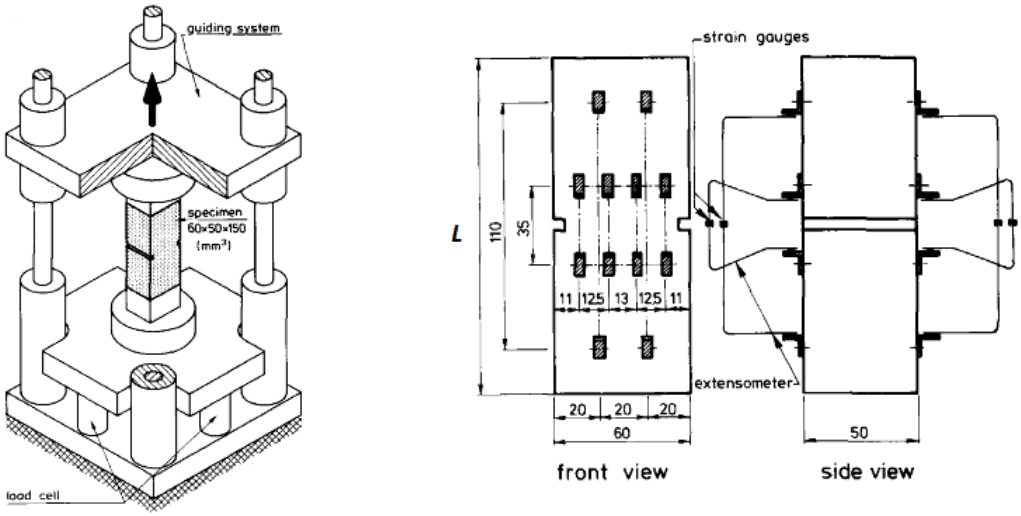

Figure 159: Concrete specimen mounted in tensile testing equipment and location of strain gauges used by Hordijk [50]

The results for the three test specimens considered here are presented as average stress-deformation curves by Hordijk [50] (see Figure 160). The stress is the engineering stress which is defined as load divided by notched original cross-sectional area. The deformation is the average deformation measured by the extensometer over the gauge length l_{gauge} = 35mm.

The stress-deformation plots for the different specimen lengths presented in Figure 160 show a smooth ascending branch first until a peak stress is reached. This is a common behaviour observed in the three considered concrete specimens. After the peak stress the engineering stress-deformation curve undergoes a steep descending branch indicating the concrete's brittle material behaviour. However, after the initial steep drop the slope levels and results in a long tail, resulting from debonding and fracture on the microscale [91]. Therefore, concrete does not lose its complete load-carrying capability upon damage initiation and undergoes a gradual degeneration of material properties due to softening [91]. It can be observed that the descending branch in Figure 160 undergoes irregularities which smooth out with decreasing specimen length. The observed irregularities were linked to an asymmetric deformation behaviour of the concrete specimens in the investigations by Peerlings et al. [91].

It can be seen in Figure 160 that the average curve for the shortest specimen with 50mm length deviates from the curves with specimen length 125mm and 250mm. The peak stress in the cross-section reached for the two longer specimens can be determined with ~3.2MPa at 0.08mm average gauge deformation. The peak stress for the shortest specimen is ~3.4MPa at 0.14mm. The difference in results is contributed

by Hordijk [50] to the set up of the stiff loading platens which might have a more significant impact on shorter specimens.

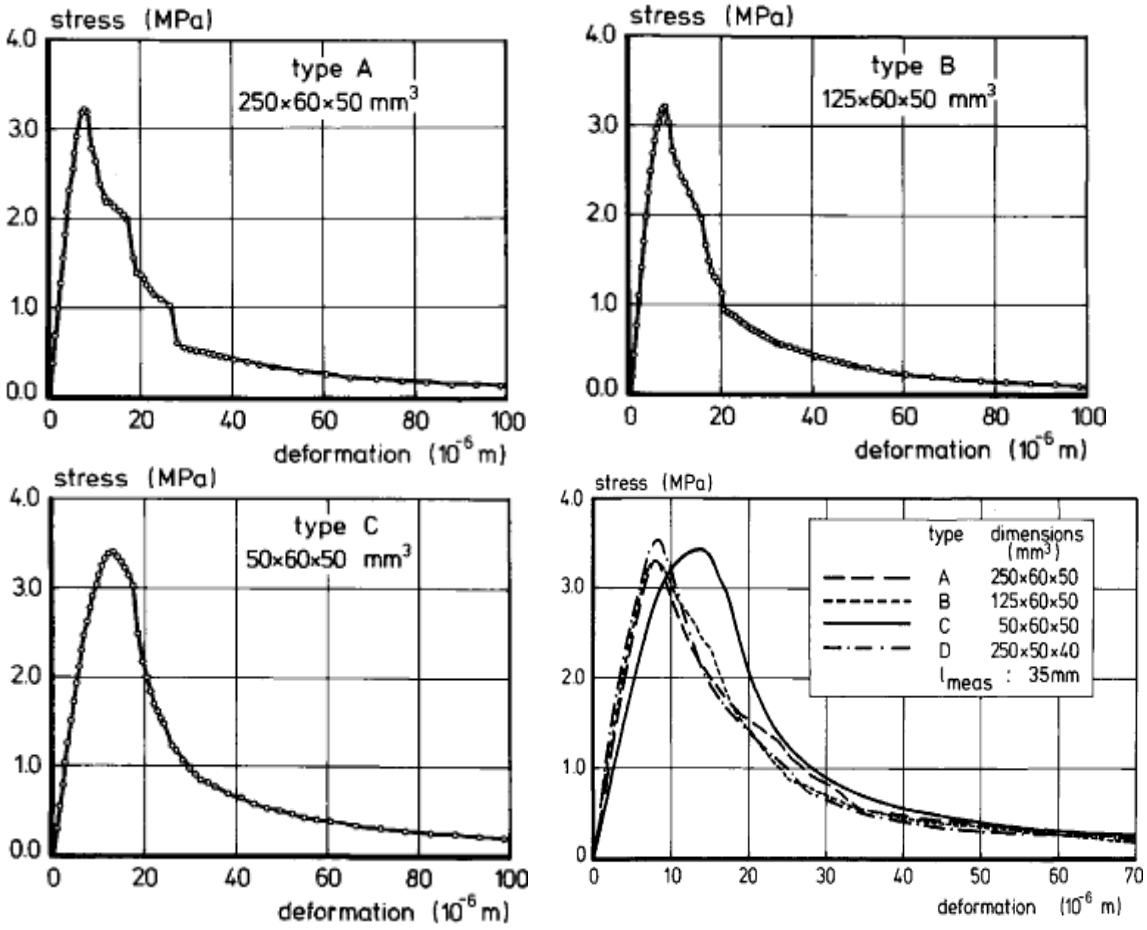

Figure 160: Average stress-deformation results obtained for the three geometries presented over 35mm gauge length by Hordijk [50]

The example of a concrete specimen under tension as it was described by Hordijk [50] was used by a number of researchers as evaluation example in the field of regularisation methods. One example is the research by Bobiński and Tejchman [12] who evaluated a nonlocal integral CDM approach by modelling a 125mm × 60mm × 50mm concrete specimen with three mesh discretisations in the gauge area for a plane stress FE example. They applied an exponential softening law for the evolution of damage to match the descending branch in the stress-deformation diagram described in Hordijk's results [50] as seen in Figure 160. The same damage model was applied to represent concrete damage behaviour by Peerlings et al. [91] to evaluate their gradient-enhanced regularisation method.

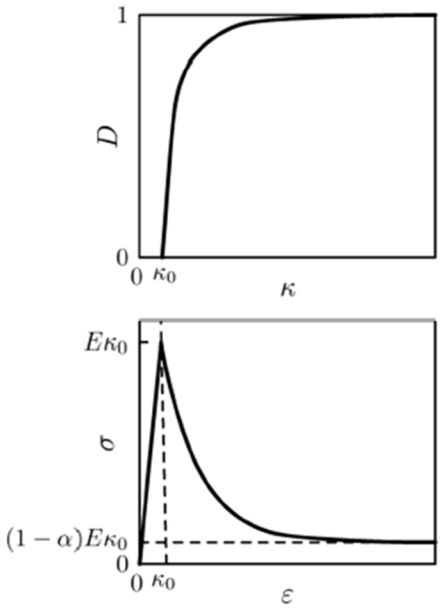

Damage variable evolution:

$$D(\kappa) = 1 - \frac{\kappa_0}{\kappa}(1 - \alpha + \alpha \cdot \exp[-\beta(\kappa - \kappa_0)])$$

with

κ: history variable representing strain

κ_0: initial value of damage threshold parameter

β: rate of damage evolution

α: limiting factor for min. stress when $\varepsilon \to \infty$

Figure 161: Exponential softening law used in numerical investigation of uniaxial tension in a notched concrete specimen by Bobiński and Tejchman [12] and Peerlings et al. [91]

Bobiński and Tejchman [12] achieved mesh-independent results by applying their nonlocal CDM model to a plane state of stress. They first applied a constant internal length parameter of $l_c = 5mm$ which resulted for all mesh discretisation in a localisation zone of the width with $22mm$ (see Figure 163). It can be seen in Figure 163 that damage originates from the notches which represent a geometric irregularity. Additionally, it can be seen that damage develops in two branches around the notched cross-section with little or no damage in the cross-section's centre depending on the mesh discretisation used. The stress-deformation curves achieved are presented in Figure 162. The curves for this example were identical for all mesh discretisations and matched the experimental results for the $125mm \times 60mm \times 50mm$ concrete specimen well although a deviation from the experimental peak stress was observed which Bobiński and Tejchman [12] contributed to the lack of hardening.

Bobiński and Tejchman [12] investigated additionally the influence of a varying internal length scale. It was observed that the peak stress increases with increasing length scale parameter l_c and that the slope of the softening branch is less steep for increasing length scale parameter l_c, therefore the modelled material behaves more ductile. The stress-deformation curves for varying internal length scales are presented in Figure 164. The size of the localisation zone increased with increasing length scale parameter as expected (see Figure 165).

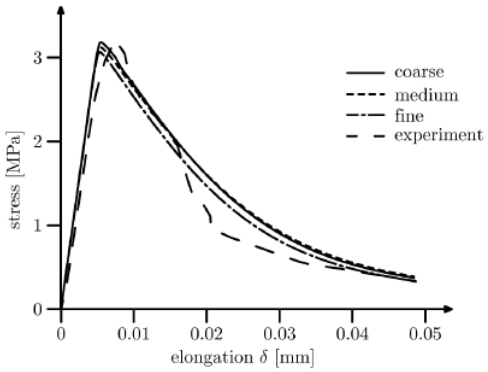

Figure 162: Stress-deformation curves for $125mm \times 60mm \times 50mm$ concrete specimen with different mesh discretisations and constant internal length scale by Bobiński and Tejchman [12]

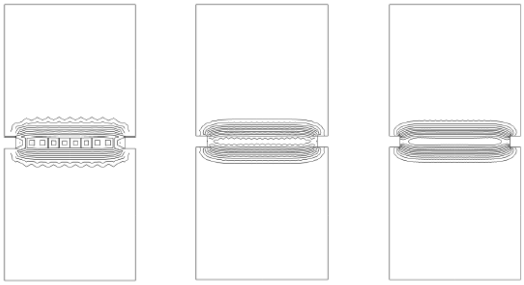

Figure 163: Damage contours for concrete specimen under uniaxial tension for nonlocal FE method with constant internal length for coarse, medium and fine mesh (left to right) by Bobiński and Tejchman [12]

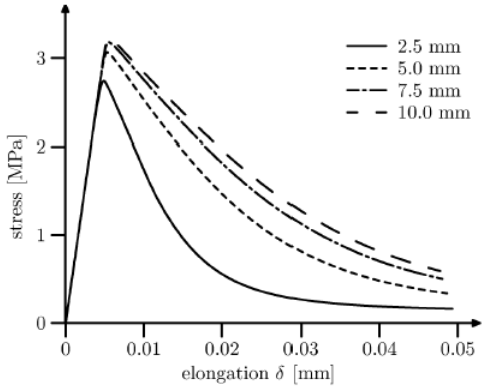

Figure 164: Stress-deformation curves for $125mm \times 60mm \times 50mm$ concrete specimen with varying internal length scale by Bobiński and Tejchman [12]

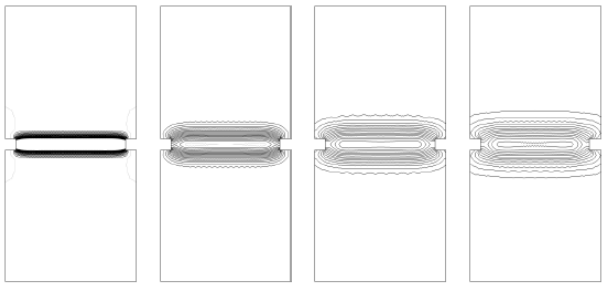

Figure 165: Damage contours for concrete specimen under uniaxial tension for nonlocal FE method with varying internal length for constant mesh size by Bobiński and Tejchman [12]

The validation study of the “Equivalent damage force” model in this work will be conducted with a $125mm \times 60mm \times 50mm$ concrete specimen as example. This example was chosen as results with the exact same specimen are available in the form of experimental results given by Hordijk [50] and nonlocal integral FE results by Bobiński and Tejchman [12]. Additionally, the results will be compared to the standard local continuum model for which the modifications required for the “Equivalent damage force” model were made. This allows a direct comparison of the impact which the “Equivalent damage force” approach makes on the strain-softening solution.

So far the investigations on strain-softening in this work were made for dynamic problems in which the ill-posed boundary value problem is caused by the change of hyperbolic to elliptic type of PDEs. However, the example of concrete failure considered in this section is a static loading case. Nevertheless, the underlying

problem, namely the ill-posed boundary value problem due to the negative tangent stiffness caused by strain-softening, is common for static and dynamic load cases. The difference is that static problems are governed by elliptic PDEs and change to hyperbolic type due to strain-softening which leaves the overall mathematical problem ill-posed and causes mesh-sensitivity of numerical results. The "Equivalent damage force" approach was developed in Section 7.1 as method to achieve a stable constitutive material model with strain-softening for dynamic cases. But it can be applied to static problems without any modifications as the static equation of motion neglects time-dependent terms and is otherwise equivalent to the dynamic equation of motion (see Chapter 2, Section 2.4).

The material model used was presented in Section 7.2.1 of this chapter. It is an isotropic material model with isotropic damage and a linear strain-softening law. The evolution of the damage variable is defined in terms of the strain at which the material's ultimate strength is reached, ε_i, and the strain at which stress vanishes, ε_f. The material input data for the initial linear elastic behaviour was chosen in accordance with input data by Bobiński and Tejchman [12] and Peerlings et al. [91] who performed numerical studies with nonlocal integral and gradient-enhanced strain-softening models for the experiment by Hordijk [50]. These are listed in Table 7-2 and are valid except for the failure strain ε_f.

Table 7-2: Input data for tension test of concrete specimen

Value	Sign	Magnitude	Unit
Density	ρ	$2.30 \cdot 10^{-9}$	t/mm^3
Young's Modulus	E	18000	MPa
Poisson's ratio	v	0.2	–
Initiation failure strain	ε_i	$2.1 \cdot 10^{-4}$	–
Failure strain	ε_f	$5.0 \cdot 10^{-3}$	–

The value ε_f is required for the linear strain-softening law used in the current "Equivalent damage force" model; however, the value could not be taken from Bobiński and Tejchman [12] or Peerlings et al. [91] because they used an exponential softening law (see Figure 161). Therefore, the determination of a feasible failure strain ε_f is done by comparing the linear softening law for the "Equivalent damage force" approach against the exponential law with α = 0.96 and β = 350 used by Bobiński and Tejchman [12] and Peerlings et al. [91]. The one-dimensional stress-strain relationships for the two softening laws are presented in Figure 166. A value of $\varepsilon_f = 5.0 \cdot 10^{-3}$ was chosen which captures the initial brittle concrete behaviour well. Using the failure strain ε_f =

$5.0 \cdot 10^{-3}$ will not lead to an exact representation of concrete behaviour while softening but this cannot be avoided with the current damage evolution in the "Equivalent damage force" approach due to its linear propagation.

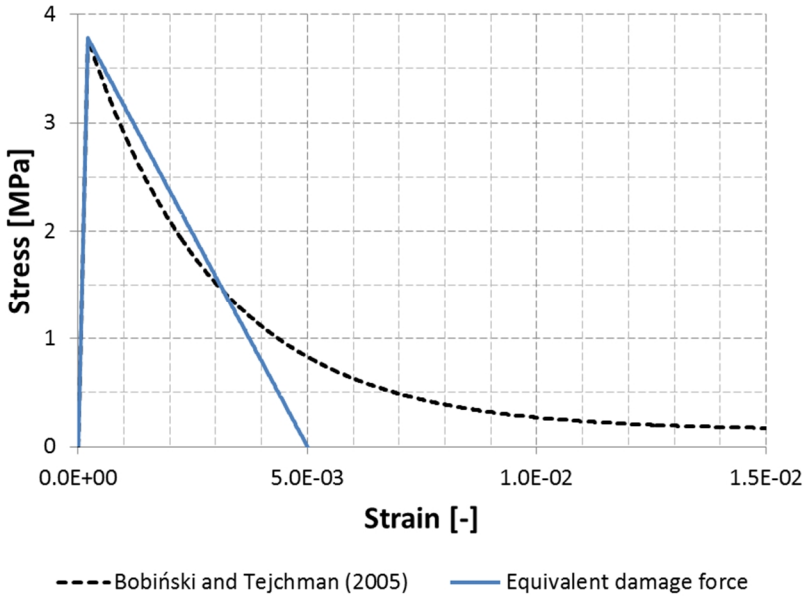

Figure 166: Comparison of stress-strain curve of exponential strain-softening law by Bobiński and Tejchman [12] and Peerlings et al. [91] with linear softening law for "Equivalent damage force" method with failure strains $\varepsilon_f = 5.0 \cdot 10^{-3}$

The concrete specimen is modelled as a three-dimensional structure with the dimensions $125mm \times 60mm \times 50mm$ and two notches with $5mm$ edge length in the specimen's centre. The specimen is meshed with three different solid mesh densities in the gauge area $l_{gauge} = 35mm$ to investigate if the "Equivalent damage force" approach shows any mesh-sensitivity due to strain-softening behaviour. The coarsest mesh has a consistent element length of $5mm$ resulting in a total of 2980 solid elements. The medium mesh has a consistent element length of $2.5mm$ in the gauge area with a total of 15200 solid elements in the specimen. The third mesh has a consistent element length of $1.25mm$ in the specimen's gauge area and a total of 121600 solid elements in the whole specimen. The three meshed specimens are shown in Figure 167.

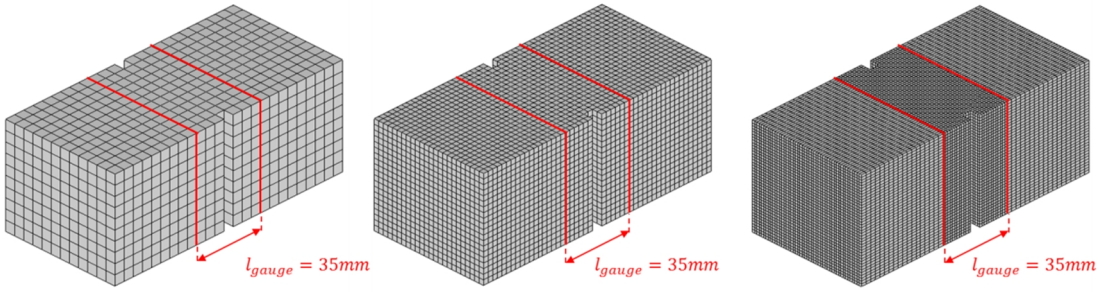

Figure 167: Three mesh discretisations used to analyse uniaxial tension test for local CDM model and "Equivalent damage force" model: coarse, medium and fine

One end of the concrete block is fully restrained and the other end allows only movement in direction of the applied load. These boundary conditions represent the fixture of the concrete block to loading platens as in Hordijk's experiment. The loading case for the uniaxial tension test of concrete is static. An implicit time integration scheme would be most suitable for the numerical calculations. However, the "Equivalent damage force" material model is implemented in DYNA3D which is an explicit solver. The displacement applied in Hordijk's work [50] is $0.08\mu m/s$ which was required in the physical experiment to avoid triggering an abrupt failure of the specimen. Nevertheless, the low loading rate used in Hordijk's experiment would be computationally very expensive in DYNA3D's explicit time integration scheme. Therefore, the loading applied in the numerical considerations is a constant velocity, $10mm/s$, to reduce computational time. The loading of $10mm/s$ is considered to be low enough to avoid significant wave propagation effects in the explicit solution.

The material behaviour in the softening domain will be very soft. This leads to the often observed numerical instability of negative volumes and a premature termination of the numerical calculations. Therefore, the "selective-reduced 8-point hexahedral element" DYNA3D stabilisation is applied to avoid negative volumes during the occurrence of strain-softening.

The conventional strain-softening CDM model with local behaviour is investigated first. The results are presented for the linear softening branch with failure strain $\varepsilon_f = 5.0 \cdot 10^{-3}$ which are representative for a local softening continuum. Figure 168 shows clearly that damage accumulates in a single row of elements in the notched area. Therefore, the size of the damaged area depends on the used mesh discretisation as expected for a local CDM model. Figure 169 compares the local results for different mesh discretisations to the recorded stress-deformation diagram in Hordijk's work [50] and nonlocal integral FE results by Bobiński and Tejchman [12]. The mesh

dependence of results obtained for the mean deformation in the gauge as well as for the determined peak stress in the notched cross-section is clearly visible. The stress-deformation slope in the softening area shows increasingly more brittle material behaviour upon mesh refinement which leads to a considerable decrease of mean deformation in the gauge area with finer mesh. The increasing brittleness with decreasing mesh size goes along with the observed narrowing of the damaged area, which is common for brittle material behaviour, presented in Figure 168. However, not only the softening slope indicates the mesh dependency of local CDM results. It can be observed in Figure 169 that the maximum reached stress in the notched cross-section decreases as well with finer mesh. This is caused by the increased brittleness of the material behaviour for the finest mesh. The effects of damage are confined to a very narrow area in the finest mesh discretisation and because of this damage cannot be smoothed out and failure occurs more rapid.

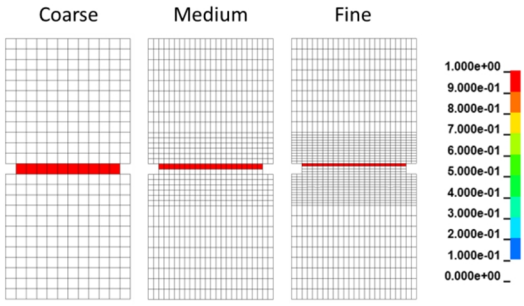

Figure 168: Localised damage in concrete specimen for three mesh discretisations in conventional local CDM model with linear softening branch (fringe level: damage [-])

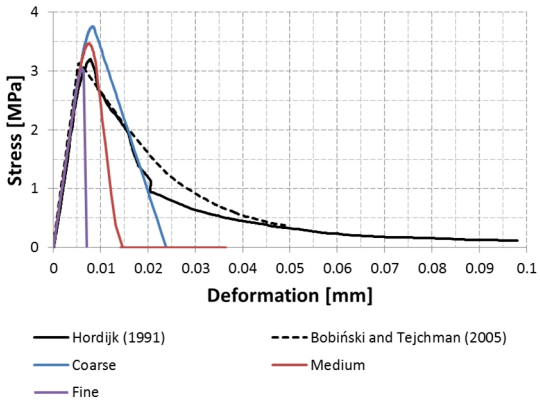

Figure 169: Stress-deformation curves in concrete gauge area for three mesh discretisations for conventional local CDM model with linear softening branch

The example of the uniaxial static tension concrete tension tests showed clearly that a physical and mesh-independent result cannot be achieved with a local CDM model. Therefore, it is difficult to apply such a model and expect meaningful results. Bobiński and Tejchman [12] showed that the application of a nonlocal integral regularisation method can improve numerical results significantly and can yield experimental results if the internal length scale l_c is chosen accordingly and an appropriate softening law is applied. Of interest in the following part of this investigation is if the “Equivalent damage force” approach, which does not require any additional terms as e.g. regularisation methods, can yield as well as regularisation methods a reliable and mesh-independent solution to the tension test of concrete.

The results for the “Equivalent damage force” approach for the three mesh discretisations and failure strain at $\varepsilon_f = 5.0 \cdot 10^{-3}$ are presented in Figure 170. The first observation which can be made is that results for the “Equivalent damage force” approach differ significantly from the results for the conventional strain-softening CDM model although the two models are equivalent with respect to the terms included in the constitutive equations. It can be seen from the damage contour plots that the damaged area is no longer confined in a single row of elements which leads in the local model to a pronounced mesh sensitivity. Damage is initiated at the specimen’s notches, representing a geometric imperfection, where stress is concentrated. During the process damage spreads for all specimens over the whole width of the notched area and propagates towards the specimen’s centre. The width of the damage band increases towards the centre with increasing damage level by forming two branches which propagate away from the notched area. This general description of damage contours in the uniaxial concrete tension example was presented by Bobiński and Tejchman [12] and was presented in Figure 163. This process is the same for all three used mesh discretisations and the width of the damaged zone can be seen as almost equivalent. However, it can be seen too that the damaged zone is more confined in the finest mesh discretisation used although this is due to the increased accuracy of the finer mesh in comparison to the coarser discretisations. Regarding these results it can be stated with confidence that the representation of damage as body force in the “Equivalent damage force” approach leads to a well-posed constitutive model and an improved damage representation in FE in comparison to a local strain-softening model.

Figure 170 includes the diagram for the stress in the notched cross-section over the average deformation in the gauge area for the “Equivalent damage force” approach. Firstly, it can be seen that the results do not match the experimental results by Hordijk [50] as well as the numerical results by Bobiński and Tejchman [12]. However, this was not expected as the damage law used for the “Equivalent damage force” approach is not capable of representing the bi-linear material behaviour of concrete. Additionally, it was rather the goal to show that the “Equivalent damage force” approach will lead to improvements of local strain-softening behaviour and is a potential solution method to strain-softening behaviour. With regards to this goal it can be stated that the results with the “Equivalent damage force” approach lead to a strong improvement of results. It is obvious that the slope of the softening branch is similar for all mesh discretisations and does not show increased brittleness for increased mesh fineness as it was observed in Figure 169.

Nevertheless, the maximum reached stress in the notched cross-section and the maximum average deformation in the gauge area seem to depend on the chosen mesh size as the linear elastic area is left earlier with decreasing mesh size and therefore a decreased maximum stress is reached in the cross-section. As the other results, namely damage propagation and slope of softening branch, indicate a well-posed constitutive model for strain-softening, the issue of mesh-dependent maximum stress must originate from another source. One source might be the geometric instability caused by the notches. Figure 170 includes the damage contour plots at damage initiation and maximum reached stress for the three mesh discretisations. It can be seen that damage initiates in the notched cross-section in the elements which are nearest to the notch. After damage development in these elements damage propagates quickly through the cross-section. The process of damage development in elements at initiation requires more time with increasing mesh size as the element size over which state variables are averaged is larger for larger element size. Therefore, the linear elastic solution is valid longer for the coarse mesh and its validity decreases with decreasing mesh size.

Another source of the not matching maximum stress values might be the not fully development symmetry of damage contours over the notched area (see Figure 170). It can be expected for the presented static tension test that stress and strain develop symmetrically over the notched area. The development of a symmetric strain would lead to a symmetric damage profile too as damage in the current implementation of the "Equivalent damage force" method is calculated from strain in the strain-softening domain. The reason might lie in the applied explicit time integration scheme which could not be avoided as the "Equivalent damage force" model is implemented in the explicit solver DYNA3D. The loading was chosen as constant velocity with $10 mm/s$ to keep computational efficiency and it was assumed that this would avoid significant propagation effects. However, propagation effects might be another reason for the not fully symmetric damage contours and the not matching maximum stress values. An additional study will be conducted at a later stage of this section to investigate maximum stress results for fully symmetric damage contours.

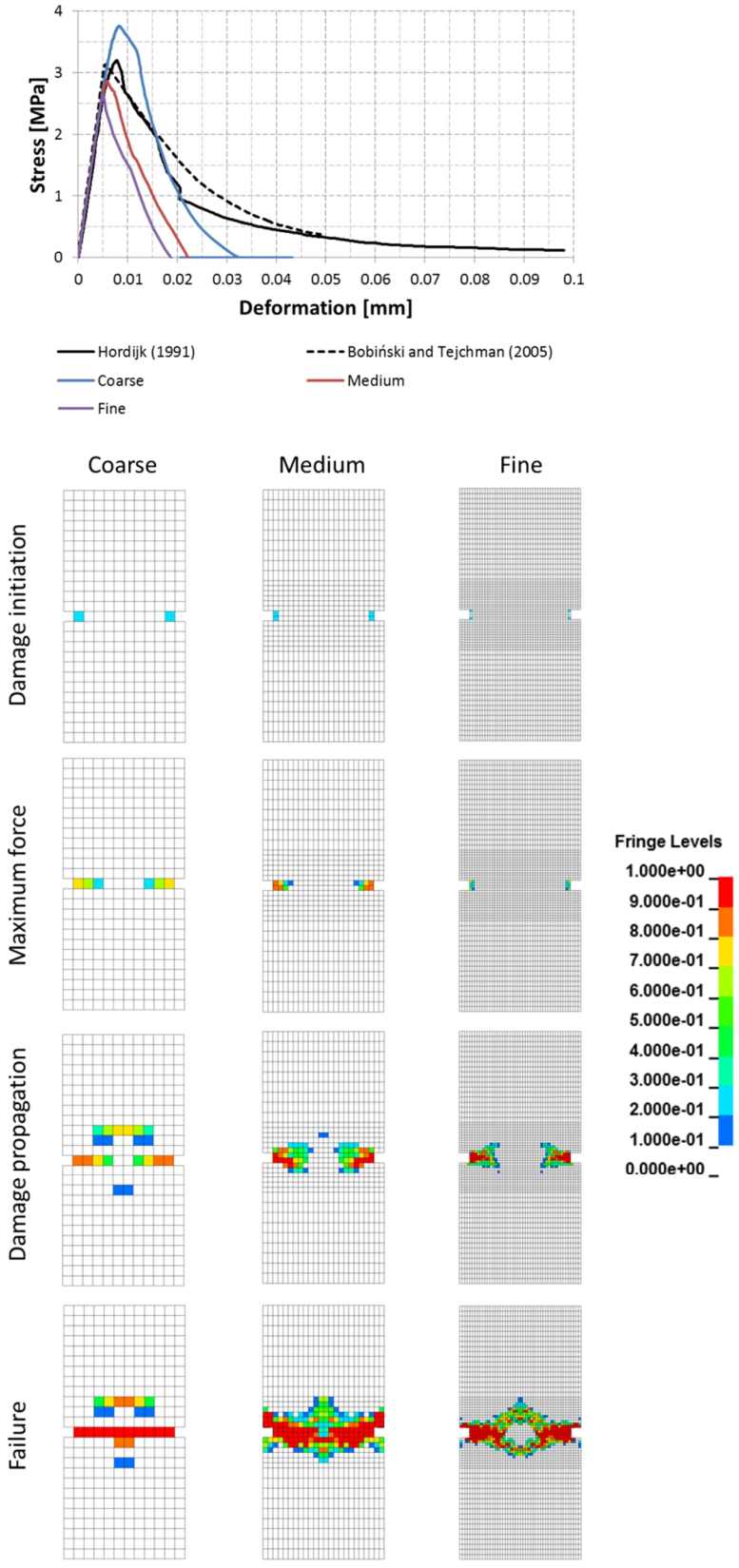

Figure 170: Stress-deformation curves and damage contours (fringe level: damage [-]) for $125mm \times 60mm \times 50mm$ concrete specimen under uniaxial tension with coarse, medium and fine mesh and equivalent failure strain $\varepsilon_f = 5.0 \cdot 10^{-3}$

Apart from the influence of the “Equivalent damage force” approach on the strain-softening results for different mesh discretisations it is of interest how a change in the linear strain-softening branch influences the results. Therefore, the slope of the linear strain-softening branch is varied by adjusting the failure strain ε_f. The one-dimensional stress-deformation diagrams for three different failure strains, $\varepsilon_f = 5.0 \cdot 10^{-3}, 1.0 \cdot 10^{-3}$ and $3.0 \cdot 10^{-3}$, is shown in Figure 171. The failure strain $5.0 \cdot 10^{-3}$ leads into a softening branch which matches the initial brittle behaviour of concrete. The failure strain $\varepsilon_f = 1.0 \cdot 10^{-2}$ matches the point at which a level of low constant stress is reached which occurs after the strain-softening response has smoothed. The final considered failure strain $\varepsilon_f = 3.0 \cdot 10^{-2}$ is chosen to match the point at which the low constant stress has been hold for a longer period. The increase in failure strain leads to a less steep slope of the softening branch which leads to a change of brittle material behaviour to more ductile material behaviour. It is expected that the increase of material ductility leads to a slowed down development of damage and with this to an enabled redistribution of strain and stress in the notched cross-section which influences the maximum reached stress in the notched cross-section as well as the maximum average deformation in the gauge area. Additionally, it is expected that the width of damaged area grows and smooths with increasing ductility. Overall, it is expected that a change of the strain-softening branch in the “Equivalent damage force” approach has the same consequences on numerical results as a change of internal length scale in nonlocal integral theory because the strain-softening branches controls the distribution of strain and with this of damage. It was demonstrated by Bobiński and Tejchman [12] (see Figure 164) that the internal length scale parameter influences brittleness of material response as well as the width of the damage band.

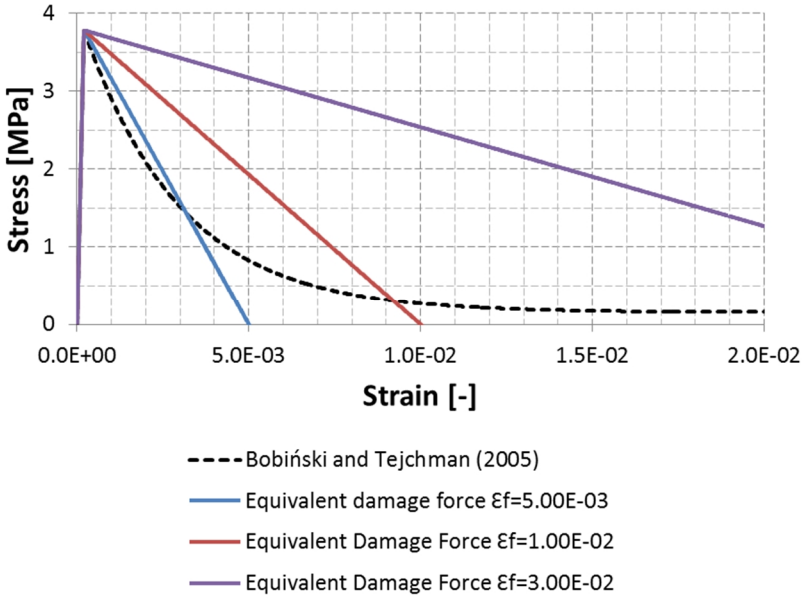

Figure 171: Comparison of stress-strain curve of exponential strain-softening law by Bobiński and Tejchman [12] and Peerlings et al. [91] with linear softening law for "Equivalent damage force" method with varying failure strains $\varepsilon_f = 5.0 \cdot 10^{-3}, 1.0 \cdot 10^{-3}$ and $3.0 \cdot 10^{-3}$

The investigation of a change of the strain-softening slope in using the "Equivalent damage force" method will be conducted with the previously used medium mesh discretisation. This discretisation was chosen as the propagation of damage contours is sharper than the coarse mesh and because the use of the fine mesh is computationally expensive.

The results for a changed strain-softening branch for the medium mesh discretisation are presented in Figure 172. It can be seen clearly that a change of the softening branch has indeed an influence on the results. It can be seen from the damage contour plots for the three failure strains that an increase of failure strain leads to a size increase of the localisation zone with smoothed out damage values. Additionally, it can be seen in the stress-deformation diagram that the maximum stress in the notched cross-section and maximum deformation in the gauge area increase with increased material ductility. This is an observation which was made by Bobiński and Tejchman [12] as well for a change in internal length scale as presented in their results in Figure 164 and Figure 165.

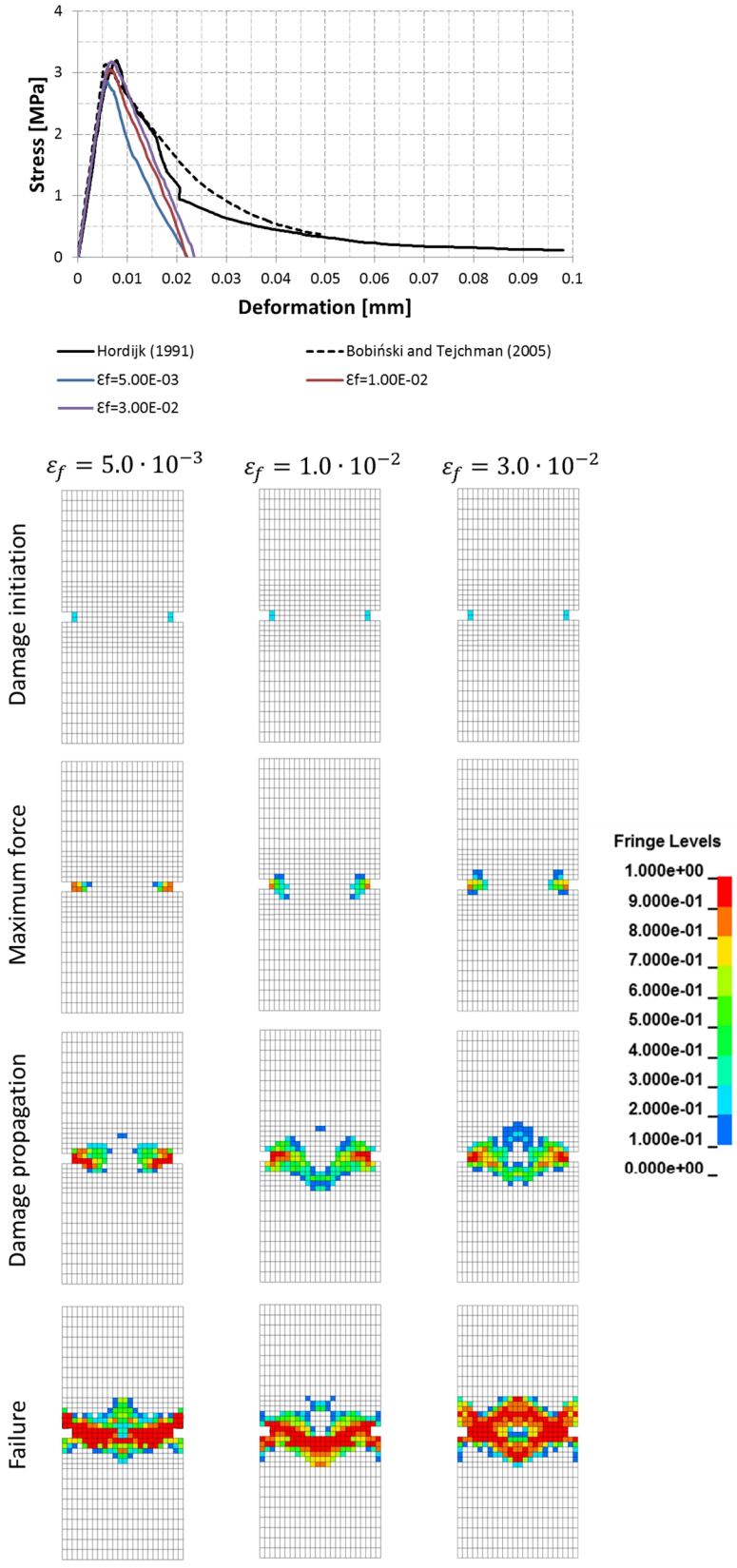

Figure 172: Stress-deformation curves and damage contours (fringe level: damage [-]) for $125mm \times 60mm \times 50mm$ concrete specimen under uniaxial tension with constant mesh size (medium) and varying failure strain $\varepsilon_f = 5.0 \cdot 10^{-3}, 1.0 \cdot 10^{-2}$ and $3.0 \cdot 10^{-2}$

It was observed in the two previous results, namely change of mesh discretisation and change of strain-softening branch, that the “Equivalent damage force” approach leads to a well-posed constitutive material model and an improved damage representation in comparison to the conventional strain-softening model. However, it was observed that the development of damage contours in Figure 173 and Figure 174 basically follows an expected pattern of propagation with some degree of symmetry with respect to the notched area. However, this pattern is not fully symmetric with respect to the plane spanned by the notched cross-section; however, a symmetric profile of strain and with this of damage was expected for a static uniaxial tension test and numerical results by other researchers [12; 91] showed a symmetric damage development over the cross-section too.

The reason for the not fully developed symmetry of damage contours in the notched cross-sectional area might lie in the use of an explicit solver for a static problem. Although the velocity applied was kept small to prevent wave propagation effects it cannot be fully avoided. Therefore, another two sets of experiments is conducted which is equivalent to the previous two except that the load is applied to both ends of the specimens. This modification of initial and boundary conditions applies symmetry of load conditions but does not change the load case itself.

The results for the three different mesh discretisations with a failure strain $\varepsilon_f = 5.0 \cdot 10^{-3}$ defining the softening branch are presented in Figure 173. It can be seen from the damage contours that the damage profile develops now fully symmetric over the notched cross-section. It can be seen too that the damage profile shape matches well for the three different mesh discretisations and a dependence of the damage profile on the chosen mesh discretisation cannot be observed.

The effect of the full symmetry of damage development on the stress-deformation diagram in Figure 173 is of high interest as well. Before it was observed that some mesh sensitivity exists for the maximum stress reached in the notched cross-section. This was previously attributed to geometric instabilities. However, in the experiment with symmetric damage profile the result curves for medium and fine mesh match almost perfectly although the reached maximum stress is lower than in the previous experiment. The maximum stress reached with the coarsest mesh does not match with the other discretisations which indicates that the mesh discretisation is too coarse to represent a defined damage development. Apart from this the slope of the softening curves still match very well for all discretisations.

The results in Figure 174 show the influence of a change in the strain-softening curve on results for the application of symmetric loading conditions. It can be seen here too that all damage profiles develop completely symmetric over the notched cross-section. It can be seen here as well that the change of the failure strain ε_f, and with this a change of strain-softening slope, has a similar effect as a change of internal length scale in the nonlocal integral approach by Bobiński and Tejchman [12]. An increase of the failure strain leads to a less steep softening slope, leading to less brittle material behaviour, and enables a redistribution of stress and strain in the notched cross-section due to a slower damaging process. Therefore, the damaged area increases in width and the maximum stress increases.

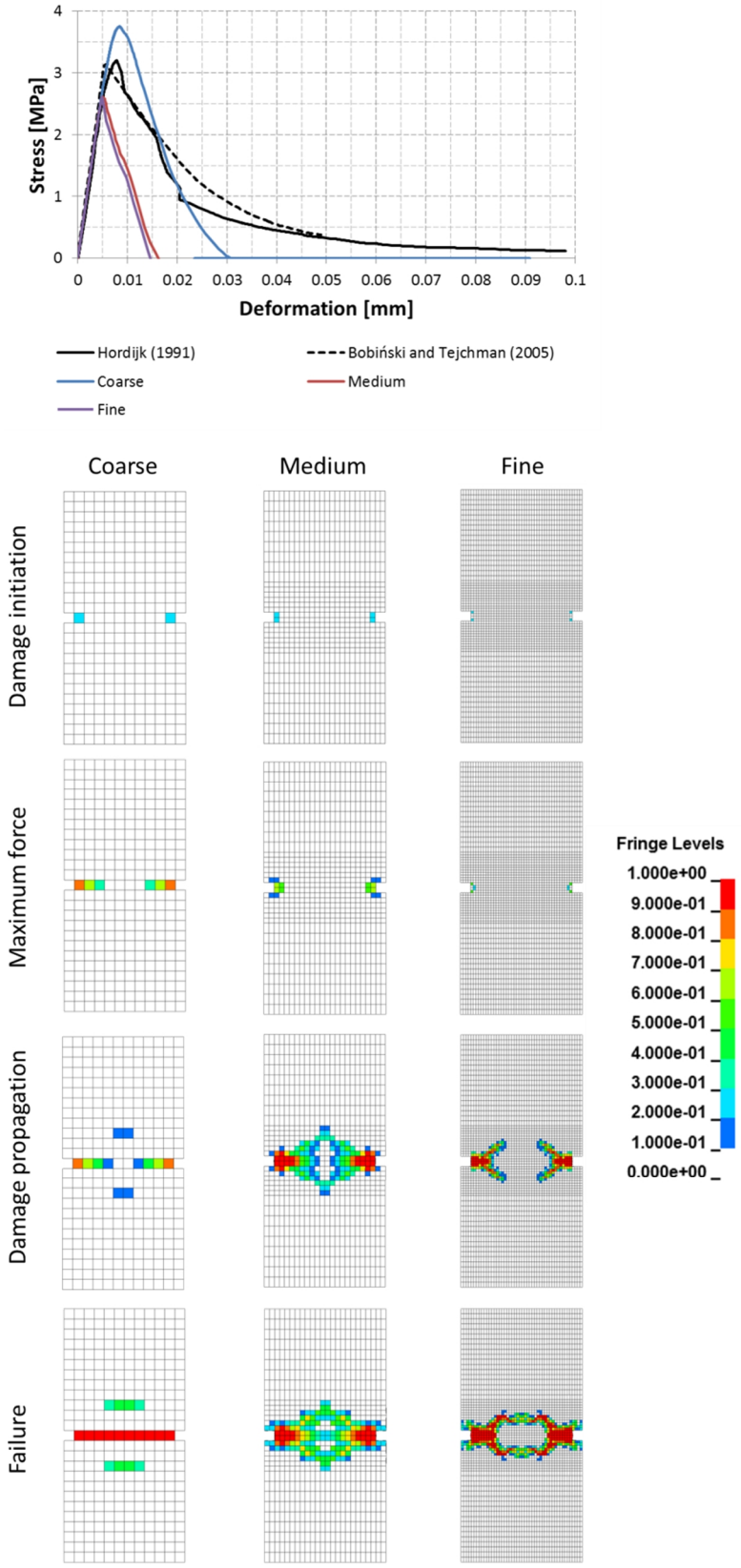

Figure 173: Stress-deformation curves and damage contours (fringe level: damage [-]) for $125mm \times 60mm \times 50mm$ concrete specimen under uniaxial tension with coarse, medium and fine mesh and equivalent failure strain $\varepsilon_f = 5.0 \cdot 10^{-3}$, symmetric load application

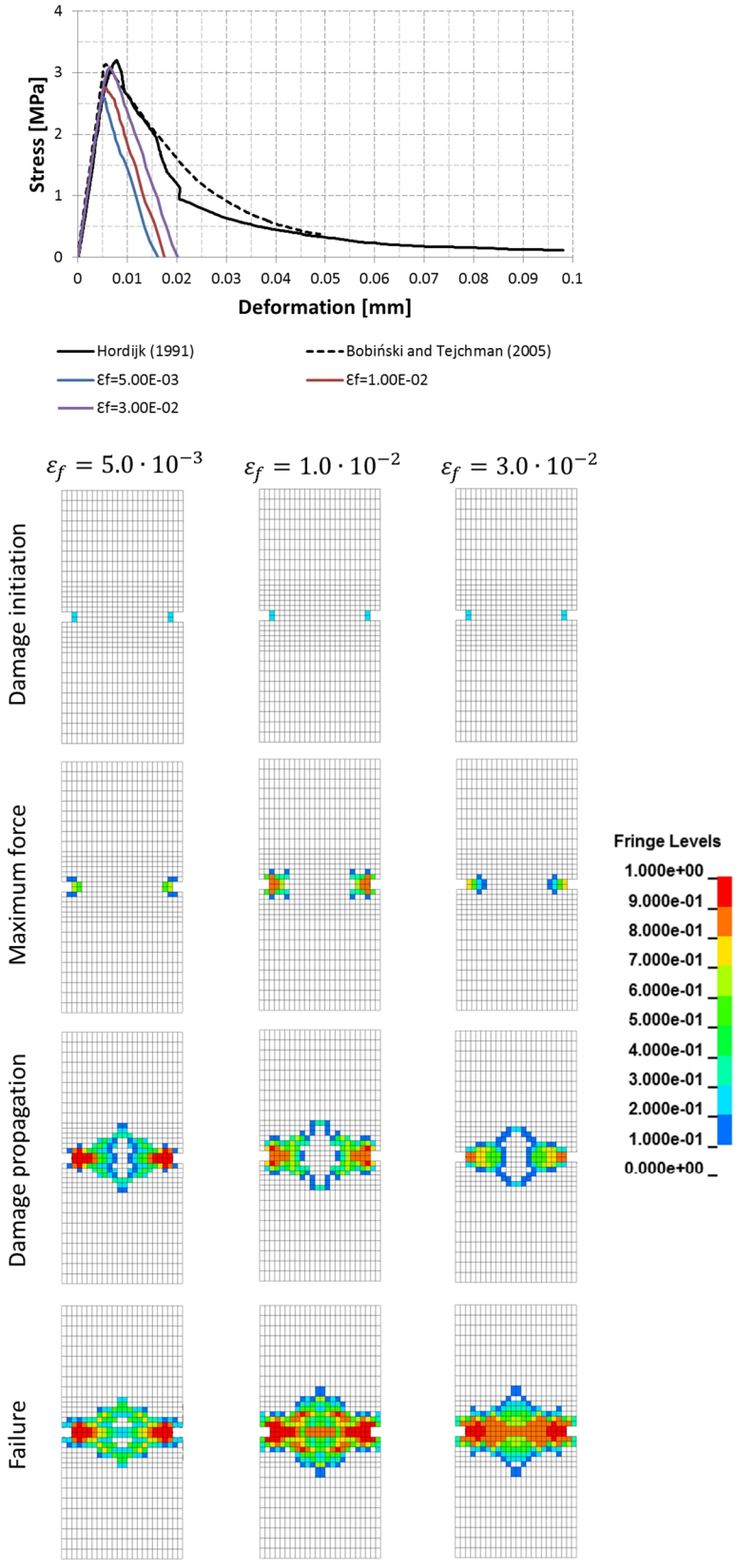

Figure 174: Stress-deformation curves and damage contours (fringe level: damage [-]) for $125mm \times 60mm \times 50mm$ concrete specimen under uniaxial tension with constant mesh size (medium) and varying failure strain $\varepsilon_f = 5.0 \cdot 10^{-3}, 1.0 \cdot 10^{-2}$ and $3.0 \cdot 10^{-2}$, symmetric load application

The presented numerical results for the uniaxial tension test of concrete showed clearly that the application of the “Equivalent damage force” approach leads to a well-posed constitutive material model. The strong instabilities of a local CDM model, namely an ill-posed boundary value problem and mesh dependency, are avoided. In difference to a regularisation method these results with the “Equivalent damage force” approach are achieved without introducing any additional terms to the constitutive equations. The development of damage is solely influenced by the development of strain in the localisation area which is controlled by the softening branch. It was shown too that a change of the failure strain ε_f, which controls the softening branch, controls the width of the localisation zone as well as the maximum stress in the localisation zone. This is an effect similar to the effect of an internal length scale in regularisation methods.

7.3 Extension of “Equivalent damage force” to Orthotropic Material Behaviour

This section will focus on the extension of the “Equivalent damage force” approach from isotropic to orthotropic materials. This work is cumbersome, as it will be shown, because orthotropy necessitates a tensorial damage variable to include directional material properties. The extension is necessary to make the approach applicable to a wider range of material models. In this work the application of the “Equivalent damage force” results in the definition of a symmetric and positive-definite 8^{th} order damage tensor. The definition of the 8^{th} order tensor for damage is not generic and goes beyond general text book knowledge. Therefore, it needed to be developed from scratch during this work.

The main issue which lead to the need for the 8^{th} order damage tensor will be stated first. Then the orthotropic material model from which the damage tensor was derived is introduced and the expression for the 8^{th} order damage tensor is derived. Then the properties of symmetry and positive-definiteness, which is required for the fulfilment of the material stability criterion by Hadamard, are verified. Finally the 8^{th} order damage tensor is simplified to 4^{th} order to make it usable for future work.

7.3.1 Problem Statement for an 8^{th} Order Damage Tensor

Isotropic material behaviour with a scalar damage variable is the simplest way to realise a full CDM model as was shown in Chapter 3 (Section 3.1.1). The application of the “Equivalent damage force” approach can be applied to these models in a straightforward fashion because the damage variable can be easily isolated.

$$\sigma_{ij} = (1-\omega)C_{ijkl}\varepsilon_{kl} \tag{7-22}$$

with

$$\tilde{C}_{ijkl} = (1-\omega)C_{mnpq} \tag{7-23}$$

in which C_{mnpq} is the virgin stiffness tensor and $\tilde{C}_{ijkl}$ is the damaged stiffness tensor.

A clear separation of damage, as it is possible with the expression in (7-23), is difficult to achieve for orthotropic material behaviour because tensor quantities are used for the representation of damage. To achieve the transformation of virgin to damaged stiffness tensor in orthotropic problems an 8th order tensor is required [22]. But 8th order tensor quantities are complex mathematical constructs with 3^8 components and are not commonly represented in literature.

In order to achieve a clear separation of damage for the application of the "Equivalent damage force" approach in orthotropy it will be necessary to define two 8th order tensors: the 8th order unit tensor $I_{ijklmnpq}$ and the 8th order damage tensor $\Omega_{ijklmnpq}$. According to Cauvin and Testa [18] the definition of $\Omega_{ijklmnpq}$ is the most general expression of damage and can represent any damage tensor in CDM models. Therefore, it is possible to represent the fraction of remaining stiffness in the form of:

$$\tilde{C}_{ijkl} = \left(I_{ijklmnpq} - \Omega_{ijklmnpq}\right)C_{mnpq} \tag{7-24}$$

In the further development of the "Equivalent damage force" approach for orthotropic materials an orthotropic material model is considered which uses the effective stress and energy equivalence. As a consequence of the energy hypothesis the transformation between damaged and virgin stiffness is achieved through the use of the damage effect tensor

$$\tilde{C}(\mathcal{D})_{ijkl} = M(\mathcal{D})^{-1}_{ijpq}C_{pqmn}M(\mathcal{D})^{-T}_{mnkl} \tag{7-25}$$

with

$$M\left(\omega_{ij}\right)_{ijkl} = (\delta_{ik}-\omega_{ik})^{-\frac{1}{2}}\left(\delta_{jl}-\omega_{jl}\right)^{-\frac{1}{2}} \tag{7-26}$$

To apply the "Equivalent damage force" approach (7-24) and (7-25) have to be equivalent; however, this equivalence is not intuitive. Literature to support the proof of equivalence of these two expressions is limited. Firstly, this is because the "Equivalent

damage force" approach is a new concept first developed in this thesis, and secondly, it is because the required 8th order tensors is complex. The author of this work is not claiming that this literature does not exist at all but research resulted only in three publications of use in this section. The first publication was done by Chaboche [22] who established an 8th order damage tensor as the most general damage expression and that this 8th order tensor can be reduced later without sacrificing quality of the damage expression. The second publication used was made by Cauvin and Testa [18]. They established (7-24) as expression which can transform any virgin stiffness tensor into the damaged stiffness tensor using an isolated 8th order damage tensor. This statement is the basis for the work in this section. The last publication used here was made by Lü and Chen [74]. Their work concerned the issue of reducing an 8th order tensor to order 4.

The author faced a number of issues in deriving a transformation in the form of (7-24). The first issue was to expand (7-25). This was required to isolate damage influenced terms from terms which represent the 8th order unit tensor. This was achieved by exploiting index notation. The second issue was to prove that the damage tensor will be symmetric. This is required to ensure that the effective stress will be a symmetric tensor as well and therefore to avoid the added complexity caused by a non-symmetric effective stress tensor. Another issue was to show that the Kronecker deltas, used in Equation (7-26), will form an 8th order unit tensor which is required in (7-24). It is vital to use a positive-definite damage tensor to guarantee the positive-definiteness of the stiffness tensor. It was pointed out (see Chapter 3, Section 3.2.2) that a loss of positive-definiteness leads to an ill-posed boundary value problem. The positive-definiteness of the damage tensor and with this of the stiffness tensor is paramount as the focus in this work lies on maintaining a stable boundary value problem. Finally, a reduction of the 8th order damage tensor to order 4 needs to be done. This is due to the complexity of 8th order tensors and that 4th order damage tensors are common tensor quantities in CDM.

7.3.2 Composite CDM Model

The choice of an orthotropic CDM model is the first step in this investigation. The further steps for the definition of an 8th order damage tensor will be rather complex and are not common text book knowledge. Therefore, it should be ensured that at least the base CDM model is using well-established concepts, such as effective stress and energy equivalence which were introduced in Chapter 3.

The CDM model presented here was designed for brittle failure of composites with orthotropic material behaviour. It assumes that damage will lead to an irreversible reduction of material stiffness and material strength. This is achieved by using the effective stress concept in which the transformation of the true stress tensor into the effective stress tensor is performed by using a 4th order damage effect tensor (see also Equation (3-14) in Chapter 3).

$$\tilde{\sigma}_{ij} = M(\mathcal{D})_{ijkl}\sigma_{kl} \tag{7-27}$$

The mapping of effective and true stress in (7-30) through the damage effect tensor is a function of a 2nd order damage tensor ω_{ij}.

$$M(\mathcal{D})_{ijkl} = M\left(\omega_{ij}\right)_{ijkl} \tag{7-28}$$

which is a diagonal tensor able to represent orthotropic damage due to reduction of effective load-carrying cross-sectional area:

$$\omega_{ij} = \begin{bmatrix} \omega_1 & 0 & 0 \\ 0 & \omega_2 & 0 \\ 0 & 0 & \omega_3 \end{bmatrix} \tag{7-29}$$

The model utilises energy equivalence hypothesis (as described in Chapter 3, Section 3.1.2) to derive the 4th order damaged stiffness tensor $\tilde{C}_{ijkl}$ from the 4th order virgin stiffness tensor C_{ijkl}. The relationship due to energy equivalence is given in (3-20) and reads:

$$\tilde{C}(\mathcal{D})_{ijkl} = M(\mathcal{D})^{-1}_{ijpq} C_{pqmn} M(\mathcal{D})^{-T}_{mnkl} \tag{7-30}$$

However, the definition in (7-30) does not ensure the symmetry of the effective stress tensor. Therefore the damage effect tensor in (7-28) is defined by product-type symmetrisation as in (3-23) [26]:

$$M\left(\omega_{ij}\right)_{ijkl} = (\delta_{ik} - \omega_{ik})^{-\frac{1}{2}}\left(\delta_{jl} - \omega_{jl}\right)^{-\frac{1}{2}} \tag{7-31}$$

The damage effect tensor will be written according to (7-29) and (7-28):

$$M_{ijkl}=\begin{bmatrix} \frac{1}{1-\omega_1} & 0 & 0 & 0 & 0 & 0 \\ 0 & \frac{1}{1-\omega_2} & 0 & 0 & 0 & 0 \\ 0 & 0 & \frac{1}{1-\omega_3} & 0 & 0 & 0 \\ 0 & 0 & 0 & \frac{1}{\sqrt{(1-\omega_2)(1-\omega_3)}} & 0 & 0 \\ 0 & 0 & 0 & 0 & \frac{1}{\sqrt{(1-\omega_1)(1-\omega_3)}} & 0 \\ 0 & 0 & 0 & 0 & 0 & \frac{1}{\sqrt{(1-\omega_1)(1-\omega_2)}} \end{bmatrix} \quad (7\text{-}32)$$

Using (7-30) and (7-32) the damaged stiffness tensor has the following form:

$$\tilde{C}(\mathcal{D})_{ijkl} = M(\mathcal{D})^{-1}_{ijpq} C_{pqmn} M(\mathcal{D})^{-T}_{mnkl} \quad (7\text{-}33)$$

$\tilde{C}_{ijkl}$

$$= \begin{bmatrix} C_{11}(1-\omega_1)^2 & C_{12}(1-\omega_1)(1-\omega_2) & C_{13}(1-\omega_3)(1-\omega_1) & 0 & 0 & 0 \\ & C_{22}(1-\omega_2)^2 & C_{23}(1-\omega_2)(1-\omega_3) & 0 & 0 & 0 \\ & & C_{33}(1-\omega_3)^2 & 0 & 0 & 0 \\ & & & C_{44}(1-\omega_2)(1-\omega_3) & 0 & 0 \\ S & & Y & M & C_{55}(1-\omega_1)(1-\omega_3) & 0 \\ & & & & & C_{66}(1-\omega_1)(1-\omega_2) \end{bmatrix} \quad (7\text{-}34)$$

7.3.3 Definition of 8th Order Damage Tensor

In a next step it is shown that an 8th order damage tensor can be derived from (7-30) through multiplication of the two damage effect tensors. This is essential to achieve an isolation of damage influenced terms. Additionally, it will be shown that this 8th order tensor will be super-symmetric. The super-symmetry will be derived from the product-type symmetrisation which was applied to the damage effect tensor in the considered orthotropic CDM model.

According to the existing composite CDM model the damaged stiffness tensor is expressed as:

$$\tilde{C}(\mathcal{D})_{ijkl} = M(\mathcal{D})^{-1}_{ijpq} C_{pqmn} M(\mathcal{D})^{-T}_{mnkl} \quad (7\text{-}35)$$

However, to apply the “Equivalent damage force” approach an expression of $\tilde{C}_{ijkl}$ in the form of (7-30) with an 8th order damage tensor is necessary which was stated as the most general form for anisotropic material behaviour with anisotropic damage [18].

$$\tilde{C}_{ijkl} = \left(I_{ijklmnpq} - \Omega_{ijklmnpq}\right)C_{mnpq} \tag{7-36}$$

The equivalence of (7-35) and (7-36) is not obvious and needs to be derived through exploitation of index notation.

Due to the product-type symmetrisation in (7-31) the damage effect tensor possesses major symmetry (see Chapter 2, Section 2.1 for the definition of tensor symmetry):

$$M\left(\omega_{ij}\right)_{ijkl} = M\left(\omega_{ij}\right)^{T}_{ijkl} = M\left(\omega_{ij}\right)_{klij} \tag{7-37}$$

And the definition in (7-35) can be rewritten:

$$\tilde{C}_{ijkl} = M^{-1}_{ijpq}C_{pqmn}M^{-1}_{mnkl} \tag{7-38}$$

As index notation is used, (7-38) can be rearranged:

$$\tilde{C}_{ijkl} = \left(M^{-1}_{ijpq}M^{-1}_{mnkl}\right)C_{pqmn} \tag{7-39}$$

$M^{-1}_{ijpq}M^{-1}_{mnkl}$ in (7-39) forms an 8th order tensor. The appearance of this 8th order tensor will be further defined by using the definition of the damage effect tensor in (7-31).

$$\tilde{C}_{ijkl} = \left(\left(\delta_{ip} - \omega_{ip}\right)^{\frac{1}{2}}\left(\delta_{jq} - \omega_{jq}\right)^{\frac{1}{2}}\left(\delta_{mk} - \omega_{mk}\right)^{\frac{1}{2}}\left(\delta_{nl} - \omega_{nl}\right)^{\frac{1}{2}}\right)C_{pqmn} \tag{7-40}$$

Next, an isolation of an 8th order unit tensor and 8th order damage tensor needs to be achieved to arrive at an expression equivalent to (7-36). This will be achieved by expanding (7-40).

$$\begin{aligned}\tilde{C}_{ijkl} = \big(&\delta_{ip}\delta_{jq}\delta_{mk}\delta_{nl} + \omega_{ip}\omega_{jq}\omega_{mk}\omega_{nl} - \delta_{ip}\omega_{jq}\omega_{mk}\omega_{nl} - \\ &\omega_{ip}\delta_{jq}\omega_{mk}\omega_{nl} - \omega_{ip}\omega_{jq}\delta_{mk}\omega_{nl} - \omega_{ip}\omega_{jq}\omega_{mk}\delta_{nl} + \delta_{ip}\delta_{jq}\omega_{mk}\omega_{nl} + \\ &\delta_{ip}\omega_{jq}\delta_{mk}\omega_{nl} + \delta_{ip}\omega_{jq}\omega_{mk}\delta_{nl} + \omega_{ip}\delta_{jq}\delta_{mk}\omega_{nl} + \omega_{ip}\delta_{jq}\omega_{mk}\delta_{nl} + \\ &\omega_{ip}\omega_{jq}\delta_{mk}\delta_{nl} - \delta_{ip}\delta_{jq}\delta_{mk}\omega_{nl} - \delta_{ip}\delta_{jq}\omega_{mk}\delta_{nl} - \delta_{ip}\omega_{jq}\delta_{mk}\delta_{nl} - \\ &\omega_{ip}\delta_{jq}\delta_{mk}\delta_{nl}\big)^{\frac{1}{2}}C_{pqmn}\end{aligned} \tag{7-41}$$

It must also be ensured that (7-41) leads to a symmetric expression. This can be proven by exploiting the minor and major symmetries of the damage effect tensor which it got from the product-type symmetrisation: $M_{ijpq} = M_{jipq} = M_{ijqp} = M_{pqij}$. Additionally, the two damage effect tensors in (7-39) are equivalent: $M_{ijpq} = M_{mnkl}$.

Therefore, any arrangement of the indices i, j, p, q, m, n, k and l is possible and the expression in (7-41) is a super-symmetric 8th order tensor.

7.3.3.1 8th Order Unit Tensor

The expression in (7-41) represents a separation of an 8th order unit tensor and 8th order damage tensor as proposed by Cauvin and Testa [18]. However, it needs to be proven that the Kronecker delta product $\delta_{ip}\delta_{jq}\delta_{mk}\delta_{nl}$ is really the 8th order unit tensor used in:

$$\tilde{C}_{ijkl} = \left(I_{ijklmnpq} - \Omega_{ijklmnpq}\right)C_{mnpq} \tag{7-42}$$

Cauvin and Testa [18] stated that (7-42) represents the most general expression of damage possible and can be applied to anisotropic damage of anisotropic materials. To recall: C_{ijkl} is the virgin stiffness tensor, $\tilde{C}_{ijkl}$ is the damaged stiffness tensor, $I_{ijklmnpq}$ is the 8th order unit tensor and $\Omega_{ijklmnpq}$ is the 8th order damage tensor in (3-7).

Equation (7-41) includes a product of four Kronecker deltas, $\delta_{ip}\delta_{jq}\delta_{mk}\delta_{nl}$, which is assumed to form the symmetric 8th order unit tensor $I_{ijklmnpq}$. To prove this equivalence it needs to be shown that $\delta_{ip}\delta_{jq}\delta_{mk}\delta_{nl}$ maps the 4th order virgin stiffness tensor on its symmetric part in case of no damage.

$$\tilde{C}(\mathcal{D} = 0)_{ijkl} = I_{ijklmnpq}C_{mnpq} = \delta_{ip}\delta_{jq}\delta_{mk}\delta_{nl}C_{mnpq} \tag{7-43}$$

It is known that the virgin stiffness C_{ijkl} possesses all minor symmetries: $pq = qp$ and $mn = nm$. Firstly, $\delta_{ip}\delta_{jq}\delta_{mk}\delta_{nl}$ will be symmetrised with respect to p and q:

$$\delta_{ip}\delta_{jq}\delta_{mk}\delta_{nl} = \frac{1}{2}\left(\delta_{ip}\delta_{jq}\delta_{mk}\delta_{nl} + \delta_{iq}\delta_{jp}\delta_{mk}\delta_{nl}\right) \tag{7-44}$$

Secondly, $\delta_{ip}\delta_{jq}\delta_{mk}\delta_{nl}$ will be symmetrised with respect to m and n:

$$\begin{aligned}&\delta_{ip}\delta_{jq}\delta_{mk}\delta_{nl}\\ &= \frac{1}{4}\left(\delta_{ip}\delta_{jq}\delta_{mk}\delta_{nl} + \delta_{iq}\delta_{jp}\delta_{mk}\delta_{nl} + \delta_{ip}\delta_{jq}\delta_{nk}\delta_{ml} + \delta_{iq}\delta_{jp}\delta_{nk}\delta_{ml}\right)\end{aligned} \tag{7-45}$$

From (3-9) it is known that the 8th order unit tensor needs to have the following appearance.

$$I_{ijklmnpq} = \frac{1}{4}\left(\delta_{im}\delta_{jn}\delta_{kp}\delta_{lq} + \delta_{im}\delta_{jn}\delta_{kq}\delta_{lp} + \delta_{in}\delta_{jm}\delta_{kp}\delta_{lq} + \delta_{in}\delta_{jm}\delta_{kq}\delta_{lp}\right) \tag{7-46}$$

Due to the super-symmetry the following is valid: $I_{ijmnpqkl} = I_{ijklpqmn}$. Therefore, (7-45) and (7-48) are equivalent and $\delta_{ip}\delta_{jq}\delta_{mk}\delta_{nl}$ in (7-41) represents the desired 8th order unit tensor.

7.3.3.2 Positive-Definite Damage Tensor

It needs to be ensured for the "Equivalent damage force" approach that the boundary value problem is well-posed at all times. Following Hadamard's definition of well-posedness [41] that means a unique solution exists and the solution depends continuously on the data. A violation of this principle would lead to the occurrence of instabilities.

To ensure that material stability in the sense of Hadamard is satisfied the stiffness tensor has to be positive-definite (see Chapter 3, Section 3.2.2) and the boundary value problem is well-posed. It has to be made sure that the stiffness tensor stays positive-definite even in the presence of damage to keep the problem well-posed. This will be the case when the damage effect tensor is also positive-definite. This is the case if the damage effect tensor is symmetric and all its eigenvalues are positive.

It has been shown that the damage effect tensor is super-symmetric previously. The last required proof for positive-definiteness is showing that the eigenvalues of the damage effect tensor are positive.

$$det\left(M(\mathcal{D})_{ijkl} - \lambda I_{ijkl}\right) = 0 \tag{7-47}$$

The damage effect tensor is diagonal in the present case. Therefore its eigenvalues can be read directly from its diagonal.

$$\left\| \begin{bmatrix} \frac{1}{1-\omega_1}-\lambda & 0 & 0 & 0 & 0 & 0 \\ 0 & \frac{1}{1-\omega_2}-\lambda & 0 & 0 & 0 & 0 \\ 0 & 0 & \frac{1}{1-\omega_3}-\lambda & 0 & 0 & 0 \\ 0 & 0 & 0 & \frac{1}{\sqrt{(1-\omega_2)(1-\omega_3)}}-\lambda & 0 & 0 \\ 0 & 0 & 0 & 0 & \frac{1}{\sqrt{(1-\omega_1)(1-\omega_3)}}-\lambda & 0 \\ 0 & 0 & 0 & 0 & 0 & \frac{1}{\sqrt{(1-\omega_1)(1-\omega_2)}}-\lambda \end{bmatrix} \right\| = 0 \tag{7-48}$$

The eigenvalues are:

$$\left(\frac{1}{1-\omega_1}-\lambda\right)\left(\frac{1}{1-\omega_2}-\lambda\right)\left(\frac{1}{1-\omega_3}-\lambda\right). \tag{7-49}$$

$$\left(\frac{1}{\sqrt{(1-\omega_2)(1-\omega_3)}}-\lambda\right)\left(\frac{1}{\sqrt{(1-\omega_1)(1-\omega_3)}}-\lambda\right)\left(\frac{1}{\sqrt{(1-\omega_1)(1-\omega_2)}}-\lambda\right)=0$$

All eigenvalues will be positive when:

$$0 \leq \omega_1, \omega_2, \omega_3 < 1 \tag{7-50}$$

The condition in (7-50) is essential for the positive-definite character of the damage effect tensor.

It was shown here that the damage effect tensor used in the considered orthotropic CDM model is positive-definite. This is crucial for the positive-definiteness of the 8th order damage tensor. The positive-definite character of the 8th order damage tensor in (7-41) is necessary to keep the stiffness tensor with damage influence in the "Equivalent damage force" approach, see Equation (7-16), positive-definite to ensure a stable boundary value problem.

7.3.4 Simplification of 8th Order Damage Tensor

With (7-41) an expression of the form $I_{ijklmnpq} - \Omega_{ijklmnpq}$ was found; however, in this case we are dealing with an 8th order tensors. This makes working cumbersome as it has 3^8 components and a simplification to a lower order is desirable.

Chaboche [22] stated that an effective 4th order damage tensor Ω^*_{ijrs} is sufficient when the 8th order tensor is diagonal and defined in a fixed principal axes system. Cauvin and Testa [18] shared this opinion.

Lü and Chen [74] worked on the issue of reducing an 8th order damage tensor to order 4. They state that the 8th order tensor $M^{-1}_{ijpq}M^{-1}_{mnkl}$ has effectively only order 4 and can be substituted with:

$$M^{-1}_{ijpq}M^{-1}_{mnkl} = M^{-1}_{ijpq}\delta_{mk}\delta_{nl} \tag{7-51}$$

Therefore the damaged stiffness tensor reads:

$$\tilde{C}_{ijkl} = \left(\delta_{ip}\delta_{jq}\delta_{mk}\delta_{nl} + \omega_{ip}\omega_{jq}\delta_{mk}\delta_{nl} - \delta_{ip}\omega_{jq}\delta_{mk}\delta_{nl} - \omega_{ip}\delta_{jq}\delta_{mk}\delta_{nl}\right)^{\frac{1}{2}}C_{pqmn} \tag{7-52}$$

The assumption is that the damage tensor of order 4 reads:

$$\Omega_{ijpq} = \sqrt{\omega_{ip}\omega_{jq} - \delta_{ip}\omega_{jq} - \omega_{ip}\delta_{jq}} \tag{7-53}$$

A comparison with the damage effect tensor

$$\mathrm{M}_{ijpq} = (\delta_{ik} - \omega_{ik})^{-\frac{1}{2}}\left(\delta_{jl} - \omega_{jl}\right)^{-\frac{1}{2}} = \frac{1}{\sqrt{\delta_{ip}\delta_{jq} + \omega_{ip}\omega_{jq} - \delta_{ip}\omega_{jq} - \omega_{ip}\delta_{jq}}} \tag{7-54}$$

leads to

$$\mathrm{M}_{ijpq} = \frac{1}{I_{ijpq} - \Omega_{ijpq}} \tag{7-55}$$

and

$$M^{-1}_{ijpq} = I_{ijpq} - \Omega_{ijpq} \tag{7-56}$$

Due to (7-56), the appearance of the damage tensor is known.

$$(-1) \cdot \Omega_{ijpq} = \sqrt{\omega_{ip}\omega_{jq} - \delta_{ip}\omega_{jq} - \omega_{ip}\delta_{jq}} \tag{7-57}$$

In matrix form it reads:

$$(-1) \cdot \Omega_{ijpq} = \begin{bmatrix} \omega_1 & 0 & 0 & 0 & 0 & 0 \\ 0 & \omega_2 & 0 & 0 & 0 & 0 \\ 0 & 0 & \omega_3 & 0 & 0 & 0 \\ 0 & 0 & 0 & -\omega_2 - \omega_3 + \omega_2\omega_3 & 0 & 0 \\ 0 & 0 & 0 & 0 & -\omega_1 - \omega_3 + \omega_1\omega_3 & 0 \\ 0 & 0 & 0 & 0 & 0 & -\omega_1 - \omega_2 + \omega_1\omega_2 \end{bmatrix} \tag{7-58}$$

7.4 Summary

During research in the presented work it was recognised that the first and paramount step in avoiding analytical and numerical strain-softening instabilities is to prevent an ill-posed boundary value problem. To achieve this it is necessary to prevent the change of the initial partial differential equation's type. Currently this is only delivered in literature by the group of regularisation methods which require the introduction of higher-order terms of space or time in constitutive equations of the CDM material model.

The “Equivalent damage force” approach was developed to address the issue of an ill-posed boundary value problem due to strain-softening and as alternative to conventional regularisation methods. The “Equivalent damage force” approach exploits the fact that inhomogeneous parts of PDEs do not influence the type of it. Therefore, damage was assumed to be a body force, the so-called “Equivalent damage force”, and with this was made an inhomogeneous part of the governing PDEs. As a consequence, the homogeneous PDE part keeps its original linear elastic form and does not lead to a type change of PDEs and the influence of damage on the solution is accounted for as inhomogeneous part of the PDE. The “Equivalent damage force” approach does not require any additional terms in the constitutive equations of a material model, such as regularisation methods, to maintain a well-posed boundary value problem. This has not been achieved by any other approach in research on strain-softening issues and makes the “Equivalent damage force" approach therefore novel in the field.

To evaluate the “Equivalent damage force” approach two material models were implemented in DYNA3D: a standard isotropic strain-softening model and the “Equivalent damage force” modification to this. These two material models include the exact same terms defining the constitutive material description and the only difference lies in the treatment of damage.

The two material models were first evaluate for the longitudinal wave propagation problem by Bažant and Belytschko [6] to investigate the characteristic properties of the “Equivalent damage force” approach against the standard strain-softening approach. Although both material models are essentially the same their behaviour in the strain-softening domain is very different. The standard strain-softening model showed the same analytical instabilities as observed in Chapter 3 and suffered from mesh-sensitivity as observed previously in Chapter 4. The “Equivalent damage force” approach in comparison showed a more physical response. Instead of strain localisation in a single element damage propagated away from the point of strain-softening. Additionally, strain and stress vanished when the damage variable reached its maximum value of one and energy dissipation did not vanish. Additionally, result sensitivity depending on the FE discretisation could not be determined.

A second validation model, the uniaxial tension test of a notched concrete specimen, was investigated to compare the performance of the “Equivalent damage force” method against physical experiments and numerical results of conventional regularisation

methods. It was found that the application of the “Equivalent damage force” approach lead into a strong improvement of results in comparison to a conventional CDM model with strain-softening. It was found too that the size of the localisation area as well as the magnitude of maximum stress is controlled by the slope of the softening branch. This is caused by the dependence of damage in the “Equivalent damage force” approach on the strain distribution in the localisation zone which in turn depends on the strain-softening branch. Therefore, the change of the softening slope has a similar impact on the solution as the internal length scale, used in regularisation methods, has on the width of the localisation zone and stress results.

Finally, the analytical ground work for the extension of the “Equivalent damage force” approach to orthotropic material behaviour was done to allow for the investigation of materials with more complex behaviour than isotropic materials. The issue in this was to achieve a clear separation of damage influenced terms from elastic ones as the orthotropy necessitates tensorial entities for the representation of the damage variable.

8 Conclusions and Future Work

8.1 Conclusions

The ***scope of the presented work*** was focused on critical issues of damage modelling within the continuum damage mechanics framework. In this the analytical and numerical issues arising from an ill-posed boundary value problem due to strain-softening behaviour was of special interest. The following section will restate and summarise the issues encountered due to strain-softening behaviour as well as solution techniques explored in this work.

The eventual failure of materials is preceded by damaging processes on the microscale which have significant influence on the macroscopic material behaviour. This shows itself as a highly localised deformation caused by the so-called strain-softening behaviour. The strain-softening phenomenon is characterised by a reduction of effective load-carrying area due to damage with increasing deformation.

The strain-softening phenomenon is observed in many engineering materials and a good phenomenological material description should therefore include the effects of damage in its description. This is commonly done by using the continuum damage mechanics approach which is able to represent linear elastic behaviour as well as the influence of damage on the macroscopic material behaviour with final failure of the structure. The continuum damage mechanics approach achieves this by introducing an average measure of material degeneration into well-known constitutive equations of continuum mechanics. The average measure is called the damage variable, which has scalar or tensorial character, and represents the loss of effective load-carrying cross-section due to damage.

Although the continuum damage mechanics approach is able to account for damage it has been established by research that the representation of strain-softening behaviour leads to severe instabilities in its analytical and numerical description of material behaviour. The work presented here was concerned with these critical issues of damage modelling in the context of continuum damage mechanics arising from strain-softening behaviour.

This work started with examining existing research on the modelling of strain-softening in the framework of conventional local continuum damage mechanics. This involved the investigation of the characteristic analytical and numerical features of the strain-

softening solution in Chapter 3 and Chapter 4 by examining a longitudinal wave propagation problem. The following characteristic properties of the strain-softening solution were established:

- The tangent modulus in the area of inelastic deformation ceases to be positive-definite due to strain-softening behaviour. This is characterised as a negative slope in the engineering stress-engineering strain diagram. The loss of positive-definiteness represents a violation of the material stability criterion in the sense of Hadamard. As a consequence the governing partial differential equations change their type from elliptic to hyperbolic in static problems and from hyperbolic to elliptic in dynamic problems. Therefore, a well-posed boundary value problem cannot be maintained and a unique solution is not achievable.
- The strain-softening solution has a characteristic impact on the representation of material behaviour which is caused by the ill-posed boundary value problem. When strain-softening occurs the change of type in partial differential equations happens immediately and the area affected is not able to interact with the rest of the structure anymore, which is still governed by the appropriate partial differential equations. All deformation is trapped in a single point, which represents an area of infinitely small width, due to strain-softening with simultaneously vanishing stress and energy dissipation. This behaviour is non-physical.
- Numerical results of continuum damage mechanics models show the same unphysical behaviour as the analytical solution. However, in contrast to the analytical solution strain-softening cannot occur in an area of infinitesimal small width because the smallest unit in finite element representation is dictated by the element size. Therefore, strain-softening accumulates in an area with the width of the element affected. As a consequence the strain-softening solution is strongly mesh sensitive in numerical simulations and a consistent solution cannot be achieved for differing spatial discretisations.

The unwanted features of the strain-softening solution in analytical and numerical investigations are well-known in research. However, instead of disregarding continuum damage mechanics models, research has focused on methods which yield physically reasonable results because the continuum approach is a widely used engineering tool which uses the well-established concept of stress and strain and its computational efficiency. Early methods dealing with physically unreasonable strain-softening solutions in numerics focused on predetermining the fracture energy released during

the strain-softening process, such as the cohesive and smeared crack methods. But these methods do not address the issue of the ill-posed boundary value problem due to strain-softening and the problem of mesh-sensitivity prevails. Another approach to the strain-softening instabilities is the group of continuum based regularisation methods. This group splits into three methods. The first one is the nonlocal integral method which introduces weighted averages of a state variable, such as plastic strain, into the constitutive equations. The second one is the gradient-enhanced method, which is closely related to nonlocal methods and uses higher-order derivatives of a state variable. The last model is the viscous method which uses rate-effects to regularise strain-softening continua. Although the regularisation mechanism depends on the specific method used regularisation methods have one aspect in common. This is the introduction of an internal length scale parameter, implicitly or explicitly, into constitutive equations. Existing regularisation methods were reviewed in Chapter 5 for dynamic problems and the two main aspects were found for the regularisation success in strain-softening models:

- Firstly and most importantly in this work is the introduction of higher-order terms of space or time in the homogeneous parts of the governing partial differential equations. This successfully prevents the change of the initial type of the partial differential equations due to the negative tangent modulus. Therefore, the well-posed character of the boundary value problem is preserved in the presence of strain-softening. Consequently, the feature of localisation of deformation in the smallest area possible, as in conventional continuum damage mechanics models, is prevented.
- Secondly, the internal length scale parameter used in regularisation methods confines the area of strain-softening to a finite area. This length scale parameter is related to the size of major microscopic heterogeneities of the considered material and if chosen correctly a localisation zone as observed in real material behaviour can be achieved.

It was concluded from the initial research on the strain-softening issue and regularisation methods that maintaining the problem's initial boundary value is crucial for a good continuum damage mechanics model. As well as this, it was found that only regularisation methods successfully deliver this at the time and alternatives to regularisation methods hardly exist.

Therefore, the ***research question*** in this work was if methods, other than regularisation methods, could maintain the problem's initial boundary value problem as well and therefore lead to an improved continuum damage mechanics representation. Based on the work presented in this thesis the indications are that the answer to this question is yes. Two methods were presented which are capable of maintaining the initial boundary value problem successfully without using the approach of a conventional regularisation method.

- **Smoothed particle hydrodynamics (SPH):**

  The study of the particle method SPH in context of strain-softening has demonstrated for the first time that SPH has nonlocal properties although SPH itself is not a nonlocal method. The nonlocal effect in SPH comes from the kernel interpolation used to approximate field variables. This is in contrast to conventional nonlocal models in which the nonlocality is part of the constitutive material model. SPH establishes particle connectivity through the smoothing function which is equivalent to a nonlocal weighting function. The size of the smoothing function's support domain is defined by the smoothing length, a quantity which is controlled by the user, which is equivalent to the internal length scale parameter in nonlocal methods. Therefore, the damage process can be controlled by the SPH user and result's sensitivity on the particle discretisation used is avoided.

  The study of SPH presented in Chapter 6 is the first study reporting the beneficial properties of SPH in the context of strain-softening issues. Therefore, it represents an ***innovative application of a pre-existing method***.

- **"Equivalent damage force" method:**

  The incentive in developing the "Equivalent damage force" method was to circumvent the issues arising from an ill-posed boundary value problem due to damage from the beginning and without the introduction of additional terms into constitutive equations of the material model.

  After investigating how strain-softening issues due to damage arise it became clear that the homogeneous parts of the partial differential equations are responsible for the ill-posed boundary value problem. It also became apparent that inhomogeneous parts of a partial differential equation are not capable of changing its type. It is known from work in this study that damage is part of the homogenous solution. And so the goal of this work was to investigate whether damage could be accounted for as an inhomogeneous term to maintain the

initial boundary value problem. To achieve this, damage was assumed to be termed a body force, the "Equivalent damage force". In doing so the homogeneous parts of the partial differential equation are not changed by damage and the linear elastic solution for the equations remains valid. Using this approach damage no longer causes the type change of partial differential equations and the initial boundary value problem is maintained.

This negates the need to change the constitutive material model used, as would be required with regularisation methods, in order to keep the boundary value problem stable. With this approach the issues previously observed in conventional strain-softening no longer occur.

This "Equivalent damage force" approach was implemented numerically in order to confirm that it is as useful numerically as it is analytically. The results showed that the numerical instabilities arising by strain-softening, namely mesh-sensitivity, were also avoided. Additionally, it was shown that the localisation zone due to strain-softening can be controlled by the user through adjusting the slope of the strain-softening branch. Therefore, an equal effect as the internal length scale has on the width of the localisation zone and maximum stress results in regularisation methods can be achieved with the "Equivalent damage force" approach. The "Equivalent damage force" approach takes a completely new approach, presented in Chapter 7, to tackle strain-softening instabilities in continuum damage mechanics. Therefore, it is a ***novel method dealing with strain-softening instabilities*** adding to the options available in the modelling of strain-softening.

- **Symmetric and positive-definite 8^{th} order damage tensor:**

  This work was part of the "Equivalent damage force" approach and aimed to extend the method to orthotropic material behaviour so that it could be applied to a wider range of materials.

  The "Equivalent damage force" approach requires that damage influenced parts in the equation of motion can be clearly distinguished from the linear elastic parts. Otherwise the "Equivalent damage force" cannot be formed as an inhomogeneous part. Unfortunately, orthotropic damage requires a tensorial representation which complicates the application of the "Equivalent damage force" approach. The study presented investigated the problem analytically and presented the formation of a damage tensor with 8^{th} order as transformation from virgin to damaged stiffness tensor. It was ensured that the tensor was

symmetric and positive-definite to maintain a well-posed boundary value problem for orthotropic material behaviour.

The 8th order damage tensor concept was developed as part of the "Equivalent damage force" method in Chapter 7. The use of an 8th order damage tensor was found to be necessary but unfortunately 8th order tensor quantities are not commonly used and described in literature. Therefore, the development of a symmetric and positive-definite damage tensor for the "Equivalent damage force" approach was conducted from scratch and represents a ***contribution to knowledge*** in itself.

The study of SPH's nonlocality and the "Equivalent damage force" approach lead to a paramount implication. Additional terms in the material's constitutive equations of a continuum damage mechanics model with strain-softening, as in regularisation methods, are not necessarily required to keep the boundary value problem stable and avoid strain-softening instabilities. In this insight lies a strong ***benefit for users of strain-softening models***. Currently, the user needs to be aware that conventional strain-softening models lead to non-physical and mesh-sensitive numerical results, and that users are required to use regularisation methods to achieve reasonable results. However, with the options studied in this work the user is not required to determine additional regularising terms for the material model and does not require a deeper understanding of the strain-softening issue to achieve mesh-independent results.

8.1 Future Work

The aim of this work was to examine critical issues of damage modelling within the continuum damage mechanics framework. More specifically, it was the goal to explore methods, other than conventional regularisation methods, which could maintain the well-posed character of the initially applied boundary value problem to circumvent critical issue of strain-softening behaviour commonly observed in continuum damage mechanics models, such as violation of the material stability criterion in analytical considerations and mesh-sensitivity of numerical results.

This work was successful in presenting two methods, namely the particle method SPH and the "Equivalent damage force" approach, which can achieve a well-posed boundary value problem and therefore contain the most crucial aspect of a good and reliable continuum damage mechanics model with strain-softening. However, some areas for improvement were determined:

- The “Equivalent damage force” approach was extended analytically to fit the more complex material behaviour of orthotropy. These analytical considerations lead to the definition of a symmetric and positive-definite 8^{th} order tensor for the transformation of the stiffness tensor to its damaged configuration. However, these considerations were kept purely analytical and need to be tested for their suitability to numeric applications as a validation step.
- The “Equivalent damage force” approach was applied numerically for an isotropic material model with linear softening law which represents the simplest way of implementing a continuum damage mechanics model with strain-softening. This representation was sufficient for the purpose of investigating the characteristic properties and feasibility of the “Equivalent damage force” approach in this work. However, it was acknowledged that the linear softening law is not the most accurate model for real material behaviour. Therefore, it is recommended to add further softening laws, e.g. bi-linear or exponential, to achieve more realistic material behaviour in the strain-softening domain.

REFERENCES

[1] Abu-Lebdeh, T., Hamoush, S., Heard, W. and Zornig, B. (2011), "Effect of matrix strength on pullout behavior of steel fiber reinforced very-high strength concrete composites.", *Construction and Building Materials,* vol. 25, no. 1, pp. 39-46.

[2] Aifantis, E. C. (1984), "On the microstructural origin of certain inelastic models.", *Journal of Engineering Materials and Technology ASME,* vol. 106, pp. 326-330.

[3] Aifantis, E. C. (1992), "On the role of gradients in the localization of deformation and fracture", *International Journal of Engineering Science,* vol. 30, no. 10, pp. 1279-1299.

[4] Barenblatt, G. I. (1962), "The mathematical theory of equilibrium cracks formed in brittle fracture.", *Advances in Applied Mechanics,* vol. 7, pp. 55-129.

[5] Bassim, M. N. and Odeshi, A. G. (2008), "Shear strain localisation and fracture in high strength structural materials.", *Archives of Materials Science and Engineering,* vol. 31, no. 2, pp. 69-74.

[6] Bažant, Z. P. and Belytschko, T. B. (1985), "Wave propagation in a strain-softening bar: Exact solution.", *Journal of Engineering Mechanics,* vol. 111, no. 3, pp. 381-389.

[7] Bažant, Z. P. and Jirásek, M. (2002), "Nonlocal integral formulations of plasticity and damage: Survey of progress.", *Journal of Engineering Mechanics,* vol. 128, no. 11, pp. 1119-1149.

[8] Bažant, Z. P. and Oh, B. H. (1983), "Crack band theory for fracture of concrete.", *Materials and Structures,* vol. 16, no. 3, pp. 155-177.

[9] Bažant, Z. P. and Zubelewicz, A. (1988), "Strain-softening bar and beam: Exact non-local solution.", *International Journal of Solids and Structures,* vol. 24, no. 7, pp. 659-673.

[10] Bažant, Z. P. and Pijaudier-Cabot, G. (1988), "Nonlocal continuum damage, localization instability and convergence.", *Journal of Applied Mechanics,* vol. 55, no. 2, pp. 287-293.

[11] Belytschko, T. and Bažant, Z. P. (1984), "Strain-softening materials and finite element solutions.", in William, K. (ed.), *Proc., ASME Symposium on Constitutive Equations: Macro, Micro and Computational Aspects,* ASME Winter Annual Meeting, New Orleans, pp. 253.

[12] Bobiński, J. and Tejchman, J. (2005), "Modelling of concrete behaviour with a non-local continuum damage approach.", *Archives of Hydro-Engineering and Environmental Mechanics,* vol. 52, pp. 243-263.

[13] Bouaziz, A., Zaïri, F., Naït-Abdelaziz, M., Gloaguen, J. M. and Lefebvre, J. M. (2007), "Micromechanical modelling and experimental investigation of random discontinuous glass fiber polymer–matrix composites.", *Composites Science and Technology,* vol. 67, no. 15-16, pp. 3278-3285.

[14] Briançon, C., Sigety, P. and G'Sell, C. (1996), "In situ study of matrix strain in carbon/resin composite materials.", *Composites Science and Technology,* vol. 56, no. 7, pp. 835-840.

[15] Cai, M., Langford, S. C., Levine, L. E. and Dickinson, J. T. (2004), "Determination of strain localization in aluminium alloys using laser-induced photoelectron emission.", *Journal of Applied Physics,* vol. 96, no. 12, pp. 7189-7194.

[16] Cao, J. J., Chen, H. H., Du, F., Zhao, H. C. and Fan, L. (2013), "Preliminary study of in situ transformed carbon fibers/Al2O3 ceramic matrix composites.", *Ceramics International,* vol. 39, no. 6, pp. 7037-7042.

[17] Carol, I., Rizzi, E. and Willam, K. (2001), "On the formulation of anisotropic elastic degradation. I. Theory based on a pseudo-logarithmic damage tensor rate.", *International Journal of Solids and Structures,* vol. 38, no. 4, pp. 491-518.

[18] Cauvin, A. and Testa, R. B. (1999), "Damage mechanics: basic variables in continuum theories.", *International Journal of Solids and Structures,* vol. 36, no. 5, pp. 747-761.

[19] Chaboche, J. L. (1981), "Continuous damage mechanics - A tool to describe phenomena before crack initiation.", *Nuclear Engineering and Design,* vol. 64, pp. 233-247.

[20] Chaboche, J. L. (1988), "Continuum damage mechanics: Part I-General Concepts.", *Journal of Applied Mechanics,* vol. 55, no. 1, pp. 59-64.

[21] Chaboche, J. L. (1988), "Continuum damage mechanics: Part II-Damage growth, crack initiation, and crack growth.", *Journal of Applied Mechanics,* vol. 55, no. 1, pp. 65-72.

[22] Chaboche, J. (1978), *Description thermodynamique et phénoménologique de la viscoplasticité cyclique avec endommagement* (PhD thesis), Université Pierre et Marie Curie, Paris.

[23] Chang, F. and Chang, K. (1987), "Post-failure analysis of bolted composite joints in tension or shear-out mode failure.", *Journal of Composite Materials,* vol. 21, no. 9, pp. 809-833.

[24] Chang, F. and Chang, K. (1987), "A progressive damage model for laminated composites containing stress concentrations.", *Journal of Composite Materials,* vol. 21, no. 9, pp. 834-855.

[25] Cheng and Hallquist, J. (unknown), *Implementation of three-dimensional composite failure model into DYNA3D* (unpublished Report), http://ftp.lstc.com/anonymous/outgoing/jday/composites/mat_059_Hallquist_Cheng.pdf.

[26] Cordebois, J. P. and Sidoroff, F. (1982), "Damage induced elastic anisotropy.", in Boehler, J. P. and Dafalias, Y. F. (eds.) *Mechanics of behavior of anisotropic solids,* No. 295 ed, Martinus Nijhoff Publishers, The Hague, pp. 761-774.

[27] de Borst, R. (1987), "Computation of post-bifurcation and post-failure behavior of strain-softening solids.", *Computers and Structures,* vol. 25, no. 2, pp. 211-224.

[28] de Borst, R., Gutiérrez, M. A., Wells, G. N., Remmers, J. J. C. and Askes, H. (2004), "Cohesive-zone models, higher-order continuum theories and reliability methods for computational failure analysis.", *International Journal for Numerical Methods in Engineering,* vol. 60, no. 1, pp. 289-315.

[29] de Borst, R., Pamin, J. and Geers, M. G. D. (1993), "On coupled gradient-dependent plasticity and damage theories with a view to localization analysis.", *European Journal of Mechanics - A/Solids,* vol. 18, pp. 939-962.

[30] de Borst, R., Sluys, L. J., Mühlhaus, H. -B. and Pamin, J. (1993), "Fundamental issues in finite element analysis of localization of deformation.", *Engineering Computations,* vol. 10, pp. 99-121.

[31] De Caso y Basalo, F. J., Matta, F. and Nanni, A. (2012), "Fiber reinforced cement-based composite system for concrete confinement.", *Construction and Building Materials,* vol. 32, pp. 55-65.

[32] Dugdale, D. S. (1960), "Yielding of steel sheets containing slits.", *Journal of the Mechanics and Physics of Solids,* vol. 8, no. 2, pp. 100-104.

[33] Dzhuraev, T. D. and Popëlek, Y. (1989), "On the canonical forms of third-order partial differential equations.", *Russian Mathematical Surveys,* vol. 44, no. 4, pp. 203-204.

[34] Gálvez, F., Rodríguez, J. and Sánchez Gálvez, V. (2000), "A wave propagation technique to measure the dynamic tensile strength of brittle materials.", *Journal de Physique IV France,* vol. 10, pp. Pr9-203-Pr9-208.

[35] Gay, D., Hoa, S. V. and Tsai, S. W. (2003), *Composite materials: design and applications,* CRC Press, Boca Raton, USA.

[36] Geers, M. G. D., Peijs, T., Brekelmans, W. A. M. and de Borst, R. (1996), "Experimental monitoring of strain localization and failure behaviour of composite materials.", *Composites Science and Technology,* vol. 56, no. 11, pp. 1283-1290.

[37] Gol'denblat, I. and Kopnov, V. A. (1965), "Strength of glass-reinforced plastics in the complex stress state.", *Polymer Mechanics,* vol. 1, no. 2, pp. 70-78.

[38] Gospodinov, G. and Kerelezova, I. (2002), "Boundary elements modeling of plain concrete notched beams by means of crack propagation formula.", *Danish Society for Structural Science and Engineering,* vol. 73, pp. 1-38.

[39] Graff, K. F. (1991), *Wave motion in elastic solids,* Dover Publications, New York, USA.

[40] Gurson, A. L. (1977), "Continuum theory of ductile rupture by void nucleation and growth: Part I-Yield criteria and flow rules for porous ductile media.", *Journal of Engineering Materials and Technology,* vol. 99, no. 1, pp. 2-15.

[41] Hadamard, J. (1903), *Leçons sur la propagation des ondes et les équations de l'hydrodynamique.* Librairie Scientifique A. Hermann, Paris, France.

[42] Hahn, H. T. and Tsai, S. W. (1973), "Nonlinear elastic behavior of unidirectional composite laminae.", *Journal of Composite Materials,* vol. 7, no. 1, pp. 102-118.

[43] Hansen, N. R. and Schreyer, H. L. (1994), "A thermodynamically consistent framework for theories of elastoplasticity coupled with damage.", *International Journal of Solids and Structures,* vol. 31, no. 3, pp. 359-389.

[44] Hashin, Z. (1980), "Failure criteria for unidirectional fiber composites.", *Journal of Applied Mechanics,* vol. 47, no. 2, pp. 329-334.

[45] Hillerborg, A., Modéer, M. and Petersson, P. -E. (1976), "Analysis of crack formation and crack growth in concrete by means of fracture mechanics and finite elements.", *Cement and Concrete Research,* vol. 6, no. 6, pp. 773-781.

[46] Hinton, M. J., Kaddour, A. S. and Soden, P. D. (2002), "A comparison of the predictive capabilities of current failure theories for composite laminates, judged against experimental evidence.", *Composites Science and Technology,* vol. 62, no. 12-13, pp. 1725-1797.

[47] Hoffman, J. D. (ed.) (2001), *Numerical methods for engineers and scientists,* 2nd ed, Marcel Dekker Inc., USA.

[48] Hoffmann, K. A. and Chiang, S. T. (1993), *Computational fluid dynamics for engineers,* Engineering Education System, Wichita, USA.

[49] Hopkinson, B. (1914), "A method of measuring the pressure produced in the detornation of high explosives or by the impact of bullets.", *Philosophical Transactions Royal Society of London A,* vol. 213, pp. 437-456.

[50] Hordijk, D. A. (1991), *Local approach to fatigue of concrete.* (PhD thesis), Delft University of Technology, Delft, The Netherlands.

[51] Hu, X. H., Jain, M., Wilkinson, D. S. and Mishra, R. K. (2008), "Microstructure-based finite element analysis of strain localization behavior in AA5754 aluminum sheet.", *Acta Materialia,* vol. 56, no. 13, pp. 3187-3201.

[52] Jirásek, M. (2002), "Objective modeling of strain localization.", *Revue Française de Génie Civil,* vol. 6, no. 6, pp. 1119-1132.

[53] Jirásek, M. (2004), "Non-local damage mechanics with application to concrete.", *Revue Française de Génie Civil,* vol. 8, no. 5-6, pp. 683-707.

[54] Jirásek, M. and Bažant, Z. P. (2002), *Inelastic analysis of structures,* Wiley, Chichester, UK.

[55] Jones, R. M. (1999), *Mechanics of composite materials,* 2nd ed, Taylor & Francis, USA.

[56] Kachanov, L. M. (1999 (1958)), "Rupture time under creep conditions.", *International Journal of Fracture (original: Izvestiya Sibirskogo Otdeleniya Akademii Nauk SSSR, Seriya Tekhnicheskikh Nauk),* vol. 97, no. 1-4, pp. 11-18.

[57] Kaddour, A. S., Hinton, M. J. and Soden, P. D. (2004), "A comparison of the predictive capabilities of current failure theories for composite laminates: additional contributions.", *Composites Science and Technology,* vol. 64, no. 3-4, pp. 449-476.

[58] Kolsky, H. (1953), *Stress waves in solids,* Clarendon Press, Oxford, UK.

[59] Kovach, L. D. (1982), *Advanced engineering mathematics,* Addison-Wesley, Reading, USA.

[60] Kozicki, J. and Tejchman, J. (2007), "Experimental investigations of strain localization in concrete using digital image correlation (DIC) technique.", *Archives of Hydro-Engineering and Environmental Mechanics,* vol. 54, no. 1, pp. 3-24.

[61] Krajcinovic, D. (1989), "Damage mechanics.", *Mechanics of Materials,* vol. 8, pp. 117-197.

[62] Krajcinovic, D. and Lemaitre, J. (1987), *Continuous damage mechanics: Theory and application. CISM Courses and Lectures No. 295,* Springer, Wien, Austria.

[63] Krug III, D. J., Asuncion, M. Z., Popova, V. and Laine, R. M. (2013), "Transparent fiber glass reinforced composites.", *Composites Science and Technology,* vol. 77, pp. 95-100.

[64] Lemaitre, J. (1985), "A continuous damage mechanics model for ductile fracture.", *Journal of Engineering Materials and Technology,* vol. 107, pp. 83-89.

[65] Lemaitre, J. (ed.) (1992), *A course on damage mechanics,* Springer, Berlin.

[66] Lemaitre, J. and Desmorat, R. (2004), *Engineering damage mechanics : ductile, creep, fatigue and brittle failures,* Springer, Berlin, Germany.

[67] Leroy, Y. and Ortiz, M. (1989), "Finite element analysis of strain localization in frictional materials.", *International Journal for Numerical and Analytical Methods in Geomechanics,* vol. 13, pp. 53-74.

[68] Lin, J. I. (2004), *DYNA3D: A nonlinear, explicit, three-dimensional finite element code for solid and structural mechanics,* User manual DYNA3D, Methods Development Group Mechanical Engineering.

[69] Lindholm, U. S. (1964), "Some experiments with the Split Hopkinson pressure bar.", *Journal of the Mechanics and Physics of Solids,* vol. 12, pp. 317-335.

[70] Livermore Software Technology Corporation (2007/2013), *LS-DYNA keyword user's manual (version 971),* User manual LS-DYNA, Livermore Software Technology Corporation (LSTC), USA.

[71] Loret, B. and Prevost, J. H. (1990), "Dynamic strain localization in elasto-(visco-)plastic solids, Part 1. General formulation and one-dimensional examples.", *Computer Methods in Applied Mechanics and Engineering,* vol. 83, no. 3, pp. 247-273.

[72] LSTC Inc and DYNAmore GmbH (2012), *LS-DYNA support*, available at: http://www.dynasupport.com/ (accessed 17/09/2012).

[73] LSTC Inc and DYNAmore GmbH (2012), *LS-DYNA support: Composite models*, available at: http://www.dynasupport.com/howtos/material/composite-models (accessed 17/09/2012).

[74] Lü, Y. B. and Chen, X. F. (1989), "The order of a damage tensor.", *Applied Mathematics and Mechanics,* vol. 10, no. 3, pp. 251-258.

[75] Lubarda, V. A. and Krajcinovic, D. (1993), "Damage tensors and the crack density distribution.", *International Journal of Solids and Structures,* vol. 30, no. 20, pp. 2859-2877.

[76] Lucy, L. B. (1977), "A numerical approach to the testing of the fission hypothesis.", *The Astronomical Journal,* vol. 82, no. 12, pp. 1013-1024.

[77] Maimí, P., Camanho, P. P., Mayugo, J. A. and Dávila, C. G. (2007), "A continuum damage model for composite laminates: Part I - Constitutive model.", *Mechanics of Materials,* vol. 39, no. 10, pp. 897-908.

[78] Maire, J. F. and Chaboche, J. L. (1997), "A new formulation of continuum damage mechanics (CDM) for composite materials.", *Aerospace Science and Technology,* vol. 1, no. 4, pp. 247-257.

[79] Marotti de Sciarra, F. (2009), "A nonlocal model with strain-based damage.", *International Journal of Solids and Structures,* vol. 46, no. 22-23, pp. 4107-4122.

[80] Mase, G. E. (1970), *Schaum's outline of theory and problems of continuum mechanics,* McGraw-Hill, New York.

[81] Matzenmiller, A., Lubliner, J. and Taylor, R. K. (1995), "A constitutive model for anisotropic damage in fiber-composites.", *Mechanics of Materials,* vol. 20, no. 2, pp. 125-152.

[82] Murakami, S. (1988), "Mechanical Modeling of material damage.", *Journal of Applied Mechanics ASME,* vol. 55, no. 2, pp. 280-286.

[83] Needleman, A. (1988), "Material rate dependence and mesh sensitivity in localization problems.", *Computer Methods in Applied Mechanics and Engineering,* vol. 67, no. 1, pp. 69-85.

[84] Needleman, A. and Tvergaard, V. (1984), "An analysis of ductile rupture in notched bars.", *Journal of the Mechanics and Physics of Solids,* vol. 32, no. 6, pp. 461-490.

[85] Needleman, A., Tvergaard, V. and Hutchinson, J. W. (1992), "Void growth in plastic solids.", in Argon, A. S. (ed.) *Topics in Fracture and Fatigue,* , pp. 145-178.

[86] Neilsen, M. K. and Schreyer, H. L. (1993), "Bifurcations in elastic-plastic materials.", *International Journal of Solids and Structures,* vol. 30, no. 4, pp. 521-544.

[87] Pankaj and Parkash, S. (1992), "Dynamic analysis of a strain softening bar.", *Earthquake Engineering, Tenth World Conference,* 1992, Rotterdam, The Netherlands, pp. 2587-2592.

[88] Pardoen, T. and Brechet, Y. (2004), "Influence of microstructure-driven strain localization on the ductile fracture of metallic alloys.", *Philosophical Magazine,* vol. 84, no. 3-5, pp. 269-297.

[89] Peerlings, R. H. J., de Borst, R., Brekelmans, W. A. M., de Vree, J. H. P. and Spee, I. (1996), "Some observations on localisation in non-local and gradient damage models.", *European Journal of Mechanics - A/Solids,* vol. 15, no. 6, pp. 937-953.

[90] Peerlings, R. H. J., de Borst, R., Brekelmans, W. A. M. and Geers, M. G. D. (1998), "Wave propagation and localisation in nonlocal and gradient-enhanced damage models.", *Journal de Physique IV,* vol. 8, no. PR8, pp. Pr8-293-Pr8-300.

[91] Peerlings, R. H. J., de Borst, R., Brekelmans, W. A. M. and Geers, M. G. D. (1998), "Gradient-enhanced damage modelling of concrete fracture.", *Mechanics of Cohesive-Frictional Materials,* vol. 3, pp. 323-342.

[92] Peerlings, R. H. J., Geers, M. G. D., de Borst, R. and Brekelmans, W. A. M. (2001), "A critical comparison of nonlocal and gradient-enhanced softening continua.", *International Journal of Solids and Structures,* vol. 38, no. 44-45, pp. 7723-7746.

[93] Peerlings, R. H., de Borst, R., Brekelmans, W. A. M. and de Vree, J. H. P. (1996), "Gradient enhanced damage for quasi-brittle materials.", *International Journal for Numerical Methods in Engineering,* vol. 39, no. 19, pp. 3391-3403.

[94] Pemberton, S. R., Oberg, E. K., Dean, J., Tsarouchas, D., Markaki, A. E., Marston, L. and Clyne, T. W. (2011), "The fracture energy of metal fibre reinforced ceramic composites (MFCs).", *Composites Science and Technology,* vol. 71, no. 3, pp. 266-275.

[95] Pijaudier-Cabot, G., ASCE, S. M. and Bažant, Z. P. (1987), "Nonlocal damage theory.", *Journal of Engineering Mechanics,* vol. 113, no. 10, pp. 1512-1533.

[96] Pijaudier-Cabot, G., Bažant, Z. P. and Tabbara, M. (1988), "Comparison of various models for strain-softening.", *Engineering Computations,* vol. 5, pp. 141-150.

[97] Pradhan, P. K., Dash, P. R., Robi, P. S. and Roy, S. K. (2012), "Micro void coalescence of ductile fracture in mild steel during tensile straining.", *Fracture and Structural Integrity,* vol. 19, pp. 51-60.

[98] Rabotnov, Y. N. (1968), "Creep rupture.", in Hetenyi, M. and Vincenti, W. G. (eds.) *12th International Congress of Applied Mechanics,* Springer, Berlin, Germany, pp. 342-349.

[99] Rice, J. R. (1976), "The localization of plastic deformation.", *Proceedings of the 14th International Congress on Theoretical and Applied Mechanics,* Vol. 1, Delft, pp. 207.

[100] Rudnicki, J. W. and Rice, J. R. (1975), "Conditions for the localization of deformation in pressure-sensitive dilatant materials.", *Journal of the Mechanics and Physics of Solids,* vol. 23, no. 6, pp. 371-394.

[101] Russo, P., Acierno, D., Simeoli, G., Iannace, S. and Sorrentino, L. (2013), "Flexural and impact response of woven glass fiber fabric/polypropylene composites.", *Composites Part B: Engineering,* vol. 54, pp. 415-421.

[102] Sandler, I. S. and Wright, J. P. (1983), "Strain-Softening", in Nemat-Nasser, S. (ed.) *Theoretical foundation for large-scale computations for nonlinear material behavior,* Northwestern University, Evanston, USA, pp. 285-301.

[103] Schreyer, H. L., Sulsky, D. and Chen, Z. (1994), "Moving surface approach to softening with localization.", in Bažant, Z. P., Bittnar, Z., Jirásek, M., et al (eds.) *Fracture and Damage in Quasibrittle Structures,* E & FN Spon, , pp. 113-120.

[104] Schweizerhof, K., Weimar, K., Münz, T. and Rottner, T. (1998), "Crashworthiness analysis with enhanced composite material models in LS-DYNA - Merits and limits.", *Proceedings of the 5th International LS-DYNA Users Conference,* 1998, Detroit, USA, pp. 1-17.

[105] Schwer, L. E. (2010), "A brief look at *MAT_NONLOCAL: A possible cure for erosion illness?", *11th International LS-DYNA Users Conference,* 2010, USA, pp. (3-19)-(3-36).

[106] Simo, J. C. and Ju, J. W. (1987), "Strain- and stress-based continuum damage models - I. Formulation.", *International Journal of Solids and Structures,* vol. 23, no. 7, pp. 821-840.

[107] Simulia (2011), *Abaqus 6.11: Analysis user's manual - Volume III: Materials,* User manual ABAQUS, Simulia, USA.

[108] Sládek, J., Sládek, V., and Bažant, Z. P. (2003), "Non-local boundary integral formulation for softening damage.", *International Journal for Numerical Methods in Engineering,* vol. 57, no. 1, pp. 103-116.

[109] Sluys, L. J. and de Borst, R. (1992), "Wave propagation and localization in a rate-dependent cracked medium - Model formulation and one-dimensional examples.", *International Journal of Solids and Structures,* vol. 29, no. 23, pp. 2945-2958.

[110] Sluys, L. J. and de Borst, R. (1994), "Dispersive properties of gradient-dependent and rate-dependent media.", *Mechanics of Materials,* vol. 18, no. 2, pp. 131-149.

[111] Song, K., Li, Y. and Rose, C. A. (2011), "Continuum damage mechanics models for the analysis of progressive failure in open-hole tension laminates.", *52nd AIAA Structures Structural Dynamics and Materials Conference* 4–7 April 2011, .

[112] Tailhan, J. -L., Rossi, P. and Dal Pont, S. (2010), "Macroscopic probabilistic modeling of concrete cracking: First 3D results.", in Oh, B. H. (ed.), *The 7th International Conference on Fracture Mechanics of Concrete and Concrete Structures,* Vol. Part II, 2010, Korea, pp. 238-242.

[113] Tsai, S. W. and Wu, E. M. (1971), "A general theory of strength for anisotropic materials.", *Journal of Composite Materials,* vol. 5, no. 1, pp. 58-80.

[114] Tsotsis, T. K., Rugg, K. L. and Cox, B. N. (2006), "Towards rapid screening of new composite matrix resins.", *Composites Science and Technology,* vol. 66, no. 11-12, pp. 1651-1670.

[115] Tvergaard, V. (1981), "Influence of voids on shear band instabilities under plane strain conditions.", *International Journal of Fracture,* vol. 17, no. 4, pp. 389-407.

[116] Tvergaard, V. (1982), "On localization in ductile materials containing spherical voids.", *International Journal of Fracture,* vol. 18, no. 4, pp. 237-252.

[117] Tvergaard, V. and Needleman, A. (1984), "Analysis of the cup-cone fracture in a round tensile bar.", *Acta Metallurgica,* vol. 32, no. 1, pp. 157-169.

[118] Vignjevic, R., Campbell, J., Jaric, J. and Powell, S. (2009), "Derivation of SPH equations in a moving referential coordinate system.", *Computer Methods in Applied Mechanics and Engineering,* vol. 198, no. 30-32, pp. 2403-2411.

[119] Vignjevic, R., Reveles, J. R. and Campbell, J. (2006), "SPH in a total Lagrangian formalism.", *Computer Modelling in Engineering and Sciences,* vol. 146, no. 3, pp. 181-198.

[120] Von Karman, T. and Duwez, P. (1950), "The propagation of plastic deformation in solids.", *Journal of Applied Physics,* vol. 21, no. 10, pp. 987-994.

[121] Voyiadjis, G. Z. and Park, T. (1997), "Anisotropic damage effect tensors for the symmetrization of the effective stress tensor.", *Journal of Applied Mechanics,* vol. 64, no. 1, pp. 106-110.

[122] Vu, D. Q., Gigliotti, M. and Lafarie-Frenot, M. C. (2012), "Experimental characterization of thermo-oxidation-induced shrinkage and damage in polymer–matrix.", *Composites Part A: Applied Science and Manufacturing,* vol. 43, no. 4, pp. 577-586.

[123] Wang, W. M., Sluys, L. J. and de Borst, R. (1997), "Viscoplasticity for instabilities due to strain softening and strain-rate softening.", *International Journal for Numerical Methods in Engineering,* vol. 40, pp. 3839-3864.

[124] Wicklein, M., Ryan, S., White, D. M. and Clegg, R. A. (2008), "Hypervelocity impact on CFRP: Testing, material modelling, and numerical simulation.", *International Journal of Impact Engineering,* vol. 35, no. 12, pp. 1861-1869.

[125] Williams, K. V., Vaziri, R. and Poursartip, A. (2003), "A physically based continuum damage mechanics model for thin laminated composite structures.", *International Journal of Solids and Structures,* vol. 40, no. 9, pp. 2267-2300.

[126] Wood, D. C., Appleby-Thomas, G. J., Hazell, P. J. and Barnes, N. R. (2012), "Shock propagation in a tape wrapped carbon fibre composite.", *Composites Part A: Applied Science and Manufacturing,* vol. 43, no. 9, pp. 1555-1560.

APPENDICES

Appendix A Product- and Sum-Type Symmetrisation

A.1 Product-Type Symmetrisation

Product-type symmetrisation was proposed by Cordebois and Sidoroff [26] and is frequently applied in literature, e.g. Carol et al. [17]. The symmetric damage effect tensor can be developed in terms of stress or strain and will be fully equivalent: $M_{ijkl} = M_{ijkl}^{-1}$.

The representation of the effective stress using the product-type symmetrisation is known from Equation (3-21).

$$\tilde{\sigma}_{ij} = (\delta_{ik} - \omega_{ik})^{-\frac{1}{2}} \sigma_{kl} (\delta_{jl} - \omega_{jl})^{-\frac{1}{2}}$$

It reads expanded in matrix notation as:

$$\begin{bmatrix} \tilde{\sigma}_{11} & \tilde{\sigma}_{12} & \tilde{\sigma}_{13} \\ \tilde{\sigma}_{21} & \tilde{\sigma}_{22} & \tilde{\sigma}_{23} \\ \tilde{\sigma}_{31} & \tilde{\sigma}_{32} & \tilde{\sigma}_{33} \end{bmatrix} = \begin{bmatrix} \frac{1}{\sqrt{1-\omega_1}} & 0 & 0 \\ 0 & \frac{1}{\sqrt{1-\omega_2}} & 0 \\ 0 & 0 & \frac{1}{\sqrt{1-\omega_3}} \end{bmatrix} \begin{bmatrix} \sigma_{11} & \sigma_{12} & \sigma_{13} \\ \sigma_{21} & \sigma_{22} & \sigma_{23} \\ \sigma_{31} & \sigma_{32} & \sigma_{33} \end{bmatrix} \begin{bmatrix} \frac{1}{\sqrt{1-\omega_1}} & 0 & 0 \\ 0 & \frac{1}{\sqrt{1-\omega_2}} & 0 \\ 0 & 0 & \frac{1}{\sqrt{1-\omega_3}} \end{bmatrix}$$

$$= \begin{bmatrix} \frac{\sigma_{11}}{1-\omega_1} & \frac{\sigma_{12}}{\sqrt{1-\omega_1}\sqrt{1-\omega_2}} & \frac{\sigma_{13}}{\sqrt{1-\omega_1}\sqrt{1-\omega_3}} \\ \frac{\sigma_{21}}{\sqrt{1-\omega_1}\sqrt{1-\omega_2}} & \frac{\sigma_{22}}{1-\omega_2} & \frac{\sigma_{23}}{\sqrt{1-\omega_2}\sqrt{1-\omega_3}} \\ \frac{\sigma_{31}}{\sqrt{1-\omega_1}\sqrt{1-\omega_3}} & \frac{\sigma_{32}}{\sqrt{1-\omega_2}\sqrt{1-\omega_3}} & \frac{\sigma_{33}}{1-\omega_3} \end{bmatrix}$$

The symmetric damage effect tensor is found by applying Voigt notation:

$$M_{ijkl} = \begin{bmatrix} \frac{1}{1-\omega_1} & 0 & 0 & 0 & 0 & 0 \\ 0 & \frac{1}{1-\omega_2} & 0 & 0 & 0 & 0 \\ 0 & 0 & \frac{1}{1-\omega_3} & 0 & 0 & 0 \\ 0 & 0 & 0 & \frac{1}{\sqrt{(1-\omega_2)(1-\omega_3)}} & 0 & 0 \\ 0 & 0 & 0 & 0 & \frac{1}{\sqrt{(1-\omega_1)(1-\omega_3)}} & 0 \\ 0 & 0 & 0 & 0 & 0 & \frac{1}{\sqrt{(1-\omega_1)(1-\omega_2)}} \end{bmatrix}$$

The representation of the effective strain using the product-type symmetrisation is as following:

$$\tilde{\varepsilon}_{ij} = (\delta_{ik} - \omega_{ik})^{\frac{1}{2}} \varepsilon_{kl} (\delta_{jl} - \omega_{jl})^{\frac{1}{2}}$$

It reads expanded in matrix notation as:

$$\begin{bmatrix} \tilde{\varepsilon}_{11} & \tilde{\varepsilon}_{12} & \tilde{\varepsilon}_{13} \\ \tilde{\varepsilon}_{21} & \tilde{\varepsilon}_{22} & \tilde{\varepsilon}_{23} \\ \tilde{\varepsilon}_{31} & \tilde{\varepsilon}_{32} & \tilde{\varepsilon}_{33} \end{bmatrix} = \begin{bmatrix} \sqrt{1-\omega_1} & 0 & 0 \\ 0 & \sqrt{1-\omega_2} & 0 \\ 0 & 0 & \sqrt{1-\omega_3} \end{bmatrix} \begin{bmatrix} \varepsilon_{11} & \varepsilon_{12} & \varepsilon_{13} \\ \varepsilon_{21} & \varepsilon_{22} & \varepsilon_{23} \\ \varepsilon_{31} & \varepsilon_{32} & \varepsilon_{33} \end{bmatrix} \begin{bmatrix} \sqrt{1-\omega_1} & 0 & 0 \\ 0 & \sqrt{1-\omega_2} & 0 \\ 0 & 0 & \sqrt{1-\omega_3} \end{bmatrix}$$

$$= \begin{bmatrix} \varepsilon_{11}(1-\omega_1) & \varepsilon_{12}\sqrt{1-\omega_1}\sqrt{1-\omega_2} & \varepsilon_{13}\sqrt{1-\omega_1}\sqrt{1-\omega_3} \\ \varepsilon_{21}\sqrt{1-\omega_1}\sqrt{1-\omega_2} & \varepsilon_{22}(1-\omega_2) & \varepsilon_{23}\sqrt{1-\omega_2}\sqrt{1-\omega_3} \\ \varepsilon_{31}\sqrt{1-\omega_1}\sqrt{1-\omega_3} & \varepsilon_{32}\sqrt{1-\omega_2}\sqrt{1-\omega_3} & \varepsilon_{33}(1-\omega_3) \end{bmatrix}$$

The symmetric inverse damage effect tensor is found by applying Voigt notation:

$$M_{ijkl}^{-1} = \begin{bmatrix} 1-\omega_1 & 0 & 0 & 0 & 0 & 0 \\ 0 & 1-\omega_2 & 0 & 0 & 0 & 0 \\ 0 & 0 & 1-\omega_3 & 0 & 0 & 0 \\ 0 & 0 & 0 & \sqrt{(1-\omega_2)(1-\omega_3)} & 0 & 0 \\ 0 & 0 & 0 & 0 & \sqrt{(1-\omega_1)(1-\omega_3)} & 0 \\ 0 & 0 & 0 & 0 & 0 & \sqrt{(1-\omega_1)(1-\omega_2)} \end{bmatrix}$$

The damage effect tensors developed through product-type symmetrisation of effective stress and effective strain are equivalent: $M_{ijkl} = M_{ijkl}^{-1}$.

A.2 Sum-Type Symmetrisation

Sum-type symmetrisation was proposed by Murakami [82] and is frequently applied in literature, e.g. Carol et al. [17]. The symmetric damage effect tensor can be developed in terms of stress or strain but will not be equivalent: $M_{ijkl} \neq M_{ijkl}^{-1}$.

The representation of the effective stress using the sum-type symmetrisation is known from Equation (3-22).

$$\tilde{\sigma}_{ij} = \frac{1}{2}\left[\sigma_{ik}\left(\delta_{kj} - \omega_{kj}\right)^{-1} + \left(\delta_{jk} - \omega_{jk}\right)^{-1}\sigma_{ki}\right]$$

It reads expanded in matrix notation as:

$$\begin{bmatrix} \tilde{\sigma}_{11} & \tilde{\sigma}_{12} & \tilde{\sigma}_{13} \\ \tilde{\sigma}_{21} & \tilde{\sigma}_{22} & \tilde{\sigma}_{23} \\ \tilde{\sigma}_{31} & \tilde{\sigma}_{32} & \tilde{\sigma}_{33} \end{bmatrix} =$$

$$= \frac{1}{2}\left\{ \begin{bmatrix} \sigma_{11} & \sigma_{12} & \sigma_{13} \\ \sigma_{21} & \sigma_{22} & \sigma_{23} \\ \sigma_{31} & \sigma_{32} & \sigma_{33} \end{bmatrix} \begin{bmatrix} \frac{1}{1-\omega_1} & 0 & 0 \\ 0 & \frac{1}{1-\omega_2} & 0 \\ 0 & 0 & \frac{1}{1-\omega_3} \end{bmatrix} + \begin{bmatrix} \frac{1}{1-\omega_1} & 0 & 0 \\ 0 & \frac{1}{1-\omega_2} & 0 \\ 0 & 0 & \frac{1}{1-\omega_3} \end{bmatrix} \begin{bmatrix} \sigma_{11} & \sigma_{12} & \sigma_{13} \\ \sigma_{21} & \sigma_{22} & \sigma_{23} \\ \sigma_{31} & \sigma_{32} & \sigma_{33} \end{bmatrix} \right\}$$

$$= \begin{bmatrix} \frac{\sigma_{11}}{1-\omega_1} & \frac{1}{2}\sigma_{12}\left(\frac{1}{1-\omega_1} + \frac{1}{1-\omega_2}\right) & \frac{1}{2}\sigma_{13}\left(\frac{1}{1-\omega_1} + \frac{1}{1-\omega_3}\right) \\ \frac{1}{2}\sigma_{21}\left(\frac{1}{1-\omega_1} + \frac{1}{1-\omega_2}\right) & \frac{\sigma_{22}}{1-\omega_2} & \frac{1}{2}\sigma_{23}\left(\frac{1}{1-\omega_2} + \frac{1}{1-\omega_3}\right) \\ \frac{1}{2}\sigma_{31}\left(\frac{1}{1-\omega_1} + \frac{1}{1-\omega_3}\right) & \frac{1}{2}\sigma_{32}\left(\frac{1}{1-\omega_2} + \frac{1}{1-\omega_3}\right) & \frac{\sigma_{33}}{1-\omega_3} \end{bmatrix}$$

The symmetric damage effect tensor is found by applying Voigt notation:

$$M_{ijkl}$$

$$= \begin{bmatrix} \frac{1}{1-\omega_1} & 0 & 0 & 0 & 0 & 0 \\ 0 & \frac{1}{1-\omega_2} & 0 & 0 & 0 & 0 \\ 0 & 0 & \frac{1}{1-\omega_3} & 0 & 0 & 0 \\ 0 & 0 & 0 & \frac{1}{2}\left(\frac{1}{1-\omega_2}+\frac{1}{1-\omega_3}\right) & 0 & 0 \\ 0 & 0 & 0 & 0 & \frac{1}{2}\left(\frac{1}{1-\omega_1}+\frac{1}{1-\omega_3}\right) & 0 \\ 0 & 0 & 0 & 0 & 0 & \frac{1}{2}\left(\frac{1}{1-\omega_1}+\frac{1}{1-\omega_2}\right) \end{bmatrix}$$

The representation of the effective strain using the product-type symmetrisation is as following:

$$\tilde{\varepsilon}_{ij} = \frac{1}{2}\left[\varepsilon_{ik}\left(\delta_{kj}-\omega_{kj}\right)^{-1} + \left(\delta_{jk}-\omega_{jk}\right)^{-1}\varepsilon_{ki}\right]$$

It reads expanded in matrix notation as:

$$\begin{bmatrix} \tilde{\sigma}_{11} & \tilde{\sigma}_{12} & \tilde{\sigma}_{13} \\ \tilde{\sigma}_{21} & \tilde{\sigma}_{22} & \tilde{\sigma}_{23} \\ \tilde{\sigma}_{31} & \tilde{\sigma}_{32} & \tilde{\sigma}_{33} \end{bmatrix} =$$

$$= \frac{1}{2}\left\{\begin{bmatrix} \varepsilon_{11} & \varepsilon_{12} & \varepsilon_{13} \\ \varepsilon_{21} & \varepsilon_{22} & \varepsilon_{23} \\ \varepsilon_{31} & \varepsilon_{32} & \varepsilon_{33} \end{bmatrix}\begin{bmatrix} 1-\omega_1 & 0 & 0 \\ 0 & 1-\omega_2 & 0 \\ 0 & 0 & 1-\omega_3 \end{bmatrix} + \begin{bmatrix} 1-\omega_1 & 0 & 0 \\ 0 & 1-\omega_2 & 0 \\ 0 & 0 & 1-\omega_3 \end{bmatrix}\begin{bmatrix} \varepsilon_{11} & \varepsilon_{12} & \varepsilon_{13} \\ \varepsilon_{21} & \varepsilon_{22} & \varepsilon_{23} \\ \varepsilon_{31} & \varepsilon_{32} & \varepsilon_{33} \end{bmatrix}\right\}$$

$$= \begin{bmatrix} \varepsilon_{11}(1-\omega_1) & \frac{1}{2}\varepsilon_{12}\left((1-\omega_1)+(1-\omega_2)\right) & \frac{1}{2}\varepsilon_{13}\left((1-\omega_1)+(1-\omega_3)\right) \\ \frac{1}{2}\varepsilon_{21}\left((1-\omega_1)+(1-\omega_2)\right) & \varepsilon_{22}(1-\omega_2) & \frac{1}{2}\varepsilon_{23}\left((1-\omega_2)+(1-\omega_3)\right) \\ \frac{1}{2}\varepsilon_{31}\left((1-\omega_1)+(1-\omega_3)\right) & \frac{1}{2}\varepsilon_{32}\left((1-\omega_2)+(1-\omega_3)\right) & \varepsilon_{33}(1-\omega_3) \end{bmatrix}$$

The symmetric damage effect tensor is found by applying Voigt notation:

$$M_{ijkl}^{-1}$$

$$= \begin{bmatrix} 1-\omega_1 & 0 & 0 & 0 & 0 & 0 \\ 0 & 1-\omega_2 & 0 & 0 & 0 & 0 \\ 0 & 0 & 1-\omega_3 & 0 & 0 & 0 \\ 0 & 0 & 0 & \frac{1}{2}\left((1-\omega_2)+(1-\omega_3)\right) & 0 & 0 \\ 0 & 0 & 0 & 0 & \frac{1}{2}\left((1-\omega_1)+(1-\omega_3)\right) & 0 \\ 0 & 0 & 0 & 0 & 0 & \frac{1}{2}\left((1-\omega_1)+(1-\omega_2)\right) \end{bmatrix}$$

The damage effect tensors developed through sum-type symmetrisation of effective stress and effective strain are not equivalent: $M_{ijkl} \neq M_{ijkl}^{-1}$.

Appendix B Single Element Test Validation

This appendix presents additional results from the LS-DYNA single element test presented in Chapter 4. Appendix B.1 and B.4 present out-of-plane results which were obtained with 3D elements in MAT_022 and MAT_059. These were not presented in Chapter 4 directly for the sake of space. Additionally, results for all materials obtained for the single element tests for strength, stiffness and failure strain are compared to LS-DYNA material input data and analytical data if available. This is meant to evaluate the accuracy of the material models. The determined failure criterion is stated as well.

The single element test was used to evaluate composite material models in LS-DYNA.

- MAT_022: Composite Damage
- MAT_054: Composite Damage with Chang-Chang
- MAT_055: Composite Damage with Tsai-Wu
- MAT_058: Laminated Composite Fabric
- MAT_059: Composite Failure

The single element test in Chapter 4 (Section 4.1.2.2.) was used to investigated and compare different composite material models in LS-DYNA. The single elements used had a consistent edge length of $1mm$ and where quasi-statically loaded with the strain-rate $\dot{\varepsilon} = 10^{-1}\frac{1}{s}$. Separate tests were conducted for three load cases (tension, compression, shear) and three different orientations (0°, 45° and 90°).

B.1 Composite Damage (MAT_022)

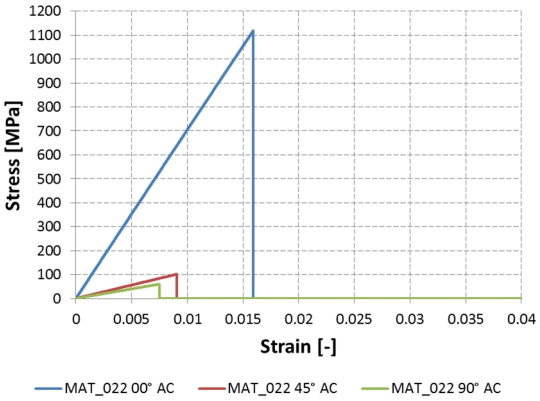

Figure 175: Single element test MAT_022: tension in ac-plane of 3D elements (00°, 45° and 90°)

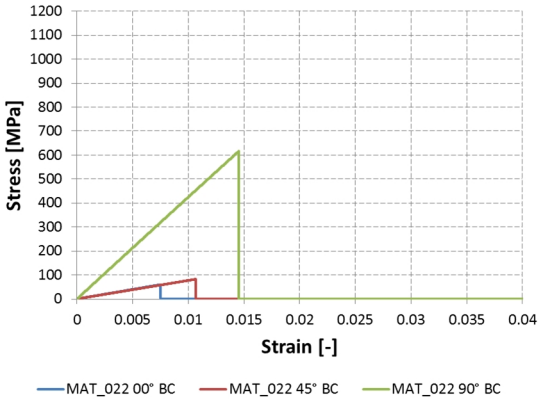

Figure 176: Single element test MAT_022: tension in bc-plane of 3D elements (00°, 45° and 90°)

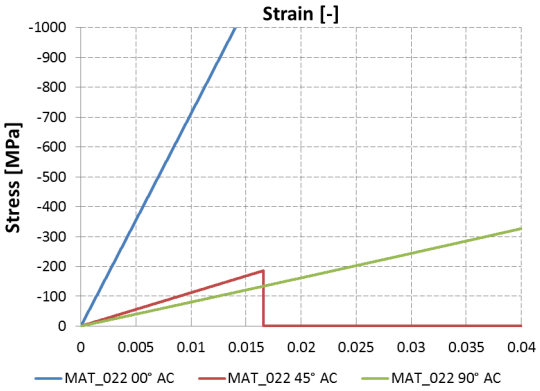

Figure 177: Single element test MAT_022: compression in ac-plane of 3D elements (00°, 45° and 90°)

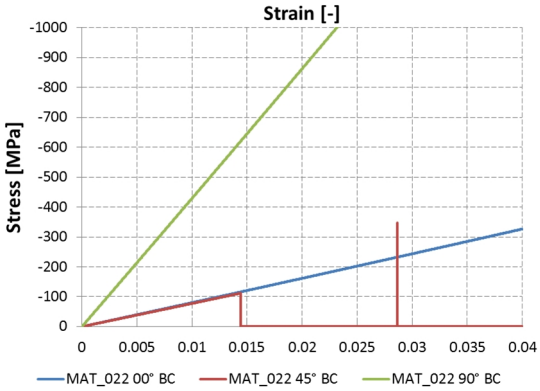

Figure 178: Single element test MAT_022: compression in bc-plane of 3D elements (00°, 45° and 90°)

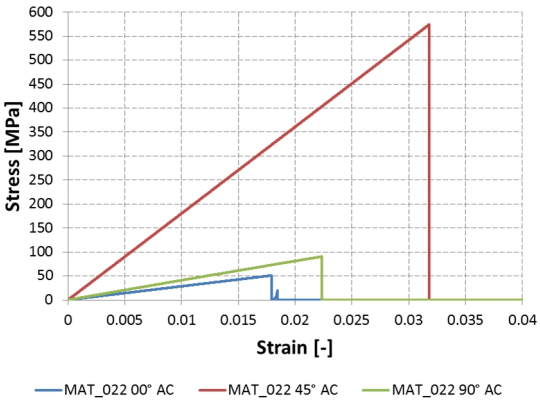

Figure 179: Single element test MAT_022: shear in ac-plane of 3D elements (00°, 45° and 90°)

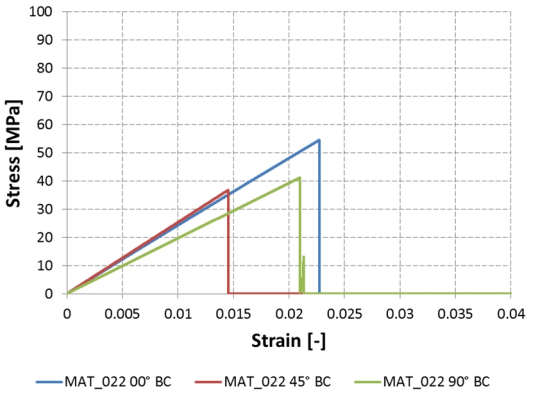

Figure 180: Single element test MAT_022: shear in bc-plane of 3D elements (00°, 45° and 90°)

Table 0-1: Comparison of failure strengths for MAT_022 (2D and 3D elements)

Shells MAT_022						Solids ab-plane MAT_022					
	Orientation	LS-DYNA input [MPa]	LS-DYNA output [MPa]	Error [%]	Failure criterion		Orientation	LS-DYNA input [MPa]	LS-DYNA output [MPa]	Error [%]	Failure criterion
Tension	00°	1119	1116.9	0.2	CC1	Tension	00°	1119	1118.9	0.000	CC1
	45°	284	281.2	0.9	CC3		45°	284	284.2	0.1	CC3
	90°	617	614.7	0.4	CC3		90°	617	617	0.000	CC3
Compression	00°	-768	N/A	N/A	N/A	Compression	00°	-768	N/A	N/A	N/A
	45°	-322	-322.2	0.1	CC4		45°	-322	N/A	N/A	N/A
	90°	-463	-459.3	0.8	CC4		90°	-463	N/A	N/A	N/A
Shear	00°	146	141.8	2.9	CC3	Shear	00°	146	140.5	3.8	shear
	45°	N/A	558.9	N/A	shear		45°	N/A	518.2	N/A	CC1
	90°	146	142.1	2.7	CC3		90°	146	142.9	2.1	CC1
Solids ac-plane MAT_022						**Solids bc-plane MAT_022**					
	Orientation	LS-DYNA input [MPa]	LS-DYNA output [MPa]	Error [%]	Failure criterion		Orientation	LS-DYNA input [MPa]	LS-DYNA output [MPa]	Error [%]	Failure criterion
Tension	00°	1119	1119	0.000	CC1	Tension	00°	60	60	0.0	DL1
	45°	101	101.6	0.6	DL1		45°	82	82.2	0.2	DL1
	90°	60	60	0.000	DL1		90°	617	617	0.0	CC3
Compression	00°	-768	N/A	N/A	N/A	Compression	00°	-30	N/A	N/A	N/A
	45°	-186	-186	0.000	CC4		45°	-111.5	-112	0.4	shear
	90°	-30	N/A	N/A	N/A		90°	-463	N/A	N/A	N/A
Shear	00°	93	50.9	45.3	CC1	Shear	00°	53	54.6	3.0	DL1
	45°	N/A	574.7	N/A	DL1		45°	N/A	36.8	N/A	DL1
	90°	93	90.6	2.6	DL1		90°	53	41.1	22.5	CC3

Table 0-2: Comparison of failure strains for MAT_022 (2D and 3D elements)

Shells MAT_022						Solids ab-plane MAT_022					
	Orientation	LS-DYNA output [MPa]	LS-DYNA input [MPa]	Error [%]	Failure criterion		Orientation	LS-DYNA output [MPa]	LS-DYNA input [MPa]	Error [%]	Failure criterion
Tension	00°	0.0158	0.0159	0.006	CC1	Tension	00°	0.0158	0.0159	0.000	CC1
	45°	0.0089	0.0089	0.000	CC3		45°	0.0089	0.0089	0.000	CC3
	90°	0.0145	0.0145	0.000	CC3		90°	0.0145	0.0145	0.000	CC3
Compression	00°	0.0109	N/A	N/A	N/A	Compression	00°	0.0109	N/A	N/A	N/A
	45°	0.0102	0.0101	0.010	CC4		45°	0.0102	N/A	N/A	N/A
	90°	0.0108	0.0107	0.009	CC4		90°	0.0108	N/A	N/A	N/A
Shear	00°	0.0138	0.0179	0.297	CC3	Shear	00°	0.0138	0.0166	0.203	shear
	45°	N/A	0.0316	N/A	shear		45°	N/A	0.0272	N/A	CC1
	90°	0.0138	0.0179	0.297	CC3		90°	0.0138	0.0156	0.130	CC1
Solids ac-plane MAT_022						**Solids bc-plane MAT_022**					
	Orientation	LS-DYNA output [MPa]	LS-DYNA input [MPa]	Error [%]	Failure criterion		Orientation	LS-DYNA output [MPa]	LS-DYNA input [MPa]	Error [%]	Failure criterion
Tension	00°	0.0158	0.0159	0.006	CC1	Tension	00°	0.0075	0.0075	0.0	DL1
	45°	0.007	0.0091	0.3	DL1		45°	0.0093	0.0107	15.1	DL1
	90°	0.0075	0.0075	0.000	DL1		90°	0.0145	0.0145	0.0	CC3
Compression	00°	0.0109	N/A	N/A	N/A	Compression	00°	0.00375	N/A	N/A	N/A
	45°	0.0129	0.0166		CC4		45°	0.0127	0.0144	13.4	shear
	90°	0.0036	N/A	N/A	N/A		90°	0.0108	N/A	N/A	N/A
Shear	00°	0.0211	0.0179	15.2	CC1	Shear	00°	0.0204	0.0228	11.8	DL1
	45°	N/A	0.0318	N/A	DL1		45°	N/A	0.0145	N/A	DL1
	90°	0.0211	0.0224	6.2	DL1		90°	0.0204	0.0210	2.9	CC3

Table 0-3: Comparison of stiffness for MAT_022 (2D and 3D elements)

Shells MAT_022						Solids ab-plane MAT_022					
	Orientation	LS-DYNA output [MPa]	LS-DYNA input [MPa]	Error [%]	Failure criterion		Orientation	LS-DYNA output [MPa]	LS-DYNA input [MPa]	Error [%]	Failure criterion
Tension	00°	70800	70243	0.8	CC1	Tension	00°	70800	70371	0.6	CC1
	45°	31684	31595	0.3	CC3		45°	31684	31933	0.8	CC3
	90°	42700	42600	0.2	CC3		90°	42700	42552	0.3	CC3
Compression	00°	70800	71185	0. 5	N/A	Compression	00°	70800	71185	0.5	N/A
	45°	31684	31901	0. 7	CC4		45°	31684	31891	0.7	N/A
	90°	42700	42925	0. 5	CC4		90°	42700	42932	0. 5	N/A
Shear	00°	10600	7923	0.253	CC3	Shear	00°	10600	8464	20.2	shear
	45°	N/A	10669	N/A	shear		45°	N/A	19051	N/A	CC1
	90°	10600	7939	25.1	CC3		90°	10600	9160	13.6	CC1
Solids ac-plane MAT_022						**Solids bc-plane MAT_022**					
	Orientation	LS-DYNA output [MPa]	LS-DYNA input [MPa]	Error [%]	Failure criterion		Orientation	LS-DYNA output [MPa]	LS-DYNA input [MPa]	Error [%]	Failure criterion
Tension	00°	70800	70377	0. 6	CC1	Tension	00°	8000	8000	0.0	DL1
	45°	14407	11165	22.5	DL1		45°	8799	7682	12.7	DL1
	90°	8000	8000	0.0	DL1		90°	42700	42700	0.0	CC3
Compression	00°	70800	71191	0. 6	N/A	Compression	00°	8000	8015	0.2	N/A
	45°	14407	11205	22.2	CC4		45°	8799	7764	11.8	shear
	90°	8000	8015	0. 2	N/A		90°	42700	42932	0.5	N/A
Shear	00°	4400	2844	35.4	CC1	Shear	00°	2600	2395	7.9	DL1
	45°	N/A	18072	N/A	DL1		45°	N/A	2538	N/A	DL1
	90°	4400	4045	8.1	DL1		90°	2600	1957	24.7	CC3

B.2 Composite Damage with Chang-Chang/with Tsai-Wu (MAT_054/055)

Table 0-4: Comparison of failure strengths for MAT_054 and MAT_055 (2D elements)

Shells MAT_054						Shells MAT_055					
	Orientation	LS-DYNA input [MPa]	LS-DYNA output [MPa]	Error [%]	Failure criterion		Orientation	LS-DYNA input [MPa]	LS-DYNA output [MPa]	Error [%]	Failure criterion
Tension	00°	1119	1116.9	0.2	CC1	Tension	00°	1119	1116.9	0.2	CC1
	45°	284	284.2	0.1	CC3		45°	284	284.2	0.1	TW1
	90°	617	617	0.0	CC3		90°	617	617	0.0	TW1
Compression	00°	-768	-768	0.0	CC2	Compression	00°	-768	-768	0.0	CC2
	45°	-322	-322.8	0.2	CC4		45°	-322	-322.8	0.2	TW1
	90°	-463	-463	0.0	CC4		90°	-463	-463	0.0	TW1
Shear	00°	146	142	2.7	CC3	Shear	00°	146	146	0.0	TW1
	45°	560	558.9	0.2	shear		45°	560	558.9	0.2	shear
	90°	146	142.1	2.7	CC3		90°	146	146.1	0.1	TW1

Table 0-5: Comparison of failure strains for MAT_054 and MAT_055 (2D elements)

Shells MAT_054						Shells MAT_055					
	Orientation	LS-DYNA output [MPa]	LS-DYNA input [MPa]	Error [%]	Failure criterion		Orientation	LS-DYNA output [MPa]	LS-DYNA input [MPa]	Error [%]	Failure criterion
Tension	00°	0.0158	0.0159	0.6	CC1	Tension	00°	0.0158	0.0159	0.6	CC1
	45°	0.0089	0.0089	0.0	CC3		45°	0.0089	0.0089	0.0	TW1
	90°	0.0145	0.0146	0.7	CC3		90°	0.0145	0.0146	0.7	TW1
Compression	00°	0.0109	0.0108	0.9	CC2	Compression	00°	0.0109	0.0108	0.9	CC2
	45°	0.0102	0.0101	1.0	CC4		45°	0.0102	0.0101	1.0	TW1
	90°	0.0108	0.0108	0.0	CC4		90°	0.0108	0.0108	0.0	TW1
Shear	00°	0.0138	0.018	30.4	CC3	Shear	00°	0.0138	0.0188	36.2	TW1
	45°	N/A	0.0316	N/A	shear		45°	N/A	0.0316	N/A	shear
	90°	0.0138	0.0179	29.7	CC3		90°	0.0138	0.0185	34.1	TW1

Table 0-6: Comparison of stiffness for MAT_054 and MAT_055 (2D elements)

Shells MAT_054						Shells MAT_055					
	Orientation	LS-DYNA output [MPa]	LS-DYNA input [MPa]	Error [%]	Failure criterion		Orientation	LS-DYNA output [MPa]	LS-DYNA input [MPa]	Error [%]	Failure criterion
Tension	00°	70800	70245	0.8	CC1	Tension	00°	70800	70245	0.8	CC1
	45°	31684	31933	0.8	CC3		45°	31684	31933	0.8	TW1
	90°	42700	42253	1.0	CC3		90°	42700	42253	1.0	TW1
Compression	00°	70800	71111	0.4	CC2	Compression	00°	70800	71111	0.4	CC2
	45°	31684	31960	0.9	CC4		45°	31684	31960	0.9	TW1
	90°	42700	42700	0.0	CC4		90°	42700	42700	0.0	TW1
Shear	00°	10600	7889	25.6	CC3	Shear	00°	10600	7766	26.7	TW1
	45°	N/A	17687	N/A	shear		45°	N/A	17687	N/A	shear
	90°	10600	7939	25.1	CC3		90°	10600	7897	25.5	TW1

B.3 Laminated Composite Fabric (MAT_058)

Table 0-7: Comparison of failure strengths and failure strains for MAT_058 (2D elements)

Strength: Shells MAT_058					
	Orientation	LS-DYNA input [MPa]	LS-DYNA output [MPa]	Error [%]	Failure criterion
Tension	00°	1119	1118.9	0.0	T1
	45°	284	284.1	0.0	T2
	90°	617	616.9	0.0	T2
Compression	00°	-768	-767.9	0.0	T1
	45°	-322	-267.3	17.0	T2
	90°	-463	-462.9	0.0	T2
Shear	00°	146	142.7	2.3	T3
	45°	560	559.2	0.1	T1
	90°	146	142.7	2.3	T3

B.4 Composite Failure (MAT_059)

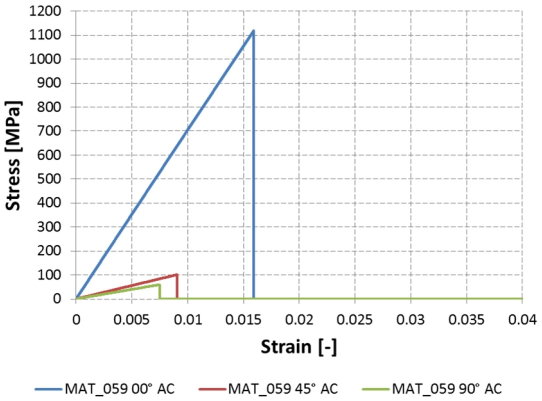

Figure 181: Single element test MAT_059: tension in ac-plane of 3D elements (00°, 45° and 90°)

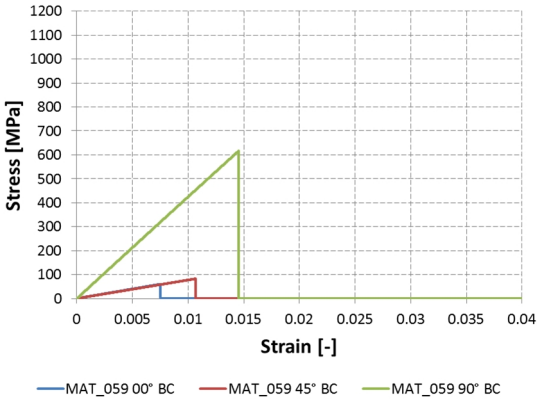

Figure 182: Single element test MAT_059: tension in bc-plane of 3D elements (00°, 45° and 90°)

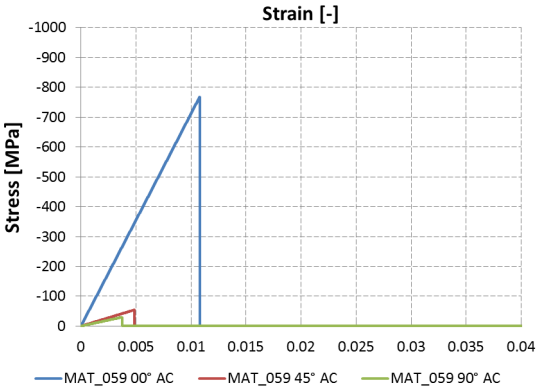

Figure 183: Single element test MAT_059: compression in ac -plane of 3D elements (00°, 45° and 90°)

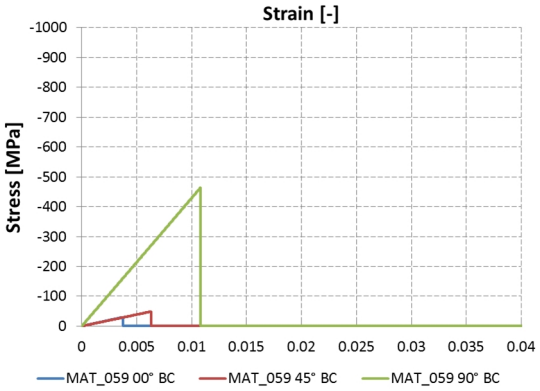

Figure 184: Single element test MAT_059: compression in bc -plane of 3D elements (00°, 45° and 90°)

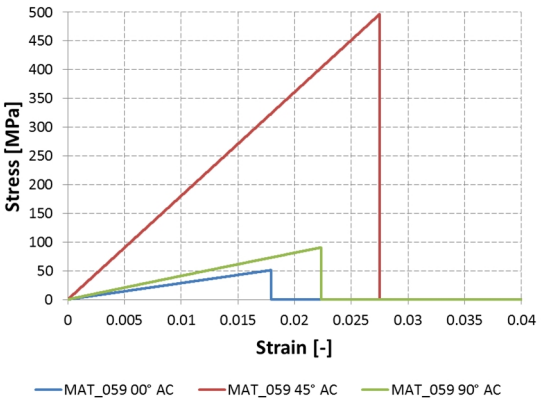

Figure 185: Single element test MAT_059: shear in ac -plane of 3D elements (00°, 45° and 90°)

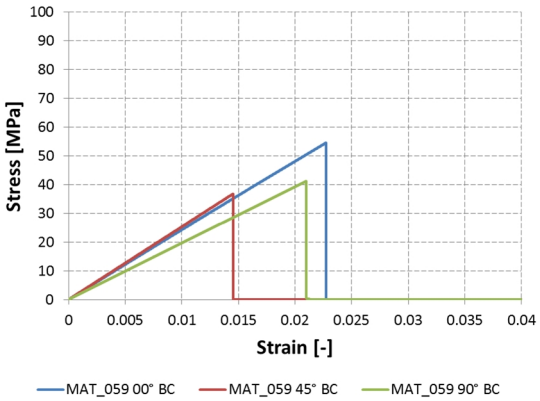

Figure 186: Single element test MAT_059: shear in bc -plane of 3D elements (00°, 45° and 90°)

Table 0-8: Comparison of failure strengths for MAT_059 (2D and 3D elements)

Shells MAT_059						Solids AB MAT_059					
	Orientation	LS-DYNA input [MPa]	LS-DYNA output [MPa]	Error [%]	Failure criterion		Orientation	LS-DYNA input [MPa]	LS-DYNA output [MPa]	Error [%]	Failure criterion
Tension	00°	1119	1119	0.0	CC1	Tension	00°	1119	1119	0.0	CH1
	45°	284	292	2.8	CC3		45°	284	284.2	0.1	CH2
	90°	617	617	0.0	CC3		90°	617	617	0.0	CH2
Compression	00°	-768	-768	0.0	CC4	Compression	00°	-768	-767.9	0.0	CH6
	45°	-292	-292	0.0	shear		45°	-322	-397.9	19.1	CH7
	90°	-463	-463	0.0	CC4		90°	-463	-463	0.0	CH7
Shear	00°	146	145.9	0.1	CC3	Shear	00°	146	140.5	3.8	CH2
	45°	560	559.2	0.1	CC1		45°	560	518.2	7.5	CH1
	90°	146	145.9	0.1	CC3		90°	146	142.9	2.1	CH1
Solids AC _MAT_059						**Solids BC MAT_059**					
	Orientation	LS-DYNA input [MPa]	LS-DYNA output [MPa]	Error [%]	Failure criterion		Orientation	LS-DYNA input [MPa]	LS-DYNA output [MPa]	Error [%]	Failure criterion
Tension	00°	1119	1119	0.0	CH1	Tension	00°	60	60	0.0	CH5
	45°	101	101.6	0.6	CH5		45°	82	82.2	0.2	CH5
	90°	60	60	0.0	CH5		90°	617	617	0.0	CH2
Compression	00°	-768	-767.9	0.0	CH6	Compression	00°	-30	-30	0.0	CH8
	45°	-186	-54.7	70.6	CH8		45°	-111.5	-48.7	56.3	CH8
	90°	-30	-30	0.0	CH8		90°	-463	-463	0.0	CH7
Shear	00°	93	50.9	45.3	CH5	Shear	00°	53	54.6	3.0	CH5
	45°	N/A	496.4	N/A	CH8		45°	N/A	36.8	N/A	CH5
	90°	93	90.6	2.6	CH5		90°	53	41.1	22.5	CH5

Table 0-9: Comparison of failure strains for MAT_059 (2D and 3D elements)

Shells MAT_059						Solids AB MAT_059					
	Orientation	LS-DYNA output [MPa]	LS-DYNA input [MPa]	Error [%]	Failure criterion		Orientation	LS-DYNA output [MPa]	LS-DYNA input [MPa]	Error [%]	Failure criterion
Tension	00°	0.0158	0.0159	0.6	CC1	Tension	00°	0.0158	0.0159	0.6	CH1
	45°	0.0089	0.0091	2.2	CC3		45°	0.0089	0.0089	0.0	CH2
	90°	0.0145	0.0146	0.7	CC3		90°	0.0145	0.0145	0.0	CH2
Compression	00°	0.0109	0.0108	0.9	CC4	Compression	00°	0.0109	0.0108	0.9	CH6
	45°	0.0102	0.0092	9.8	shear		45°	0.0102	0.0125	22.5	CH7
	90°	0.0108	0.0108	0.0	CC4		90°	0.0108	0.0108	0.0	CH7
Shear	00°	0.0138	0.0184	33.3	CC3	Shear	00°	0.0138	0.0166	20.3	CH2
	45°	N/A	0.0317	N/A	CC1		45°	N/A	0.0272	N/A	CH1
	90°	0.0138	0.0184	33.3	CC3		90°	0.0138	0.0156	13.0	CH1
Solids AC _MAT_059						**Solids BC MAT_059**					
	Orientation	LS-DYNA output [MPa]	LS-DYNA input [MPa]	Error [%]	Failure criterion		Orientation	LS-DYNA output [MPa]	LS-DYNA input [MPa]	Error [%]	Failure criterion
Tension	00°	0.0158	0.0159	0.6	CH1	Tension	00°	0.0075	0.0075	0.0	CH5
	45°	0.007	0.009	28.6	CH5		45°	0.0093	0.011	18.3	CH5
	90°	0.0075	0.0075	0.0	CH5		90°	0.0145	0.0145	0.0	CH2
Compression	00°	0.0109	0.0108	0.9	CH6	Compression	00°	0.00375	0.00374	0.3	CH8
	45°	0.0129	0.0049	62.0	CH8		45°	0.0127	0.0063	50.4	CH8
	90°	0.0036	0.0037	0.3	CH8		90°	0.0108	0.0108	0.0	CH7
Shear	00°	0.0211	0.0179	15.2	CH5	Shear	00°	0.0204	0.0228	11.8	CH5
	45°	N/A	0.0275	N/A	CH8		45°	N/A	0.0145	N/A	CH5
	90°	0.0211	0.0224	6.2	CH5		90°	0.0204	0.0209	2.5	CH5

Table 0-10: Comparison of stiffness for MAT_059 (2D and 3D elements)

Shells MAT_059						Solids AB MAT_059					
	Orientation	LS-DYNA output [MPa]	LS-DYNA input [MPa]	Error [%]	Failure criterion		Orientation	LS-DYNA output [MPa]	LS-DYNA input [MPa]	Error [%]	Failure criterion
Tension	00°	70800	70377	0.6	CC1	Tension	00°	70800	70377	0.6	CH1
	45°	31684	32444	2.4	CC3		45°	31684	31933	0.8	CH2
	90°	42700	42260	1.0	CC3		90°	42700	42552	0.3	CH2
Compression	00°	70800	71111	0.4	CC4	Compression	00°	70800	71102	0.4	CH6
	45°	31684	31739	0.2	shear		45°	31684	31832	0.5	CH7
	90°	42700	42870	0.4	CC4		90°	42700	42870	0.4	CH7
Shear	00°	10600	7929	25.2	CC3	Shear	00°	10600	8464	20.2	CH2
	45°	N/A	17640	N/A	CC1		45°	N/A	19051	N/A	CH1
	90°	10600	7929	25.2	CC3		90°	10600	9160	13.6	CH1
Solids AC _MAT_059						**Solids BC MAT_059**					
	Orientation	LS-DYNA output [MPa]	LS-DYNA input [MPa]	Error [%]	Failure criterion		Orientation	LS-DYNA output [MPa]	LS-DYNA input [MPa]	Error [%]	Failure criterion
Tension	00°	70800	70377	0.6	CH1	Tension	00°	8000	8000	0.0	CH5
	45°	14407	11289	21.6	CH5		45°	8799	7473	15.1	CH5
	90°	8000	8000	0.0	CH5		90°	42700	42700	0.0	CH2
Compression	00°	70800	71102	0.4	CH6	Compression	00°	8000	2778		CH8
	45°	14407	11163	22.5	CH8		45°	8799	7730	12.1	CH8
	90°	8000	8108	1.4	CH8		90°	42700	42870	0.4	CH7
Shear	00°	4400	2844	35.4	CH5	Shear	00°	2600	2395	7.9	CH5
	45°	N/A	18051	N/A	CH8		45°	N/A	2538	N/A	CH5
	90°	4400	4045	8.1	CH5		90°	2600	1967	24.3	CH5

Appendix C One-Dimensional Wave Propagation: Solution for Several Time Instances

This appendix includes analytical wave propagation results obtained for a standard local CDM model presented in Chapter 3 (Section 3.2).The longitudinal wave propagation problem used was described originally by Bažant and Belytschko [6] and consists of a bar which is loaded at both ends with a constant velocity. This model was introduced in Chapter 3 to observe and analyse strain-softening phenomena and to evaluate different methods concerning this behaviour. The results presented here were derived analytically for different time instances of the probem and are presented for the sake of completeness.

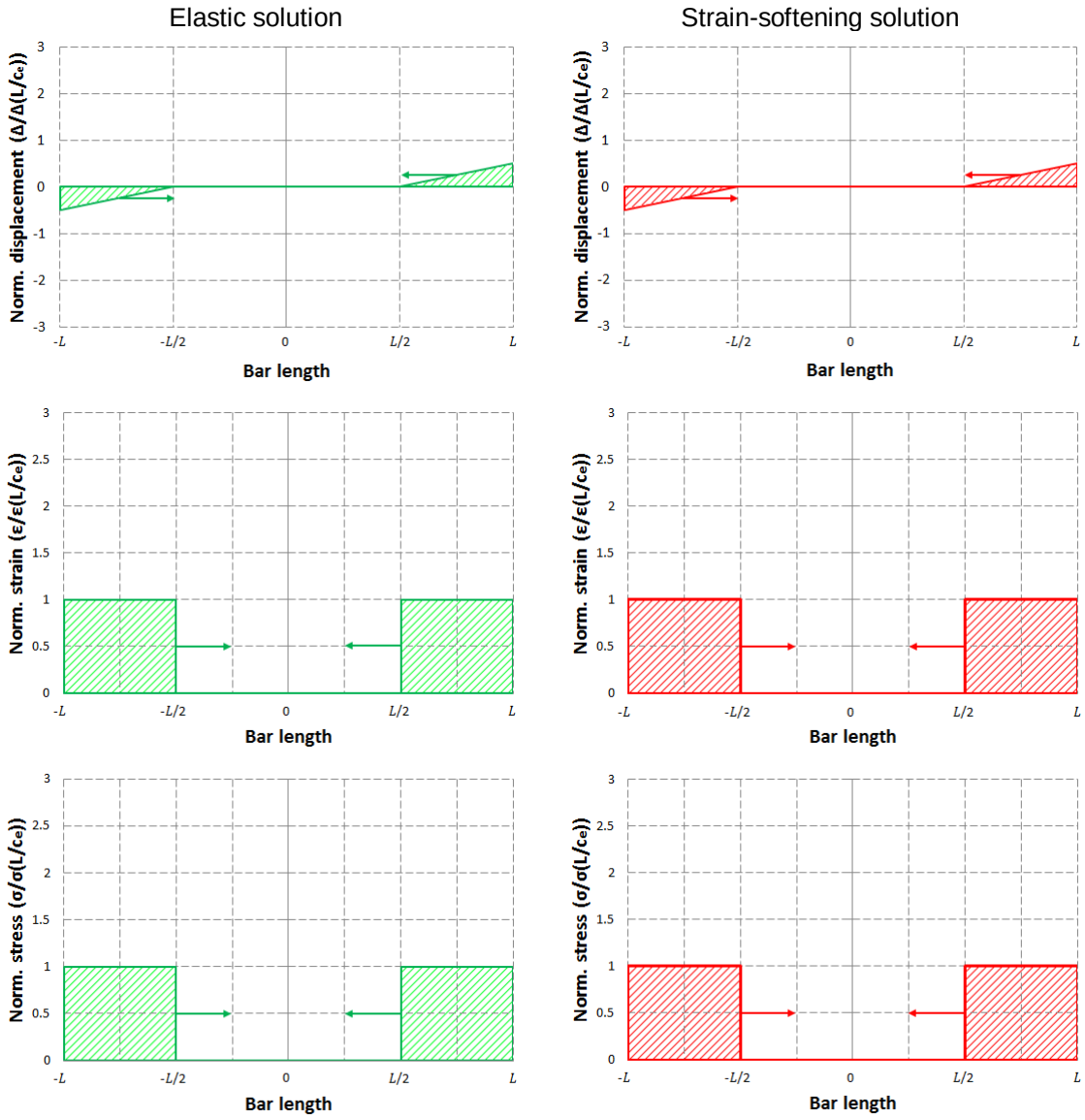

Figure 187: Analytical solution for normalised longitudinal displacement, strain and stress at $t = 1/2 \cdot L/c_e$

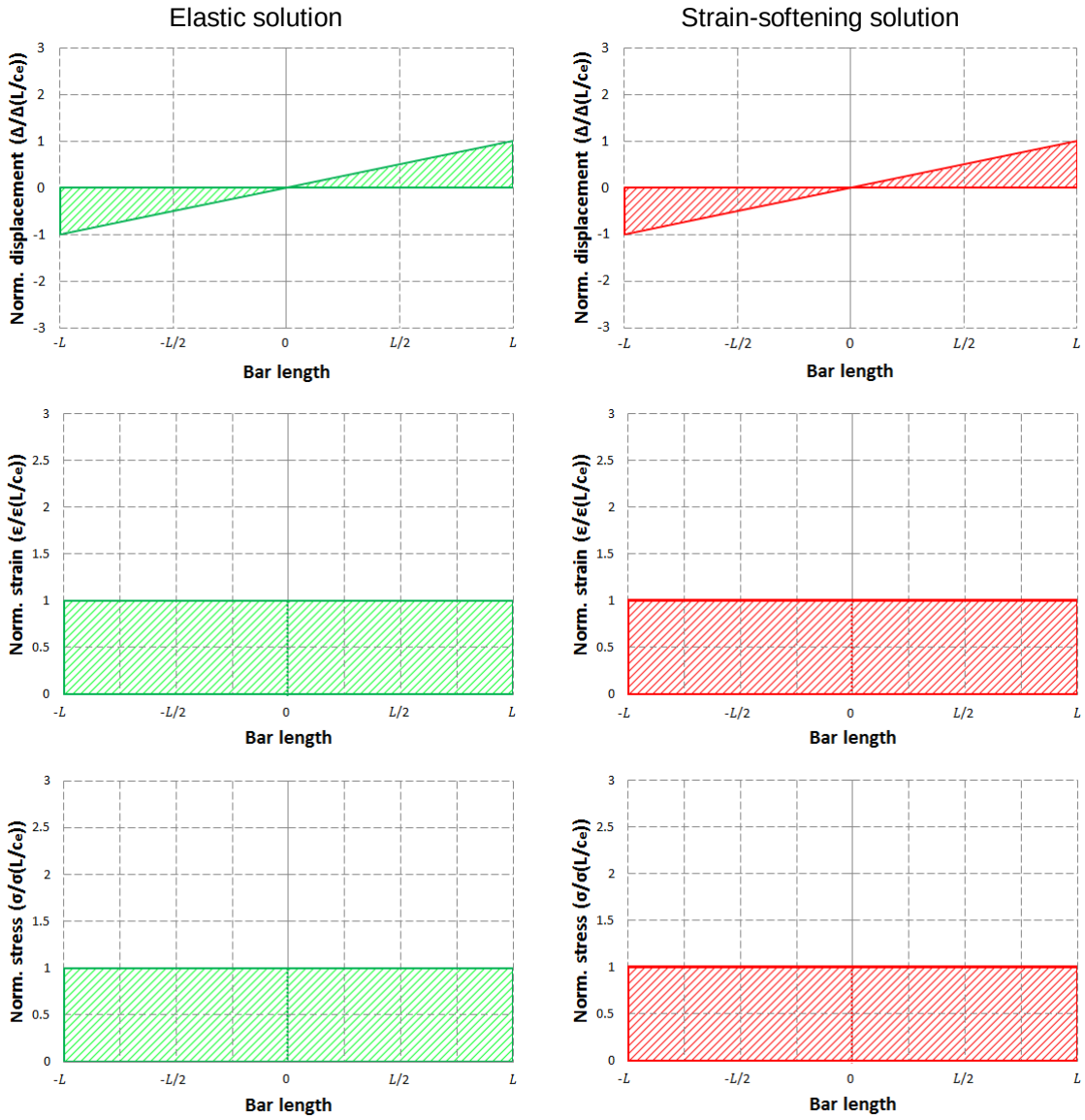

Figure 188: Analytical solution for normalised longitudinal displacement, strain and stress at $t = L/c_e$

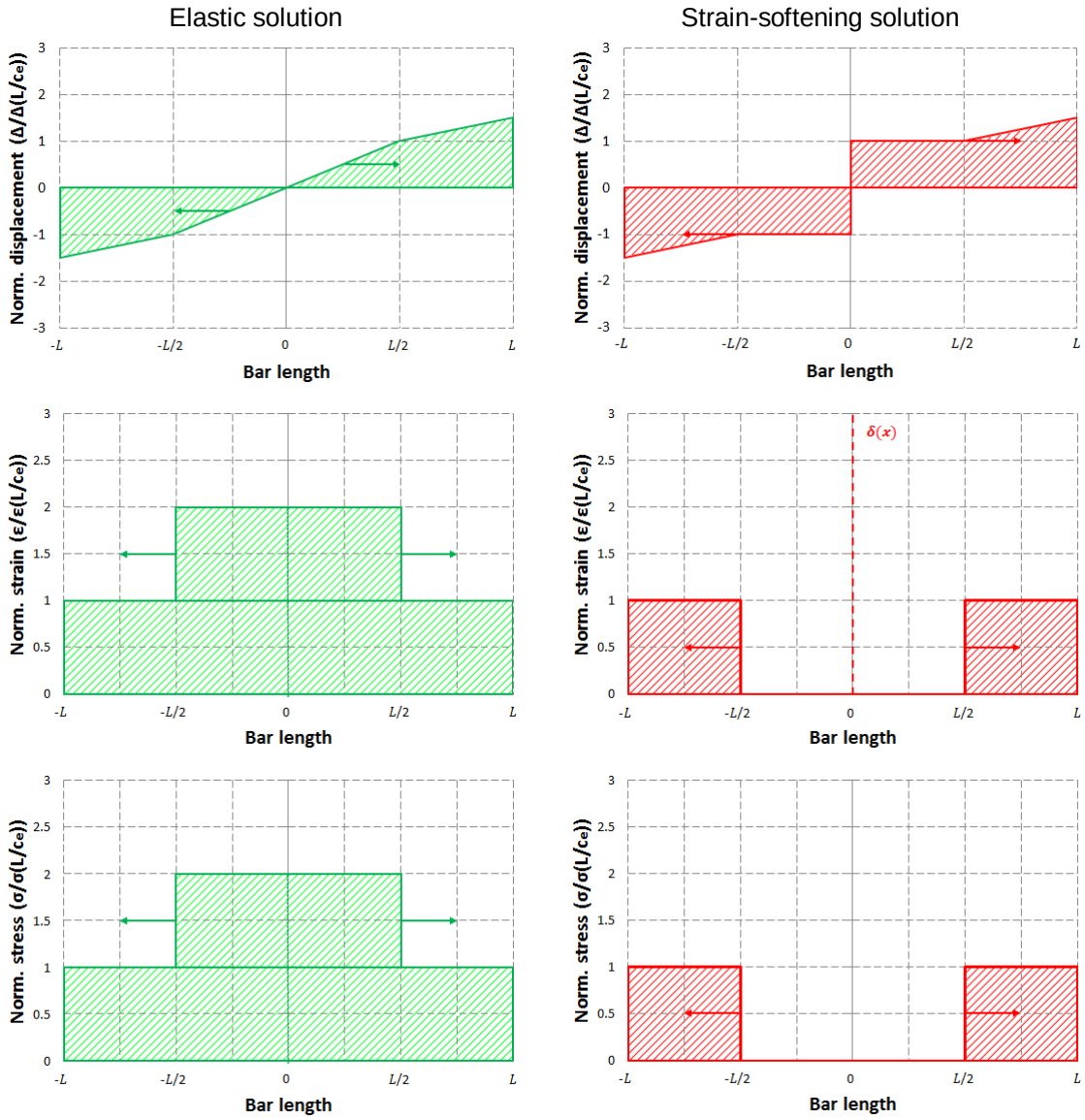

Figure 189: Analytical solution for normalised longitudinal displacement, strain and stress at $t = 3/4 \cdot 2L/c_e$

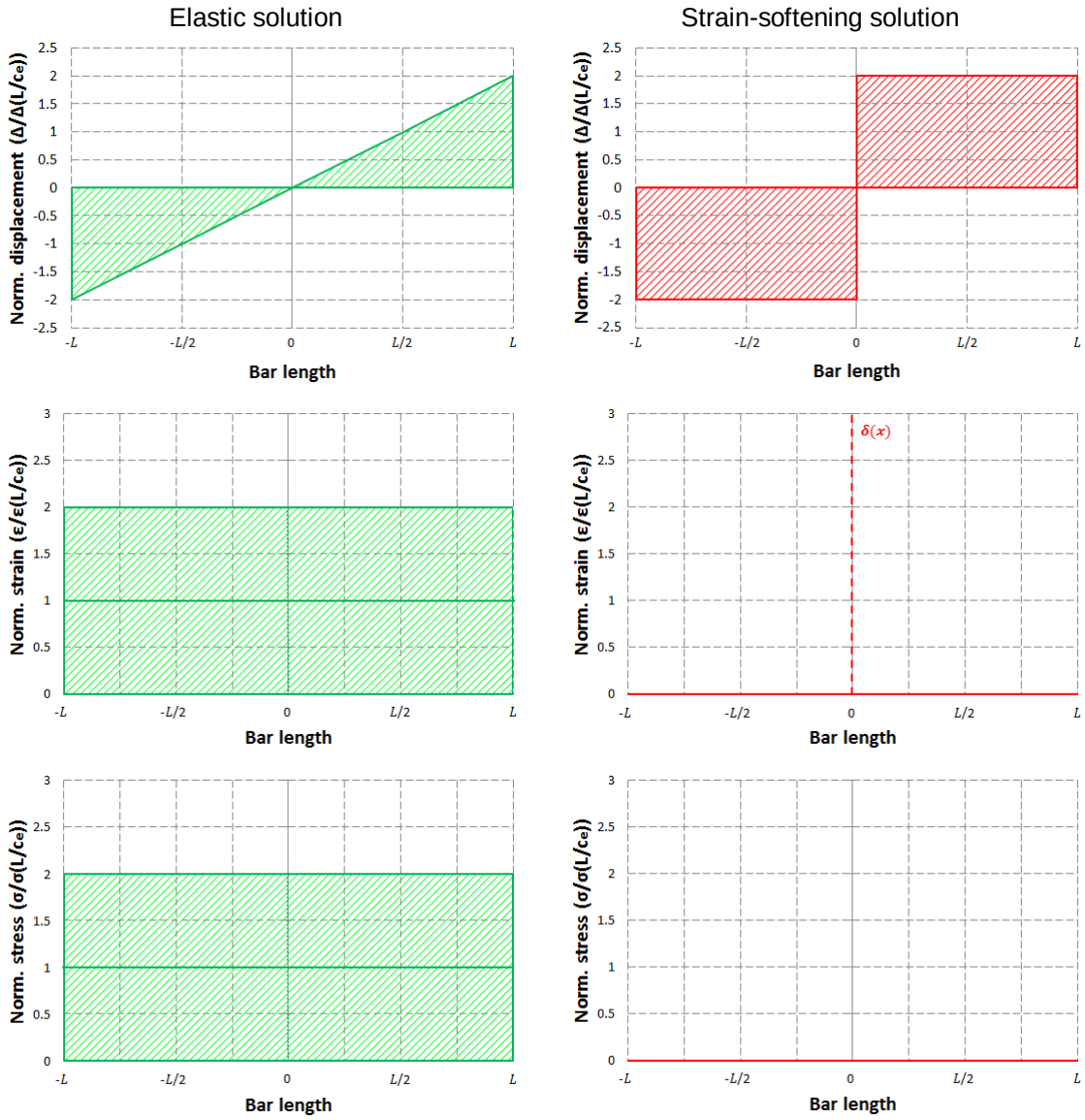

Figure 190: Analytical solution for normalised longitudinal displacement, strain and stress at $t = 2 \cdot L/c_e$